Synthesis of highly fluorinated precursors and their deposition conditions for self-assembled monolayers with defined small-scale surface structures as templates for the manipulation of wetting behavior

---

Jan Knauf

Univ.-Diss.

zur Erlangung des akademischen Grades
„doctor rerum naturalium“
(Dr. rer. nat.)
in der Wissenschaftsdisziplin „Colloid and Interface Science“

eingereicht an der
Mathematisch-Naturwissenschaftlichen Fakultät
Institut für Chemie
der Universität Potsdam

Ort und Tag der Disputation: Potsdam, 20. Juli 2020

Hauptbetreuer: Prof. Dr. Alexander Böker
Zweitbetreuer: Dr. Karsten Reihs

1. Gutachter: Prof. Dr. Alexander Böker
2. Gutachter: Dr. Karsten Reihs
3. Gutachter: Prof. Dr. Hans-Jürgen Butt

Published online in the
Institutional Repository of the University of Potsdam:
https://doi.org/10.25932/publishup-47380
https://nbn-resolving.org/urn:nbn:de:kobv:517-opus4-473804

Synthesis of highly fluorinated precursors and their deposition conditions for self-assembled monolayers with defined small-scale surface structures as templates for the manipulation of wetting behavior

Jan Knauf

Meiner Familie

Sonne auf, Sonne unter, Sonne hier, Sonne da, Sonne weg.

Quichotte

Danksagung

Ich bedanke mich bei meiner Familie, allen Freunden und Kollegen in Köln, Aachen und Potsdam, die mich in den letzten nicht immer einfachen Jahren begleitet und unterstützt haben. Diese Zeit hat auf unglaublich vielfältige Weise deutlich gemacht, was mir wirklich wichtig ist und immer sein wird. Ohne Euch würde ich diese wenigen, kurz gehaltenen Zeilen gerade vielleicht nicht mehr schreiben. Danke!

Ich möchte mich hierbei noch besonders bei Prof. Böker und Herrn Reihs bedanken, die mir während meiner Arbeit immer unterstützend zur Seite standen und auf deren hilfreiche Einwände, Ideen und Bestätigungen ich in unseren Diskussionen immer zählen konnte. Herrn Böker gilt zudem ein weiterer Dank für die konsequente Weiterverfolgung meiner Arbeit während des Wechsels von der RWTH Aachen zur Universität Potsdam.

Meiner Frau Annika gilt sicherlich der größte Dank für die Geduld und das Verständnis für die vielen Stunden, die in die Bearbeitung neuer Gedanken, Ideen und die vermutlich noch langwierigere textliche Aufarbeitung des Ganzen geflossen sind.

Abstract

"How Wenzel and Cassie were wrong" – this was the eye-catching title of an article published by Lichao Gao and Thomas McCarthy in 2007, in which fundamental interpretations of wetting behavior were put into question. The authors initiated a discussion on a subject, which had been generally accepted a long time ago and they showed that wetting phenomena were not as fully understood as imagined. Similarly, this thesis tries to put a focus on certain aspects of liquid wetting, which so far have been widely neglected in terms of interpretation and experimental proof. While the effect of surface roughness on the macroscopically observed wetting behavior is commonly and reliably interpreted according to the well-known models of Wenzel and Cassie/Baxter, the size-scale of the structures responsible for the surface's rough texture has not been of further interest. Analogously, the limits of these models have not been described and exploited. Thus, the question arises, what will happen when the size of surface structures is reduced to the size of the contacting liquid molecules itself? Are common methods still valid or can deviations from macroscopic behavior be observed?

This thesis wants to create a starting point regarding these questions. In order to investigate the effect of smallest-scale surface structures on liquid wetting, a suitable model system is developed by means of self-assembled monolayer (SAM) formation from (fluoro)organic thiols of differing lengths of the alkyl chain. Surface topographies are created which rely on size differences of several Ångströms and exhibit surprising wetting behavior depending on the choice of the individual precursor system. Thus, contact angles are experimentally detected, which deviate considerably from theoretical calculations based on Wenzel and Cassie/Baxter models and confirm that sub-nm surface topographies affect wetting. Moreover, experimentally determined wetting properties are found to correlate well to an assumed scale-dependent surface tension of the contacting liquid. This behavior has already been described for scattering experiments taking into account capillary waves on the liquid surface induced by temperature and had been predicted earlier by theoretical calculations.

However, the investigation of model surfaces requires the provision of suitable precursor molecules, which are not commercially available and opens up a door to the exotic chemistry of fluoro-organic materials. During the course of this work, the synthesis of long-chain precursors is examined with a particular focus put on oligomerically pure semi-fluorinated *n*-alkyl thiols and *n*-alkyl trichlorosilanes. For this, general protocols for the syntheses of the desired compounds are developed and

product mixtures are assayed to be separated into fractions of individual chain lengths by fluorous-phase high-performance liquid chromatography (F-HPLC).

The transition from model systems to technically more relevant surfaces and applications is initiated through the deposition of SAMs from long-chain fluorinated *n*-alkyl trichlorosilanes. Depositions are accomplished by a vapor-phase deposition process conducted on a pilot-scale set-up, which enables the exact control of relevant process parameters. Thus, the influence of varying deposition conditions on the properties of the final coating is examined and analyzed for the most important parameters. The strongest effect is observed for the partial pressure of reactive water vapor, which directly controls the extent of precursor hydrolysis during the deposition process. Experimental results propose that the formation of ordered monolayers rely on the amount of hydrolyzed silanol species present in the deposition system irrespective of the exact grade of hydrolysis. However, at increased amounts of species which are able to form cross-linked molecules due to condensation reactions, films deteriorate in quality. This effect is assumed to be caused by the introduction of defects within the film and the adsorption of cross-linked agglomerates. Deposition conditions are also investigated for chain-extended precursor species and reveal distinct differences caused by chain-elongation.

Parts of this work were funded by the German Federal Ministry of Education and Research (Grant 16SV5761K).

Content

1. Introduction: Manipulation of Surface Properties via Functional Coatings

The formation of functional coatings on solid substrates yields almost unlimited possibilities for the manipulation of surface properties. Particularly in terms of wetting behavior, tailored properties can be achieved and designed in order to suit a desired application.

Surfaces represent a means of "chemomechanical communication" of natural and artificial objects with their environment and direct the response of ambient materials towards these objects. Thus, it is not surprising that diverse kinds of surface structures, shapes, regular geometries and chemical modifications are found in nature. The most prominent example is probably the leaf of the lotus plant *Nelumbo nucifera*, which inspired researchers to develop super-water-repellent surfaces and applications ("lotus effect"). The lotus leaf achieves its superhydrophobic properties by the combination of a naturally rough surface which is covered with a waxy substance. [1,2] This very same principle can be applied in technical applications, where hierarchical structures are obtained by equipping solid rough structures with a liquid-repellent top-layer coating.

Historically, already Benjamin Franklin described the effect of surface coatings and the influence of thin layers of oil spread on water. [3] Later, Irving Langmuir and Katherine Blodgett developed the means to form ordered films of surfactants on liquids and transferring them onto solid substrates. [4,5] Unfortunately in terms of stability, these Langmuir-Blodgett-films are only loosely physisorbed onto a substrate and most often lack the stability required for technical applications. In contrast to this, self-assembled monolayers (SAMs) from organic compounds represent an important technique for the robust application of top-layer coatings onto substrate surfaces. Precursor molecules within SAMs are chemisorbed onto a substrate's surface and exhibit a high stability due to this covalent binding. Their application enables the creation of effective surface properties, which may be the exact opposite of the properties of the underlying substrate. For example, a hydrophobic organic coating inversely mirrors the hydrophilic wetting behavior of an underlying oxide prior to SAM-deposition.

The foundations of current SAM-techniques were established by Zisman *et al.* already in the 1940s, who prepared films of organic molecules on platinum and glass substrates. [6] Several years later, Nuzzo and Allara reported on the formation of stable films from alkyl disulfides on gold surfaces and initiated a new era of research for this

class of films. [7] Based on their findings, SAMs from alkyl thiol precursors developed into the standard system of SAM-deposition. Analogously, Maoz and Sagiv transferred their work on the modification of chromatographic silica gels with alkyl silanes to flat oxide substrates, which lead to further development of SAM-formation on technically relevant surfaces. [8]

SAMs from fluorinated alkyl precursors represent a distinct class of monolayers within the vast variety of substrate/precursor systems. They exhibit properties, which distinctly differentiate them from common alkyl SAMs and lead to unique film characteristics. Moreover, SAMs from fluorinated precursors enable the formation of omniphobic materials. These materials possess strong water- as well as oil-repellent properties and pave the way to new applications and techniques in terms of surface manipulation.

Due to their structural variety and diversity of surface properties, SAMs represent an active section of current research in many areas of science. Apart from studies concerning the wettability of surfaces, SAMs are, for example, employed in the directed adsorption of proteins or in biosensors [9,10], drug delivery [11], as barrier layer in ALD depositions [12,13], in the fabrication of nano-wires [14,15], as anti-stiction layers in micro-electromechanical systems (MEMS) [16–18], or in organic electronic devices [19].

The task of this thesis is two-fold. On the one hand, it aims to evaluate the effect of molecular roughness on surfaces introduced via the deposition of binary mixed SAMs from alkyl thiols with an initial focus on semi-fluorinated precursors. On the other hand, the results of the investigation of vapor-phase deposition parameters of SAMs from semi-fluorinated alkyl trichlorosilanes and their effect on the film's wetting properties are presented. Moreover, the synthesis and provision of oligomerically pure, commercially not available fluorous precursors is described and discussed. Following the definition stated in the “Handbook of Fluorous Chemistry”, the term "fluorous" will be used throughout the text to universally describe fluoroorganic molecules with a high degree of fluorination. [20]

In Chapter 2, the fundamental aspects of wetting on rough surfaces and methods to manipulate effective wetting behavior will be presented along with the introduction of the characteristic features of SAMs. The chapter focuses on fluorous functionalities and their unique influence on SAM-properties as well as the two most prominent SAM-systems of alkyl thiols and alkyl silanes. Binary mixed monolayers as a template for molecular roughness will be introduced and the importance of controlling

deposition conditions for silane-based SAMs will be discussed with special regard to the risk of precursor cross-linking.

Chapter 3 introduces methods of SAM-deposition as well as analysis and highlights the influence of high degrees of fluorination on experimental and analytical procedures. Moreover, fluorous-phase high-performance liquid chromatography (F-HPLC) will be presented as a new means of chromatographic provision of yet inaccessible compounds.

Chapters 4 to 6 cover the results-section of the thesis and are divided into the discussion of precursor syntheses, binary mixed SAMs from (fluoro)alkyl thiols and the investigation of deposition conditions for SAMs from fluorous trichlorosilanes. The results of precursor syntheses are presented in Chapter 4, where the provision of compounds for SAM-deposition from telomeric mixtures of crude educts will be explained. While Chapter 5 will present and discuss the creation of sub-nm roughness by means of fluorous thiol-based SAMs, Chapter 6 focuses on the investigation of process conditions for the deposition of high-quality monolayers from fluorous trichlorosilanes.

The concluding chapters contain additional information regarding experimental details, bibliographic resources, scientific contributions, and lists of figures, tables, and abbreviations.

2. Theoretical Background

2.1. Common methods to modify wetting behavior of surfaces

Current techniques for the modification of wetting behavior of liquids on rough surfaces all rely on two methods. While Wenzel introduced the ratio of actual to geometric surface area as a new, seminal measure of effective wetting, Cassie and Baxter extended his work and differentiated between different contact areas incorporated into one macroscopic surface.

The contact angle θ_Y of a liquid droplet resting on a solid substrate has been described by Young according to an equilibrium of forces (equation (1), Figure 1).[21] Incorporated are the surface tensions of the corresponding interfaces solid/vapor γ_{SV}, solid/liquid γ_{SL} and liquid/vapor γ_{LV}. This description assumes a system being in thermodynamic equilibrium with a liquid droplet resting on a flat, homogeneous surface.

$$\cos\theta_Y = \frac{\gamma_{SV} - \gamma_{SL}}{\gamma_{LV}} \qquad (1)$$

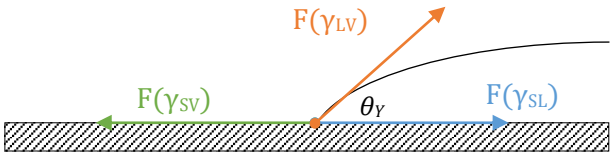

Figure 1: Contact angle of a liquid droplet on a flat homogeneous surface corresponding to Young.

For the interpretation of wetting experiments on rough substrate surfaces, Wenzel introduced the "roughness factor" *r* in order to account for the difference between actual and geometric (or "projected") surface area (equation (2)).[22] In practice, this

difference increases the surface area which is actually wetted under a liquid droplet (Figure 2).

$$r = \frac{actual\ surface}{geometric\ surface} \tag{2}$$

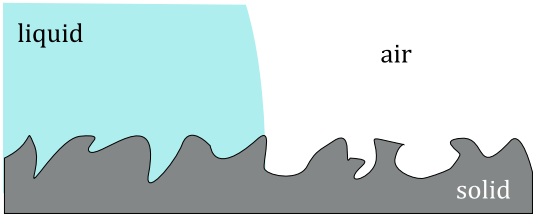

Figure 2: Schematic illustration of wetting on rough surfaces according to Wenzel. The surface under the droplet is completely wetted by the contacting liquid.

The Young contact angle of a homogeneous surface is thus enhanced by r and an apparent Wenzel contact angle θ_W is deduced. By increasing the effective surface to be wetted, roughness amplifies the wetting properties of a contacting liquid. Using water as an example, a hydrophilic surface ($\theta_Y < 90°$) becomes more hydrophilic, whereas a hydrophobic surface ($\theta_Y > 90°$) exhibits even increased hydrophobicity.

$$\cos\theta_W = \cos\theta_Y \cdot r \tag{3}$$

Extending Wenzel's model, Cassie and Baxter assigned different wetting properties to different areas of a rough surface, originally meant for the interpretation of wetting on porous surfaces.[23] The most prominent example for this model is air trapped within surface structures below liquid water contacting a hydrophobic, solid surface (Figure 3).

Figure 3: Schematic illustration of wetting on rough surfaces according to Cassie-Baxter. Air pockets are formed between solid substrate and liquid droplet so that the effective contact area solid/liquid is strongly reduced on very rough surfaces.

Here, the surface tension of the liquid is not identical when in contact with air or the solid substrate, so that according to Cassie-Baxter, the individual contributions of the relative surface areas (area fractions f_1, f_2) are considered for deriving the effective contact angle of the whole system.

$$\cos\theta_{CB} = f_1 \cdot \cos\theta_{Y1} + f_2 \cdot \cos\theta_{Y2} \qquad (4)$$

As the contact angle of liquids on air is assumed as $\theta_{Y2} = 180°$ (i.e. $\cos 180° = -1$), the total surface tension of a system is significantly reduced, when a large area of the liquid is brought into contact with trapped air, e.g. through the introduction of high degrees of roughness. In consequence, very large contact angles are observed when the solid/liquid contact area is reduced.

The Cassie-Baxter method has been increasingly exploited during the past years and research on distinct surface geometries and features has revealed several interesting possibilities. The size of these geometries scales down to nanometer levels and several different aspects of size and shape have been investigated. Further refinement of the surfaces and thus improvements concerning their wetting behavior can be

achieved by the creation of hierarchical structures through the introduction of functional coatings. [24–33] Applying self-assembled monolayers as top-layer coatings, the structural size of the effective structures is reduced even further down to the molecular level of the corresponding precursor molecules. One example for these hierarchical structures is presented in Figure 4. The image shows an alumina substrate that has been exposed to repeated etch and growth processes in order to obtain solid structures in the micro-/nanometer range. Applying a hydrophobic monolayer coating renders the surface super-hydrophobic and enables the observation of liquid water slippage. [32]

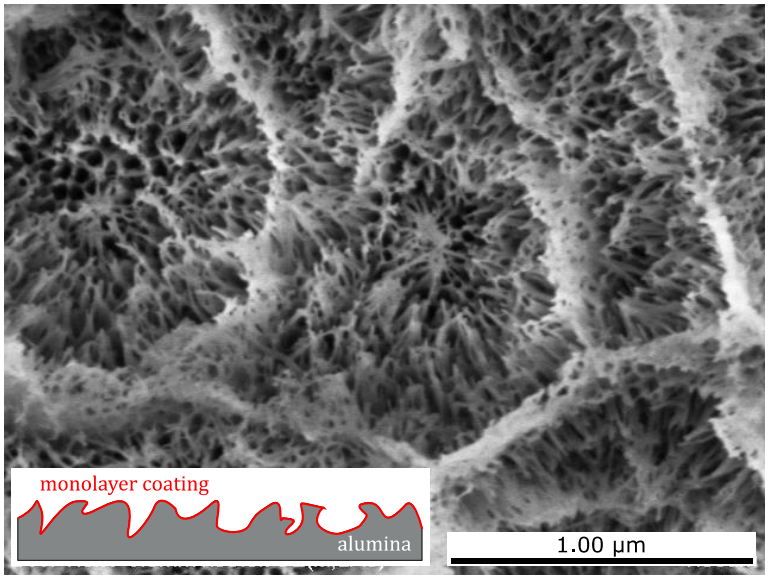

Figure 4: FE-SEM image of an etched alumina substrate for the formation of hierarchical structures. [32]

Non-ideal surfaces exhibit deviations from ideal wetting behavior due to surface defects which lead to local pinning of a contacting liquid. In consequence, differences between contact angles can be observed during the motion of a droplet over a surface. During the expansion of a droplet by the addition of liquid from a reservoir, an advancing contact angle θ_{adv} is observed, while on reduction of the drop volume a receding contact angle θ_{rec} is detected that can be significantly smaller than θ_{adv}. This effect is caused by inhomogeneities within the solid surface and resulting local differences in wetting properties. Thus, local pinning of the droplet leads to a change

of the localized contact angle. Contact angle hysteresis Δθ, the difference between θ_{adv} and θ_{rec}, is therefore regarded an important measure of surface homogeneity and represents a main criterion of surface quality. If only static contact angles on surfaces are determined, the measured value may reflect any value between the underlying advancing or receding contact angles. [34] Within the scope of this thesis, films of high quality are therefore characterized by a large advancing contact angle and low contact angle hysteresis.

$$\Delta\theta = \theta_{adv} - \theta_{rec} \tag{5}$$

2.2. Nomenclature

In order to simplify reading and understanding, a simple nomenclature for specifying (fluoro)alkyl precursors will be used throughout the text. Compounds are designated F*n*H*m*-*X* based on their number of fluoromethylene (*n*) and methylene (*m*) units in combination with the corresponding functional group (*X*). For example, *1H,1H,2H,2H*-perfluorodecyl thiol (F-$(CF_2)_8$-$(CH_2)_2$-SH) with eight fluoromethylene and two methylene units will be abbreviated F8H2-SH (Figure 5), while for *1H,1H,2H,2H*-perfluorododecyl trichlorosilane (F-$(CF_2)_{10}$-$(CH_2)_2$-$SiCl_3$) the form F10H2-$SiCl_3$ and for *n*-hexadecyl thiol (H-$(CH_2)_{16}$-SH) the form H16-SH will be used.

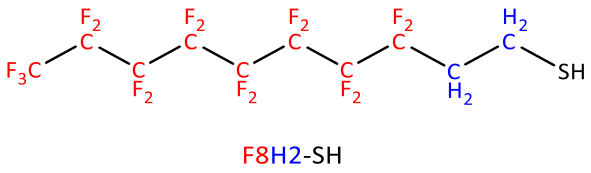

Figure 5: Example for the abbreviated nomenclature of *1H,1H,2H,2H*-perfluorodecyl thiol (F8H2-SH).

2.3. Self-assembled Monolayers

2.3.1. From molecular layers to macroscopic properties: Fundamental aspects of self-assembled monolayers

Self-assembled monolayers (SAMs) represent a distinct type of molecularly thin layers, which are prepared on suitable substrates from individual precursor molecules resulting in a quasi-continuous structure.[35–38] As stated by their name, ideal SAMs consist of a single layer of densely-packed molecules, so that layer thickness is mainly determined by the size of the precursor molecules. SAMs are characterized by their spontaneous assembly onto a substrate without the need of an external force to initiate film growth. The resulting overlayers can experience a remarkably high degree of structural order and are able to dramatically alter the effective properties of the surface towards contacting media. Several reviews, books and seminal papers have been published during the past 30 years, so that the list of references cited in this work is far from complete but tries to introduce the main aspects of research on these films by exemplary reports.

The very basic and simplified structure of an individual precursor molecule is depicted in Figure 6 with F4H2-SH (*1H*,*1H*,*2H*,*2H*-perfluorohexyl thiol) as a practical example. It consists of a reactive head-group, a functional tail-group and an optional spacer unit, which may as well be regarded a part of the tail-group (depending on its exact chemical structure). While the head-group of a precursor is often predetermined by the underlying substrate, the exact choice of the further sub-units is of key importance for the final properties of the resulting material.

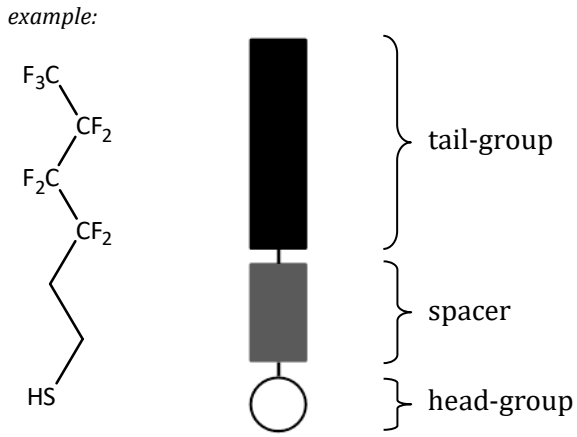

Figure 6: Simplified presentation of the general structure of a precursor molecule. Within the example of F4H2-SH, the thiol functionality -SH serves as the reactive head-group, the two methylene units -$(CH_2)_2$- as spacer and the perfluorobutyl chain -$(CF_2)_3$-CF_3 as tail-group.

In contrast to Langmuir-type films, which are referred to as ordered surfactant films on liquid media [4], SAMs are formed on solid substrates, onto which they are covalently chemisorbed. This further distinguishes them from Langmuir-Blodgett films which are only loosely physisorbed on solid substrates. [5,39,40] Covalent attachment of the SAM is achieved via the functional head-group which is able to covalently bind to anchor sites on the substrate surface. As depicted in Figure 7, the precursor chains are not confined in their spatial arrangement but will adopt a structural configuration based on the energetically most favorable state. In most cases, alkyl backbones are slightly tilted in comparison to the surface normal and spacer as well as tail-group may adopt differing configurations.

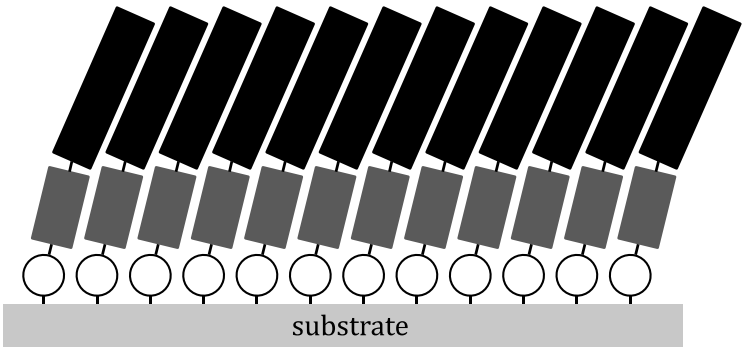

Figure 7: Schematic illustration of an idealized SAM structure. Head-groups are covalently attached to the substrate and precursor chains direct a regular and dense packing. Spacer- and tail-groups are allowed to adopt the most favorable configuration.

The driving forces of spontaneous self-assembly are the covalent binding of precursor head-groups to the substrate surface and stabilizing intermolecular interactions of precursor chains. Various head-group functionalities have already been applied in the deposition of SAMs, so that several different precursor/substrate-systems are known today. A short introduction into some of these diverse possibilities is given in Table 1.

Precursor	**Substrates**
R-SH, R-S-S-R	Au, Ag, Cu, Hg, GaAs [7,41–46]
R_n-$SiX_{(3-n)}$, X = Cl, OEt, OMe	SiO_2, Al_2O_3, GeO_2, SnO_2, Ti-alloys, diamond-like carbon [47–55]
R-$P(OH)_3$	Ti-alloys [53]
R-COOH	Ag, Pt, Al [56–60]
R-NH_2, R-CN	mica, Ag, Au, Si-Cl [61–63]
R-NC	Pt, Au [64]
R-SeH	Au, Ag [65–68]
R-OH	Si-Cl [69]
R-CH=CH_2, R-C≡CH	Si, Au [70–72]

Table 1: Introductory overview of some SAM systems.

The two most important SAM-systems are films deposited from alkylated thiols and alkylated mono-, di- or trifunctional silanes, respectively. On the one hand, thiols are mainly deposited on noble metals and have been proven to be well-suited particularly as model-systems in the investigation of fundamental SAM properties. On the other hand, films from silanes offer a wider variety of substrates, which are relevant to industrial processes and applications, but are more sensitive to deposition conditions and bare an increased risk of defects within the monolayer. Both systems have in common that the details of formation mechanisms and monolayer structure are still not fully understood and many questions remain unsolved. This is caused to some extent by the fact that many different deposition protocols exist which are often conducted under varying conditions. Published results therefore range from, e.g. uniform to island-like film growth for work with thiols and from highly cross-linked to mobile structures for work with silanes.

Although precursor headgroups are among the main driving forces in the process of self-assembly and are responsible for the stability of chemisorption, they commonly have no effect on the properties of the final layer towards surrounding liquids or gases. These properties are determined by the choice of the precursor's tail group, which commonly adopts orientations tilted relative to the surface normal but is

always directed towards contacting media. Similar to the variety of head-groups, the selection of the tail-groups is almost unlimited and is, due to the lack of necessity for distinct chemical bonding, even wider than for substrate-selective head-groups. Principal limitations in the choice of tail-groups are mainly given in the cases of very bulky functionalities, which hinder the ordered packing of a monolayer, and functionalities that compete with the head-group for direct reactions with the surface or react with the head-group itself. The most prominent tail-groups are unsubstituted *n*-alkyl chains, due to their simplicity and seminal character, and ω-substituted alkyl chains, which enable the simple introduction of chemical reactivity into an alkyl monolayer. The lengths of such reported alkyl chains may vary over a wide range and the corresponding properties of these layers can differ tremendously. Thus, the contact angles of several liquids (e.g. water, hexadecane, dimethylformamide, oleic acid, iodomethane) on *n*-alkyl, *n*-fluoroalkyl and ω-substituted alkyl monolayers are known to distinctly increase for increasing chain-lengths of the applied precursor molecules.[41,42,73,74] Moreover, SAMs deposited from precursors bearing longer relative chain lengths were observed to exhibit superior properties compared to short chains and, e.g., were more densely packed and exhibited increased thermal stability and reduced ion permeability.[75–78] As a consequence of monolayer packing and the dominating role of the tail-group in the interaction with a surrounding ambient, the influence of substrate/head-group interaction and buried polar functional groups, e.g. in terms of contacting liquids, becomes evident only in cases of very short precursor chain lengths.[73,79,80] Hence, still naming only a few, functionalities introduced into a monolayer range from "non-specific" alkyl or perfluoroalkyl tail-groups, aromatic species, specific protein receptors, polar or pH-responsive substituents to buried functionalities like ether, alkene or alkyne modifications.[46,81–84] Within this variety, this thesis will focus on the possible modification of surfaces by the application of *n*-(fluoro)alkylated precursor molecules.

A "spacer" or "linker" group is not necessarily found in every SAM system or may be regarded a sub-unit of the tail-group. Within an ideal monolayer with a tail-group of suitable length, the spacer unit is buried within the film and has no immediate effect on the properties of the monolayer/ambient interface. However, it can play a crucial role in the structural integrity of a SAM as attractive interactions between long spacer chains may direct the ordering process and certain types of precursor-molecules require a spacer for chemical stability. On the other hand, an increase in hydrocarbon-spacer chain-length was observed to lead to a decrease in order within the perfluoroalkyl tail-group, although the packing of the methylene sub-layer was improved.[85–87] This effect exemplarily highlights the consequence of competing ordering mechanisms during SAM formation.

The structural simplicity of SAMs along with the wide modular variety of precursor/substrate combinations allow the formation of a vast number of different materials with the principal possibility of tailor-made properties. The actual deposition is nonetheless dependent on often tiny details, so that great care and sometimes advanced methods are required in order to obtain well-ordered, defect-free monolayers with the desired properties. During deposition, typical defects within a SAM may originate from the precursor itself, the substrate, or from contaminants, which can easily be introduced into the deposition system. Defects induced by the choice of precursor or by contaminants within the precursor or the substrate may be prevented with relative ease or by adaptions to the deposition system/procedure. Substrate-induced effects on the other hand are more principal in nature and even largely homogeneous substrate surfaces may give rise to the creation of defect-sites, which in turn cause the development of larger areas with a lower degree of structural order. A conclusive introduction into SAM-defects, also considering the dynamic character of these monolayers, is given by Love *et al.*.[88] While the authors' focused on monolayers from thiol precursors, other systems are more strongly affected by the deposition conditions and the introduction of contaminants or the occurrence of undesired side-reactions. Nonetheless, the basic causes of defects remain the same, with individual, system-dependent weaknesses.

SAMs are deposited by either solution-based or vapor-based methods, with the majority of depositions reported for solution deposition. This approach was already used for the very first examples of monolayer deposition due to its straightforward and simple operation even with standard laboratory equipment. Thus, in its most basic form, SAMs can be deposited by immersion of a substrate in a solution of the chosen precursor in a suitable solvent. Immersion times may range from several seconds to days, depending on the formation characteristics of the chosen system and the required quality of the film. As film formation relies on spontaneous, dynamic ordering processes on the substrate, an extension of the immersion time leads to films of higher quality if interfering processes are excluded.

A crucial aspect of any SAM deposition is the reproducibility of the chosen method, which can already be influenced easily during the simplest process as stated above regarding sample immersion time. Monolayer formation is influenced by several parameters during a deposition process, with some being more and some being less important for the final outcome. It is therefore important to know and be aware of parameters and conditions that can have a detrimental effect on the films' properties, may it be their mechanical and chemical stability, their behavior in liquid wetting, or their defect density to name only a few. In consequence, it is essential that strictest care has to be taken in order to prevent any contamination of substances or

laboratory equipment. Although SAMs of various kinds have been studied during the past decades, the exact mechanisms involved in adsorption and ordering processes are still not fully understood. Great interest is therefore placed in gaining more insight into these mechanisms and the parameters influencing them.

The advantage of the simplicity of liquid-phase deposition techniques is often annihilated by the difficulties posed by maintaining very clean and defined conditions during the coating process. This involves not only the purity of the initial precursor and substrate but as well traces of impurities within the solvents, residual adsorbed contaminants from the ambient onto the substrate or moisture uptake from air during the deposition process. Although this kind of deposition is very reliable and robust for several SAM systems (as long as certain minimum standards of purity of the chemicals and cleanliness are maintained), there are other systems that create difficulties when liquid-phase methods are applied (e.g. uncontrolled hydrolysis in silane-based deposition due to residual humidity, Chapter 2.3.4).

In an alternative approach, SAMs can be deposited via a vapor-phase process, which avoids several risks of possible contaminations if depositions are conducted appropriately in a closed system. Here, the substrate is brought into contact with the vapor of the corresponding precursor and, if necessary, with further reactive components, e.g. water vapor. This eliminates solvent effects on the formation process and enables the deposition in an isolated, possibly *in-situ* pre-cleaned, vessel but requires the sufficient vaporization of the respective compounds. There are of course several different variants of vapor-phase deposition setups to think of and SAM formations have been reported from very simple setups using desiccators to advanced ultra-high vacuum deposition systems. In order to obtain as-perfect-as-possible SAMs, the use of an advanced experimental setup is unavoidable. The use of closed vacuum systems simplifies the control of deposition parameters, e.g. temperature and partial pressures of the components, and the isolation of the deposition environment from ambient contaminants. Moreover, analytical equipment can be easily added to a deposition system in order to conduct *in-situ* experiments. Altogether, the use of vapor-phase deposition, particularly in combination with advanced vacuum equipment, enables a route of deposition that outperforms classical solution-based methods when it comes to delicate SAM systems. Further advantages of vapor-phase depositions are the possibility to uniformly coat substrates with demanding shapes and to avoid the excessive use of potentially harmful solvents.

Both methods of SAM deposition, liquid- and vapor-phase, lack the existence of a "standard-protocol" and deposition processes differ from research group to research

group. This makes it difficult to systematically compare the influence of individual results, although general trends have been deduced from experimental work (compare sections 2.3.3 and 2.3.4).

2.3.2. Standing Out of the Ordinary: SAMs with Fluorous Tail-groups

"Fluorous" chemistry in general is still regarded a very special area of organic chemistry and deals with the chemistry of fluoro-organic compounds with a very high degree of fluorination. [20,89] It is thus not surprising, that also SAMs based on fluorous precursor molecules exhibit special, not to say unique, properties compared to standard organic SAMs. They enable the creation of surfaces with properties strongly different to common methods and possibilities. [90–94] On the other hand, perfluorinated compounds are subject of an active discussion concerning their environmental impact and are essayed towards substitution with less detrimental substances. [95–97] As a recent example, public recognition has focused particularly on perfluorooctanoic acid (PFOA) which is used as a surfactant and common coating compound in textiles. Conscious use in terms of efficient application and waste management are therefore advised to be implemented already on a laboratory scale.

The reason for the extraordinary behavior of fluorous or only fluorinated compounds and SAMs deposited from them lies in the outstanding polarity and stability of the carbon-fluorine bond and the very low polarizability of the fluorine atom. Within the C-F-bond the most electronegative element fluorine causes a strong polarization of the bond, what results in a dramatic change of molecular properties when nonpolar C-H-bonds are substituted for C-F-bonds. The low polarizability in combination with a high ionization energy leads to only weak intermolecular forces which probably has the most important influence on macroscopically observable properties. The results are low interfacial energies and consequently characteristic properties in terms of liquid wetting. Thus, fluorinated surfaces show highly hydrophobic as well as oleophobic properties, what has made them ideal candidates for the development of omniphobic surfaces. [31,98,99] As a rough comparison, fluorination of a precursor commonly causes an increase of the water contact angle of a smooth SAM of approximately 10°. [17,100] Compared to hydrocarbon SAMs, fluorinated films exhibit an increased stability against mechanical and thermal stresses and a characteristical chemical inertness. [17,100–105] Despite this, fluorinated monolayers are sensitive towards decomposition induced by UV-light, electron irradiation and x-rays. [90,106]

It has been shown for SAMs from semi-fluorinated alkyl thiols that liquid repellency increases with increasing grade of fluorination of the precursor's tail-group. [17,48,50,74,90,107–109] Contact angles increase with increasing fluorous chain length and approach a plateau value larger than the hydrocarbon SAM reference, particularly regarding water and other polar liquids.

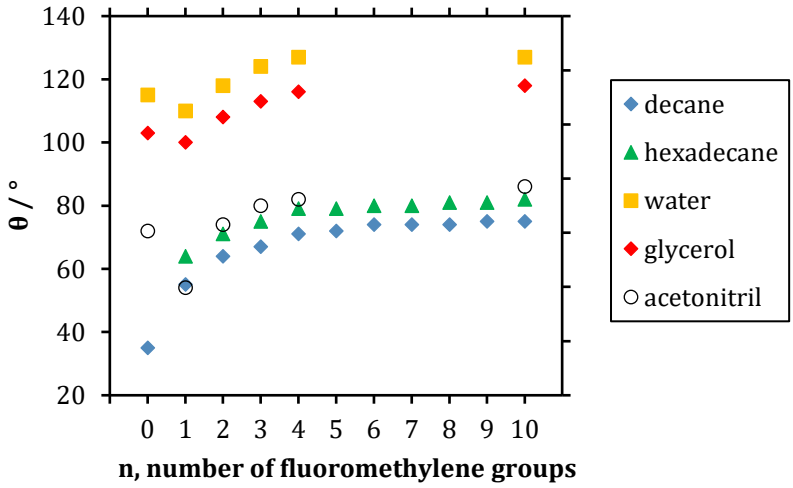

Figure 8: Effect of increased grade of fluorination in SAMs from (fluoro)hexadecyl thiols F/H-$(CF_2)_n$-$(CH_2)_{16-n}$-SH on the contact angle. Values are adapted from references [108] (decane, hexadecane) and [107] (water, glycerol, acetonitril).

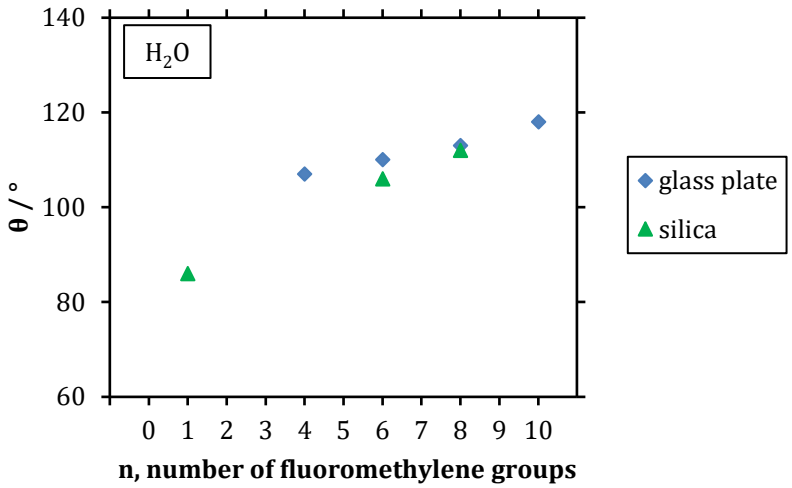

Figure 9: Effect of increased grade of fluorination in SAMs from (fluoro)alkytrimethoxy silanes F-$(CF_2)_n$-$(CH_2)_2$-Si(OMe)$_3$ on water contact angle. Values are adapted from references [74] (glass substrate) and [48] (silica substrate).

An interesting exception are SAMs deposited from precursors with only a trifluoromethyl end group without further fluorination. Due to the polarity which is introduced into the more exposed part of the chain in comparison to the purely hydrocarbon precursor, the wettability towards polar liquids is effectively increased despite the fluorination (Figure 8, n = 1). [108,110] By extended elongation of the fluorous part of the chain, the highly polar section of the precursor becomes more and more buried within the SAM and has no direct influence on wetting any more. [107,108] Further effects of increased fluorous chain lengths are a decrease in contact angle hysteresis and improved packing of the precursor chains within the monolayer, what in turn results in an increased thermal stability. [44,45,85]

The electrostatic repulsion between the fluorine atoms within the carbon backbone results in another important aspect of fluorous precursors. It forces the chains to adopt a rigid helical structure in contrast to the common hydrocarbon chains with high conformational flexibility. [111–113] Helices are intramolecularly stabilized and have a remarkable effect on the SAMs deposited from fluorous precursors. Rigid, helical fluorous precursor chains require an increased volume per adsorption site compared to their non-fluorinated analogs. In consequence, SAM structures differ from hydrocarbon SAMs in terms of structure and packing density and smaller tilt angles are observed. [44,114,115] Moreover, fluorocarbon helices enable the creation of rigid surface morphologies (Section 2.4).

The strong electronegativity of fluorine has an effect on fluorous precursors and SAMs beyond structure-related aspects. Caused by its strong eletron-withdrawing effect, it can increase the reactivity of neighboring functional head-groups via the introduction of additional induced polarity. This enhancement of reactivity becomes particularly evident in the case of semifluorinated trichloro-/trialkoxysilanes $F\text{-}(CF_2)_n\text{-}(CH_2)_m\text{-}SiX_3$ (X = Cl, alkoxy). Here, a hydrocarbon spacer unit between head-group and fluoroalkyl tail-group is not only a structural detail but is essentially required for maintaining chemical stability after SAM deposition. The introduction of a fluoromethylene unit in α/β-position of the silane head-group would effectively weaken the stability of a silane-substrate bond and would thus lead to the deterioration of the monolayer. [116,117] This induced enhancement of reactivity leads to distinct differences between fluorinated and non-fluorinated precursor molecules even when a spacer-unit is present. While purely hydrocarbon silane precursors do not form SAMs on anhydrous silica surfaces even at elevated temperatures, their fluorinated analogs already react at room temperature and appear to form monolayers faster in general. [118,119] Moreover, it was reported that solutions of fluorous precursor analogs became cloudy after a few minutes due to the formation of hydrolyzed agglomerates while non-fluorinated precursor solutions did not show signs of degradation. [120]

A major drawback concerning the application and research of fluorous monolayers is the limited commercial availability of required precursors. Particularly, long-chain tail-groups $-C_nF_{2n+1}$ with $n > 8$ are not readily available. The synthetical provision of these compounds is therefore an inevitable prerequisite of any research related to these types of monolayers.

Table 2 presents some results of wetting properties for fluorous SAMs reported in literature. The table gives comparative values relevant to this thesis and contains different methods of preparation as well as precursor compounds. As a matter of clarity, further experimental details are omitted in this overview.

θ_{adv} [°]	Δθ [°]	Precursor / substrate	Method	Test liquid
71	-	F6H2-SH / Au	solution	*n*-hexadecane [41]
118	-	F6H2-SH / Au	solution	water [41]
69	-	F6H2-$SiCl_3$ / SiO_2	solution	*n*-hexadecane [120]
80	19	F6H2-$SiCl_3$ / SiO_2	solution	*n*-hexadecane [78]
105	-	F6H2-$SiCl_3$ / SiO_2	solution	water [120]
104	-	F6H2-$SiCl_3$ / SiO_2	vapor	water [121]
112	-	F6H2-$SiCl_3$ / SiO_2	vapor	water [17]
120	15	F6H2-$SiCl_3$ / SiO_2	solution	water [78]
118	-	F8H2-SH / Au	solution	water [115]
79	-	F8H2-SH / Au	solution	*n*-hexadecane [115]
76	5	F8H2-$Si(OEt)_3$ / Al_2O_3	vapor	*n*-hexadecane [122]
75	3	F8H2-$Si(OEt)_3$ / Al_2O_3	vapor	*n*-hexadecane [52]
107	-	F8H2-$Si(OEt)_3$ / SiO_2	vapor	water [121]
113	-	F8H2-$Si(OMe)_3$ / SiO_2	solution	water [74]
68	-	F8H2-$SiCl_3$ / SiO_2	solution	*n*-hexadecane [103]
83	4	F8H2-$SiCl_3$ / SiO_2	vapor	*n*-hexadecane [123]
67	-	F8H2-$SiCl_3$ / SiO_2	vapor	*n*-hexadecane [124]
110	-	F8H2-$SiCl_3$ / SiO_2	vapor	water [125]
112	10	F8H2-$SiCl_3$ / SiO_2	solution	water [126]
110	-	F8H2-$SiCl_3$ / SiO_2	vapor	water [127]
115	-	F8H2-$SiCl_3$ / SiO_2	vapor	water [17]
117	9	F10H2-SH / Au	solution	water [128]
118	-	F10H2-$Si(OMe)_3$ / SiO_2	solution	water [74]
64	6	F10H2-$SiCl_3$ / SiO_2	solution	*n*-heptane [129]
124	9	F10H2-$SiCl_3$ / TiO_2	solution	water [130]

Table 2: Literature examples of wetting on fluorinated SAMs deposited from FnH2-X. If no value of contact angle hysteresis Δθ is cited, the original authors did only conduct static wetting experiments.

2.3.3. Thiol monolayers as a reliable standard

Among the various SAM systems, monolayers deposited from alkyl thiol precursors have developed into a reliable reference system. [36,88,131–134] Reasons for this are the extensive research conducted on this type of SAMs and its robust method of preparation in conjunction with the films' stability. Typical substrates are coinage metals like silver, copper and particularly gold, which has also been used for depositions during the course of this thesis. While polycrystalline substrates dominated by Au(111) textures are commonly applied and well-suited for the study of macroscopic SAM properties like wetting, monocrystalline Au(100) surfaces are required for in-depth studies of monolayer structural details. Fresh Au(111) substrates are relatively simple in preparation and are inert against atmospheric deterioration, although the adsorption of contaminants onto the surface prior to SAM deposition has to be avoided. [41,135,136]

In addition to the inertness of the substrate it is an important advantage that also the precursors' thiol functionality is relatively stable under controlled laboratory conditions so that precursors can be handled with relative ease as long as no chemically sensitive tail group functionality is involved. A decisive exception from this overall stability is the risk of pre-deposition oxidation of the thiols to dialkyl disulfides or alkyl sulfonates. While SAMs from symmetric dialkyl disulfides have been reported to yield monolayers undistinguishable from SAMs deposited from identically substituted alkyl thiols [43,137], alkyl sulfonates may hamper the formation of closely packed monolayers of thiols and have been detected to be a main product of photoinitialized oxidative degradation. [138–140] The protection of thiol precursors and the SAM deposition system from sources of oxidative degradation thus becomes a distinct prerequisite of any thiol deposition and even more so in cases where tiny details of the deposited film influence the sample's properties to a major extent. The deposition of molecularly rough thiol monolayers within this thesis is one such example, particularly as during the course of preparing depositions, the required glassware has to be cleaned under very harsh oxidizing conditions ("piranha" solution, peroxymonosulfuric acid).

The method-of-choice for SAM formations from alkyl thiol precursors on gold is a liquid-phase deposition from precursor solutions. Although the processes involved during the formation of chemisorbed monolayers are not fully understood in all details, a number of parameters and its influence on SAM deposition have been investigated. Bain *et al.* proposed a two-step model for the deposition kinetics of liquid-phase deposition from thiol precursor solutions, which is widely accepted today and has been supported experimentally by further groups. [41,141] According to

this model, thiol molecules adsorb onto the substrate surface during the initial first stage of film formation in a random manner. This first adsorption takes place on rather short time-scales of seconds to several minutes and generates films with similar but not identical properties (e.g. contact angle, film thickness) compared to the final films, which are obtained after prolonged deposition times. During the second phase of film formation, ordering processes within the pre-formed thiol layer accompanied by further adsorption of precursor molecules are assumed to lead to the formation of the final SAM. This second stage requires a far longer time-scale and may require durations of several days. The transition from first to second stage of solution-based SAM formation is often reported to be accompanied by an island-like evolution of growing patches of uniform monolayer regions. [142–144]

The deposition temperature, precursor concentration, choice of solvent and the duration of substrate/solution contact have been identified as the most important parameters during deposition. In terms of ordering processes based on the adsorption/desorption of precursor molecules, it is assumed that an increase of solution temperature will increase the rate and quality of monolayer formation. [145,146] Moreover, as already introduced in the two-stage deposition model, film formation is strongly influenced by the time that substrate and precursor solution are allowed to stay in contact. Prolonged deposition times are reported to yield monolayers of improved packing and quality. The time which is necessary to obtain a certain degree of ordered monolayer coverage is connected to the concentration of the deposition solution and growth rates have been found to increase with thiol concentration. [41,141,142,146–148]

During SAM depositions, the choice of solvent can have a profound effect on the formed monolayer. It has been reported, for example, that the application of *n*-heptane and other rather strong solvents for alkyl thiols results in an increased initial rate of thiol deposition onto the substrate. [148,149] On the other hand, monolayers from weakly solvating liquids (e.g. ethanol) yield SAMs of higher structural order and films are discovered to be more uniform and more densely packed than films prepared from solutions of strong solvents (e.g. *n*-heptane). [150,151] This behavior is assumed to be a consequence of the circumstance that a strong solvent may inhibit the formation of precursor aggregations on the substrate. Moreover, the exchange of pre-adsorbed solvent-molecules on the substrate surface for thiol molecules has been discussed to have a rate-limiting effect. [41,142] As faster adsorption is also detected in non-polar *n*-hexane compared to ethanol for the deposition of thiols bearing polar tail-groups, the exchange of solvent molecules appears to have a stronger influence on early deposition kinetics than thiol solubility. [149] Interestingly, the choice of solvent does not appear to have a striking effect on the overall properties of the final

monolayer.[41,42] More practical reasons for the preferred choice of ethanol as deposition solvent are its low costs and low toxicity.

The combination of parameters of deposition time, temperature and concentration of the precursor solutions becomes particularly important in the case of mixed monolayers from multiple precursors which are simultaneously adsorbed. Here, the interplay of temperature and deposition duration leads to the establishment of a structural and compositional state approaching a quasi-equilibrium state, where no further change in composition and structure is assumed to take place. Results obtained from adsorptions of radiolabeled alkyl thiols and dialkyl disulfides suggest that precursor chains once adsorbed onto the substrate surface may be subject to an exchange for precursor thiols provided from a contacting precursor solution.[152–154] Thus it is of particular interest for the deposition of binary mixed monolayers that deposition conditions allow the formation of monolayers close to their thermodynamic equilibrium. The conditions during the experiments described in this thesis were adjusted to fulfill this requirement and monolayers were allowed to form for 70 hours.

In conclusion, there are many parameters which have been discovered to have an important effect on the results of SAM deposition from alkyl thiol precursors. Nonetheless, the exact nature and extent of these effects are yet to be determined and remain parts of an active discussion.

2.3.4. Alkyl silanes as precursors for durable SAMs on industrially relevant substrates

Next to SAMs from alkyl thiols on gold, monolayers deposited from mono-/di-/trifunctional alkyl silanes on silica are one of the most prominent and best-investigated SAM systems.[36,155,156] They cover a wide variety of tail-groups similar to thiol monolayers but are not as limited in terms of possible substrates and can be deposited on numerous, mostly hydroxylated or oxide, surfaces. This makes silane-based SAMs an ideal tool for the investigation and transfer of model-systems to more industrially relevant substrates. Commonly, chloro- or alkoxy-functional (-OMe, -OEt) head-groups are applied with chlorosilane precursors being the more reactive choice compared to relatively stable alkoxy compounds.[116] In general, mono-, di- and trifunctional silanes can be applied for monolayer deposition. The most important difference between the resulting SAMs is the steric hindrance and increased required volume of the head-groups which is introduced by additional alkyl

substituents in mono- and difunctional silanes. [123,157,158] This leads to a decreasing degree of order and less densely packed SAMs in comparison to films from trifunctional precursors. For recent studies and reviews on the work on SAMs from mono- and difunctional silanes the reader is referred to referenced publications, while this thesis focuses on SAMs from trifunctional precursor silanes.

It is generally accepted that the formation of monolayers from trichlorosilane precursors (and related alkoxysilanes) proceeds via the physisorption, hydrolysis and subsequent chemisorption of precursor molecules onto the substrate surface. Although the stepwise hydrolysis of the chlorine moieties to silanol functionalities (Figure 10) is an essential part of film formation, it has not been clarified yet, in which order physisorption and hydrolysis take place. Depending on the extent of hydrolysis, different species of mono-, di- and trisilanols can be present next to each other during the deposition process. Moreover, HCl is liberated during the hydrolysis, which may influence the formation of ordered films and has to be removed from the process.

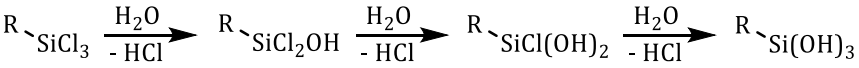

Figure 10: General process of hydrolysis during the deposition of silane-based SAMs.

After precursor hydrolysis, monolayers are formed from the deposition of silanols onto a suitable substrate, during which anchoring to the substrate is accomplished by the formation of siloxane bonds. These substrate/head-group-bonds are distinctly more stable than gold/sulfur-bonds in SAMs from alkylthiols. Despite their extraordinary stability against mechanical and thermal wear, [159–163] silane-based films may deteriorate rapidly in use or storage. Especially aqueous basic media lead to hydrolysis of siloxane bonds and subsequent decomposition of the monolayer structure. [73,100,164]

The most critical aspects for film formation are the hydrolysis and subsequent deposition of precursors onto the substrate, which are closely connected to the concentration of water within the deposition system. Optimum as well as minimum amounts of water required for the formation of well-ordered monolayers are still a matter of discussion and range from hydrated substrates to anhydrous conditions. Best results, however, have been reported to be obtained when depositions were

carried out under conditions allowing traces of water. [165–169] Increased mobility of precursor molecules and reversible adsorption/desorption processes have been discussed under the assumption of a thin physisorbed layer of water on top of the substrate surface. [170–172]

Hydrolysis of the precursor is already initiated by traces of water within the deposition system (liquid- and vapor-based), which may as well lead to highly undesired side-effects during the deposition process. Due to the highly reactive nature of the precursor molecules, coupling reactions between precursor head-groups can occur prior to self-assembly. For short-chain alkyl trichlorosilanes, DFT calculations have shown that condensation can take place as soon as precursor hydrolysis with water has begun. [173] Excess water accelerated hydrolysis and lead to enhanced condensation rates at increased levels of hydrolysis. Thus, pre-adsorption agglomeration of hydrolyzed precursor molecules can occur and condensed species are incorporated into the film leading to irreversible defects and preventing ordered monolayer formation. [126,174,175] Zhuang *et al.* reported that films with high amounts of aggregates exhibited lower thermal stability than smooth, defect-free films. [102] Bunker *et al.* observed during their work on solution depositions that an increase in surface roughness by particle formation only appeared at deposition times that exceeded a certain nucleation time for the formation of objects in the deposition solution found by light scattering experiments. [176] Moreover, films grown under anhydrous conditions were reported to be smoother, free of particulate defects and exhibited more uniform mechanical properties than films grown under non-anhydrous conditions. [160] Gnanappa *et al.* studied the effect of annealing of a vapor-deposited sample in order to reduce the number of particles after film deposition. [164] They found that post-deposition annealing was able to reduce particle density even after exposure of the samples to water. However, they were not able to produce films which showed no particle defects in the first place. De Boer *et al.* assumed the particles to be the result of a surface phase reconfiguration to polymeric and hydrophobic bulk phase mounds. [177] Those reconfigurations have also been discussed by other groups and may originate from cross-linking defects within the monolayer as water molecules can diffuse into the layer leading to hydrolytical cleavage of siloxane bonds to the substrate. [50,102,164,178] Michalske *et al.* reported particle formation during gas-phase depositions with a large excess of water over fluoroalkylated trichlorosilane precursors but did not further investigate this phenomenon. [179]

In addition to the formation of particles, the uncontrolled hydrolysis of precursor silanes is known to generate several types of side-reactions and structures besides the formation of well-ordered and aligned monolayers. [157,158,180–182] This can cause the

formation of extensive cross-linked networks of precursor molecules deposited as a molecular monolayer on the substrate or the formation of multilayers through distortions introduced via cross-linking (Figure 11).

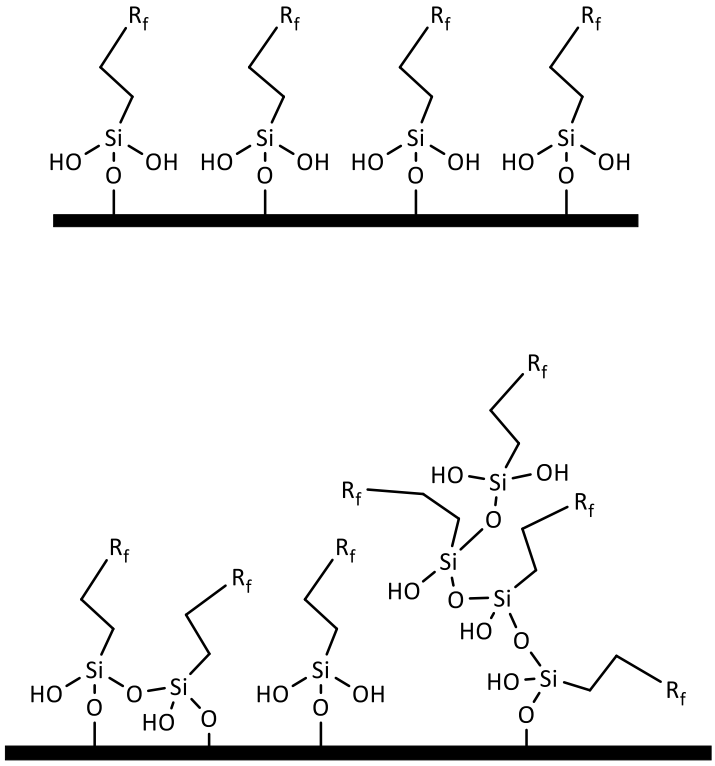

Figure 11: Illustration of possible defects caused by precursor condensation. In contrast to an ordered array of precursor molecules (upper section), cross-linking may lead to defective formation of siloxane networks and multilayer growth (bottom section). R_f represents a fluoroalkyl chain of arbitrary length.

Apart from that, the definite shape and structure of SAMs deposited from this type of precursors are still a matter of discussion and, ultimately, there is no consent yet, how exactly a perfect silane monolayer looks like. Depending on the point-of-view, the perfect SAM is either regarded as highly cross-linked, what results in a very stable film with probably the surface properties as desired, or as a most-densely packed film, which rather resembles the image of an ideal monolayer. The problem arising from these two options is that both cannot coincide in one system. Although for many years it had been assumed that intermolecular cross-linking is a major characteristic of

silane SAMs (and is still reported as such nowadays), it is now known that this image cannot be correct. The van-der-Waals-diameter of the precursor alkyl chains is actually too large in order to accommodate siloxane bridging between neighboring head-groups.[157,158,183] With a vdW-diameter of ≈ 5.6 Å for fluoromethylene and ≈ 4.2 Å for hydrocarbon alkyl chains, even a fully stretched Si-O-Si bond is essentially too short (≈ 3.2 Å) and precursor chains would have to overlap if they were tried to be forced into parallel alignment.[184–186] In consequence, precursor chains in cross-linked SAMs have to tilt away from each other, which causes a loss of structural uniformity (Figure 12). This effect is even increased for the deposition of fluoroalkylated SAMs because of the larger vdW-diameter of fluorous chains compared to hydrocarbon backbones. Besides the loss of densest packing, the defect-sites introduced by cross-linked precursors can cause multilayer growth via the addition of further molecules to the available silanol functionalities.

In conclusion, the control of the amount of water supplied to SAM formation has been found to be a decisive parameter during the deposition process. Preventing cross-linking, therefore, is essential for the formation of dense and uniform monolayers.

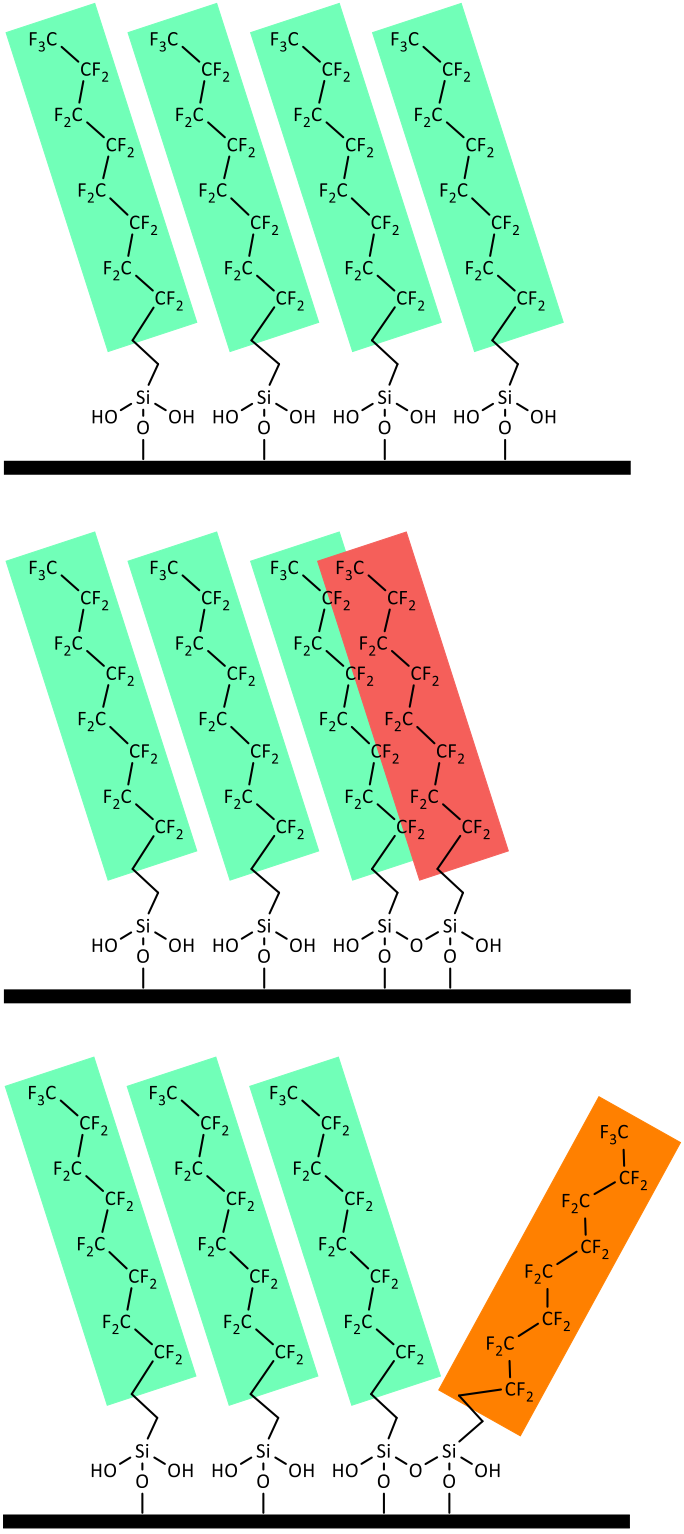

Figure 12: Schematic representation of the consequences of cross-linking for the structure of semifluorinated silane-based SAMs. Colored boxes symbolize the space required by the fluorocarbon chains. Without cross-linking of precursor head-groups dense packing of the precursor chains is possible (top image). The introduction of short siloxane bonds would cause an overlap of the alkyl backbone (middle) so that precursors have to tilt away from each other (bottom image), thus causing defects within the SAM.

Related to the impact of cross-linking is the question, to what extent the anchoring of silane headgroups to the substrate takes place. These subjects are in so far similar, as neither a highly cross-linked network, nor a densely packed structure of parallelly aligned precursors are assumed to exhibit a very high degree of substrate/head-group bonding due to the lack of exact overlap of anchoring sites and head-groups. Thus, IR-, XPS- and SHG-experiments (second harmonic generation) suggested only a low density of substrate/head-group bonding and Le Grange *et al.* proposed that only 10-20 % of precursor molecules are actually anchored to the substrate. [168,169,171,187] Moreover, studies of monolayer formation on non-hydroxylated substrates showed that stable monolayers could be obtained even for these systems, which, however, were formed at the cost of cross-linked networks. This further lead to the assumption, that internal condensation of precursor molecules was an important feature of SAMs prepared from alkyl silanes. [183,188–190] In contrast to these findings, Wang *et al.* noted that films grown under anhydrous conditions, i.e. minimizing the risk of precursor condensation, were smoother than SAMs prepared under the presence of water and were very resistant to mechanical damage. They assumed that substrate bonding alone is sufficient to create stable monolayers. [160] More recently, an umbrella-like structure has been proposed, which combines cross-linking and low-density substrate-bonding via the introduction of gauche-defective rearrangements of the alkyl chains. [191]

As the details of monolayer formation mechanism and monolayer structure remain unresolved so far, both the deposition of silane SAMs from solution and from the vapor-phase are still subject of active current research.

2.4. Binary mixed monolayers from (fluoro)alkylated thiols as a template to investigate molecular roughness

Methods to manipulate wetting behavior according to Wenzel and Cassie-Baxter (Section 2.1) are both assumed to be valid independent from the structural scale of the investigated rough system. In the light of SAMs, which are composed of molecular size building blocks, the question arises, whether sub-nm topographical structures can affect macroscopic wetting properties. Thus, this thesis aims to provide the means to prepare monolayers with sub-nm topographies for the investigation of wetting behavior on these structures.

Binary mixed SAMs from fluoroalkylated precursors serve as the ideal toolbox for this kind of model surface structures. [192] While SAMs from (fluoro)alkylated thiols are known for their reliable and robust preparation, the stiff helix of the fluoroalkyl backbone allows for the introduction of vertical structural features with a height difference defined by the chain length difference of the thiol components. Thus, the proper choice of precursor molecules enables the preparation of a binary mixed monolayer with defined topographic features on a sub-nm, molecular size scale. The lateral scale of surface structures is determined by the molar composition of the binary mixture and, assuming an ideal densest molecular packing, by the van-der-Waals-diameter of the individual precursor chains. Here, the relative molar composition affects the probability of identical thiols being adsorbed directly next to each other on the substrate surface, so that structures of same height are formed. The larger same-height-areas grow, the smaller will be their contribution to surface roughness.

The effect of chain length difference in systems from varying combinations of long- and short-chain fluorous thiols has been investigated for several molar compositions. Figure 13 illustrates an example of a binary mixed monolayer from F8H2-SH and F12H2-SH with a molar fraction x_{F12H2} = 6 %. The long-chain backbones of the F12H2-thiolates sticking out of the "surface" of F8H2-thiolates are prominently distinguishable. The chain-length difference between the two different precursor backbones defines the vertical scale of the formed topography and creates a height difference of 5 Å.

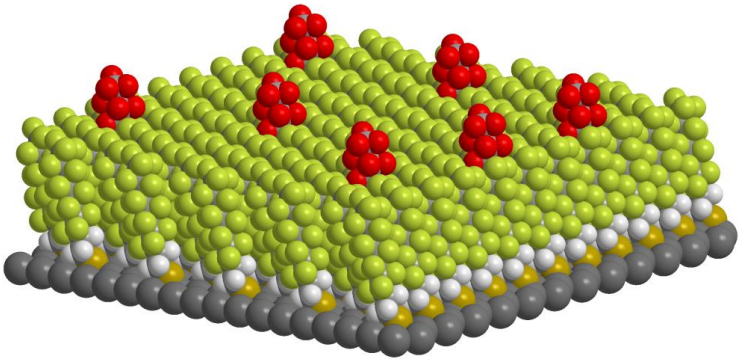

Figure 13: Illustration of a binary mixed SAM from F8H2-SH and F12H2-SH on Au. x_{F12H2} = 6%, Δh = 5 Å.

The high degree of fluorination yields SAMs with strong hydrophobic as well as oleophobic properties. Moreover, fluorous thiol monolayers have been intensively studied and their structural parameters are well-known. Thus, it is possible to derive mixed systems with established structural features whose theoretically expected properties can be reliably modeled. As for all highly fluorous depositions throughout this work, a major drawback is the scarce availability of the compounds and their characteristic behavior within standard methods of organic chemistry.

Parameter	**FnH2-SH**	**Hm-SH**
vdW-diameter	5.6 Å [184]	4.5 Å [185]
Δh per -$(CX_2)_2$-	2.5 Å [134]	2.2 Å [75]
next-neighbor distance	5.8 Å [87,114,193]	5.0 Å [194–196]

Table 3: Structural features of (fluoro-) alkylated monolayers from FnH2-SH and Hm-SH precursors.

The exact molar composition of a mixed monolayer depends on the individual adsorption properties of the corresponding thiol components and has to be determined for each binary system. Thus, a reliable method is required in order to determine monolayer compositions. As already stated by other authors, the composition of a binary mixed SAM does not necessarily match the concentration ratio of components in the corresponding deposition solution but strongly depends on details of precursor chemistry and deposition solvent. [192,197–204] Folkers *et al.* investigated the composition of binary mixed thiol monolayers deposited from two-component long- and short-chain thiol solutions on gold substrates and evaluated adsorption isotherms for several systems. [205] According to their work, SAM composition in thermodynamical equilibrium as a function of the composition in the contacting solution can be described by equation (6) (with R_0: required concentration ratio for an equimolar composition within the SAM; x_{long}: molar fraction of long-chain thiolates within the SAM; ω: interaction parameter; k: Boltzmann constant; T: Temperature):

$$\ln\left(\frac{R_{sol}}{R_0}\right) = \ln\left(\frac{x_{long}}{1 - x_{long}}\right) + \left(1 - x_{long}\right)\frac{\omega}{kT} \tag{6}$$

Equation (6) can be derived analogously for x_{short} by substituting x_{long} for $(1 - x_{short})$. It contains two important fitting parameters, which can both be determined experimentally: the concentration ratio R_0 and the interaction parameter ω. While R_{sol} represents the actual composition of a deposition solution in the form of a concentration ratio $R_{sol} = c_{long}/c_{short}$, R_0 describes the concentration ratio of long over short thiols in a deposition solution that is required in order to prepare a monolayer of equimolar composition. Thus, with $R_{sol} = R_0$ an equimolar SAM of $x_{long} = x_{short} = 0.5$ is obtained. Moreover, the value of R_0 allows to determine a preferred adsorption of one thiol over the other, so that the longer chain thiol preferentially adsorbs onto the surface if $R_0 < 1$.

The second fitting parameter is the interaction parameter ω. It represents the degree of interaction between thiol molecules and represents a measure of the miscibility of the corresponding thiols within the SAM. Thermodynamically, ω originates from the Gibbs free enthalpy of mixing and is a measure of the ideality of a solution, as given here in the form of a binary solution of thiols. The value of ω can fall into three different regions. In the case of $\omega = 0$, the solution represents an ideal mixture with only entropic contributions to the mixing behavior. For $0 < \omega < 2$ kT, entropy between like molecules overcomes the tendency to form aggregates and complete mixing of the solution's components is expected. When ω adopts a critical value of $\omega \geq 2$ kT, phase separation occurs due to increased attractive interactions between like molecules. The consequence for this study and for the preparation of new combinations of binary SAMs is that all systems, which are meant to yield randomly mixed monolayers, have to fall into the regime of $0 < \omega < 2$ kT. This requirement is expected to become more difficult to achieve when very large chain-length differences between chosen thiol components occur.

Examples of typical adsorption isotherms are presented in Figure 14, with the molar fraction of thiolates in the SAM x_{SAM} plotted as a function of R_{sol}, the ratio of long- over short-chain thiol concentration in the contacting solution. The effect of changes in ω and R_0 is easily visualized in the corresponding adsorption isotherms. As $x_{long} + x_{short} = 1$, the isotherms show inverted shapes. In contrast to an ideal system in terms of thiol/thiol interaction and preferred adsorption of long alkyl chains ($\omega = 0$ kT, $R_0 = 0.1$), the example of an isotherm for non-ideal behavior ($\omega = 2$ kT,

R_0 = 0.1) is strongly compressed. For systems close to ω = 2 kT this means that, in practice, mixed monolayers can only be obtained within a very narrow range of R_{sol}. The third example additionally depicts the influence of adsorption behavior in terms of R_0. It is represented by a shift of the isotherm to smaller or, as given here, to larger values of R_{sol} without affecting the isotherm's overall shape. The chosen value of ω = 1 represents an intermediate value and visualizes the trend from low to high values of the interaction parameter.

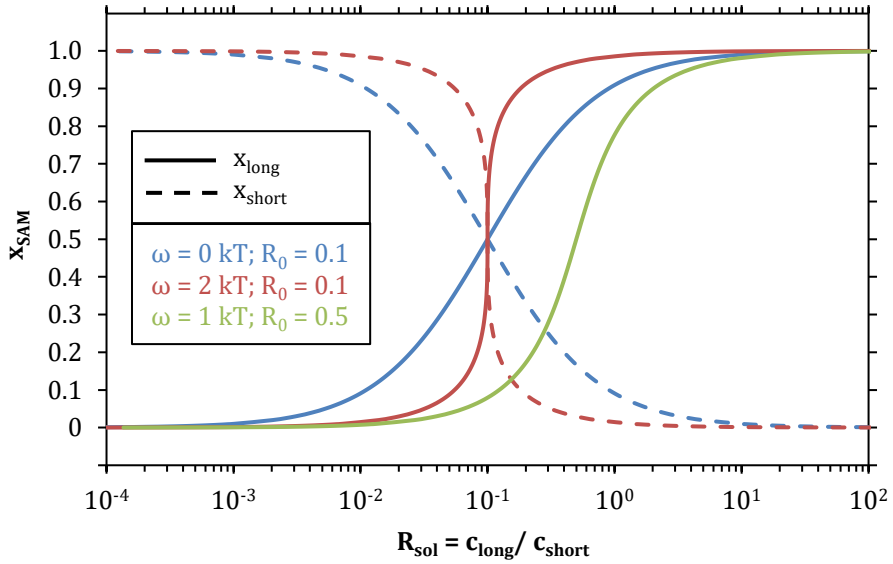

Figure 14: Adsorption isotherms for binary mixed SAMs and the effect of variations in R_0 and ω. The molar fractions of long (x_{long}, solid lines) and short chains (x_{short}, dashed lines) within the SAM are given as a function of the concentration ratio in the solution R_{sol}.

The molar composition of prepared SAMs can be determined by means of static secondary ion mass-spectrometry (sSIMS). This technique has been proven particularly useful for the investigation of this kind of monolayers for mainly two reasons. First, sSIMS yields characteristic fragment ions, particularly negatively charged ions, so that the concentration of long/short precursor species within the SAM can be quantitatively determined from the corresponding fragments (Section 3.3.2). Other techniques like XPS yield highly fragmented ions and do not allow for a quantitative analysis of molecular species. An overview of some secondary ions for

(fluoro)alkylated monolayers carrying molecular chain information is given in Table 4. Within this work, monomeric fragment $AuF(M_{FnH2-SH} - H)^-$ was commonly evaluated for the determination of the molar composition of a fluoroalkyl monolayer, while $Au_2(M_{Hm-SH} - H)^-$ was used for non-fluorinated monolayers (with M being the thiol molecule of interest).

M = FnH2-SH	**m/z = kn [Th]**	**M = Hm-SH**	**m/z = km [Th]**
$(M - H)^-$	79 + 50n	$(M - H)^-$	33 + 14m
$Au(M - H)^-$	276 + 50n	$Au(M - H)^-$	230 + 14m
$AuF(M - H)^-$	295 + 50n		
$Au_2(M - H)^-$	473 + 50n	$Au_2(M - H)^-$	427 + 14m
$(Au(M - H)_2)^-$	355 + 100n	$(Au(M - H)_2)^-$	263 + 28m
$Au(M_1 - H)(M_2 - H)^-$	$355 + 50n_1 + 50n_2$	$Au(M_1 - H)(M_2 - H)^-$	$263 + 14m_1 + 14m_2$

Table 4: Overview of some monomeric and dimeric secondary ions carrying molecular chain information during sSIMS.

Second, Monte Carlo simulations have shown that the immediate environment of thiolate chains within the monolayer can be probed by sSIMS. [206] This is possible via the analysis of dimeric species carrying two thiolate chains of the forms long-long $[Au(M_{long} - H)_2]^-$, long-short $[Au(M_{long} - H)(M_{short} - H)]^-$ and short-short $[Au(M_{short} - H)_2]^-$. Simulations showed that these combinations in fragments are almost exclusively formed from chains which have been nearest neighbors within the SAM prior to ion bombardment. Thus, it is possible to evaluate the grade of random chain distribution within a probed SAM.

At such very small scales of surface structures the description of wetting in terms of surface energies is known to deviate from macroscopic models and requires an independent description. According to the pioneering work of Tolman, the surface tension of very small liquid droplets has to be assumed a function of the droplet's size. [207] Induced by the droplet's curvature, the effective surface tension is assumed to deviate from its value on planar surfaces. Corresponding to this effect, an experimental observation of wave-vector dependent surface energies for several organic liquids, water and liquid gallium was recently accomplished. [208–210] The

wave-vector $q_{||} = \frac{2\pi}{\lambda}$ represents the wavelength λ of effective capillary waves according to capillary wave theory of liquids. This theory states that surfaces of liquids are not intrinsically flat on a smallest scale but exhibit deviations in form of thermally excited capillary waves whose amplitudes are affected by surface tension, which serves as a restoring force.

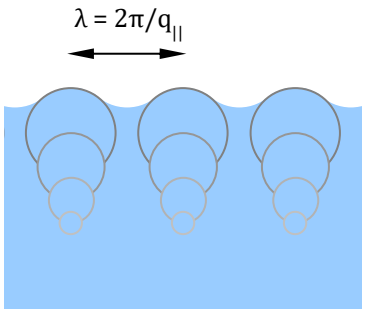

Figure 15: Illustration of thermally excited capillary waves on a liquid surface and the wave-vector $q_{||}$.

Mora *et al.* reported for scattering experiments with increasing wave-vector (synchrotron grazing incidence x-ray scattering, GIXD) that the surface tensions of probed liquids first decreased from their macroscopic values and then strongly increased if the wave-vector of the incident beam was further increased (Figure 16). [209] Their results correspond well to predictions made earlier by Mecke and Dietrich based on density functional theory calculations. [211] Although the determining wave-vector for the onset of increase/decrease behavior was found to be characteristic for a given liquid, the curve shapes of the relative surface tensions were identical for all samples. As the wave-vector is a measure of smallest-scale roughness, these results may be referred directly to the manipulation of wetting properties by the introduction of molecular roughness through the means of SAMs.

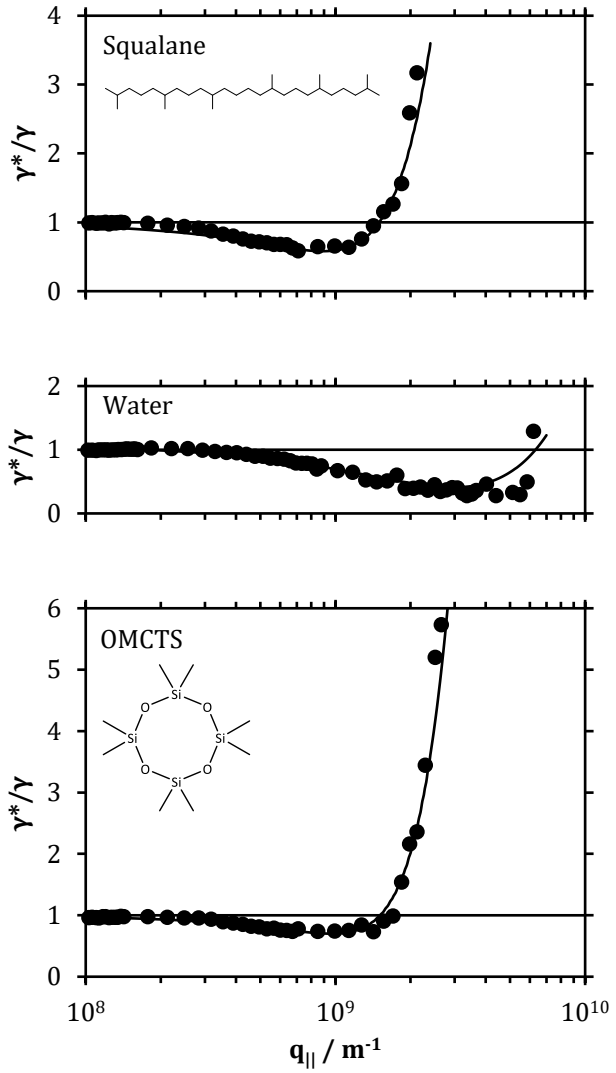

Figure 16: Wave-vector dependence of the effective surface tension γ* for chemically diverse liquids as observed by GIXD. [209] Results are given as relative values in comparison to the macroscopic surface tensions. Uncertainties at large wave-vectors (≈ 10^{10} m^{-1}) are due to low scattering intensities at the detection wavelength (λ = 15.5 Å). Data were kindly provided by J. Daillant.

2.5. Investigation and Optimization of the Conditions for Vapor-Phase Monolayer Deposition from Fluorous Silane Precursors

In preceding sections, the fundamental aspects of monolayer formation from trifunctional fluoroalkylsilane precursor molecules were introduced and the significance of precursor cross-linking was explained. It has already been highlighted there, that early efforts of explaining silane monolayer formation assumed a highly

cross-linked nature of the precursor headgroups, which neglects the steric constraints given by the length difference of siloxane bonds versus precursor chain diameter. Nonetheless, the picture of cross-linked headgroups might be correct for probably most of silane SAM depositions accomplished under standard laboratory conditions due to residual humidity within the deposition system. It has to be emphasized though, that in consequence, these SAMs do not represent a perfect monolayer in terms of densest-packing and that defects will occur within the film.

This discrepancy between preparational aspiration and (often neglected) structural reality still is a current problem concerning the reliable formation of silane SAMs and "ideally cross-linked" structures are still common to be reported. An important aspect related to this problem is the circumstance that there is no common agreement on the deposition conditions for specific SAMs so that numerous individual recipes for solution-based and vapor-phase depositions exist and monolayer preparations differ from researcher to researcher. [13,18,47,48,50,121,125,127,179,212–214] In consequence, results of individual groups are difficult to be compared systematically not only in terms of exact values.

The risk of uncontrolled hydrolysis, subsequent cross-linking and formation of agglomerates is a seminal example for the strong dependence of silane-based monolayer formation on the exact conditions during the deposition process. It emphasizes the need to meticulously control deposition parameters in order to obtain well-ordered monolayers. Considering the type of deposition, this control is easier to achieve for vapor-phase depositions, as the technical setup allows for more adjustments than possible during solution-based depositions. While traces of residual humidity are often difficult to abandon from liquid solvents and glassware, vacuum systems for vapor-phase deposition can be thoroughly prepared for dry conditions.

Among the numerous results published in literature, only a few publications report on intentionally changing the amount of water supplied during the deposition process in terms of a systematic comparison. Vapor-phase depositions were mainly conducted using simple deposition setups at ambient conditions or desiccators which were evacuated to some extent. For example, Genzer *et al.* achieved good wetting results for vapor phase depositions at ambient conditions without further control of silane or water partial pressure. [123] In another study, the group used a desiccator system which was evacuated to approximately 10^{-2} to 10^{-3} Torr after placing the substrate and F8H2-$SiCl_3$ in the deposition chamber. [215] Thus in both studies, a sufficient amount of water was left within the system's atmosphere. Hozumi and McCarthy deposited low-hysteretic films from F8H2-$Si(OMe)_3$ on alumina under

reduced humidity inside a sealed deposition container.[122] Ekerdt *et al.* tried to elucidate the required water content for optimum deposition conditions on silica in a flow-system vapor deposition process.[216] The authors hydrated silica surfaces (T = 25 °C) in a humid gas flow prior to the addition of F6H2-$SiCl_3$ silane vapor and varied the duration of water vapor flow. They reported that controlled substrate hydration was detected to be crucial for the outcome of the deposition and assumed that approximately one monolayer of water adsorbed on the uncoated silica surface was required to obtain an optimized dense film. They suggested multilayer growth at excess water contents as roughness, film thickness and F/Si intensity ratio increased with increasing substrate hydration. In general, however, deposition methods and conditions vary between the groups. Detailed information on deposition conditions is often missing or control of relevant parameters (water and silane partial pressures, exact temperatures and deposition times, etc.) was not accomplished.

Similar to SAMs deposited from alkyl thiols, deposition temperature affects film formation with alkylated silanes. For solution based silanizations an upper critical deposition temperature has been reported, i.e. temperature influences formation mechanisms and deposition above a threshold temperature leads to less ordered films.[51,170,217–219] On mica, a decrease of the deposition temperature was reported to lead to a decrease of the size of ordered clusters but simultaneously no regions of unordered domains were found.[188] Concerning vapor-phase depositions, process temperatures have rather been acknowledged in terms of the vapor pressure of the precursor molecules in order to control sufficient vaporization.

Although the underlying chemistry in silanization processes consists of fast reactions, deposition duration may alter the properties of the final films and analogous to the variety of deposition recipes, several optimum deposition times have been reported.[121,123,179,213,215,220] Improved layer quality was detected for processes with extended reaction times and "saturation" of layer properties occurred. While in thiol depositions only one overall deposition time is considered, there are more temporal parameters to be investigated in silane deposition chemistry. Depending on the details of a deposition process, for example individual adsorption times of single components or separate heating or desorption durations may be considered.

Optimization of deposition conditions does not exclude improvements from a chemical point of view, i.e. variations in the precursor molecule itself. In terms of fluoroalkylated precursors, the most obvious variation can be achieved by changing the length of the fluorous alkyl chain segment. Reports suggest an improvement of monolayer properties by elongation of the fluoroalkyl chain within fluorous

n-alkyl-substituted monolayers. [48,50,90,107] Extending the fluorous segment increases its influence on monolayer formation and its final structure, so that more stable films with increased structural order are formed. In consequence, films prepared from silanes with larger chain-lengths than commonly used are expected to show improved properties in terms of liquid wetting in comparison to monolayers prepared from short-chain precursors. Despite this expected improvement, its development does not only involve a simple and straightforward implementation of a new precursor molecule. Quite in contrast, the introduction of a new precursor requires not only its (synthetical) provision, but a thorough investigation of its applicability to the deposition process, for example in terms of a required minimum vapor pressure or its reactivity against other deposition conditions or substances.

Gaining a deeper understanding of the technical requirements and chemical processes involved in monolayer depositions apart from individual recipes is an important aim of this thesis. For this, fundamental aspects of a vapor-phase deposition process were systematically investigated in order to identify the most critical parameters during SAM preparation and to yield a practical guideline for deposition conditions. On a technical basis, this meant as well to find a compromise between optimum film properties and the limits of technical practicability, where necessary. Although the results for deposition conditions obtained during this study are still subjective in technical terms, they are aimed to be as general and representative as possible in comparison to other vapor-phase deposition processes. Based on the identification of important process characteristics, a further improvement of the resulting monolayers was assessed through the introduction of chain-extended fluorous precursors. On the whole, the optimization of a vapor-phase deposition process on a has been conducted, which is meant to enable a large-scale, automated deposition process yielding monolayers of reproducibly high quality.

3. Methods and Materials: How Fluorination Affects Experimental Procedures

3.1. Challenges during synthesis and analysis

The characteristic features of fluorous precursor molecules, which are strongly desired to give rise to the special properties within the final monolayer, bear major drawbacks during the course of synthesis and analysis of the compounds. The high degree of fluorination in combination with long chain lengths renders almost any of the compounds only sparingly soluble in standard organic solvents. An issue that affects synthesis and work-up as well as analytical experiments. In terms of syntheses, this problem can be overcome by the choice of appropriate solvents, e.g. fluorinated solvents, or adaptions to the synthetic procedure, although costs and efforts increase by increasing grade of fluorination of the desired products. During the post-synthetic work-up, the fluorous features may actually be regarded a simplification as the unique partitioning into fluoroorganic and organic solvent layers helps separating the fluorous products from organic reagents. Moreover, water is only sparingly soluble in fluorous solvents, so that dissolved products are protected from humidity to a certain degree. In many cases, the low solubility even in fluorous solvents undermines these positive effects.

In analytical experiments, solvents cannot be substituted as easily as during syntheses. For example, within NMR experiments solvents should not only enable a sufficient solubility of the analytes but in addition have to be deuterated. A combination that is difficult to be found in common solvents and is only fulfilled by rather exotic and thus expensive materials. After all, the solubility in solvents like, for example, hexafluoro *iso*-propanol is still not sufficient in many cases. Another alternative is the use of external referencing capillaries, which contain a standard NMR-solvent and are inserted into the actual sample tube containing the analyte in a fluorous, non-hydrogenated solvent. However, experience showed that external referencing capillaries did not yield satisfying results in all cases. Therefore, NMR analysis was conducted using standard techniques with standard solvents like chloroform-d1, accepting the drawback of low solubilities and thus low signal intensities.

In terms of analyzing telomeric mixtures of fluorous compounds with varying chain lengths, field-desorption mass-spectrometry (FDMS) has been found to serve as a suitable analytical technique. [221–224] In contrast to common ionization techniques of

mass-spectrometry (e.g. electron ionization, electrospray ionization, chemical ionization), field desorption gives only little fragmentation of the fluorinated analytes and is particularly useful for the study of solid substances. Thus, pure substances and mixtures of fluorous long-chain compounds can be conveniently investigated and the relative composition of the analyte mixture can be obtained. Due to the experimental procedure (repeated measurements during a continuous heating cycle), the results represent only an estimate of the actual relative amounts.

How simple methods reveal important details can be observed exemplarily for contact angle measurements which have been conducted extensively during this work. As macroscopic wetting behavior of the prepared samples was a major means of interpretation, the evaluation of dynamic contact measurements was accomplished with great efforts and care. Advancing and receding contact angles were automatically recorded and subsequently analyzed after meticulously selecting drop baselines manually. In consequence, the reported values are the average of at least eight independent droplets applied to one sample with approximately 150 individual data points per video. The achieved results showed very small deviations across a sample and were an important contribution to gaining insights into the effect of preparative details on SAM properties.

3.2. Fluorous phase high-performance liquid chromatography (F-HPLC)

The chromatographic method of fluorous phase high-performance liquid chromatography (F-HPLC) is similar to standard reversed phase HPLC (RP-HPLC) and uses fluoroalkylated stationary phases instead of alkylated silica gels for the separation or purification of compound mixtures.[20,225] Initially, these kinds of fluorous silica gels were used for the separation of organic molecules, which contained no fluorine at all or only small fluorous tags. Fluorous silica gels are standard gels modified with a (commonly linear) fluorinated alkyl chain, which in most cases is a perfluorohexyl ($-C_6F_{13}$) or perfluorooctyl ($-C_8F_{17}$) end group. Care has to be taken during the choice of the proper gels, as trademark names can be confusing and sometimes "fluorous C8" can mean a true perfluorooctyl group $-C_8F_{17}$ or only $-(CH_2)_2-C_6F_{13}$. F-HPLC columns separate compound mixtures depending on the fluorine content of the individual components. Regarding linear fluoroalkyl precursor molecules this means that the longer the fluorous part of a chain is, the stronger the retention of fluorous molecules becomes.

The interaction of a molecule with the stationary phase is primarily dominated by the fluorine-containing group. Interactions with the "purely" organic part are only of secondary nature, and although these organic interactions can be relatively strong, they will always be weaker than fluoro-organic interactions. Thus, F-HPLC has found some routine use in the separation of organic compounds which have been tagged with a fluorine containing functional group. In most cases, these tags are small fluorinated alkyl chains (-CF_3 to -C_6F_{13}) and some tags are reversibly substituted after separation. Its main use therefore consists of the separation of fluorinated from non-fluorinated compounds, independent from the fate of the compounds' fluorous tag(s). On the other hand, fluorous stationary phases have been proven to be surprisingly effective in the separation of non-fluorinated compounds due to their characteristically different behavior towards analytes as well as mobile phases compared to standard silica gels. The main difference compared to standard RP-HPLC (e.g. C18 silica gel) is the much weaker retention of organic molecules, which commonly elute with or near the solvent front. Introducing polarity to a molecule increases the retention time.

However, the very basic principle of F-HPLC is the separation by fluorine content, which makes it, in principle, the ideal method for the separation of organic molecules bearing long fluorinated alkyl chains of different lengths. The substances of interest to this thesis are oligomeric mixtures consisting of either fluoroalkylated iodides, olefins or thiols, which are sought for as pure oligomers of a single chain length. Several challenges have to be met in order to fully adapt F-HPLC to this task. There is no reference found in literature concerning similar separations, so that the general feasibility has to be clarified and if successful, method development has to be accomplished. This comprises every aspect that is routinely looked at in standard (RP-)HPLC but also adds the characteristic peculiarities of fluoroorganic chemistry. The long fluoroalkyl chains require appropriate solvents or mixtures of solvents in order to enable sufficient solubility along with a suitable concentration that is still high enough for viable compound recovery. Excess usage of fluorous solvents would increase the costs per recovered milligram of product. However, the general applicability of F-HPLC separation is the major goal, as there is no other possibility to obtain the desired products. Method optimization in terms of processing time and costs are therefore of secondary importance.

3.3. Thiol Monolayers

3.3.1. Liquid-phase deposition

In order to study the effect of molecular scale roughness on the wetting characteristics of surfaces, the preparation of proper samples becomes an essentially important aspect and the samples' quality has to be ensured tidiously. For this work, thiol monolayers were deposited onto Au substrates from ethanolic and *n*-heptane solutions following standard procedures described in literature under slight adaptions. [88,131,132] Benzotrifluoride (α,α,α-trifluoro toluene, 99 %) was obtained from ABCR, Germany, while all other solvents and deionized water were obtained from Chemsolute Th. Geyer, Germany, and were used as received if not stated otherwise. Short-chain thiols F4H2-SH (≥ 97 %, Sigma Aldrich, Germany), F6H2-SH (> 99 %, Fluoryx, USA) and F8H2-SH (> 99 %, Fluoryx, USA) were obtained from commercial sources while thiols used for deposition experiments with n ≥ 12 were synthesized according to literature procedures (Section 7.1.1). F10H2-SH was prepared following the same experimental protocol and was kindly supplied by Udo Adels (Qiagen, Germany). Non-fluorinated alkyl thiols Hm-SH with n = 8, 10, 12, 14, 16, 18, 20, 22 were commercially available and were used as received: H8-SH (98 %, Alfa Aesar), H10-SH (96 %, Alfa Aesar), H12-SH (98 %, Alfa Aesar), H14-SH (97 %, TCI), H16-SH (>97 %, TCI), H18-SH (96 %, Alfa Aesar), H20-SH (98 %, Alfa Aesar), H22-SH (>97 %, TCI). Thiols H30-SH and H38-SH were synthesized according to procedures described in Section 7.1.1.

All glass instruments used during deposition and bare silicon wafers (test grade, Si-Mat, Germany) were cleaned with fresh piranha etch solution (peroxymonosulfuric acid, H_2SO_5) prepared from concentrated sulfuric acid H_2SO_4 (95 wt-% aqueous solution, analytical grade, Chemsolute Th. Geyer, Germany) and hydrogen peroxide H_2O_2 (35 wt-% aqueous solution, analytical grade Chemsolute Th. Geyer, Germany) in a volume ratio of 7:3. Parts to be cleaned were soaked in hot etch solution for 30 minutes before they were rinsed intensively with deionized water and cleaned in an ultrasonic bath filled with deionized water for another 15 minutes. Subsequently, glass instruments were rinsed with deionized water again and were dried at 200 °C for 12 hours. Silicon wafers were rinsed with deionized water and analytical grade ethanol and were dried in a stream of argon (Ar 4.6).

Au-substrates were prepared by sputter coating a layer of gold onto cleaned silicon wafers. For this, bare wafers were transferred into a vacuum deposition system with a base pressure < $5 * 10^{-7}$ Torr and were sequentially coated with 20 nm titanium

(2.5N, deposition rate: 0.09 nm/s) and 200 nm gold (4N, deposition rate: 1.12 nm/s) using argon plasma (Ar 6.0, Ar-pressure 2 * 10^{-3} Torr).

Deposition of binary mixed monolayers was performed in ground joint weighing glasses from 1 mM ethanolic (FnH2-SH) or *n*-heptane (Hm-SH) solutions (99 %, HPLC grade, saturated with argon 4.6 in order to reduce the amount of dissolved oxygen [42]) of the respective thiols. Immediately after sputter coating, substrates were immersed into the deposition solutions at room temperature and stored for 70 hours at 60 °C. After removal from the solutions, samples were soaked in benzotrifluoride for 15 min and were then exposed to a series of rinsing steps. Thus, samples were rinsed with copious amounts of benzotrifluoride, dichloromethane, toluene and ethanol and were dried in a stream of argon (Ar 4.6). All rinsing solvents were of analytical grade. Analytical experiments were conducted within three days of sample preparation.

3.3.2. Methodology

Within this work, single-component monolayers and several series of binary mixed samples were prepared and analyzed towards their wetting properties. A series of samples is based on two thiol precursors of differing chain-lengths which are applied in selected concentration ratios during the deposition of the monolayers. As described earlier, it is thus possible to create binary mixed monolayers of different compositions with defined molar ratios within the sample surface. With these samples the effect of an increasing amount of a precursor species can be studied. Here, the precursors are simply referred to as "long" or "short" precursors, as the chain length difference is the defining parameter of the precursor system. The compositional ratio R_{sol} of a deposition solution is given by the concentrations of the corresponding thiols in the deposition solution:

$$R_{sol} = \frac{c_{long}}{c_{short}} \tag{7}$$

The total concentration of the deposition solution was adjusted to c_{sol} = 1 mM. Within a series of samples, R_{sol} was varied in such a manner that sample compositions were distributed homogeneously over the range of the molar ratio x_{long} = 0…1 within the

SAM and wetting properties could be determined for each system. The molar composition within a monolayer was determined through sSIMS analyses by quantification of suitable secondary ions. These ion intensities were referenced with the intensity of Au^- (m/z = 197 Th) according to equation (8).

$$J_{197}^{kn} = \frac{I(^m/_z = kn)}{I(^m/_z = 197)} \tag{8}$$

The molar ratios x_{long} and x_{short} of a deposited binary monolayer were determined using sSIMS results of the mixed and pure monolayers. Thus, relative ion intensities J_{197}^{kn} of a binary SAM were referenced to the relative intensity obtained from the single-component SAM.

$$x_{long} = \frac{J_{197}^{kn}(x_{long})}{J_{197}^{kn}(x_{long} = 1)} \tag{9}$$

$$x_{short} = \frac{J_{197}^{kn}(x_{short})}{J_{197}^{kn}(x_{short} = 1)} \tag{10}$$

Relative ion-intensities of dimeric fragments $n_{long\text{-}long}$, $n_{long\text{-}short}$, $n_{short\text{-}short}$ were determined analogously.

$$n_{long-long} = \frac{J_{197}^{kn}(x_{long})}{J_{197}^{kn}(x_{long} = 1)} \tag{11}$$

$$n_{long-short} = \frac{J_{197}^{kn}(x_{long})}{J_{197}^{kn}(x_{long} = 0.5)} \quad (12)$$

$$n_{short-short} = \frac{J_{197}^{kn}(x_{short})}{J_{197}^{kn}(x_{short} = 1)} \quad (13)$$

Precursor molecule combinations were varied in terms of the fluorinated alkyl chain lengths of both long and short species, so that various systems of different combinations of chain lengths differences were prepared. For all individual samples of one series, the wetting properties were tested using water and hydrocarbon squalane as contacting liquids. Thus, it was possible to monitor the effect of chain length differences and molar compositions and to deduce general trends and characteristics in wetting behavior.

3.4. Silane Monolayers

3.4.1. Vapor-phase deposition

Monolayers of the respective fluoroalkylated trichlorosilanes were deposited onto flat silicon wafers as substrates (prime grade, University Wafer, Boston, MA, USA). All substrates were treated with UV/ozone for 20 min prior to loading them into the deposition chamber using an UV-minidrier (BE 7/1, Beltron GmbH, Germany) with a mercury low pressure vapor lamp with a quartz window, emitting light of wavelengths 185 nm and 254 nm.

Deposition was carried out in the vapor phase under specified conditions within a stainless steel hot-wall chemical vapor deposition (CVD) system at a base pressure of $< 1 * 10^{-6}$ Torr. Figure 17 presents a technical schematic of the deposition system. Before use, reagents underwent a degassing sequence of several freezing, pumping and thawing steps. Moreover, silane precursors were supplied in individual glass ampoules in order to prevent decomposition of the reagents. Substrates were placed in a cylindrical 250 mm diameter deposition chamber of about 15 L volume. Prior to the deposition process the UV-cleaned samples were additionally treated by an *in-situ*

oxygen plasma excited by a 350 kHz discharge at 20 W in a 30 sccm O_2 flow (O_2 4.5) for 20 s. Except for this plasma treatment, the system was operated under static conditions, so that no flow-system or carrier gas was used for the inlet of reactive components. This reduced the risk of possible contamination and lead to very small amounts of silane being used.

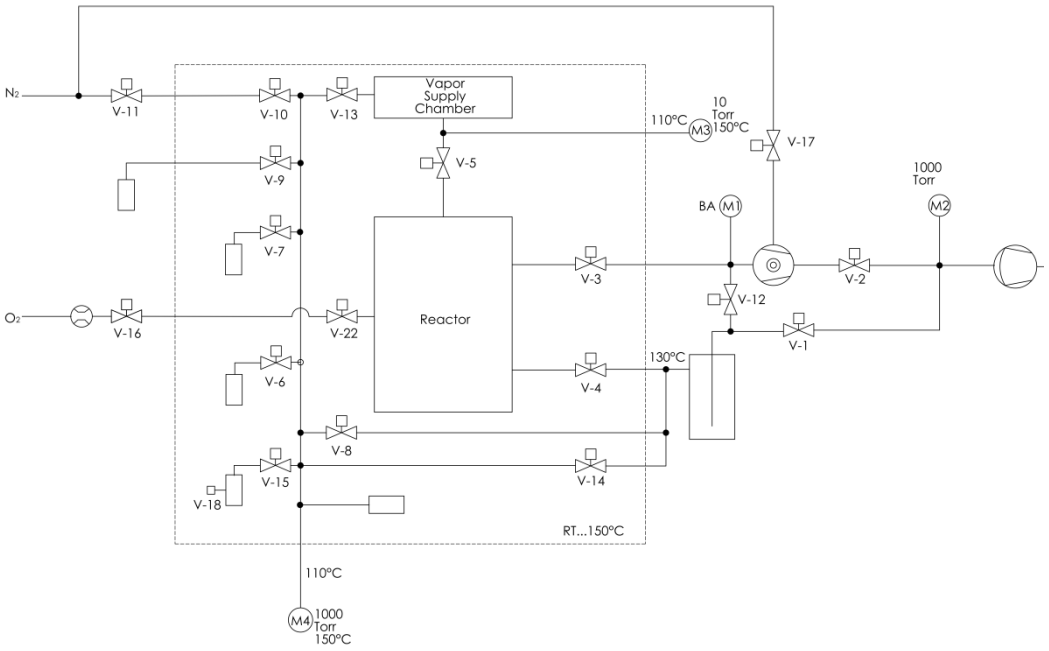

Figure 17: Schematic representation of the CVD-system for vapor-phase depositions. Reagent vapors can be prepared in a vapor supply chamber independently from a parallel coating reaction in the reactor chamber.

Upon completion of the *in*-situ plasma cleaning, the preparation of monolayers was started by dosing of the precursor vapor and subsequent inlet to the reaction chamber containing the substrate. During this adsorption phase (hereafter referred to as "silane adsorption time" t(silane)) only silane vapor with a partial pressure p(silane) was present in the reaction chamber and was thus able to adsorb onto the substrate. After silane adsorption phase was finished, the desired amount of water vapor was automatically measured, added to the reaction chamber and the system was kept under these conditions for a pre-determined time with the additional water partial pressure p(H_2O). This phase, when silane and water vapor were able to react both with each other as well as with the substrate is referred to as "water reaction time" t(H_2O). Afterwards, all reactants were pumped out and the system was purged

repeatedly with dry nitrogen in order to remove any residuals. Further desorption of reagents from the substrate surface was allowed before the sample was removed from the system ("silane desorption time").

Process conditions like temperatures, reaction times and particularly the partial pressures of the components were varied in the course of this study. An illustration of the process sequence as a history of pressure is given in Figure 18. For each part of the sequence, temperature and duration can be set individually. Additionally, preparation/cleaning conditions and most important the partial pressures of any reactant can be controlled, which enabled full individual control over the process parameters and lead to highly reproducible results. Parameters and their definitions are summarized in Table 5.

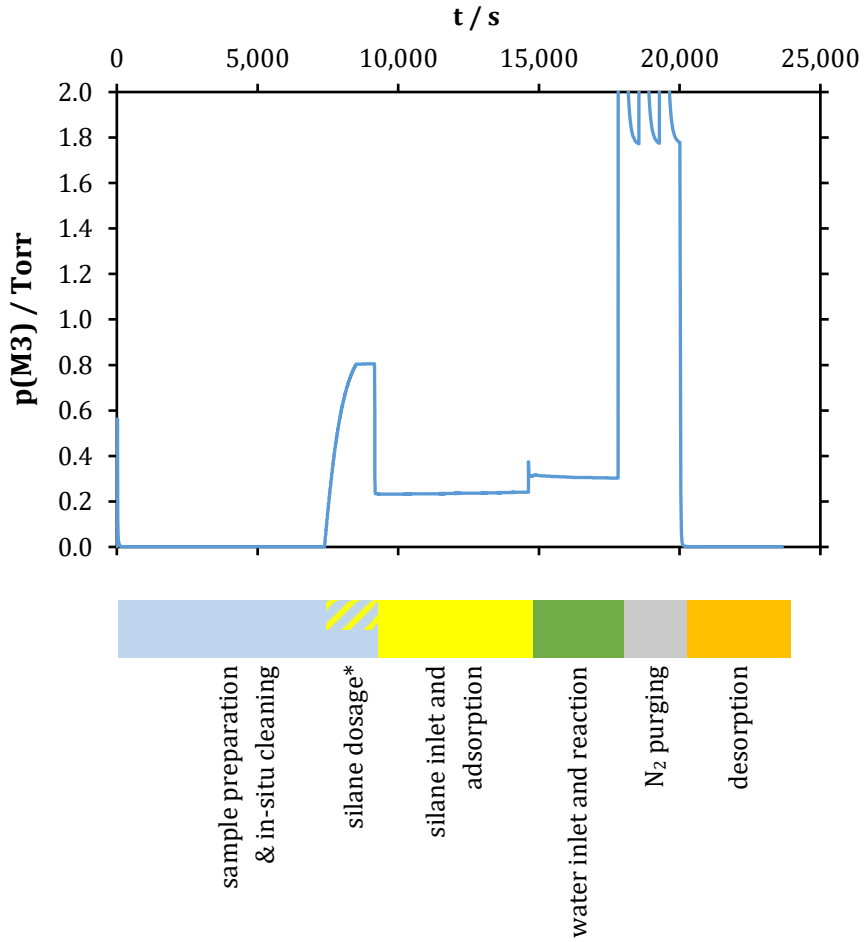

Figure 18: Example of the history of pressure (manometer position M3) during a vapor-phase deposition process (SF-Si-0133, p(H20) = 71 mTorr, p(F8H2-$SiCl_3$) = 232 mTorr, T(dep.) = 80 °C). Values > 2 Torr are not shown within the scale chosen here. *Silane dosage is conducted simultaneously in a separate vapor supply chamber (pressure shown here) while sample preparation and cleaning is conducted in the isolated main reactor chamber.

Parameter	**Function**
Water partial pressure: $p(H_2O)$	Partial pressure of water in the reaction chamber.
Silane partial pressure: p(silane)	Partial pressure of the respective silane precursor in the reaction chamber.
Deposition temperature: T(dep.)	System temperature for all process steps (except from desorption phase).
Silane adsorption time: t(silane)	Duration, for which only silane is present in the reaction chamber.
Water reaction time: $t(H_2O)$	Duration, for which both silane and water vapor are present in the reaction chamber.
Desorption time and temperature: t(des.), T(des.)	Parameters during desorption of excess material after purging of the system.

Table 5: Overview and explanations of process parameters.

3.4.2. Methodology

The objective of this part of this thesis was the determination of optimized coating conditions while maintaining high coating quality in terms of wetting properties and layer stability. This goal was to be achieved by a systematic approach looking at individual processing parameters and their effects on the final coating. Ideally, an optimized coating process would result in a fast, inexpensive, clean and reliable method.

Starting from general standard values, which were determined during initial studies, individual parameters were varied while all other parameters were kept constant. The result of each coating process was monitored by analyzing the wetting properties of the respective sample. Thus, the influence of a certain parameter on the coating process could be systematically investigated and optimum conditions were deduced. The application of this methodology to all relevant process parameters yielded information about the most important factors influencing monolayer deposition and enabled not only the optimization of the coating itself but the deposition process as a whole.

4. Fluorous Precursor Synthesis

4.1. A Fluorosynthetical Prologue: Zonyl™ Telomers as Starting Materials

Highly fluorinated, or „fluorous“, compounds as they are used within this study are still rather special substances in everyday chemistry, what makes them rare materials in terms of commercial availability. In this very case, the precursor molecules of fluoroalkylated thiols and trichlorosilanes which are used throughout this work are similar in chemical structure and only differ in their functional headgroups depending on the precursor/substrate system we are looking at. The “fluorous functionality” remains a long fluoroalkyl chain only differing in the length of the fluorocarbon backbone. Therefore, it is not surprising that both these precursors may share the same synthetic origin and can be derived from the corresponding fluoroalkyl iodides. While the thiols can be obtained directly from the iodides via an intermediate, the synthesis of trichlorosilanes requires the prior synthesis of the fluorinated olefin.

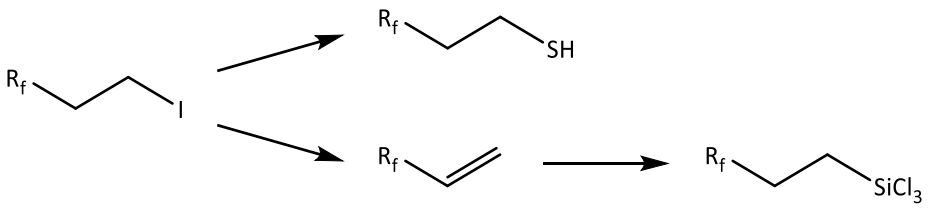

Figure 19: Synthetic routes to fluorous thiols and trichlorosilanes applied during this study. R_f represents a perfluoroalkyl substituent of arbitrary chain length.

More important than a common chemical source is a prerequisite that both types of precursors share. In order to be able to deposit neat monolayers that are suitable to serve the scientific purpose of this work, all precursor compounds have to be available as pure oligomers of defined chain lengths. Oligomeric mixtures of unknown compositional ratio cannot be applied to any of the deposition experiments.

Only a very small number of fluorous precursor molecules or reactants that are required for precursor synthesis can be obtained from commercial suppliers. Those commercial sources are commonly limited to substances carrying a

1H,*1H*,*2H*,*2H*-perfluorodecyl chain as the longest possible chain. Therefore, in case of thiol-based monolayers on gold F8H2-SH is the longest precursor available and any other substance is required to be synthesized. Concerning monolayers from fluorous alkyl silanes with n > 8, all alkene and trichlorosilane substances except for the F10H2-olefin have to be synthesized.

What makes the situation even more challenging is that also the very basic starting materials for the corresponding syntheses, i.e. fluorinated iodides, are only available as pure oligomers to some extent (≤ F12H2-I). Readily available are, however, telomeric mixtures, which are marketed by DuPont under the Zonyl trade name. The mixtures contain FnH2-I oligomers in the range of approximately n = 4…30, with n being limited to even numbers. This series originates in the telomerization production method, in which perfluoroethylene monomers are sequentially added to alkyl iodides. [226]

An earlier attempt to separate the Zonyl telomers by high-temperature vacuum distillation had proven unsuccessful and resulted in fractions of mixed iodides with narrower distributions in n compared to the Zonyl starting material (boiling points > 200 °C at 1 bar). Different ranges of n within the fractions could be obtained by repeated distillation of previous fractions. A distinct isolation of individual oligomers was not possible by this method, due to the strong tendency of the substances to sublimate well below their actual boiling points and their very similar properties. Exemplarily, FDMS analysis of a fraction denoted “R2”, which was acquired at a pressure of 10 mbar over a boiling point range of 161-175 °C, yielded a composition as shown in Figure 20. The sequential difference of 100 M/z per C_2F_4-unit is easily observable.

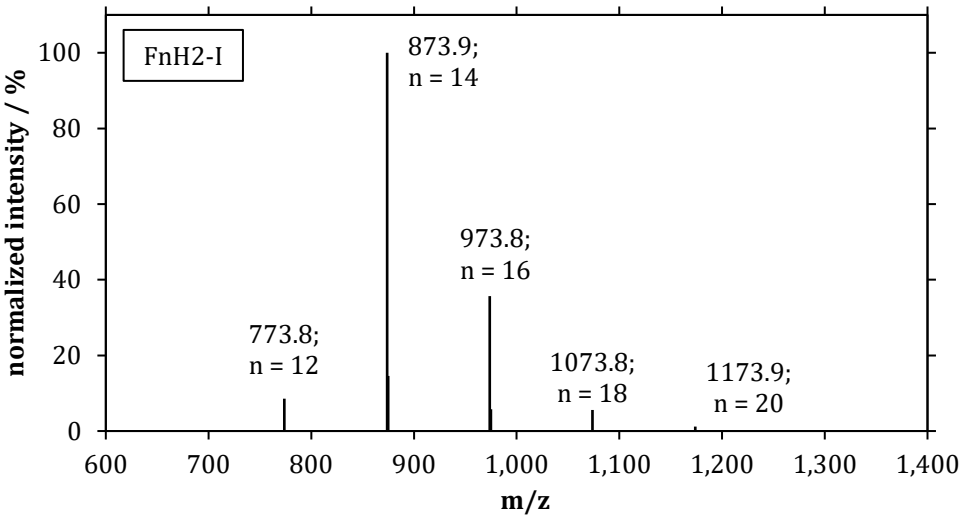

Figure 20: FD mass spectrum of fluorinated iodide fraction R2 after vacuum distillation (acquired at 10 mbar over a boiling point range of 161-175 °C). Intensities are normalized to the most intensive peak.

These mixtures have been successfully converted to oligomeric mixtures of thiols, olefins and trichlorosilanes in this thesis. However, for the deposition of monolayers from these products oligomerically pure precursors are required, so that at some stage during the course of production a separation of individual oligomers has to be accomplished.

Therefore, in order to further separate these fractions and to obtain isolated oligomers, an alternative method of separation had to be established. Although fluorous phase high-performance liquid chromatography (F-HPLC) had not been reported for this kind of separations, it turned out to be a suitable alternative. Early tests had already confirmed the general applicability of F-HPLC for the separation of FnH2-iodides and baseline separation appeared feasible. The method's actual capability in terms of baseline separation, solvent flux and temperature had yet to be determined.

Method development yielded conditions under which oligomeric mixtures of Zonyl iodides could be separated into pure oligomer fractions. However, the separation turned out to be very time-consuming and expensive. The necessity to sufficiently dissolve the fluorous compounds in the mobile phase lead to the use of large amounts of semifluorinated solvent (perfluorobutyl)methylether (Figure 21), which is marketed under the trade name Novec® HFE-7100 by 3M. Although HFE-7100 can be used in a mixture with methanol in a ratio MeOH:HFE-7100 of 4:1 (v/v), the solvent generated high costs, particularly because recycling of the mobile phase has not been

developed, yet. Moreover, the overall solubility especially of higher fluorinated compounds still turned out to be very poor and the sample volume per separation cycle was limited due to saturation of the HPLC column. The overall yield per solvent volume of products was < 10 mg/L. These restrictions resulted in only small amounts of obtained products per cycle and many cycles had to be accomplished in an extended time frame and under the consumption of large amounts of solvents.

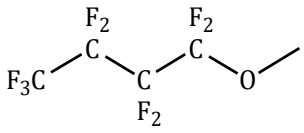

Figure 21: Chemical structure of the semifluorinated solvent HFE-7100.

As an example, F-HPLC chromatography of fluorous iodide fraction R3b (acquired by vacuum distillation at 300 mbar over a boiling point range of 233-242 °C) was successfully accomplished with baseline-separation as depicted in Figure 22. Separation was conducted under isocratic conditions (MeOH:HFE-7100, 4:1 (v/v)) using a preparative HPLC column (ES industries, 250 x 30 mm, Fluorosep RP Octyl packing) under a solvent flux of J = 8 mL/min and a column temperature of T = 45 °C. It has to be noted that an increase in column temperature certainly increases the solubility of the analytes. Due to the low-boiling nature of fluorinated solvents (HFE-7100: b.p. = 61 °C) and in order to minimize the risk of temperature gradients within the system, the column temperature was not increased above 45 °C. Separation of alternative starting mixtures yielded the same results and identical reproducible retention times for the corresponding iodides were obtained. Iodides with chain-lengths of n = 12, 14 were identified by means of FDMS but spectra contained contaminations from unsuitable tubing of the fraction collector. Further experiments, which were focused on the separation of fluorous thiols, were therefore conducted after exchange of the tubing for PTFE-materials. Obtained quantities of samples from longer chain-length iodides were too small to be identified by FDMS.

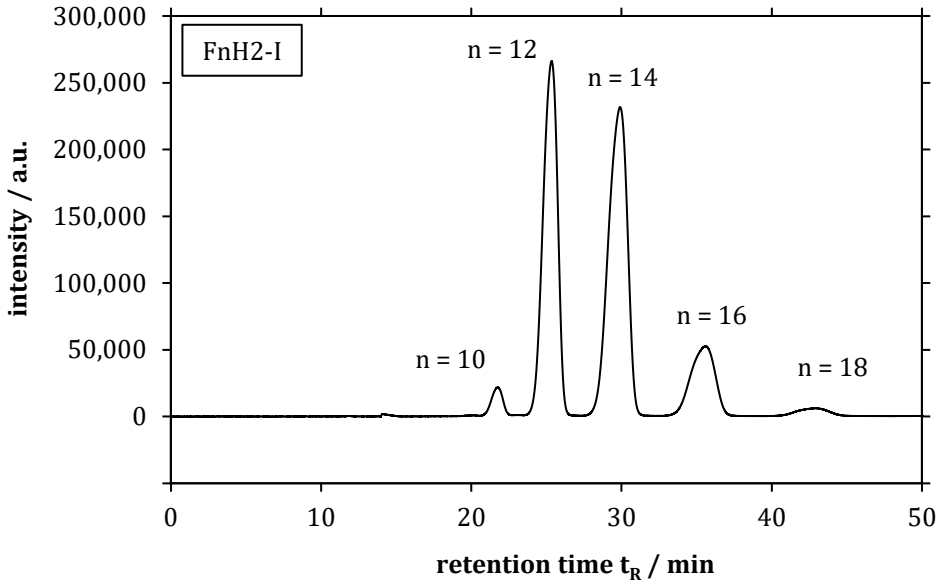

Figure 22: Preparative F-HPLC chromatogram of iodide mixture R3b (λ = 258 nm, T = 45°C, J = 8 mL/min., isocratic MeOH: HFE-7100 4:1 (v/v)), which was initially acquired by vacuum distillation at 300 mbar over a boiling point range of 233-242 °C. Peaks correspond to FnH2-I with n = 10…18. FDMS predicted chain lengths of n ≈ 12…16.

	analytical column		**preparative column**	
n	**t_R [min]**	**FWHM**	**t_R [min]**	**FWHM**
10	5.13	0.33	21.76	0.82
12	6.10	0.36	25.35	1.10
14	7.37	0.39	29.91	1.44
16	9.01	0.41	35.58	1.86
18	11.17	0.45	42.86	2.45

Table 6: F-HPLC retention times of fluoroalkylated iodides FnH2-I.

4.2. Precursors for Thiol Monolayers

4.2.1. Fluorinated *n*-alkyl thiols

The synthesis of alkylthiols for monolayer deposition has been reported several times due to the intensive study of this monolayer system during the past decades. The general route of formation of (fluoro-)alkyl thiols from the corresponding alkyl halides via nucleophilic substitution is well-studied and has been reported for various types of nucleophiles (e.g. thiourea or thiolacetic acid). [227,228] These different methods share the same motif of a nucleophilic exchange of the halide followed by the hydrolysis of the resulting intermediate yielding the alkyl thiol. This circumstance enabled the relatively straightforward transition from literature procedures to reliable recipes for the formation of fluorinated alkyl thiols required for this study.

As for many highly fluorinated compounds and especially long-chain fluorous substances, also the fluoroalkylated thiols required for this work are not commercially available in a sufficient variety. Like the chemically similar telomeric iodides, the thiols are available as pure substances up to a certain chain length only. Commonly available are compounds with chain-lengths not longer than F8H2-SH, although F10H2-SH is rarely to be found. In order to study monolayers from this type of thiols in a broad variety, the synthesis of these compounds is unavoidable. While fluorous thiols bearing short alkyl chains ($n \leq 10$) and their corresponding syntheses have been described in literature, no information can be obtained for longer fluoroalkyl chains. Thus, the application of the desired long fluoroalkylated chains caused certain adaptions nonetheless, but experimental research did not require a broader variety of synthetical pathways as during the work on fluoroalkylated trichlorosilane precursors. Moreover, fluorous thiols are essentially easier to handle compared to the highly moisture-sensitive trichlorosilanes, so that standard chemical methods during synthesis and work-up can be applied.

Prior efforts of synthesizing *1H,1H,2H,2H*-perfluoroalkyl thiols had already focused on the nucleophilic substitution of the corresponding iodides by the application of thiourea, so that this route was soon established as the major means of obtaining the desired precursors. Extending reaction temperature and duration accompanied by an optimization of the chosen solvents resulted in the successful synthesis of long-chain thiols and mixtures thereof containing different chain lengths. Nonetheless, the basic reaction scheme remains the same for all conversions and is depicted in Figure 23. Substitution of the iodide with thiourea gives the thiouronium salt as an intermediate which is not isolated. Instead, it is subsequently hydrolyzed *in-situ* with basic NaOH and the thiol is extracted after acidification with aqueous HCl.

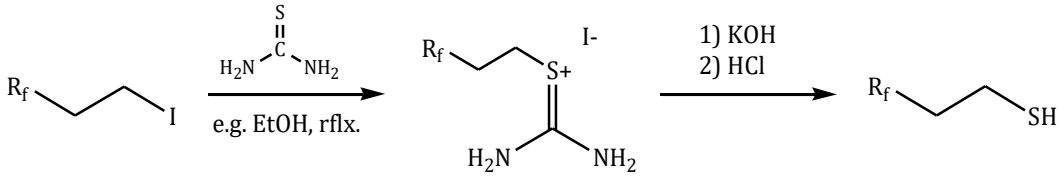

Figure 23: Reaction scheme of the conversion of fluorous iodides to thiols with thiourea employed as nucleophile. The intermediate thiouronium salt is not isolated but hydrolyzed with KOH *in-situ*. The positive charge is delocalized over the thiouronium moiety and only one possible mesomeric form is shown here.

The choice of solvent mainly depends on the chain length of the reactant/product or the composition of the oligomeric mixture. Problems arise from the solubility of the reactants and the boiling point of the chosen solvent. While short-chain iodides are sufficiently soluble in ethanol, longer-chain compounds cannot be completely dissolved even in refluxing ethanol and the final degree of conversion is rather poor. For long-chain iodides and especially for oligomeric mixtures containing different types of long-chain iodides, 1,4-dioxane is a more appropriate solvent. Its higher boiling point enables sufficient solubility in most cases. In the case of oligomeric mixtures with high amounts of very long fluoroalkyl chains an almost solvent-free procedure is found efficient where the reaction takes place in a melt of the fluorous iodides.

In conclusion, oligomeric mixtures of iodides as well as pure oligomers can be converted to the respective thiols successfully under appropriate conditions. Figure 24 gives the results of an FDMS experiment conducted on an oligomeric mixture synthesis of fluorous thiols. Analogous to the results presented earlier for fluorous iodides, the chain length difference is clearly observable in terms of the mass difference of 100 M/z per C_2F_4-unit.

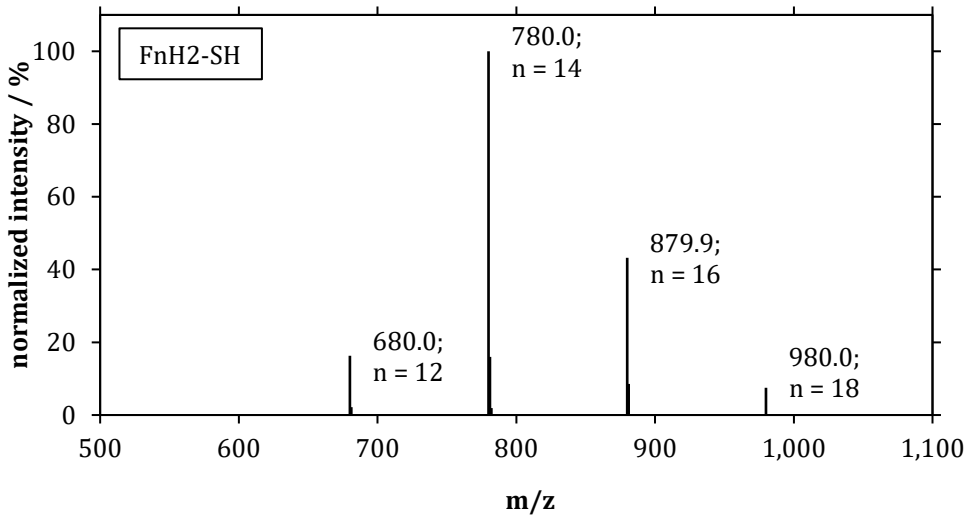

Figure 24: FD mass spectrum of fluorinated thiol sample JK109 synthesized from iodide fraction R3b (acquired by vacuum distillation at 300 mbar over a boiling point range of 233-242 °C). Intensities are normalized to the most intensive peak.

4.2.2. Non-fluorinated *n*-alkyl thiols

Initially, *n*-Triacontanethiol H30-SH was prepared by iodination of *n*-triacontanol H30-OH and subsequent conversion of the *n*-alkyl iodide to the thiol H30-SH. For this, the alcohol was converted with elemental iodide in presence of imidazole and triphenylphosphine to give the corresponding iodide, which was further converted to the thiol following the general thiourea route described above. As *n*-alkyl alcohols with m > 30 were not commercially available, this protocol could not be applied for chain-extended thiols with m > 30.

Chain-extended thiols with m ≥ 30 were synthesized via a recursive protocol by consecutive stages (Figure 25). It consisted of the formation of an active Grignard reagent from a linear chloro alkyl alcohol (stage I [229–232]), which was subsequently converted by Grignard reaction with an *n*-alkyl bromide for chain-extension (II). Bromination (III) of the obtained alcohol and conversion of the thus obtained alkyl bromide with thiourea gave the corresponding thiol (thiolation, IV). Within this route, the main portion of the intermediate bromide obtained after the bromination stage (III) could be isolated and applied as chain-extension reagent (II) within the initial Grignard reaction of a new conversion cycle. The consecutive stages of this method can be repeatedly applied until a desired chain length is achieved. For this study, H22-

Br served as initial halide and 1-chlorooctan-8-ol was used as chain-extension reagent. H38-SH is the longest thiol that has been synthesized, so far.

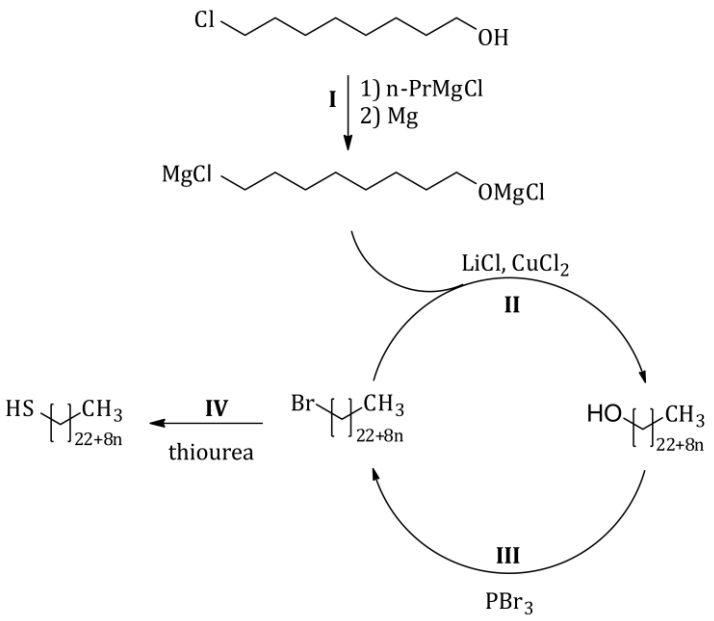

Figure 25: Recursive method of production of chain-extended non-fluorinated *n*-alkyl thiols.

4.2.3. Provision of oligomerically pure fluorinated thiol precursors

Apart from the successful synthesis of fluorous thiols with large chain lengths, the provision of pure thiol oligomers of an individual chain length represented another challenge. For this, routes enabling the provision of iodide reactants as well as thiol products were followed during the course of this study. The separation of fluorous iodide mixtures by means of F-HPLC has been described in Section 4.1 and enables the provision of pure iodide oligomers which may serve as starting materials for the synthesis of fluorous thiols FnH2-SH. Alternatively, it is possible to convert iodide oligomeric mixtures batch-wise to the corresponding thiols without prior chromatography and to separate the obtained thiol oligomeric mixture afterwards. While both types of compounds (iodides, thiols) can be processed equally well via F-HPLC, the choice of thiol separation over iodide separation offers an important advantage. After the chromatographic separation of iodides it is necessary to conduct

individual syntheses and purifications for each thiol chain length desired. Thus, pure thiol oligomers are at hand right away after synthesis but it means a lot of time and efforts to be spent as several syntheses have to be performed. In the case that thiol oligomeric mixtures are synthesized as a first step, the subsequent separation by F-HPLC immediately yields pure thiol oligomers which can be applied in monolayer deposition. The conversion of oligomeric mixtures therefore enables a time-saving route with less synthetic steps to be conducted.

Analogous to the F-HPLC separation of Zonyl iodides method development yields baseline separation of the fluorous thiols by chain length so that individual oligomers can be collected. Chromatographic separation is accomplished under identical conditions as with fluorous iodides except for a different UV-detection wavelength. UV/Vis-spectra of fluorous thiols are presented in Figure 26.

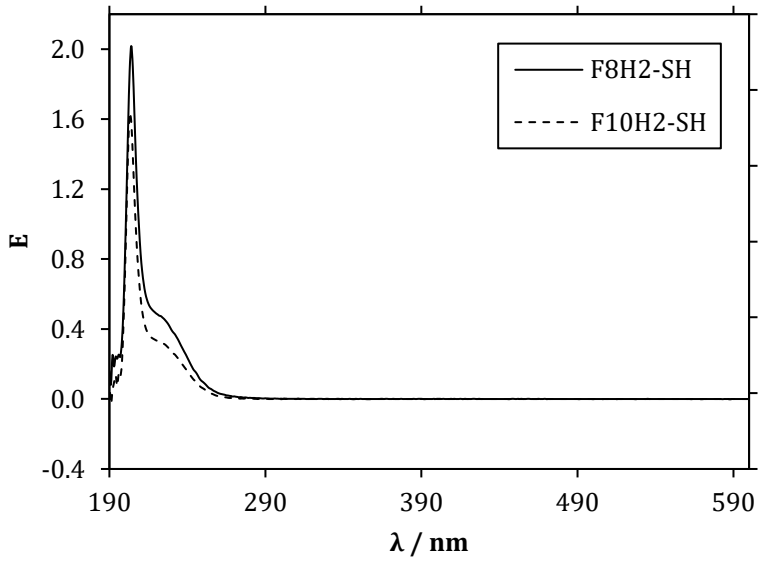

Figure 26: UV/Vis-spectrum of fluorous thiols F8H2-SH (c = 3.5 mM) and F10H2-SH (c = 3.2 mM). Sample solvent and reference background: MeOH:HFE-7100 4:1 (v/v). Maximum absorption is detected at λ_{max} = 204 nm.

Exemplarily, Figure 27 represents a chromatogram obtained from separation of a thiol oligomeric mixture. Separation was conducted under isocratic conditions

(MeOH:HFE-7100, 4:1) using an analytical HPLC column (ES industries, 4.6 x 30 mm, Fluorosep RP Octyl packing) under a solvent flux of J = 1 mL/min and a column temperature of T = 45 °C. Short chain thiol F10H2-SH is not resolved as a part of the solvent front, which, however, is of no further concern as this chain length can be obtained independently from HPLC separation. Preparative scale HPLC yielded the same results with baseline separation at shifted retention times as a consequence of analytical to preparative upscaling. Despite the observed baseline separation, SSIMS analyses of monolayers deposited from collected individual thiol oligomers did show characteristic fragments of chain lengths other than the desired oligomer in some batches. Contaminated films deposited from FnH2-SH contained up to 7 % of thiols with chain-lengths of n ± 1 based on normalized sSIMS intensities. This is assumed to be a consequence of the very large quantities of required solvent compared to the small yield of product, as even small amounts of impurities are being concentrated upon removal of the liquid solvent.

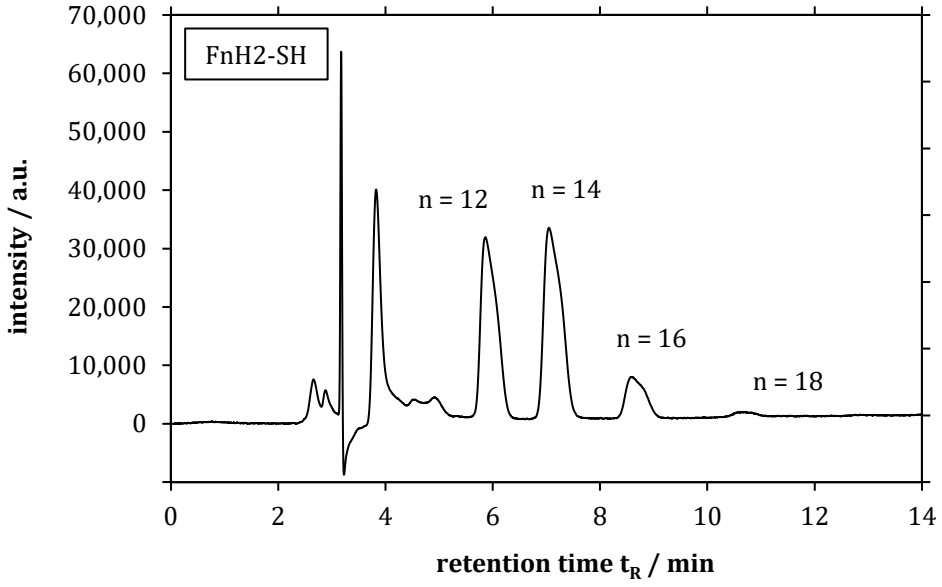

Figure 27: Analytical F-HPLC chromatogram of thiol mixture sample JK109 (λ = 204 nm, T = 45°C, J = 1 mL/min., MeOH: HFE-7100 4:1 (v/v)). Peaks correspond to FnH2-SH with n = 12,14,16,18. F10H2-SH elutes together with the solvent front and is not resolved.

	analytical column		preparative column	
n	**t_R [min]**	**FWHM**	**t_R [min]**	**FWHM**
12	5.86	0.35	24.91	1.00
14	7.04	0.39	29.25	1.30
16	8.58	0.43	34.84	1.55
18	10.58	0.50	-	-

Table 7: F-HPLC retention times of fluoroalkylated thiols FnH2-SH.

As for separations of fluorous iodide mixtures, the solubility of thiols in the mobile phase during F-HPLC is quite poor and the same problems concerning chromatographic yields and excessive consumption of solvents arise. Commonly, a standard separation of fluorous thiols consisted of 75 runs, which per cycle took 50 minutes and 400 mL of solvents. The yield of such a separation was approximately 150 mg of thiols in total. Although this amount is very small, it was still sufficient to conduct a number of experiments with thiols of $n \leq 14$, due to the small concentration required for thiol deposition solutions. Thiols with chain lengths of $n \geq 16$ are observed in the chromatogram but could not be recovered in sufficient quantities for film deposition.

4.3. Precursors for Silane Monolayers

Precursor molecules of the form FnH2-$SiCl_3$ have been commonly reported in publications on SAMs during the past decades. Despite this, variations of the alkyl chain length of the precursor molecule are rarely to be found and most of the published work focuses on chain lengths ranging from F6H2-$SiCl_3$ to F10H2-$SiCl_3$, with F8H2-$SiCl_3$ being the most prominent precursor of this type. A major reason for this selectivity might be the lack of commercial availability of longer-chain precursor derivatives, as even F10H2-$SiCl_3$ is not available by standard (and in satisfying quality) and custom syntheses are very expensive, even in comparison to the high-prized smaller compounds. Therefore, the successful synthesis of the

compounds of interest was essential for the outcome of this study. The synthesis of fluoroalkylated trichlorosilane compounds was investigated for chain lengths with $n \geq 8$, with the commercially available compound of $n = 8$ serving as an initial reference substance for the synthetic studies.

Trichlorosilanes have been chosen for this thesis instead of the corresponding trialkoxy silanes for mainly three reasons. Trichlorosilanes are more reactive than their alkoxy counterparts and thus appear to be more suitable for the vapor-phase reaction of long fluorous precursors with unknown reactivities. [116] Moreover, HCl as unavoidable by-product of chlorosilane hydrolysis is assumed to desorb more readily from the reaction-site than alcohols formed from alkoxysilanes due to its smaller size and higher vapor pressure. The third reason acknowledges practicability, as the alkoxy compounds are commonly synthesized from their trichlorosilanes. Thus, by applying trichlorosilanes, a further synthetic step and additional risk of hydrolytical degradation can be avoided.

The synthetic route via the hydrosilylation of fluoroalkylated 1-ethenes (*1H*,*1H*,*2H*-perfluoroalkenes) was found to be the most effective method to synthesize the desired trichlorosilanes. [233–235] Moreover, this method is well-documented in literature - even in terms of fluoroalkyl compounds [74,129,236] - and the fluorinated olefins can be easily obtained from the corresponding iodides. Alternative routes based on literature reports had been investigated in preceding and initial studies but did not yield positive results. [237–246] Especially the possibility to convert fluorous iodides directly to the corresponding silanes using amines or tetrabutylphosphonium chloride (TBPC) as a catalyst appeared desirable. However, it has already been reported in literature that the choice of alkyl bromides over chlorides resulted in higher amounts of side-products due to the higher reactivity of bromides. [244] It is therefore not surprising that the even more reactive alkyl iodides, which were used within this work, gave only semifluorinated alkanes as a reduction product instead of the fluorinated trichlorosilane (Figure 28). Further optimization of this method may serve as a suitable alternative avoiding the need to initially prepare the fluorous olefins one day. As the elimination and subsequent hydrosilylation of Zonyl iodides are conducted with relative ease and in good yields, there is no immediate need to put further efforts in the TBPC route.

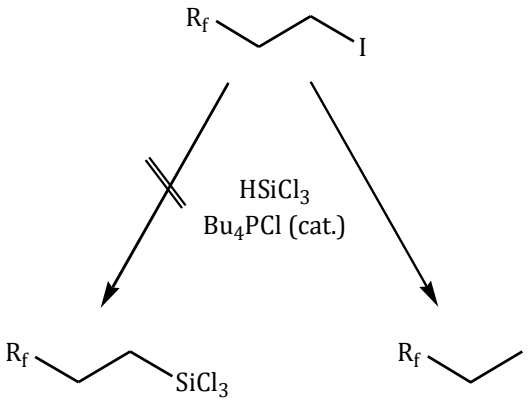

Figure 28: Conversion of Zonyl iodides with catalytic TBPC yields fluorinated alkanes instead of trichlorosilanes.

The general synthesis of FnH2-$SiCl_3$ using FnH2-I as starting materials is depicted in Figure 29. As long-chain derivatives of the *1H,1H,2H*-perfluoralkenes are not commercially available, the synthesis of the olefins from the iodides is an important step for prospective syntheses.

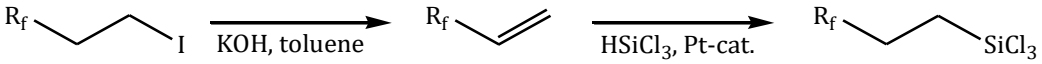

Figure 29: General reaction scheme for the synthesis of fluorous trichlorosilanes from Zonyl iodides via the corresponding olefin.

The formation of the fluorinated olefins is achieved by a simple elimination step and both short and long chain olefins are formed in good yields > 85 %. Pure iodides with $n \leq 10$ as well as telomeric mixtures (n = 10…24) were successfully converted. The elimination is performed in the presence of excess KOH in refluxing organic solvents with toluene being the preferential solvent. Although the conversion succeeded equally well in ethanol, side-reactions have been reported with this solvent and the higher boiling point of toluene facilitates the conversion of higher fluorous iodides. [247]

Despite the evident ease of conversion of the iodides, this first stage of silane production affords a substantial effort, especially taking into account long-chain derivatives of n ≥ 12. On the one hand, the solubility of the iodides strongly decreases with increasing chain length, which causes additional precautions during the synthesis. On the other hand, the work-up and purification procedures of the resulting olefins become increasingly tedious, as these solid products cannot be purified easily by distillation and removal of solvents after recrystallization becomes time-consuming. However, fluorinated olefins can be synthesized successfully and even oligomeric mixtures of varying chain lengths can be converted in a one-pot-synthesis.

The conversion of terminal alkenes to trichlorosilanes by hydrosilylation was intensively studied by Speier and is a common method to introduce silane functionality. [233] This addition of various types of hydrosilanes to carbon double bonds is catalyzed by noble metals, with platinum complexes being the most important catalysts. Within this study, the so-called "Karstedt-catalyst" was used, which describes organic complexes of platinum with 1,3-divinyltetramethyldisiloxane (Figure 30).

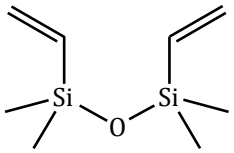

Figure 30: 1,3-divinyltetramethyldisiloxane, complexing agent within the so-called "Karsted-catalyst".

Although the method of hydrosilylation has been commonly used for decades the exact mechanism and active species still remain unclear. Yet it is assumed that colloidal platinum serves as an active species catalyzing the reaction. The general mechanism is depicted in Figure 31.

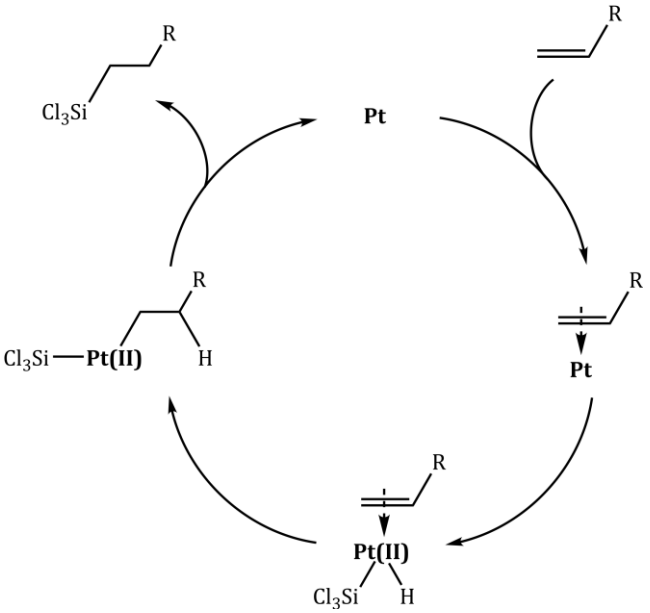

Figure 31: Assumed catalytic cycle of Pt during hydrosilylation mechanism. Colloidal Pt(0) is coordinated by the alkene's double bond and directs the addition of $HSiCl_3$.

The hydrosilylation of fluorous olefins was carried out in sealed stainless steel tubes under inert, solvent-free conditions, which eliminates the risk of solvent-related side-reactions and reduces not only costs but as well solvent-waste. Oligomerically pure silanes FnH2-$SiCl_3$ with n = 8,10,12 were obtained with typical yields of 80-90 %.

It was discovered during the experiments that reaction temperature has the strongest effect on the outcome of the synthesis. As to be expected, the required minimum reaction temperature increases with increasing chain length (n = 8: 70 °C; n = 10: 120 °C; n = 12: 160 °C). At lower reaction temperatures during the formation of F10H2-$SiCl_3$, an increased formation of the fluorinated alkane F-$(CF_2)_{10}$-CH_2-CH_3 as side-product was detected. Moreover, increased amounts of residual olefin were detected after low-temperature syntheses, so that a minimum temperature during conversion has to be maintained in order to achieve high yields of the trichlorosilane (Figure 32). It is unclear, whether this is purely an effect of temperature or rather a consequence of the increased pressure within the reaction tube induced by temperature.

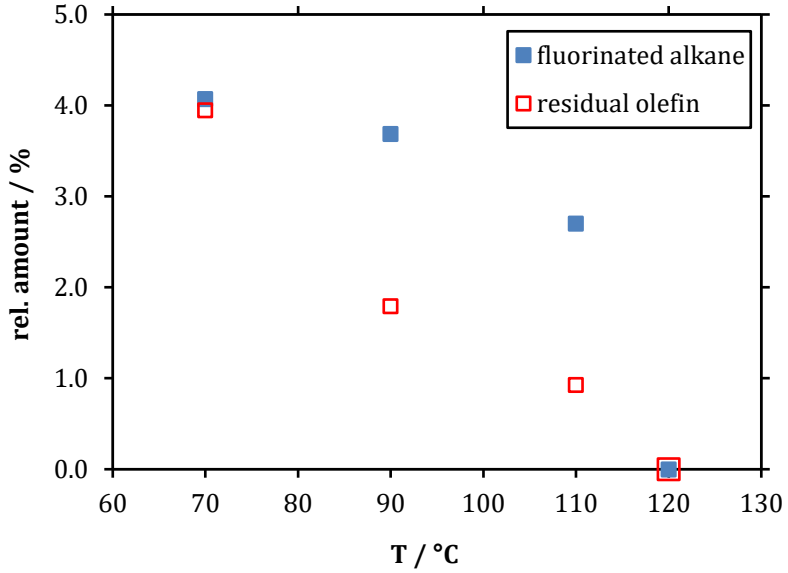

Figure 32: Effect of temperature on the hydrosilylation of fluorous olefins (n = 10). With increasing temperature, the amounts of residual olefin and fluoroalkane side-product decrease. Relative amounts are estimated based on 1H-NMR-integrals

Reaction durations were typically about 20 hours and although this minimum time should be maintained, no further improvement was detected at extended reaction times. The purification of the highly reactive and air-sensitive trichlorosilane products was accomplished via extractive methods using moisture-free organic and fluoro-organic solvents. Both during work-up and product analysis the low solubility particularly of long-chain compounds became a major difficulty in providing precursor substances. For example, in the case of F12H2-$SiCl_3$ NMR-analysis was only possible with fluorous perfluorohexane as a solvent and using an insert for external referencing. Even in this solvent, solubility was low and it has to be expected that longer-chain fluorous silanes will require more special solvents which assure both sufficient solubility and deuteration.

As for the formation of fluorinated olefins, also the hydrosilylation step was successfully applied for the formation of individual oligomers of long-chain trichlorosilanes and for oligomeric mixtures thereof. Apart from the general synthetic success, it confirms the applicability of this method to even higher olefins. These

long-chain olefins have not been converted individually so far, due to the lack of oligomerically pure starting materials. Apart from that, the obtained mixtures of fluorinated trichlorosilanes are of no further use for the preparation of monolayers because the individual oligomers of these highly reactive compounds cannot be separated effectively without major loss of material.

4.3.1. Provision of oligomerically pure silane precursors

The provision of reactants for precursor synthesis is a major concern during the work with fluorous monolayers. Although the reactions described can be accomplished successfully, long-chain products ready for monolayer deposition can only be obtained via separation of the oligomeric mixtures. As explained above, mixtures of fluorinated trichlorosilanes cannot be separated without major loss of material due to the highly reactive nature of these compounds. Any way of separation is limited to mixtures of fluorinated iodides or olefins.

Fluorous HPLC has already been introduced for the separation of Zonyl iodide telomers and serves as the method-of-choice during the synthesis of fluorous trichlorosilanes as well. As the separation by means of F-HPLC can be applied to either fluorous iodides or olefins as starting materials, it has to be decided which separation is to be preferred. This decision is easily made in favor of the separation of fluorous iodides for several reasons. The most evident reason is the simple observation of the iodides by standard UV-absorption during F-HPLC. While fluorous iodides show strong UV-absorption ($\varepsilon_{max} \approx 400$ L mol^{-1} cm^{-1}, $\lambda_{max} = 258$ nm, Figure 33), olefins absorb only weakly ($\varepsilon_{max} < 10$ L mol^{-1} cm^{-1}, $\lambda_{max} \approx 210$ nm, Figure 34) and high concentrations of the olefin, which would be detectable more easily, are difficult to achieve under chosen conditions.

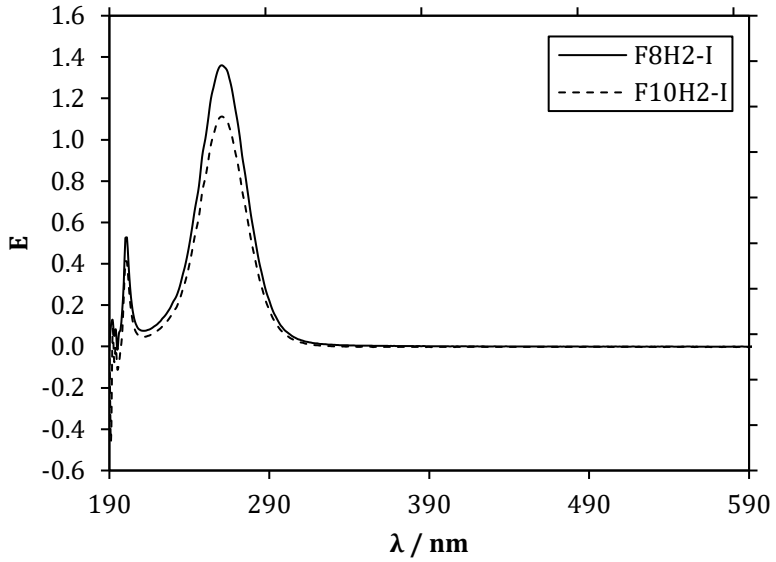

Figure 33: UV/Vis-spectrum of fluorous iodides F8H2-I (c = 3.3 mM) and F10H2-I (c = 2.5 mM). Sample solvent and reference background: MeOH:HFE-7100 4:1 (v/v). Maximum absorption is detected at λ_{max} = 258 nm

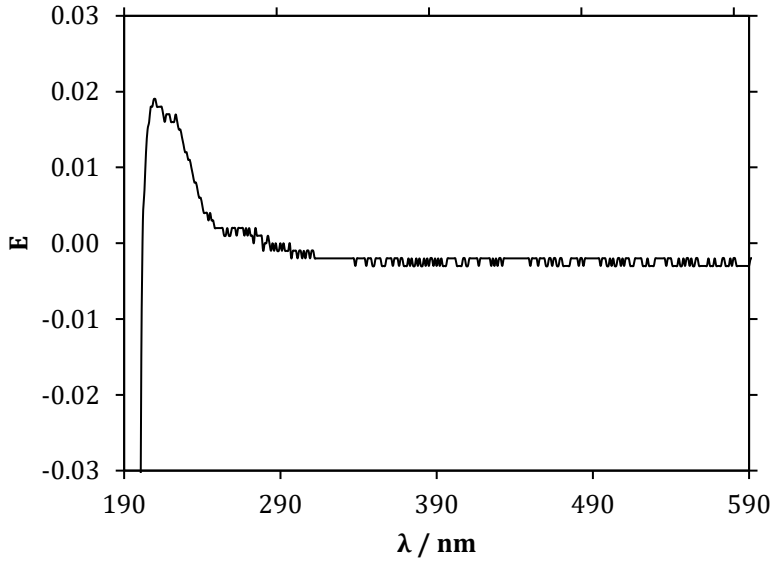

Figure 34: UV/Vis-spectrum of fluorous F8H2-olefin (c = 4.5 mM). Sample solvent and reference background: MeOH:HFE-7100 4:1 (v/v). Note the distinctly weaker absorbance compared to UV/Vis-spectra of fluorous iodides, which have been determined at lower concentrations (Figure 33).

Moreover, although the preparation of one olefinic mixture seems to be advantageous over several preparations of individual olefins at first (similar to the batch-wise preparation of fluorous thiols), this is not necessarily true. The synthesis of olefinic mixtures creates difficulties if a large variety of alkyl chain lengths is present. Long-chain iodides require high temperatures for the conversion to olefins and show poor solubility under standard conditions in general. Short-chain iodides however, tend to sublimate easily at high temperatures and are thus removed from a (high-temperature) reaction solution, so that mixtures of these iodides cannot be converted as controlled as individual iodides. In terms of the conversion of iodides it is therefore advisable to specifically adjust the reaction conditions (solvent, temperature, duration, etc.) to individual oligomers instead of using averaged conditions for mixtures. In addition to that, the synthetically straightforward conversion of iodides to olefins does not result in a mentionable increase of effort if individual syntheses are conducted.

During the introduction of Zonyl iodide telomers it has already been shown that optimization of the F-HPLC methodology yields conditions under which baseline separation is possible and fractions of individual iodide oligomers can be collected (Figure 22). These chain-length selected oligomers can serve as starting materials for the conversion to fluorous olefins and trichlorosilanes. Due to the limited technical capabilities for the deposition of monolayers from $FnH2\text{-}SiCl_3$ with $n > 10$, no further separations of iodides by means of F-HPLC were accomplished. Instead, resources of F-HPLC were focused on the provision of long-chain fluorous thiols, which could be applied successfully in the deposition of SAMs.

4.3.2. Handling of trichlorosilane precursors

Fluorinated trichlorosilanes are highly reactive compounds and are very sensitive to moisture. It is therefore crucial to ensure proper handling and storage of the precursors in order to avoid hydrolysis and condensation of the molecules. For commercial compounds, inert gas storage under argon was found to be sufficient as long as the inert atmosphere was maintained. During and after handling of the compounds, great care has to be taken in order to ensure the substance's integrity.

In terms of safe storage and simple processing during the coating process individual glass ampoules (4 mL total volume) filled with the silane of choice were developed during this work. One ampoule is used per deposition process and can be filled with a silane and volume of choice before it is degassed and sealed. Sealed ampoules can

be safely stored until they are required for a coating process, so that decomposition within a large precursor container is avoided.

Surprisingly, it was observed during the course of experiments that the silanes' reactivities differ dependent on the fluorous chain length in an unexpected manner. In contrast to the expected behavior, an increase in chain length seemed to increase the sensitivity towards hydrolysis. This lead to the circumstance that liquid short-chain trichlorosilane F8H2-$SiCl_3$ could be easily (though quickly) transferred into ampoules under ambient atmosphere, whereas the solids F10H2-$SiCl_3$ and F12H2-$SiCl_3$ hydrolyzed fast. Within a few moments of contact with ambient atmosphere, these solid silanes hydrolyzed and thus did not dissolve in chloroform any more, while the silanes itself are at least sparingly soluble in this solvent. Unfortunately, due to the special nature of these fluorous molecules, no further independent proof for this increased tendency towards hydrolysis could be obtained yet. Initial experiments based on similar effects published in literature using NMR spectroscopy [174] and light scattering methods [176] did not yield definite results and revealed that increased efforts beyond the scope of this work are necessary in order to investigate this effect under appropriate conditions. Reaction kinetics are simply too fast, so that a controlled hydrolysis of these trichlorosilanes cannot be accomplished and investigated by routine measures and equipment. However, Améduri *et al.* reported in their work on the same type of fluorous silanes that they observed an increased reactivity of the longer-chain compounds during the synthesis of trichlorosilanes from the respective olefins. [236] Moreover, Paso *et al.* detected an increased number of defects when they increased the chain length of fluorous silanes during SAM deposition from anhydrous solutions. [126] They attributed this effect to an increased number of particles that originated partly from the formation of hydrolyzed oligomers within the solution. Although the deposition of particles may have been a result of the silanes' low solubility in the solvent of choice (70 % *iso*-octance, 30 % carbon tetrachloride), it might as well be a consequence of increased reactivity and agglomeration of hydrolyzed molecules. These observations may relate to the effect of increased reactivity and might show that there actually is an increase in the tendency towards hydrolysis if the fluorous alkyl chain is extended. Certainty however, will only be obtained by further experiments explicitly addressing this issue.

Without the use of an inert gas glove box, solid silanes F10H2-$SiCl_3$ and F12H2-$SiCl_3$ could only be transferred under increased efforts and without knowledge of the exact amount of silane. For this, product silane was dissolved under inert conditions in a fluorous solvent in order to ensure a high amount of dissolved product per solvent volume. This solution (as a whole or in parts) was transferred into a glass ampoule

under inert atmosphere and the solvent was evaporated under a stream of argon, which was applied via a canula. Once the solvent was evaporated (almost) completely, the ampoule was attached to a vacuum system, cooled with liquid nitrogen and evacuated. By carefully warming the ampoule, all the residual solvent was removed and the ampoule was sealed. This procedure enabled the safe storage over several months and processing with no risk of hydrolysis. However, depending on the amount of silane which should be transferred, preparing only a single ampoule could take several hours. Moreover, the exact amount of silane transferred could only be estimated via the original concentration of the silane solution. The evident difficulties connected to this approach emphasize the need for improved technical abilities in handling and precursor provision.

4.4. Conclusion & Outlook

In conclusion, the synthesis of long-chain fluorous precursors can be achieved by organic chemistry methods in good yields at acceptable efforts. Thus, both fluorous silanes as well as fluorous thiols are available from commercial telomeric mixtures of the corresponding iodides. Nonetheless, great care has to be taken to ensure the purity of the individual oligomers.

A limiting factor is the poor solubility of reactants and products, so that measures have to be taken in order to guarantee sufficient solubility during F-HPLC-separation, synthesis and work-up. High-boiling toluene is therefore preferred over ethanol during the conversion of iodides to olefins and fluorous solvents enable good solubility for purification purposes of the final trichlorosilane. During the synthesis of fluorous thiols, product solubility is of importance during product recovery. In all cases, syntheses become more demanding when higher derivatives are to be converted what is caused both by lower solubility and higher melting points. Besides the precautions to be taken during synthesis, proper and careful handling is required with the final products. Particularly the highly reactive trichlorosilanes require special attention but also thiols have to be handled with care in order to avoid oxidation and formation of fluorous disulfides or sulfonates.

The successful synthesis of fluorous precursors is only half the way towards products that are ready for the deposition of SAMs and any of the longer-chain precursors can only be obtained after a tedious separation of telomeric mixtures along the way. It has

been shown in this work, that separation by means of F-HPLC is a suitable method to provide pure oligomers of thiols and iodides, which can be further converted to trichlorosilanes. Although this method is highly material- and time-consuming, there is no alternative source for these compounds yet. Future research and further development of this method, especially in terms of solvent and solvent recovery, are likely to yield improvements and a particular focus has to be put on the purity of the obtained materials. Once fluorous trichlorosilanes of substantially longer chain-length are available it will also be possible to develop new types of fluorous stationary phases, which will further improve the separation capabilities.

Another possible alternative are new synthetic pathways based on compounds that are easier to obtain than long-chain fluorous iodides. For example, the synthesis of fluorous olefins may be achieved by the conversion of fluorous carboxylic esters F-$(CF_2)_n$-COOR (R: *n*-alkyl substituent, commonly methyl/ethyl) via a multi-step chain extension. Fluorous esters are available with chain lengths $n \leq 17$, which exceeded available chain lengths of thiols and silanes in the beginning of this work. This highly experimental route has been developed based on individual literature syntheses and has not been described as a whole process in literature, especially in terms of very long fluorous chains. However, apart from problems arising from solubility, the strong inductive effect of the fluorocarbon chain is assumed to increase the overall reactivity of the compounds in comparison to hydrocarbon molecules. The overall synthetic route is presented in Figure 35. Chain extension is already conducted within the first stage (I) of the protocol by addition of dimethylsulfoxide (DMSO) to the ester of the fluorous carboxylic acid under basic conditions.[248,249] Geminal diol side-products of this reaction can be transferred to the next synthetic step (II) as both products may be used for the reduction to the corresponding alcohol.[248] After protection of the alcohol, the sulfoxide is reduced with trifluoroacetic acid (TFA) in the presence of NaI and the protective group is removed (III).[248] Subsequently, the olefin is formed by an elimination reaction via an intermediate episulfonium species (IV).[250] During the course of this work, this method had been initially tested for its applicability. Although the individual stages represent common reactions of organic chemistry, the extraordinary high grade of fluorination poses a huge challenge already with short fluoroalkyl chains. It was thus soon experienced that synthesis development required more attention than advisable and should be postponed as an individual project instead of getting in the way of "standard" procedures and F-HPLC development. By now, F-HPLC is able to deliver chain lengths greater than those accessible by commercially available fluorous carboxylic acids. Nevertheless, the method of chain-extension may be of interest in the future.

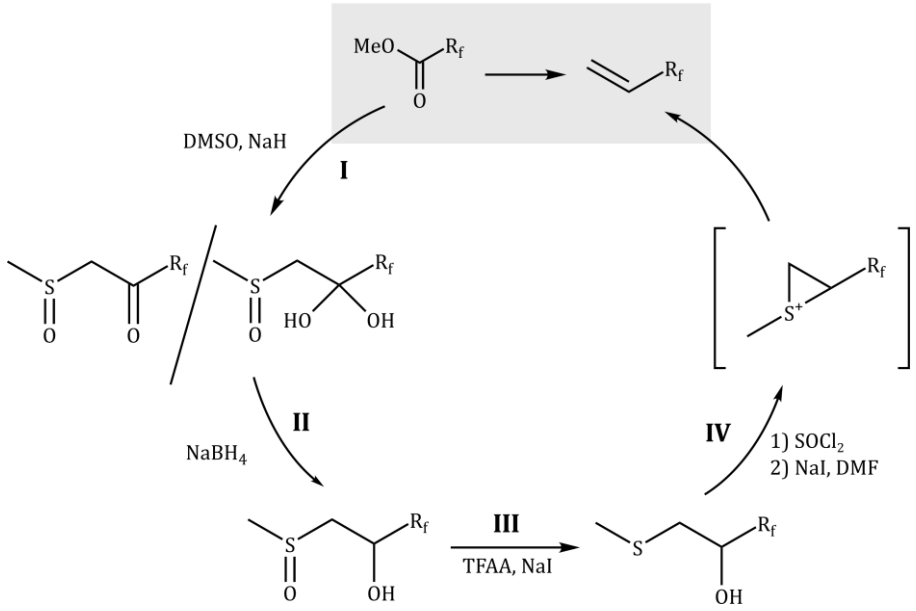

Figure 35: Suggested synthetic route for the chain extension of carboxylic esters.

This work has successfully opened up a route to the provision of long-chain fluorous compounds for the formation of SAMs and further applications. Although separation by F-HPLC is still at its beginnings it has already shown its potential for the provision of even longer chains and represents the only viable method to date that provides the means to supply these types of pure substances. Future improvements concerning F-HPLC solvents and chromatography columns have the potential to strongly simplify this process of telomer separation.

5. Binary SAMs from (fluoro-)alkyl thiols as a model system for molecular roughness

5.1. Deposition of single-component monolayers

The deposition of thiol monolayers from diluted solutions is a well-documented and robust method of preparation. Nonetheless, it requires a certain amount of experience and strictest care has to be taken in terms of cleanliness of substances and glassware.

Wetting experiments on monolayers deposited from singular thiol precursors yielded advancing contact angles with water of approximately $\theta_{adv}(W) \approx 120\,°$ and thus correspond well to values published in literature (see section 2.3.2, Table 2). This value represents an approximate value and only serves as a rough means of comparison. It was observed during the experiments that short-chain thiols (n = 6) are rather prone to relatively low values of $\theta_{adv}(W)$ and often lead to results of $\theta_{adv}(W) \approx 118.5°$ while thiols with chain-lengths of $n \geq 8$ show stable results of $\theta_{adv}(W) \approx 120.0°$ (Table 8, Figure 37). Similar to observations discussed in literature on the effect of increasing chain-lengths, this behavior may be interpreted as an indication of increased depositional integrity for longer-chain thiols, especially taking into account the risk of pre-depositional oxidation introduced later in this section. Nonetheless, all these values correspond to well-ordered monolayers and contact angles of pure, non-mixed samples served as a reliable first indication for the quality of a whole sample series. Samples not meeting these criteria were not considered for further experiments, although these cases were very rare.

Wetting experiments applying hydrocarbon squalane (Figure 36) as contacting liquid revealed a slightly larger variation in determined contact angles. On average, an advancing contact angle of approximately $\theta_{adv}(Sq) \approx 80\,°$ was observed. Similar to water experiments, the average contact angle was found to be smaller for short chains than for longer chains (Table 8, Figure 38). Initial wetting experiments with ethylene glycol showed the same increase with chain-length and yielded advancing contact angles of roughly $\theta_{adv}(Gly) \approx 96\,°$. However, experiments with ethylene glycol appeared to show stronger deviations between measurements, which may be a consequence of the strong hygroscopic character of this liquid. The results of wetting experiments and average contact angles determined throughout several systems are presented in Table 8.

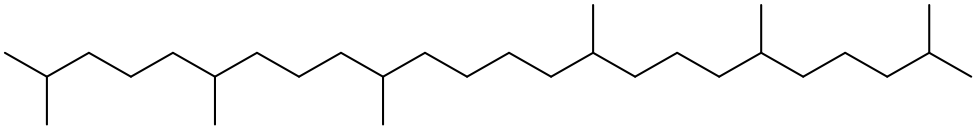

Figure 36: Chemical structure of hydrocarbon squalane (2,6,10,15,19,23-hexamethyltetracosane). Despite its size, squalane is a liquid while comparable paraffins are waxy solids.

FnH2-SH	**θ_{adv}(W) [°]**	**θ_{adv}(Sq) [°]**	**θ_{adv}(Gly) [°]**
6	118.6 ± 0.3	77.5 ± 0.5	93.0 ± 1.0
8	119.3 ± 0.4	80.1 ± 0.8	93.0*
10	119.5 ± 0.1	81.2 ± 0.6	96.0*
12	120.0 ± 0.4	81.5 ± 0.4	97.7 ± 0.8
14	120.7 ± 0.2	82.0 ± 0.4	98.3 ± 0.4

Table 8: Average advancing contact angles and standard deviations for water, squalane and ethylene gylcol wetting experiments on single-component monolayers prepared from fluoroalkylated thiols. *Only a small number of experiments with ethylene glycol was conducted. In these very cases, only a singular value was determined.

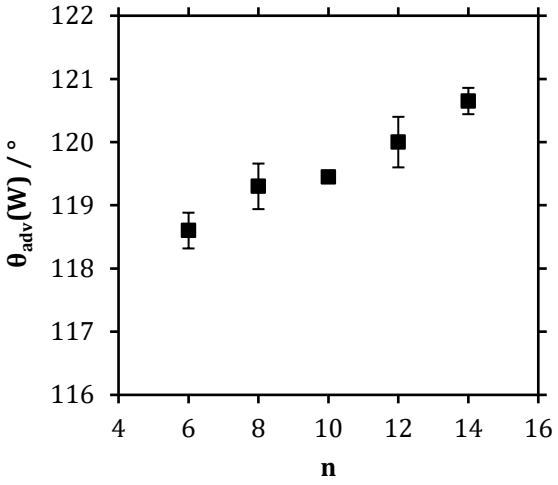

Figure 37: Advancing contact angle of water on single-component monolayers deposited from precursors FnH2-SH. Similar to literature, θ_{adv}(W) increases with increasing chain length.

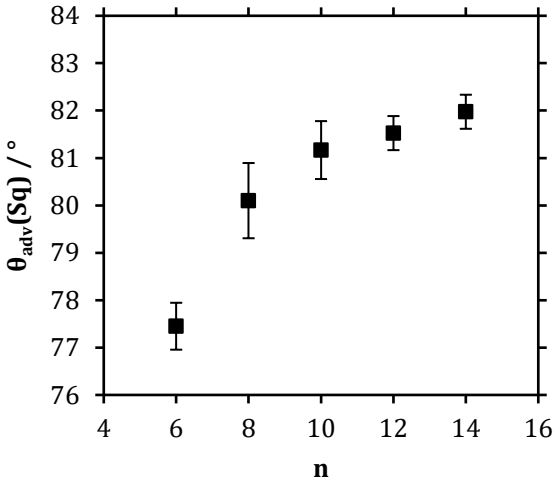

Figure 38: Advancing contact angle of squalane on single-component monolayers deposited from precursors FnH2-SH.

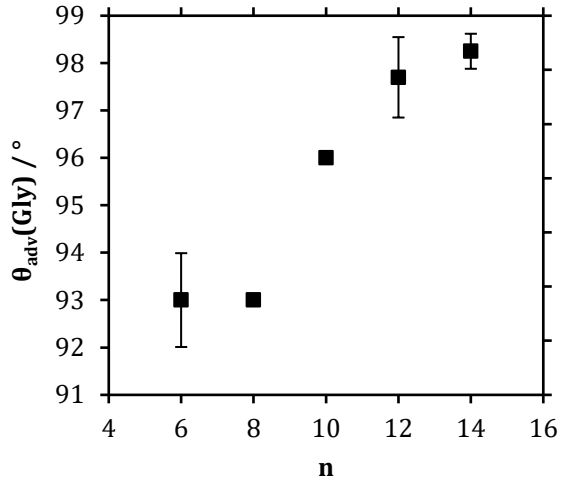

Figure 39: Advancing contact angle of ethylene glycol on single-component monolayers deposited from precursors FnH2-SH. The low value of n = 8 had only be measured once and is assumedly caused by an improper preparation concerning this very sample. For n = 8, 10 only singular measurements were conducted so that no standard deviation is given.

Monolayer deposition was extended to non-fluorinated SAMs from Hm-SH thiols during the course of this work. Analogously to fluoroalkylated SAMs, wetting properties of the single-component monolayers were determined. As expected, advancing contact angles increased with increasing chain-lengths of the thiol precursors and appeared to approach a saturation state. However, a decrease of θ_{adv} was detected for very long alkyl chains of H38-SH and to some extent H30-SH. As these precursors had been synthesized instead of being obtained commercially and were only applied for a few initial experiments, an undetected impurity might be assumed. Although post-synthetic analyses did not show residual impurities, already small amounts of introduced contaminations may lead to deteriorating effects within this sensitive environment.

Hm-SH	**θ_{adv}(W) [°]**	**θ_{adv}(Sq) [°]**	**θ_{adv}(Gly) [°]**
8	108.5	39.1	79.2
10	110.3	49.7	82.4
12	111.2	53.6	83.7
14	111.0	54.1	85.4
16	112.5	55.7	-
18	112.0	55.7	-
20	112.8	56.0	85.8
22	112.7	55.9	85.7
30	112.3	53.9	85.4
38	111.7	50.4	-

Table 9: Average advancing contact angles for water, squalane and ethylene gylcol wetting experiments on single-component monolayers prepared from non-fluorinated alkyl thiols.

As introduced in Section 2.4, sSIMS experiments were conducted as a reliable means of compositional analysis of the deposited monolayers. Characteristic fragment ions carrying intact precursor chains were observed in the experiments, which allowed the quantification of monolayer constituents within the SAM. These important fragment ions have been presented in Table 4.

During sSIMS analyses of SAMs from fluoroalkylated thiols, most intensive peaks were observed for gold (cluster) ions of Au_n^- and associated fragment ions of the form $Au_nF_yS_k^-$. Gold cluster ions Au_n^- were observed with decreasing intensities for increasing cluster sizes and weak intensities for clusters of n ≥ 6. Moreover, detected intensities were commonly stronger for cluster ions of odd-numbered n. Fragment ions $Au_nF_yS_k^-$ were detected in various combinations throughout the mass spectra. Commonly, fluorine and sulfur fractions were limited to values of y ≤ 2 and k ≤ 5 with decreasing peak intensities for increasing y and k. Moreover, odd/even effects could be observed for these ion species with n > 1. Species with even-numbered values of n showed ion intensities $Au_nF_1^- > Au_n^-$, while for odd-numbered ions observed intensities followed $Au_nF_1^- < Au_n^-$. Similar behavior was observed for species $Au_nF_1^-$ and $Au_nS_1^-$. Here, even-numbered values of n lead to $Au_nF_1^- > Au_nS_1^-$, while species with odd values of n caused behavior of $Au_nF_1^- < Au_nS_1^-$. Several fragment ions $C_xF_y^-$ were detected with y ≤ 2x+1. Among these ions, most intensive peak intensities were

observed for small ions with approximately $x \leq 4$. Within a mass range of approximately m/z = 250…400 Th several species of the form $AuC_xF_y^-$ were observed with intensities decreasing with increasing mass. Most intensive peaks were observed for ions with x = 2,3,4 and y = 4…8. These ion intensities decreased strongly for corresponding ions carrying more than one gold atom. Similar larger ion species $AuFC_xF_{2x+1}^-$ with supposedly intact small fluoroalkylated chains of $x \geq 4$ were observed analogously, although these species showed weaker intensities.

Monolayers from fluoroalkylated thiols were commonly analyzed by quantification of ion intensities from fragment ions $AuF(M-H)^-$ with M representing the molecular mass of the thiol of interest FnH2-SH. Further fragments carrying intact precursor chains were of lower intensities. Among these fragments were ions $(M-H)^-$, $Au(M-H)^-$ and corresponding cluster ions $Au_nF_y(M-H)_l^-$ and $Au_n(M-H)_l^-$. The latter species $Au_n(M-H)_l^-$ were commonly observed for fragments of l = n ± 1 and were of only low intensities for n > 3. Intensities of ions $Au_nF_y(M-H)_{l>1}^-$ decreased strongly compared to $AuF(M-H)^-$, were only observed for $n \leq 3$ and thus were not used for analyses.

Quantification of $AuF(M-H)^-$ ion intensities was in some cases hampered by the appearance of alternative fragments of identical nominal masses. However, these ion intensities could be resolved according to their exact molar masses or could be attributed to adducts of thiolate fragments. Thus, particularly low-molecular-weight thiolate fragment ions of F4H2-SH and F6H2-SH were obscured by fragment ion species of the form $C_xF_{2x+1}S_2C^-$ (x = 8, 10) during the analysis of single-component monolayers from FnH2-SH with $n \geq 8$ and indicated short-chain residues within the monolayers. Analysis of exact molar masses revealed that the apparent peak was shifted to lower masses than expected for the characteristic fragments $AuF(M-H)^-$ from F4H2-SH and F6H2-SH. This shift was clearly evident via the comparison of the correct peak intensities from short-chain versus long-chain monolayers. The slight shift of ion intensities from the $C_xF_{2x+1}S_2C^-$ series could be reliably assigned through the accuracy of mass intensity assignments exhibited for the whole of sSIMS analyses. For example, the experimental masses for ions $AuF(M_{F4H2}-H)^-$ and $AuF(M_{F8H2}-H)^-$ within their single-component monolayers showed only slight deviations from their theoretical, exact masses and could be commonly assigned with a deviation of approximately 0.005 %. Additionally, slight shifts in observed masses were usually detected for positive deviations to larger masses, only. Assigning the exact masses of ions $AuF(M_{F4H2}-H)^-$ or $AuF(M_{F6H2}-H)^-$ to the experimentally determined, "shifted" peak masses leads to a

negative deviation of -0.007 % while assignment of $C_8F_{17}S_2C^-$ or $C_{10}F_{21}S_2C^-$, respectively, resulted in a deviation of only +0.0002 %.

Additionally, the analysis of single-component monolayers commonly revealed mass intensities which corresponded to masses of twice the chain-length than applied during monolayer preparation. For example, next to ion intensities from $AuF(M_{F4H2} - H)^-$ (m/z = 495 Th), considerable intensities were detected for $AuF(M_{F8H2} - H)^-$ (m/z = 695 Th) in monolayers from F4H2-SH. The intensities of supposed long-chain impurities were typically within a range of 5-8 % of the intensity of the primary thiol fragment ion. Actual contaminations could be excluded by analysis of characteristic fragment ions other than $AuF(M - H)^-$ for the long-chain thiolate. The appearance of high-mass ion intensities in low-mass samples was attributed to the formation of fragment ions of the form $Au(M_{FnH2} - H)(C_nF_{2n+1})^-$, which lead to adducts of identical molecular composition as expected from chain-extended thiolates. Similar types of adducts were assumed for the appearance of equivalent masses at $Au(M_{FnH2} - H)(C_xF_{2x+1})^-$ with x < n, which would correspond to residues of precursors F_{n+x}H2-SH with slightly larger chain-lengths. Also in these cases, no further characteristic fragment ions of the corresponding thiolates were detected and these adducts were observed with lower intensities than adducts of x = n.

fragment ion	**commonly observed species**
$Au_nF_yS_k^-$	n ≤ 10, 0 ≤ y ≤ 2, 0 ≤ k ≤ 5 (≤ 2 if y = 0)
Au_n^-	n ≤ 13, $I(Au_{n,even}) < I(Au_{n,odd})$
$C_xF_y^-$ / $AuC_xF_y^-$	various x, y
$AuFC_xF_y^-$	y = 2x+1
$Au_n(M - H)_l^-$	n ≤ 3, l = n ± 1, and n=0, l = 1
$Au_nF_y(M - H)_l^-$	n = y = l = 1

Table 10: Overview of most intensive fragment ions detected during sSIMS experiments with fluorinated monolayers

In some cases, particularly films deposited from liquid short-chain thiols (n = 6, 8) exhibited considerable amounts of impurities of the corresponding fluoroalkyl sulfonates FnH2-SO_3^- detected by sSIMS. These impurities can result from pre-deposition oxidation of thiols as well as degradation of improperly stored deposited samples. In most cases, sulfonate species were primarily detected for samples prepared from older thiol batches, which suggests pre-deposition oxidation. Interestingly, solid thiol precursors with n ≥ 10 almost exclusively did not show any sign of oxidative degradation, independent from the original source, indicating an improved stability compared to shorter-chain liquid thiols. Such pre- and post-deposition oxidation can already be caused by dilute ozone under ambient atmosphere conditions and has been discussed primarily on the basis of non-fluorinated thiols and SAMs thereof. [138–140,251,252] At least for (non-fluorinated) alkylated thiols it has been reported that sulfonate residues within a monolayer could be substituted for thiolate chains by simple exposition of the degraded sample to a fresh thiol solution. [252] This behavior would rather suggest a post-deposition degradation during storage in contrast to the assumption of deteriorated thiol batches. In any case, the exact methods of handling, deposition and storage will have a vital effect on the fate of the respective sample. During this work, the exact origin of the increased risk of oxidation, including the influence of fluorous alkyl substitution, was not investigated in detail, particularly as for the majority of thiols no sulfonate impurities were detected. Nonetheless, the preparation of samples containing liquid thiols was conducted with even increased caution and care, which lead to a significant improvement and the occurrence of contaminated films was effectively reduced.

Analogously to sSIMS experiments with fluoroalkylated monolayers, non-fluorinated SAMs showed various fragment ions corresponding to species $C_xH_zS_k^-$. Most intensive peaks were observed for CH^-, C_2H^-, $C_3H_2^-$, $C_4H_3^-$ and SH^-, CSH^- and C_2SH^-. Fragment ions $Au_nS_k^-$ were observed with medium to strong intensities decreasing with increasing n. Further decrease was observed with increasing k, leading to weak intensities for k ≥ 4. Exceptionally increased intensities were observed for fragments of k = 2 in ions of even-numbered n. Related species $Au_nS_kH_z^-$ were detected with varying intensities, commonly similar to their non-hydrogenated form if z = 1. Ions $Au_nH_z^-$ were detected with decreasing intensities for increasing n or z. Relative to Au_n^-, peaks are found more intensive if n was odd-numbered.

Fragment ions $(M-H)_l^-$ were only detected with medium intensities, strongly decreasing for l ≥ 2. Suitable fragments for quantification with high intensities were ions $Au_n(M-H)_l^-$, which were particularly detected for $l = n \pm 1$ with $(l = n-1) > I(l = n+1)$. For $l \neq n \pm 1$, the H-adduct $Au_nH(M-H)_l^-$ was found to be

more intensive than its parent-ion. The intensity of $Au_n(M-H)_l^-$ was observed to decrease with increasing n + l, and most intensive species were $Au_2(M-H)_1^-$, $Au_1(M-H)_2^-$ and $Au_2(M-H)_3^-$. Oxidized species $(M-H)_lS_kO_p^-$ were particularly detected for l = 1 with k = 0,1. Intensities of higher species were very low. Sulfonate species occurred more frequently than in fluorinated monolayers and commonly, weaker intensities were observed for increasing chain-lengths.

fragment ion	**commonly observed species**
$C_xH_z^-$	$x \le 6, z \le 5; I(C_xH_{z,even}) < I(C_xH_{z,odd})$
$C_xH_zS_k^-$	various x, z, k
Au_n^-	$n \le 15; I(Au_{n,even}) < I(Au_{n,odd})$
$Au_nH_z^-$	$n \le 8, z \le 2; I(Au_{n,odd}H_1) < I(Au_{n,even}H_1)$
$Au_nS_k^-$	$n \le 13$, various k; $I(Au_{n,even}S_1) < I(Au_{n,odd}S_1)$
$Au_nS_kH_z^-$	analogous to $Au_nS_k^-$
$(M-H)_l^-$	l = 1
$(M-H)_lSO_3^-$	l = 1
$Au_n(M-H)_l^-$	$n \le 5$, $l = n \pm 1$, and $n = l$ for $n \le 2$; $I(Au_nM_{q=n+1}) < I(Au_nM_{q=n-1})$
$Au_nH(M-H)_l^-$	$n \le 3, l \le n+1$
$Au_n(M-H)_lS_k^-$	$n \le 3$ for l, k = 1

Table 11: Overview of most intensive fragment ions detected during sSIMS experiments with non-fluorinated monolayers.

5.2. Random composition of binary mixed monolayers

Besides the requirement of well-ordered monolayers, the verification of the random distribution of thiolate chains within a film is the most important prerequisite for this study. Films exhibiting separated domains of long or short thiolate chains lack the existence of random topographical features in the sub-nm regime and are not suitable to study effects beyond the macroscopic Wenzel and Cassie-Baxter models.

The randomness of chain distribution can be independently confirmed by two different methods based on sSIMS. While the first method relies on thermodynamic parameters of film formation, the second method is based on the evaluation of the occurrence of dimeric species during sSIMS experiments.

According to Folkers *et al.* the compositional homogeneity of a binary mixed monolayer system deposited from two precursor species can be evaluated by its interaction parameter ω ([205], Section 2.4). In consequence, a monolayer with $0 \leq \omega < 2$ kT can be regarded as fully miscible in terms of its thiolate species and thus represents a randomly mixed film. Analysis of charactersitic precursor fragment ions by means of sSIMS allows for the quantitative determination of the amount of deposited long or short precursor chains within the monolayer. [253] Thus, the adsorption isotherm of a specific system can be obtained via a series of deposition experiments and thermodynamic parameters ω and R_0 can be derived and evaluated. Interaction parameter ω as a measure of random distribution of chains within the binary thiol SAMs is thus directly accessible as a first proof of the desired random mixture within a film.

Exemplarily, Figure 40 represents the adsorption isotherm for a system deposited from F8H2-SH and F12H2-SH obtained from curve fitting of the experimental results. With ω = (1.4 ± 0.15) kT the interaction parameter is below the threshold value of 2 kT and complete mixing of the precursor molecules can be expected resulting in a random distribution of the film's constituents. Depending on the choice of precursor molecules de- and increased values of ω are obtained for the systems investigated in this study. The sum of the molar ratios x_{long} and x_{short} is represented by the open triangles and yields the expected value of 1 within a typical error of ± 2 %.

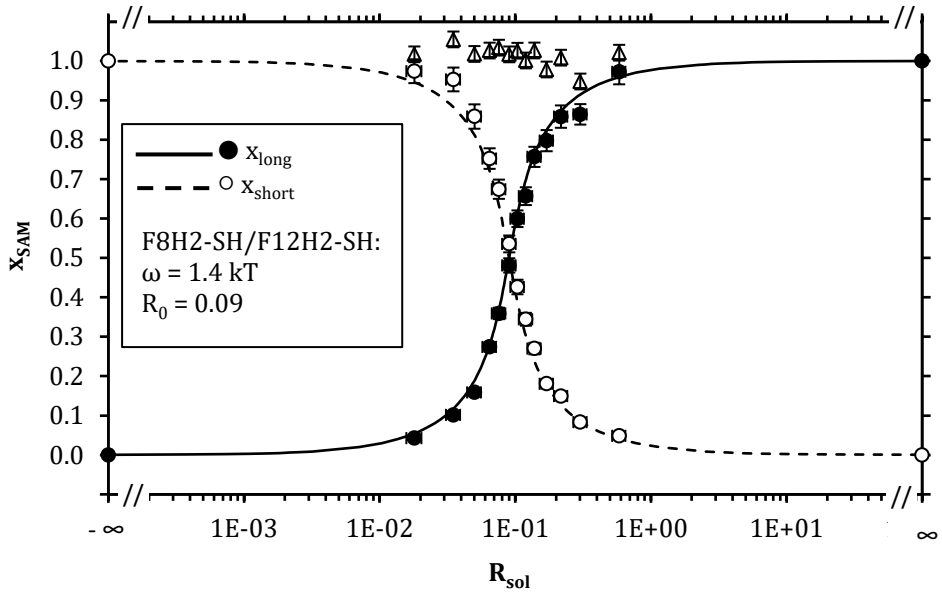

Figure 40: Adsorption isotherm for a SAM with x_{long} = F12H2-SH and x_{short} = F8H2-SH. Solid and dashed lines represent the results of curve fitting of the experimental values obtained by sSIMS (circles), which yield the interaction parameter ω = 1.4 kT. Hence, complete mixing of thiolate chains is expected. Open triangles represent the sum of x_{long} and x_{short}.

The second possibility to confirm the random nature of a film relies on the quantitative analysis of dimeric fragment ions from sSIMS. As investigated by Arezki *et al.* it can be shown by Monte Carlo simulation studies that in sSIMS fragmentation certain dimeric ion species are almost exclusively formed by thiolate chains which have been nearest neighbours in the film prior to ion bombardment ([206], Section 2.4). The binary systems investigated here consist of long and short thiolate chains, so that dimeric fragments of long-long, short-short and long-short combinations ("n_{xx}") are observed ($\left[\mathrm{Au}(\mathrm{M_{long}}-\mathrm{H})_2\right]^-$, $\left[\mathrm{Au}(\mathrm{M_{long}}-\mathrm{H})(\mathrm{M_{short}}-\mathrm{H})\right]^-$, $[\mathrm{Au}(\mathrm{M_{short}}-\mathrm{H})_2]^-$). The experimentally observed relative intensities of these dimeric ions can be compared with the intensities expected from statistical calculations (equation (14)). This comparison is presented in Figure 41 for a F8H2-SH/F12H2-SH system and it is easily observed that the experimental results match the theoretical expectations very well.

$$n_{long-long}: n_{long-short}: n_{short-short} = x_{long}^2 : 2x_{long}x_{short} : x_{short}^2 \qquad (14)$$

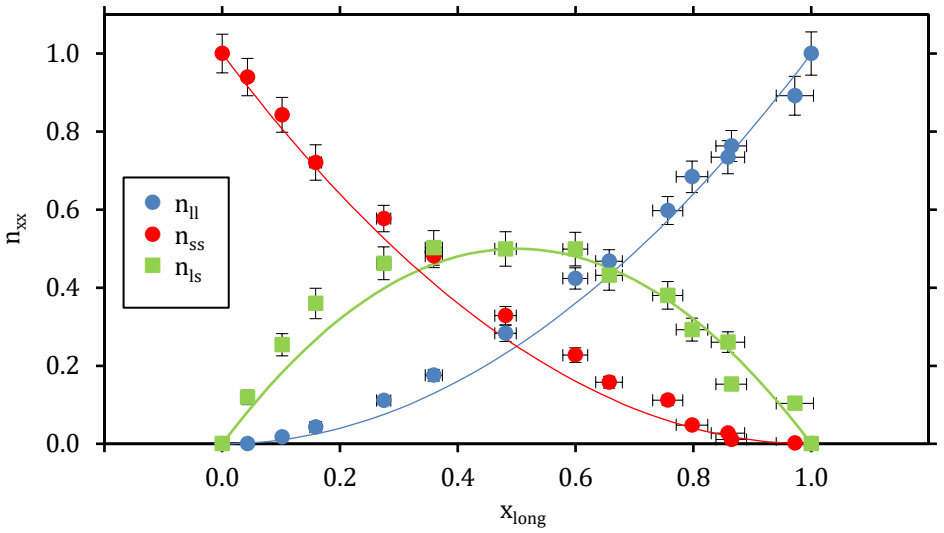

Figure 41: Relative amounts of dimeric secondary ions n_{xx} as detected in sSIMS for a SAM with x_{long} = F12H2-SH and x_{short} = F8H2-SH (ll: long-long, ss: short-short, ls: long-short). Solid lines represent the expected theoretical amounts.

Both these criteria have been applied for the confirmation of the random distribution of thiolate chains within the deposited monolayer films throughout this study (Table 12). The investigated SAMs were completely mixed on the molecular scale according to these methods, although distinct trends in the miscibility could be observed. These effects will be discussed in correlation with the films' wetting properties later in this chapter. R_0 and ω of the monolayer systems were determined with approximate uncertainties of $\Delta R_0 = \pm 0.01$ and $\Delta\omega = \pm 0.15$ kT.

n_{short}	n_{long}	Δn	R_0	ω/kT
6	10	4	0.07	0.90
6	12	6	0.03	1.80
6	14	8	0.02	2.00
8	10	2	0.30	0.30
8	12	4	0.10	1.40
8	14	6	0.04	1.70
10	12	2	0.53	0.05
10	14	4	0.21	0.70
12	14	2	0.55	0.05

Table 12: Overview of compositional parameters R_0 and ω/kT for fluoroalkylated SAMs. Approximate uncertainties of the determinations are $\Delta R_0 = \pm 0.01$ and $\Delta\omega = \pm 0.15$ kT.

For non-fluorinated hydrocarbon monolayers, an increased tendency to form phase-separated domains due to attractive van-der-Waals interactions of equal-length alkyl chains may be assumed to occur. However, sSIMS results did not support this effect in case of the prepared systems and random distribution of thiolate chains was confirmed analogously to fluoroalkylated thiol SAMs (Table 13).

m_{short}	m_{long}	Δm	R_0	ω/kT
8	20	12	0.05	1.8
10	22	12	0.05	1.9
12	18	6	0.17	1.2
12	20	8	0.09	1.4
12	30	18	0.02	1.4
14	30	16	0.04	1.3
14	38	24	0.05	0.7
16	20	4	0.27	0.8
18	20	2	0.46	0.2

Table 13: Overview of compositional parameters R_0 and ω/kT for non-fluorinated alkyl SAMs. Approximate uncertainties of the determinations are $\Delta R_0 = \pm 0.01$ and $\Delta\omega = \pm 0.15$ kT.

5.3. Increase of film thickness corresponds to molar composition

Ellipsometry experiments were conducted in order to investigate the films' thicknesses, particularly regarding the relative increase of layer thickness per fluoromethylene unit throughout a sample series. Considering the limited accuracy of ellipsometry, the absolute values of film thickness are not compared in detail.

In any sample series the molar ratio of the longer-chain component is increased per subsequent samples, so that one finds a steady enrichment of longer chains compared to a decreasing fraction of short chains. This circumstance leads to the effect that the average film thickness of the series increases with increasing molar ratio of longer chains and eventually approaches the value of a monolayer consisting of long-chain precursors only. The determination by ellipsometry lacks the accuracy that is necessary to determine absolute values for film thicknesses. [134,254,255] However, the determination of relative thicknesses between individual samples is possible with sufficient accuracy. Figure 42 and Figure 43 present the results of film thicknesses determined by ellipsometry as a function of the molar fraction of the longer-chain component in a F8H2-SH/F14H2-SH- and F8H2-SH/F10H2-SH-series. Linear

regression yields an increase of 1.24 Å per CF_2-unit for the F8H2-SH/F14H2-SH system and 1.58 Å for F8H2-SH/F10H2-SH. These results compare well to the value of 1.23 Å per CF_2-unit reported in literature. [134] Other systems give similar results reflecting the increase of long-chain components and ellipsometric data relate well to data published in literature.

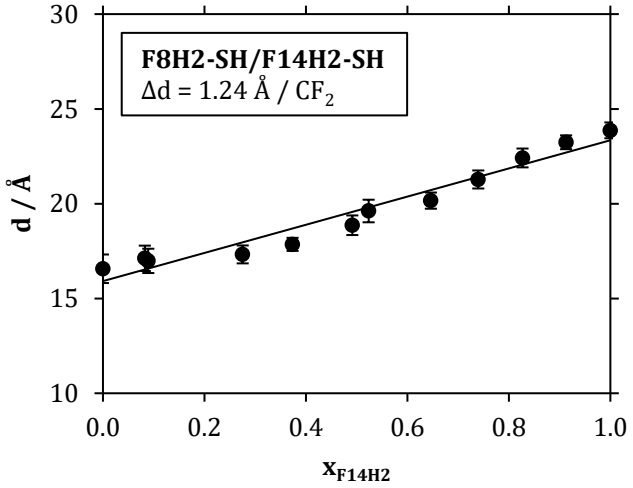

Figure 42: Ellipsometric thicknesses of a series of binary mixed monolayers of the system F8H2-SH/F14H2-SH.

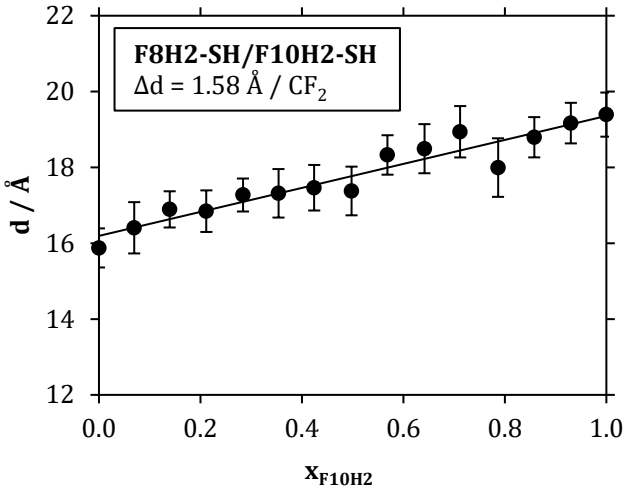

Figure 43: Ellipsometric thicknesses of a series of binary mixed monolayers of the system F8H2-SH/F10H2-SH.

5.4. Effect of sub-nm topography on wetting properties

The impact of molecular roughness on the wetting properties of different (fluoro)alkylated thiol SAM-systems has been studied using polar and non-polar liquids as contacting media during dynamic contact angle experiments. Binary mixed monolayers were deposited from varying combinations applying thiols FnH2-SH with chain lengths of n = 6…14 and complementary Hm-SH with m = 8…38.

Exemplarily, the results of dynamic wetting experiments with water as contacting liquid on a binary mixed monolayer deposited from thiols F8H2-SH and F12H2-SH are depicted in Figure 44. Results are presented as a function of the molar composition of the monolayer in terms of the molar fraction x_{F12H2} of the longer chain thiol F12H2-SH. Hence, flat surfaces are expected at $x_{F12H2} = 0$ (pure F8H2-SH monolayer) and $x_{F12H2} = 1$ (pure F12H2-SH monolayer), whereas in-between mixtures of long and short thiolate chains create structured surfaces. From a thermodynamic point-of-view, this binary monolayer represents a quasi-ideal system exhibiting complete miscibility and random distribution of precursor molecules in the deposited film ($\omega = 1.4$, $R_0 = 0.10$, see Table 14). The choice of precursor thiols results in only a small difference in molecular chain length ($\Delta h = 5.0$ Å [134]) but despite this

small scale of topographical features an effect on wetting properties is clearly observable. While pure monolayers yield wetting behavior well-comparable to literature as described above, binary mixed films lead to an increase in advancing contact angle θ_{adv}(W) with increasing surface roughness. Maximum θ_{adv}(W) is detected at $x_{F12H2} \approx 0.5$, which represents a surface of equimolar amounts of long and short thiolate chains and therefore the film of largest molecular roughness within this system. The difference between the maximum increase of θ_{adv} at $x_{long} = 0.5$ and an averaged base value of the pure monolayers is introduced as a parameter $\Delta\theta_{adv,max}$ (equation (15)).

$$\Delta\theta_{adv,max} = \theta_{adv}(x_{long} = 0.5) - \frac{\theta_{adv}(x_{long} = 1) + \theta_{adv}(x_{long} = 0)}{2} \qquad (15)$$

Compared to the pure films prepared from single-component precursor solutions the increase of θ_{adv}(W) for a film with $x_{long} = 0.5$ is $\Delta\theta_{adv,max}$(W) ≈ 4°.

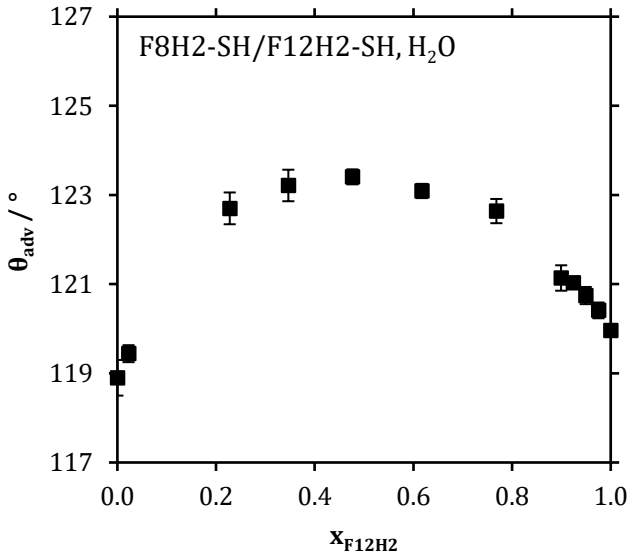

Figure 44: Results of dynamic contact angle measurements with water on a sample series deposited from F8H2-SH/F12H2-SH (NT-849(12)).

In contrast to the evident effect at this scale of surface roughness on liquid wetting with water, there is no noticeable effect on the contact angle using hydrocarbon squalane as contacting liquid (Figure 45). For samples with increasing x_{F12H2} θ_{adv}(Sq) shows a linear increase towards the value obtained for the pure F12H2-SH monolayer without detectable deviations.

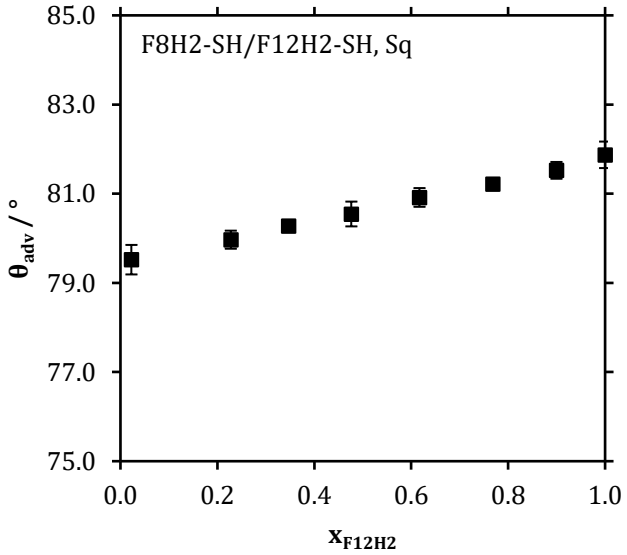

Figure 45: Results of dynamic contact angle measurements with squalane on a sample series deposited from F8H2-SH/F12H2-SH (NT-849(12)).

For monolayer systems with larger chain length differences, an effect can be detected even for wetting experiments with squalane. For example, Figure 46 represents the squalane-results for a monolayer deposited from F8H2-SH and F14H2-SH with a difference in chain length of Δh = 7.5 Å. Although small compared to the effect for wetting experiments with water, a decrease in θ_{adv}(Sq) can be detected for squalane, attaining values of $\Delta\theta_{adv,max}$(Sq) ≈ -1.7°. Wetting experiments with water yield a maximum increase of $\Delta\theta_{adv,max}$(W) ≈ 6.2° (Figure 47).

Along with an increase in chain length difference a tendency to form less homogeneously mixed films is detected. Evaluation of sSIMS experiments yield values of ω = 1.7 and R_0 = 0.04 (see Table 14) and suggest an increased risk of aggregation of identical precursor chains. Consequently, both the results for water as well as for

squalane show that complete mixing of the components may be less favored for this system than it was for smaller chain-length differences and therefore suffer a certain deviation from the expected "idealized" behavior. Thus the changes in θ_{adv} are not as centered around $x_{long} = 0.5$ anymore as they are for small values of Δh and deviations from idealized behavior become more evident.

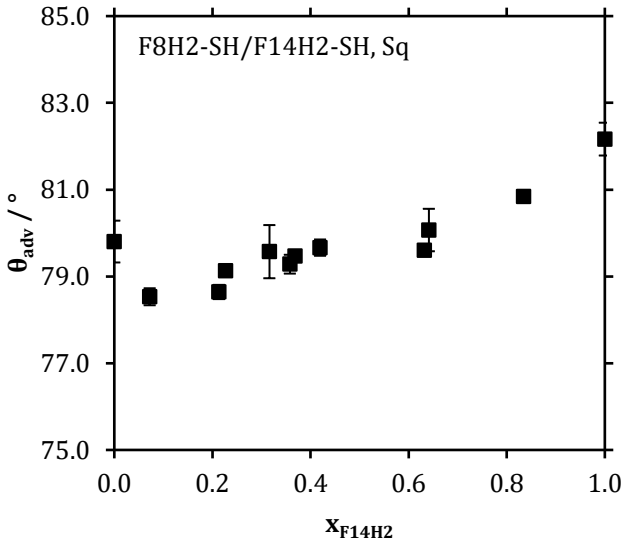

Figure 46: Results of dynamic contact angle measurements with squalane on a sample series deposited from F8H2-SH/F14H2-SH (NT-977(12)).

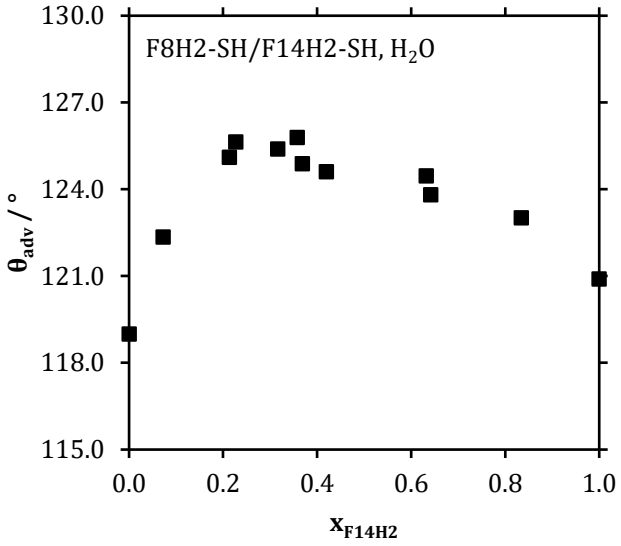

Figure 47: Results of dynamic contact angle measurements with water on a sample series deposited from F8H2-SH/F14H2-SH (NT-977(12)).

The monolayer system prepared from F10H2-SH and F12H2-SH serves as an example for two solid precursors with the smallest chain length difference of $\Delta h = 2.5$ Å. This small difference accompanied by the circumstance that two solid precursors are applied instead of one liquid and one solid thiol leads to a high degree of homogeneity within the film. Thus, values of $\omega = 0.05$ and $R_0 = 0.53$ are obtained by sSIMS analysis. In terms of wetting properties, these characteristics lead to only a small increase in θ_{adv} with water ($\Delta\theta_{adv,max}(W) = 2.8°$) and no roughness-induced effect for wetting experiments with squalane is observed. This behavior is in agreement with the expectations from previous experiments. The results of this and the two previous systems are summarized in Table 14 together with further systems which have been investigated.

n_{short}	n_{long}	Δn	R_0	ω/kT	$\Delta\theta_{adv,max}$(W) [°]	$\Delta\theta_{adv,max}$(Sq) [°]	$\Delta\theta_{adv,max}$(Gly) [°]
6	10	4	0.07	0.90	-*	-*	-*
6	12	6	0.03	1.80	6.0	-1.0	6.9
6	14	8	0.02	2.00	5.3	-0.9	-
8	10	2	0.30	0.30	1.7	-0.1	-
8	12	4	0.10	1.40	4.2	-0.2	5.1
8	14	6	0.04	1.70	6.6	-2.0	6.3
10	12	2	0.53	0.05	3.2	0.0	-
10	14	4	0.21	0.70	4.4	-0.7	4.2
12	14	2	0.55	0.05	1.7	-0.1	2.2

Table 14: Overview of wetting experiments with fluoroalkylated binary mixed monolayer systems studied in this work. *For F6H2-SH/F10H2-SH samples, only sSIMS-experiments have been conducted.

5.5. Discussion of surface roughness and its effect on wetting results

The observed effects of increasing water contact angles are expected to be the result of molecular scale roughness which is introduced by varying the chain lengths of the precursor molecules. It is therefore reasonable to take a closer look at the experimental results as a function of chain length difference Δn or height difference Δh, respectively.

Figure 48 presents the cumulated results of Table 14 in terms of the maximum increase of the advancing water contact angle $\Delta\theta_{adv,max}$(W) as a function of Δn. Except for the low value at largest chain length difference (Δn = 8) $\Delta\theta_{adv,max}$(W) steadily increases with increasing Δn by approximately 2° per two fluoromethylene units. As the height of topographical features increases with Δn this result supports the assumption of increased dewetting on binary mixed layers with increasing precursor chain lengths. The behavior is in accordance to an increase of the Wenzel roughness factor.

The relatively low value at $\Delta n = 8$ is assumed be a consequence of the increased tendency of phase-separation within this system. The applied thiol precursors possess fluorous backbones of highly different chain lengths which results in a high value of interaction parameter ω. This means that surface roughness would decrease for this system in comparison to systems with lower ω due to an increased fraction of same-height-areas consisting of identical precursors. Moreover, the increased sensitivity of liquid F6H2-SH and monolayers thereof towards oxidation and incorporation of sulfonate impurities might cause wetting results to deviate from an expected idealized behavior. Investigations of even higher chain length differences (for liquid/solid as well as solid/solid thiol combinations) will be necessary to gain more insight into wetting effects at the scale of $\Delta n \geq 8$.

As the observed changes in $\theta_{adv}(Sq)$ for experiments with squalane are very small, no conclusive tendency concerning a maximum decrease in $\theta_{adv}(Sq)$ can be derived. Nonetheless it is assumed that $\Delta\theta_{adv,max}(Sq)$ will decrease with increasing chain length difference Δh, which will be accessible with future precursor chain lengths.

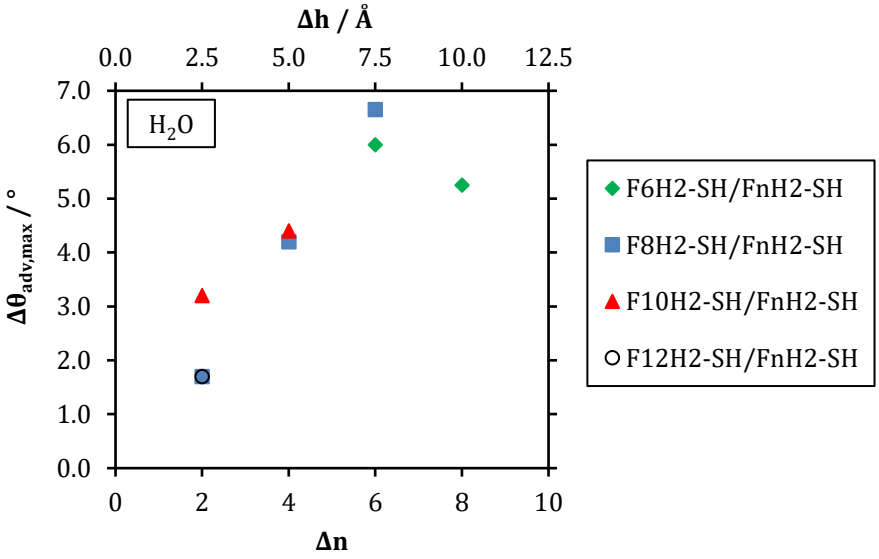

Figure 48: Results for maximum increase of advancing water contact angle $\Delta\theta_{adv,max}(W)$ on binary mixed fluorinated monolayers with respect to the choice of short-chain thiol.

It has already been observed for the samples' wetting behavior that at high degrees of Δn also ω tends to increase and that contact angles are affected accordingly. The effect on ω is visualized in Figure 49, where the increase of ω with Δn is clearly evident over the entire number of systems.

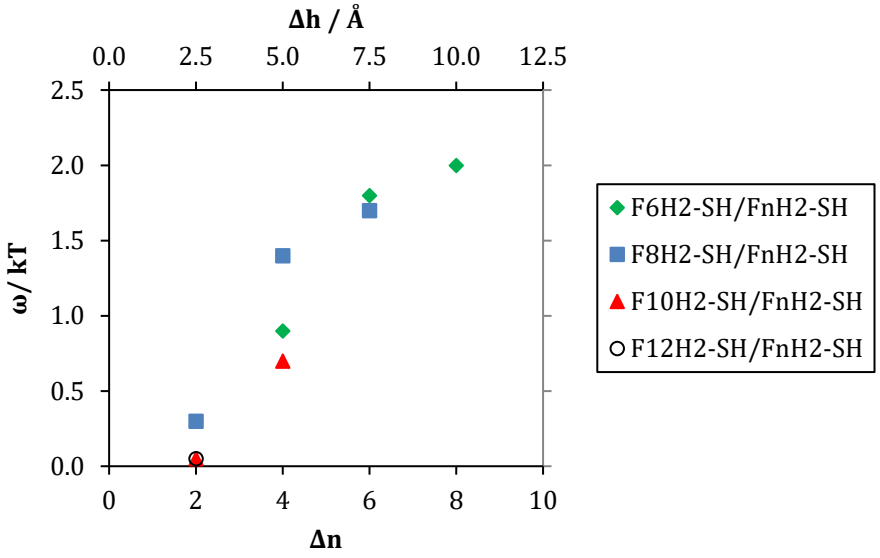

Figure 49: Analysis of ω as a function of chain length difference Δn with respect to the choice of short-chain thiol.

Taking into account only samples with identical short-chain thiol (e.g. $n_{short} = 6$) the influence on ω reoccurs in the same manner and the interaction parameter increases with chain length difference Δn for all possible sub-groups. These results suggest that ω, as expected, increases with increasing chain length difference and leads to an increased risk of phase separation within the binary films. Apart from one deviation for systems with Δn = 4 (i.e. F8H2/F12H2), the obtained experimental results for ω within one group of identical Δn are of similar size and suggest that, primarily, ω depends solely on the chain length difference and not on total chain lengths. However, particularly this "suspicious" system is very well investigated and documented, so that obtained values are assumed to be correct (compare sections 5.2 and 5.4). A reason for this behavior may be found in the structural characteristics of the corresponding pure monolayers. Figure 50 summarizes the results of tilt angle determinations for thiol monolayers of different chain lengths published in literature.

Although deviations occur among the data, which have been determined using varying experimental methods, it can be deduced that the tilt angle of thiolate chains within pure monolayers decreases with increasing chain length. In terms of binary mixed monolayers this means that additional structural stress is introduced into a system if thiol precursors of highly different tilt angle are combined. As tilt angles appear to adopt similar values at large chain lengths (approximately n ≥ 12), this kind of structural stress is expected to be most influential if liquid thiols are used as the short-chain component and are mixed with solid precursors. For solid/solid combinations the effect is assumed to be less relevant the longer both thiolate chains get. Hence, while the rough magnitude of ω can be related to the chain length difference Δn, the exact choice of thiol precursors still has an effect on the final structural parameters.

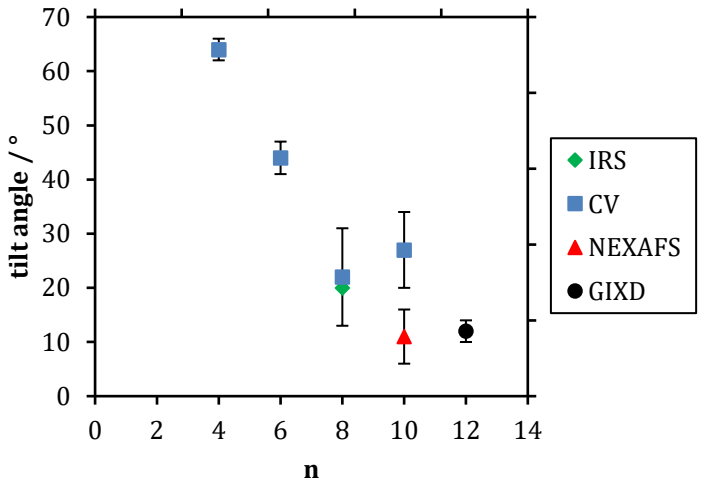

Figure 50: Tilt angles of thiol monolayers deposited from FnH2-SH determined by various experimental methods (CV [256], IRS [114], NEXAFS[257], GIXD [193]).

The influence of tilt angles might as well explain the comparably strong increase of ω in transition from the system F8H2/F10H2 to F8H2/F12H2 or F6H2/F10H2 to F6H2/F12H2, respectively. A distinct change of the tilt angle for thiols F10H2-SH and F12H2-SH would lead to an observable effect on ω for corresponding monolayer systems, whereas the similar tilt angle for F12H2-SH and F14H2-SH may show a

smaller effect in higher systems. According to this assumption, it will be highly interesting to obtain values for a system of e.g. F10H2/F16H2 as ω would be expected to only slightly increase compared to F10H2/F14H2. Thus, mixed films could be obtained, which would still be completely miscible in terms of ω. High values of Δn could be accessible by combining long-chain precursor thiols with similar tilt angle, while a random composition could be maintained.

The development of R_0 depending on the choice of monolayer system is depicted in Figure 51 and Figure 52. As a reminder, R_0 is a measure of the probability for the preferred adsorption of one type of precursor molecule over the other. The smaller R_0, the stronger is the preferential adsorption of the corresponding longer-chain thiol. Results show that R_0 decreases with increasing Δn and that for systems with identical Δn, R_0 increases with increasing length of the shorter chain (n_{short}). Particularly for low values of Δn = 2,4, this increase suggests that the applied thiols approach each other in terms of adsorption behavior (i.e. R_{sol} = 1). Related to this is the finding, that for Δn = 2, the increase in R_0 is relatively strong between the systems F8H2-SH/F10H2-SH and F10H2-SH/F12H2-SH, which may reflect the transition from a liquid/solid to a solid/solid system, as the tendency to adsorb will be more similar for the latter system's thiols (solid thiols are expected to be less soluble in deposition solvents). At Δn = 6, the determined values of R_0 are practically identical, which may suggest that, for this chain-length difference, an increase of R_0 rather depends on Δn than on the chosen short-chain thiol. However, data sets are too thin here in order to be decisive.

Moreover, results show that for systems with identical n_{short} R_0 decreases with increasing Δn. This observation is in agreement with the expected behavior and is assumed to be a consequence of decreasing thiol solubility for increasing chain-lengths. Thus, thiols bearing very large chain-lengths will exhibit an increased tendency to permanently adsorb onto the gold surface, which leads to a preferential adsorption of longer-chain thiols over their short-chain counterparts and to a decrease of R_0 if n_{short} is kept constant.

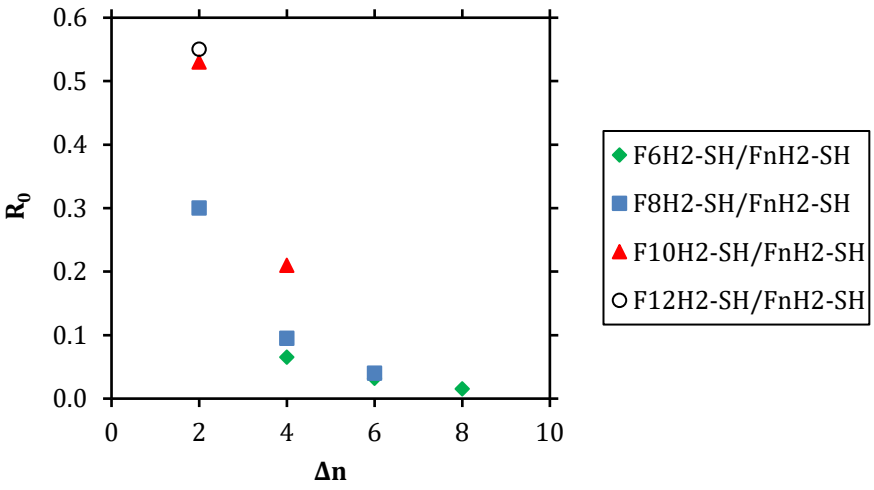

Figure 51: Influence of the chain length difference Δn on R_0 for fluorinated SAMs.

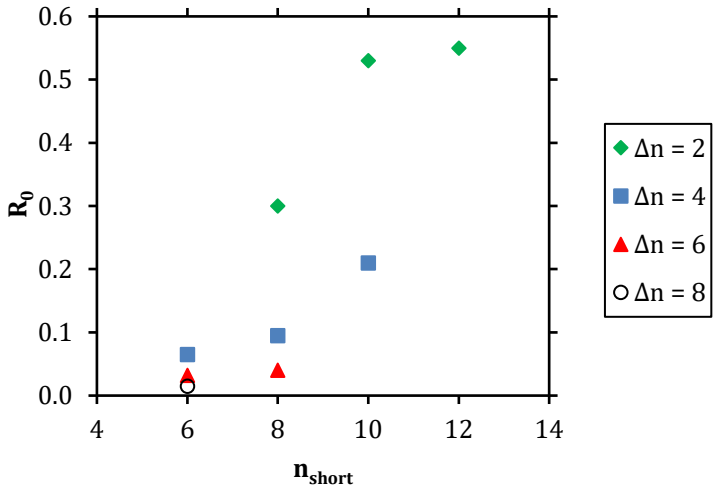

Figure 52: Influence of the choice of short-chain thiol on R_0 with respect to chain length difference Δn.

Similar to fluorinated monolayers, SAMs deposited from Hm-SH show a decrease of R_0 with increasing chain-length difference Δm, i.e. long-chain precursors adsorb preferentially.

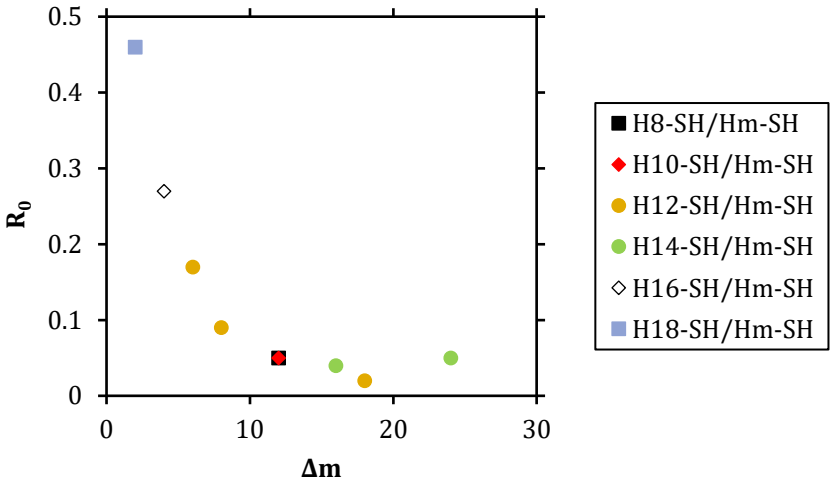

Figure 53: Influence of the chain length difference Δm on R_0 for non-fluorinated SAMs.

So far, it has been shown successfully that even sub-nm structures of molecular length scales have a measurable effect on the wetting behavior of contacting liquids. However, the important question remains in how far these results compare to the wetting behavior expected from well-established macroscopic models. Wetting on rough surfaces is commonly described by the Wenzel and Cassie-Baxter models as introduced in Section 2.1. In order to predict the wetting characteristics of surfaces with sub-nm topographies as prepared in this work, model calculations have been conducted according to the corresponding Wenzel and Cassie-Baxter states of liquid wetting. For this, wetting on the surface of a hexagonal array of closely packed cylinders was calculated, in which the top- and sidewall-areas of the cylinders were attributed with distinct wetting properties. Detailed information on the model calculations are presented in the appendix. Here, it is important to state that all parameters that were applied throughout the calculations are well-known and have been published in literature repeatedly.

In Figure 54, the results of these model calculations and the corresponding experimental contact angles are compared for the system of F8H2-SH/F12H2-SH, which has been presented earlier in Section 5.4.

Although the theoretical values predict an increase in $\theta_{adv}(W)$ and $\Delta\theta_{adv,max}(W)$ for highest degree of surface roughness at $x_{long} = 0.5$ as expected, it is obvious that the experiment does not fit the model calculations. While experiments yielded a maximum increase of $\Delta\theta_{adv,max}(W)$ of approximately 4°, model calculations predict a change of approximately 19°. Moreover, it is not possible to make the model data fit the experiment by variation of structural parameters unless highly unrealistic values are used (Table 15). In summary, none of the monolayer systems prepared during this study matched their theoretical models for water wetting.

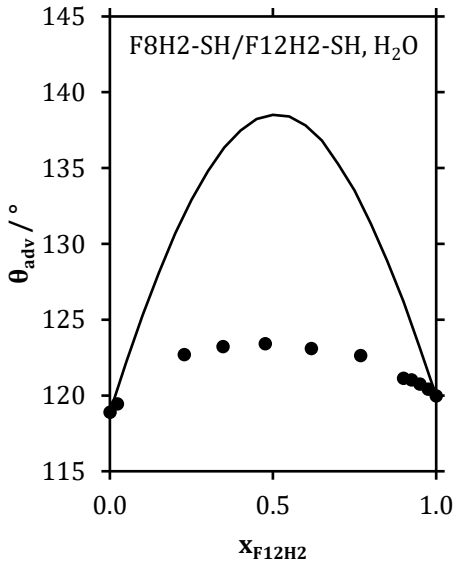

Figure 54: Comparison of the results obtained from wetting experiments with water (•) and values calculated from theory (solid line) for a monolayer system F8H2-SH/F12H2-SH.

Parameter	**Value**	**Required to fit experimental data**
vdW-diameter	(5.6 ± 0.1) Å [184]	1.4 Å
Δh per -$(CF_2)_2$-	(2.5 ± 0.5) Å [134]	0.65 Å
next-neighbor distance	(5.8 ± 0.1) Å [87,114,193]	11.5 Å
$\theta_{CF2}(H_2O)$	(110 ± 2)° [258–261]	95°

Table 15: Comparison of documented structural parameters of fluorous thiol SAMs and the corresponding values which would be required in order to make the model fit the experimental data.

Analogous behavior is observed when squalane wetting experiments are compared with the theoretical calculations. As already discovered for water, experimentally determined values do not match the expected values for macroscopic models (see Figure 55). However, in contrast to a decrease of the expected contact angle for water, the effect of surface topography on squalane wetting is expressed by a relative increase of experimentally determined contact angles compared to their calculated values. In contrast to water wetting, squalane wetting increases on rough surfaces due to a contact angle < 90° on flat fluoroalkylated surfaces. Thus, both experiments have in common that the effect of surface roughness known from macroscopic systems is apparently decreased on this kind of structures.

As depicted in Figure 56, the increase of θ_{adv} at $x_{long} = 0.5$ in comparison to the mean average of wetting on pure monolayers differs dramatically in terms of modeled and experimentally determined values for all samples. Moreover, the influence of molecular roughness on wetting properties increases with increasing chain-length difference of the corresponding thiols.

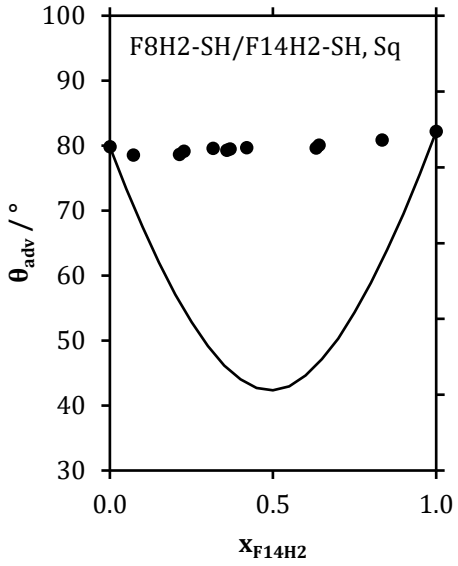

Figure 55: Comparison of the results obtained from wetting experiments with squalane (•) and values calculated from theory (solid line) for a monolayer system F8H2-SH/F14H2-SH.

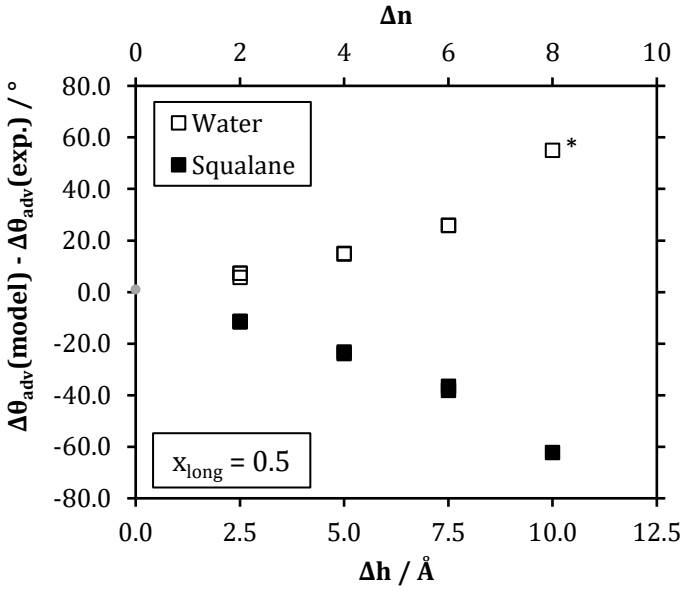

Figure 56: Difference between experimentally determined and calculated values of $\Delta\theta_{adv}$ at $x_{long} = 0.5$ as a function of Δh or Δn, respectively (irrespective of the exact combination of long/short thiol). The deviation between model and experiment increases with increasing chain length. *At Δh = 10.0 Å, Wenzel modeling predicts complete dewetting with water ($\theta_{adv}(W) > 180°$), so that the value given here is determined from the difference to $\theta_{adv}(W) = 180°$.

The experimental results most evidently cannot be explained by known models and the question arises, what effects might cause this behavior. At this point it is important to remember the context of the samples and the actual size of their topological structures, which are of similar size as the solvent molecules themselves. Wenzel and Cassie-Baxter models, which were used for the theoretical calculations, describe macroscopic phenomena and rely on thermodynamic properties of the contacting liquids. Thus, these approaches make use of the properties of an ensemble of molecules, which might not be adequate for wetting at the scale of the presented surface topographies anymore.

Effective surface tensions for very small structures are known to deviate from their macroscopic values and have already been described originally by Tolman in the 1940s and more recently by Fradin and Mora (Section 2.4,Figure 16). Thus, a second approach of explaining the experimental results was conducted based on the assumption of an effective surface tension that deviates from its macroscopic value. For this, the common Girifalco-Good-model [262] (equation (16)) is applied in combination with the Young-equation (1) in order to derive an expression for γ_{LV} (equation (17)) that allows for the modelling of the experimental data in accordance with an effective surface tension liquid/vapor γ_{LV}^{*}. Scale dependent surface tension γ^{*} is assumed both for solid/liquid and liquid/vapor interfaces with particular regard to the importance of wetting at the triple line. As discussed by Gao and McCarthy, the wetting behavior of a liquid droplet depends mainly on the situation observed at its triple line. [263] Thus, within this small size-scale, an effect on γ_{LV} next to γ_{SL} can be reasonably assumed. The increased effective surface area on rough surfaces according to Cassie-Baxter is considered in terms of the roughness factor r (Section 2.1).

$$\gamma_{SL} = \gamma_{SV} + \gamma_{LV} - 2\Phi\sqrt{\gamma_{SV}\,\gamma_{LV}} \tag{16}$$

$$\gamma_{LV}\cos\theta = \gamma_{SV} - \gamma_{SL} \tag{1}$$

$$\left(\frac{\cos\theta}{r} + 1\right)^{2} \cdot \gamma_{LV} = \text{const.} \tag{17}$$

The obtained values of γ_{LV}^{*} can be further expressed in relation to the macroscopically effective surface tension γ_{LV} as $\frac{\gamma_{LV}^{*}}{\gamma_{LV}}$. Based on equation (17), it is possible to successfully model the experimental results taking advantage of the assumption of a reduced surface tension for water or an increased surface tension for squalane, respectively. Resulting calculated values for wetting on binary mixed monolayers are depicted exemplarily in Figure 57 for water and Figure 58 for squalane.

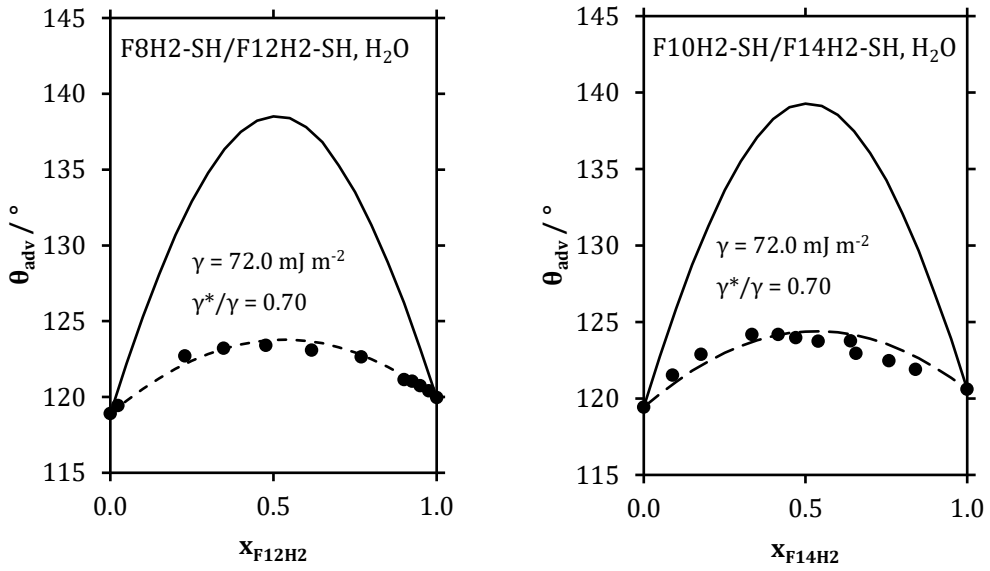

Figure 57: Exemplary comparison of results obtained from wetting experiments with water (•) and values calculated from theory (solid lines) or modeling with reduced surface tension (dashed lines).

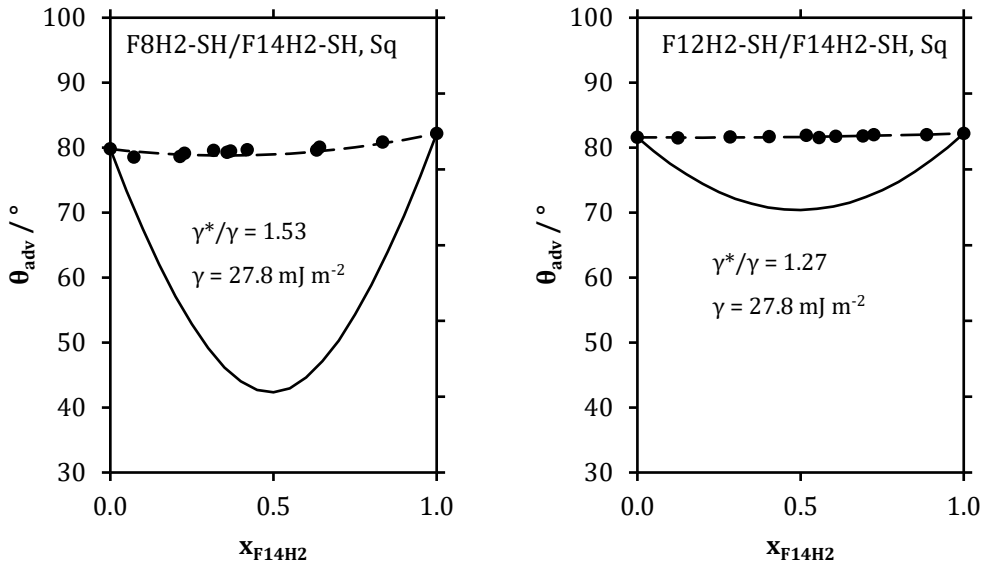

Figure 58: Exemplary comparison of results obtained from wetting experiments with squalane (•) and values calculated from theory (solid lines) or modeling with increased surface tension (dashed lines).

Figure 59 and Table 16 summarize the results of effective surface tension calculations for wetting experiments with water and squalene on binary fluoroalkylated SAMs (at x_{long} = 0.5). It is easily observable for both contacting liquids that the relative deviation from the macroscopic surface tension $\frac{\gamma_{LV}^{*}}{\gamma_{LV}} = 1$ increases with increasing differential height of the underlying surface topography. In the case of water, the maximum height difference of Δh = 10.0 Å results in an effective reduction of surface tension by a factor of approximately 0.6, while for squalane an increase by a factor of approximately 1.6 is observed. The calculated values of both liquids appear to fall onto one fitted curve but further experiments will be necessary in order to obtain a definite image of this effect. Nonetheless, the relative effective surface tension is a characteristic feature of any of the prepared thiol monolayers and can be controlled by the choice of deposition parameters in order to enable desired wetting properties.

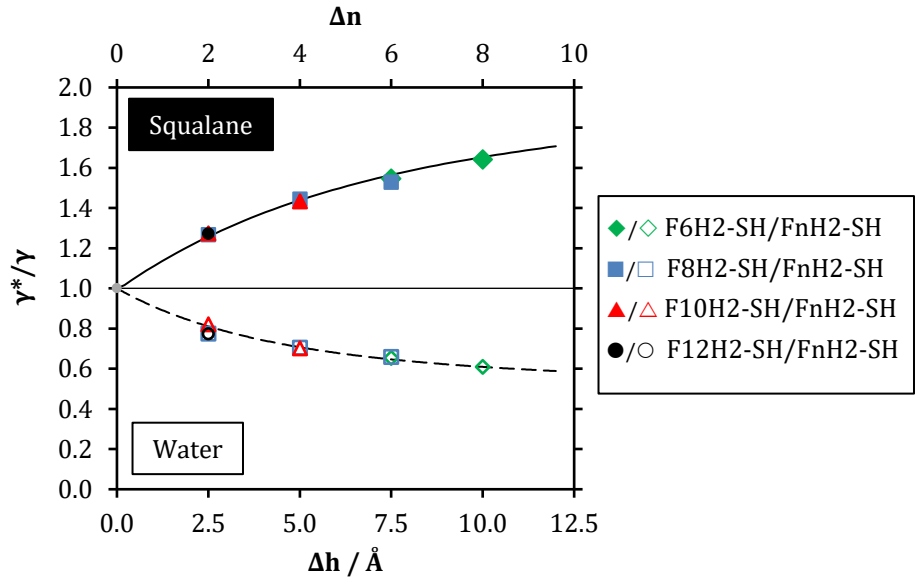

Figure 59: Results of calculated effective surface tensions at x_{long} = 0.5 for water and squalane wetting experiments on fluorinated monolayers. Given lines present a guide to the eye only.

Contacting liquid	**System, n_{short} / n_{long}**	**Δh [Å]**	γ_{LV}^{*} $\left[{}^{mJ}/_{m^2}\right]$	$\frac{\gamma_{LV}^{*}}{\gamma_{LV}}$
Water	Reference	0.0	72.0 [264]	1.00
	6 / 12	7.5	47.0	0.65
	6 / 14	10.0	43.7	0.61
	8 / 10	2.5	55.7	0.77
	8 / 12	5.0	50.6	0.70
	8 / 14	7.5	47.4	0.66
	10 / 12	2.5	59.0	0.82
	10 / 14	5.0	50.5	0.70
	12 / 14	2.5	55.6	0.77
Squalane	Reference	0.0	27.8 [265]	1.00
	6 / 12	7.5	42.9	1.54
	6 / 14	10.0	45.6	1.64
	8 / 10	2.5	35.2	1.27
	8 / 12	5.0	40.1	1.44
	8 / 14	7.5	42.4	1.53
	10 / 12	2.5	35.3	1.27
	10 / 14	5.0	39.8	1.43
	12 / 14	2.5	35.3	1.27
Ethylene glycol	Reference	0.0	48.0 [266]	1.00
	6 / 12	7.5	52.6	1.10
	8 / 12	5.0	51.3	1.07
	8 / 14	7.5	52.3	1.09
	10 / 14	5.0	51.6	1.07
	12 / 14	2.5	50.5	1.05

Table 16: Overview of calculated effective surface tensions on fluorinated surfaces at x_{long} = 0.5 for water, squalane and ethylene glycol wetting experiments.

Comparison of these results with the experiments published by Mora *et al.* yield a surprisingly good match in terms of the resulting value of effective relative surface tensions. As depicted in Figure 60, the results obtained for fluorinated monolayers with $\Delta h = 10.0$ Å refer to an effective structural length $d_{eff} = \frac{\lambda}{2} = 17$ Å of the topographical structures if a capillary wave length of $\lambda = 34$ Å is assumed. This structural length is distinctly larger than the van-der-Waals-diameter of the applied precursor chains ($d_{vdW} = 5.6$ Å).

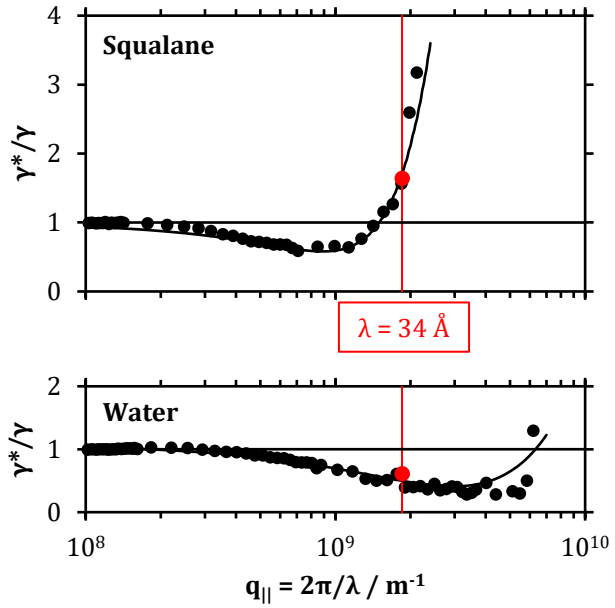

Figure 60: Comparison of the scattering results obtained by Mora and Fradin (black) with the calculated effective surface tensions of fluorous binary mixed monolayers with Δn = 10 (red). The red lines indicate a capillary wavelength of λ = 34 Å ($q_{||} = 1.9 \cdot 10^9$ m^{-1}).

However, this finding is not in contradiction to the known structural parameters of the monolayers but actually underlines the random distribution of thiolate chains within the films. As a consequence of the random deposition, surface structures are formed that contain different local fractions of chain lengths. The randomness of distribution does not imply that preferentially different chain lengths are placed next to each other but that the deposition of same-height chains is equally probable. Figure 61 represents an illustrative example of a surface consisting of equimolar amounts of two types of precursors which share the same chain diameter but differ in chain length. Obviously, only a very small number of separated precursors of a single chain

length are found on this surface and the majority of structures is deposited as same-height-agglomerations of different dimensions. Thus, structures are formed that on average will be unavoidably larger than the diameter of individual chains, which is assumed to be reflected by the effective structural wavelength observed in the comparison with the Mora results.

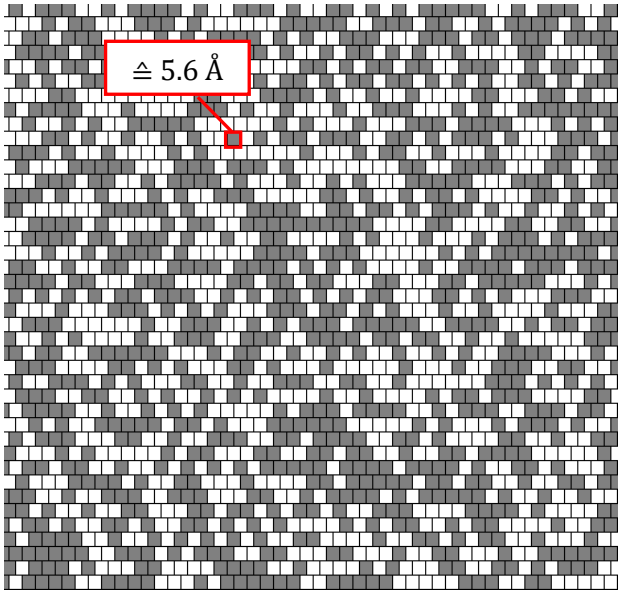

Figure 61: Illustration of a binary mixed monolayer surface deposited from equimolar amounts of two thiol precursors of different chain length.

In an effort to obtain experimental data for surfaces with even smaller structural features, the results of fluoroalkylated SAMs were compared to binary mixed monolayers from non-fluorinated analogs Hm-SH with m = 8…38. As the vdW-diameter of hydrocarbon chains is smaller than the diameter of their fluorocarbon counterpart (Table 3), an effect on the change in effective surface tension could be expected.

Wetting experiments on non-fluorinated monolayers were observed to show similar behavior as their fluorinated analogs and a strong discrepancy between experimental results and predictions of the Wenzel model were observed, which is exemplarily shown in Figure 62.

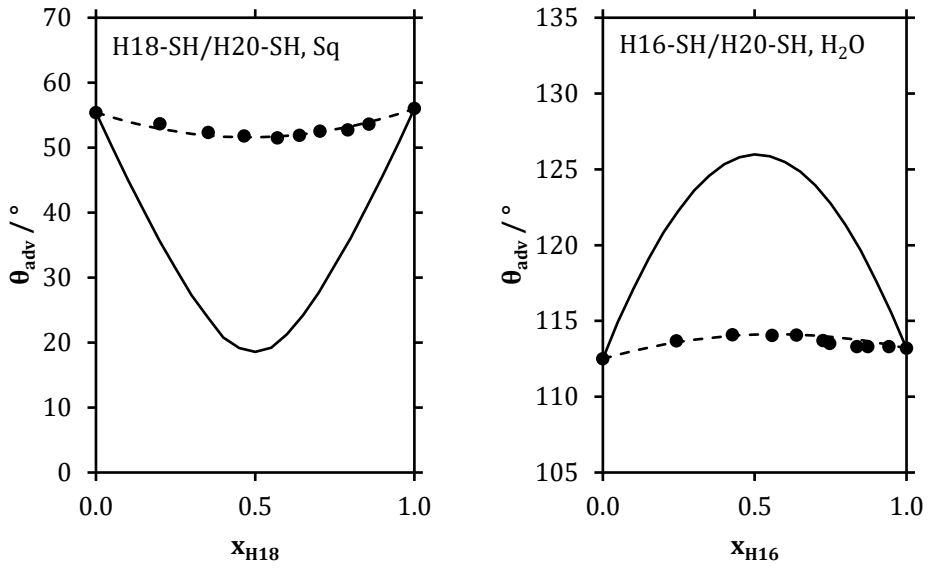

Figure 62: Exemplary comparison of results obtained from squalane/water wetting experiments (•) with values calculated from Wenzel/Cassie-Baxter theory (solid lines) or modeling with scale-dependent surface tension (dashed lines).

The strong difference between theoretical model values and the corresponding wetting results observed experimentally are presented in Table 17 and Figure 63 for hydrocarbon squalane. Theory predicts complete wetting of squalane on non-fluorinated binary mixed SAMs already for chain-lengths differences of $\Delta m \geq 4$. Thus, -cos θ was used for a direct comparison of the corresponding values.

Δm	**Δh [°]**	**$\theta(Sq)_{theo}$ [°]**	**$-\cos\theta(Sq)_{theo}$**	**$\theta(Sq)_{exp}$ [°]**	**$-\cos\theta(Sq)_{exp}$**
2	2.4	18.6	-0.95	51.7	-0.62
4	4.7	compl. wetting	-1.33	43.8	-0.72
6	7.1	compl. wetting	-1.73	35.3	-0.82
8	9.4	compl. wetting	-2.10	27.4	-0.89
12	14.2	compl. wetting	-2.97	26.3	-0.90
12	14.2	compl. wetting	-2.91	28.4	-0.88
12	14.2	compl. wetting	-2.91	18.7	-0.95
16	18.9	compl. wetting	-3.66	32.0	-0.85
18	21.2	compl. wetting	-4.07	39.2	-0.78
24	28.3	compl. wetting	-5.21	39.7	-0.77

Table 17: Comparison of the experimental results for squalane wetting on non-fluorinated binary monolayers with the results predicted from model calculations. As theory predicts complete wetting already at small surface structures, the results are presented in terms of -cos θ as well.

Analogous to the results observed for fluorinated SAMs, the deviation from modelled values increase with increasing size of the topographical features of the deposited monolayers. Referring to wetting experiments with squalane, a tendency to obtain values of $-\cos\theta_a > 0$ or even > 1 at further increased Δm may be expected (Figure 63). This would mean an inversion of wetting behavior induced by surface structures and will have to be investigated during future studies.

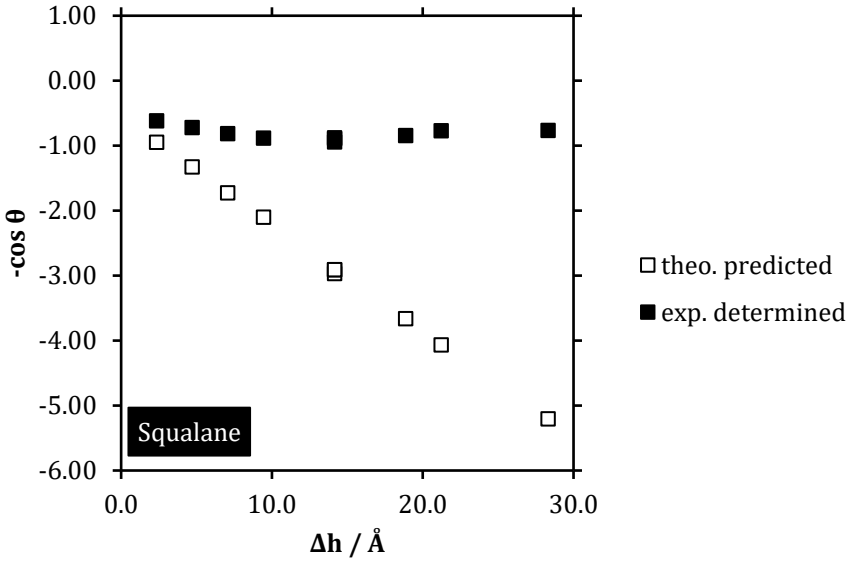

Figure 63: Comparison of the experimental results for squalane wetting on non-fluorinated binary monolayers with the results predicted from model calculations in terms of -cos θ.

The evaluation of the obtained results according to the model of an effective surface tension yielded again a relative change in effective surface tension as a function of the height-difference of the structural features. These results enabled a direct comparison of fluorinated to non-fluorinated structures and the effect of the smaller size of the non-fluorinated alkyl-chains.

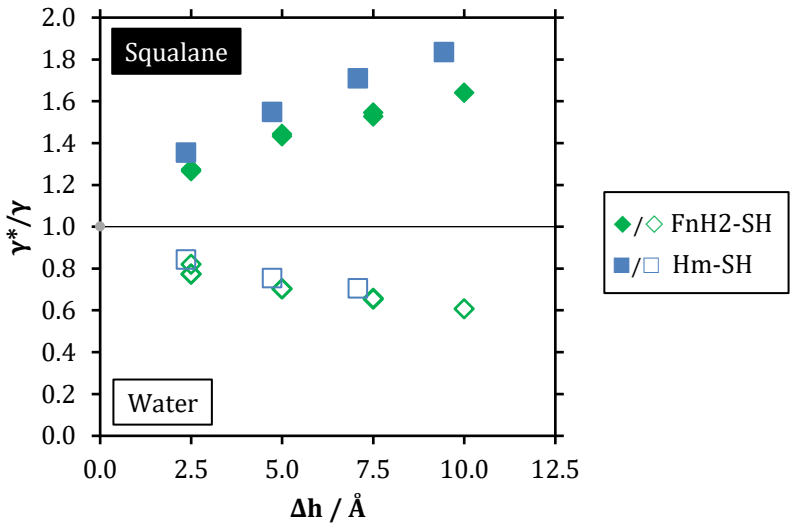

Figure 64: Results of calculated effective surface tensions at x_{long} = 0.5 for water and squalane wetting experiments on fluorinated and non-fluorinated monolayers (Δn = 2…8 or Δm = 2…8, respectively).

Further results for calculated values of the effective surface tension on non-fluorinated surfaces are summarized in Table 18. The extended availability of Hm-SH precursors enabled the investigation of a wider range of height differences Δh compared to SAMs from FnH2-SH. Monolayers with large structural height-differences were only examined with squalane, as polar contacting liquids like water might induce an increased tendency of chain-coiling in comparison to hydrocarbon squalane. Thus, wetting experiments with water may be hampered with increased chain-length difference. The continuous increase of the effective surface tension compared to its macroscopic value for squalane on fluorinated and non-fluorinated SAMs is presented in Figure 65.

Contacting liquid	**System, m_{short} / m_{long}**	**Δh [Å]**	γ_{LV}^{*} $\left[mJ/m^2\right]$	$\frac{\gamma_{LV}^{*}}{\gamma_{LV}}$
Water	Reference	0.0	72.0 [264]	1.00
	18 / 20	2.4	60.7	0.84
	16 / 20	4.7	54.3	0.75
	12 / 18	7.1	50.7	0.70
Squalane	Reference	0.0	27.8 [265]	1.00
	18 / 20	2.4	37.6	1.35
	16 / 20	4.7	43.0	1.54
	12 / 18	7.1	47.5	1.71
	12 / 20	9.4	51.0	1.83
	8 / 20	14.2	62.0	2.23
	10 / 22	14.2	61.3	2.20
	18 / 30	14.2	59.4	2.13
	14 / 30	18.9	68.6	2.47
	12 / 30	21.2	73.7	2.65
	14 / 38	28.3	79.9	2.87

Table 18: Overview of calculated effective surface tensions on non-fluorinated surfaces at x_{long} = 0.5 for water and squalane wetting experiments.

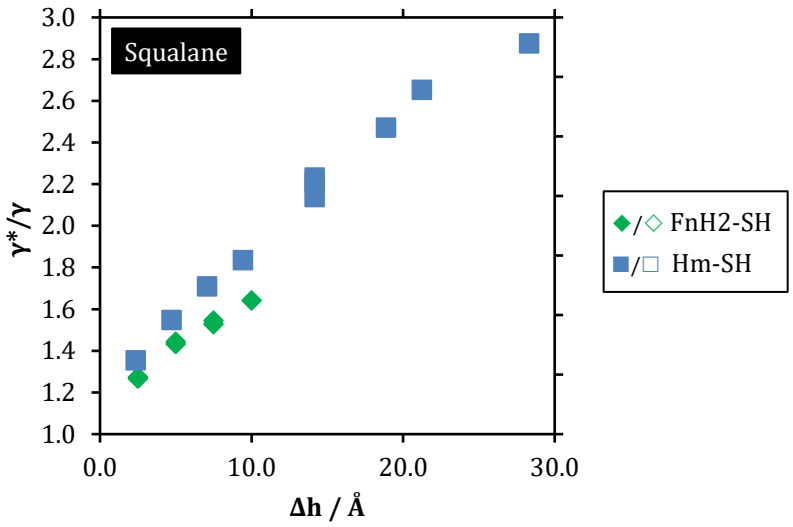

Figure 65: Results of calculated effective surface tensions at x_{long} = 0.5 for squalane wetting experiments on fluorinated and non-fluorinated monolayers.

The application of hydrocarbon precursor molecules enabled the formation of smaller structures compared to surfaces prepared from fluoroalkylated precursors. This small decrease of the vdW-diameter lead to a measurable difference in effective surface tension and larger values of γ* were detected. This result corresponds to the results presented by Mora and Fradin, who reported an increase in effective surface tension for squalane with a decrease of structural size.

5.6. Conclusion & Outlook

The initial motivation of this work was the development of surfaces with molecular-scale topographies and the investigation of these structures' response towards contacting liquids. The question whether such small structures could still have an effect on liquids' wetting behavior was successfully answered. Thus, it has been successfully shown that even surface topographies in the range of some Ångstroms do have an observable effect on the wetting behavior of contacting liquids. This effect, however, deviates considerably from the one expected from generally accepted models of wetting on macroscopic surface structures and it is assumed to be a first experimental proof of scale-dependent surface tensions and their influence on

solid surface wetting. Moreover, it has been shown that binary mixed monolayers from fluoroalkylated thiols can be deposited from thiols of differing chain lengths and that the exact choice of precursor chain length significantly influences the thermodynamic properties of monolayer formation. It was observed that the risk of phase separation increases with increasing chain length difference, particularly when thiols with $n \leq 8$ are chosen as short-chain component. Results suggest that the effect of increasing interaction parameter ω may be reduced by the choice of longer-chain solid precursors ($n \geq 10$) and the provision of even longer chain lengths will enable the investigation of such systems in the future. Further improvement through the application of long-chain solid fluorous thiols was also observed regarding the results of R_0. As expected, R_0 increases with decreasing Δn and for small Δn, the results of solid/solid binary systems appear to adopt similar values. The obtained results show that by variation of surface topographies in the sub-nm regime it is possible to generate surfaces, which reveal wetting properties that are completely different compared to common concepts of surface manipulation.

The agreement of the results by Mora and Fradin with the wetting behavior on sub-nm topographies of binary mixed thiol monolayers supports the assumption of a scale-dependent surface tension. As an increase in the observed effective structural length can be explained by the formation of equal-height structures within the monolayer film, it appears obvious that a reduction of the effective structural length may be obtained by the reduction of effective equal-height area fractions within the surface structure. This approach could provide the means to prepare universally dewetting surfaces outperfoming the current methods of omniphobic surfaces. These kinds of smallest-scale structures may be obtainable via the application of carbon nanotubes (CNTs), which have been reported with CNT diameters as small as 3 Å. [267] Appropriate choice of CNT diameter and height may lead to structures which would enable the preparation of sufficiently small topographies. Unfortunately, this approach requires not only the successful preparation of isolated CNTs but also their deposition or *in-situ* growth on appropriate surfaces as free-standing and isolated objects, which is, for now, a very ambitious concept.

The reduction of an effective equal-height area fraction may, however, be successfully achieved by other less ambitious methods. Introduction of further thiol precursors with different chain lengths would enable the preparation of ternary, quaternary or higher monolayer systems, which would contain an increased variability of structural heights. Moreover, symmetric dialkyl sulfides have already been published to form monolayers which cannot be distinguished from monolayers deposited from the corresponding alkyl thiols. It is conceivable that asymmetric dialkyl sulfides may be deposited in the same manner as alkyl thiols and symmetric dialkyl sulfides, so that

an increased fraction of next-neighbor height difference could be introduced into the surface topography. Either of these methods would enable the preparation of surfaces with topographies bearing a higher fraction of different height scales than binary mixed monolayers can provide.

Besides the development of structures with smaller lateral dimensions, the increase of structural height differences and implementation of fluorous thiols with $n \geq 16$ will be a subject of future relevance. Although monolayer systems with a height difference of $\Delta n = 8$ have already shown first indications of phase separation, the extension to longer-chain thiols may lead to further improvements, particularly taking into account the assumed effect of stabilizing tilt angles in pure monolayers. Moreover, observed problems concerning the oxidation of short-chain thiols ($n = 6, 8$) could be overcome by an increased variety of accessible thiols. Increased height differences with non-fluorinated thiol precursors may bear the risk of less stable structures compared to fluoroalkylated structures. Pure hydrocarbon thiols may, however, be easier to obtain than their fluorocarbon analogs.

The ultimate goal of all these investigations will of course be the transition of the acquired knowledge towards suitable applications in industry, academia and everyday life. With surface functionalization, especially regarding wetting manipulation, being important in many obvious and hidden aspects of life, this technique, once successfully implemented, will surely find its way to greater recognition.

6. Optimization of Vapor-deposited SAMs from Chain-extended Fluorous Silanes

6.1. Effect of Deposition Conditions on Film Properties

The characterization of films deposited from F8H2-$SiCl_3$ and F10H2-$SiCl_3$ was conducted with the main interest being placed in the wetting properties of the films. The influence of several deposition parameters was examined by dynamic contact angle measurements with hexadecane (HD). Some samples were tested for their wetting properties against water as well, but the main focus was put on testing non-polar HD. Thus, oleophobic properties of the samples could be investigated and a quick and easy characterization of the large number of samples was enabled. For further characterization XPS, AFM, sSIMS, and ellipsometry experiments were performed. Films from F12H2-$SiCl_3$ were not studied as a consequence of the difficult handling of the precursor and the high tendency to deteriorate during preparation (see chapters 3 and 4). Moreover, its low vapor pressure would have required high deposition temperatures beyond the technical capabilities of the deposition setup.

An overview of the process parameters that were studied is given in Table 5. The corresponding value or range of parameters for individual sections is presented in Table 19. During the discussion of the effect on film properties by the variation of single parameters, other parameters will not be mentioned explicitly but can be retrieved from Table 19.

Silane	Investigated parameter	Parameters and their values during experiments				
		T(dep.) [°C]	**t(silane) [min]**	**t(H_2O) [min]**	**p(silane) [mTorr]**	**p(H_2O) [mTorr]**
F8H2-$SiCl_3$	p(H_2O)	80	90	45	262 ± 4	10…11000
	p(silane)	80	90	45	20…670	62 ± 3
	t(silane)	80	1…180	45	274 ± 16	180 ± 6
	t(H_2O)	80	90	1…180	275 ± 15	180 ± 5
	T(dep.)	80…120	90	45	254 ± 3	134 ± 9
F10H2-$SiCl_3$	p(H_2O)	100	90	45	275 ± 19	10…2100
	p(silane)	100	90	45	30…620	159 ± 7
	T(dep.)	80…120	90	45	147 ± 13	152 ± 12

Table 19: Overview of deposition conditions during the study of individual process parameters. Within a set of experiments, one parameter was varied while all other parameters were kept at a constant value. Thus, the influence of a parameter of interest on film formation and film properties could be determined.

6.1.1. Films Deposited from F8H2-$SiCl_3$

6.1.1.1. Water partial pressure p(H_2O)

The influence of water partial pressure on the wetting properties of films deposited from F8H2-$SiCl_3$ was examined by dynamic contact angle measurements with HD. The results are shown in Figure 66 in terms of advancing contact angle θ_{adv} and contact angle hysteresis $\Delta\theta$.

θ_{adv} is found to steadily increase with increasing p(H_2O) from approximately 73° until apparently reaching a plateau at 80° at higher water concentrations. Although no change in $\Delta\theta$ is observable at low p(H_2O), a sharp increase in hysteresis occurs at p(H_2O) ≈ 200 mTorr, where $\Delta\theta$ increases from 2° to 10°. Maximum hysteresis is observed at approximately 3,000 mTorr water partial pressure and hysteresis tends to decrease slightly until the maximum pressure tested at 10,000 mTorr. Wetting properties with HD at optimum conditions (p(H_2O) ≈ 200 mTorr) are θ_{adv} ≈ 76.5° and $\Delta\theta$ ≈ 2.0°.

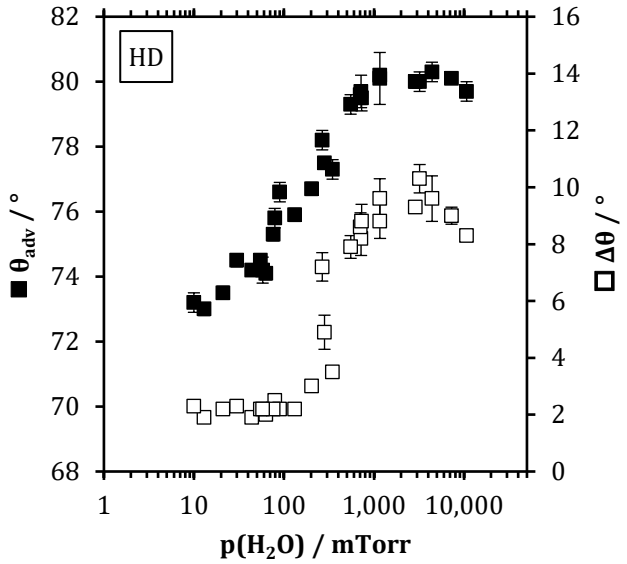

Figure 66: Results of wetting experiments with HD for films deposited from F8H2-$SiCl_3$ prepared at varying water partial pressures $p(H_2O)$. θ_{adv} steadily increases with increasing $p(H_2O)$ whereas $\Delta\theta$ remains constant at low $p(H_2O)$ and sharply increases at $p(H_2O) \approx 200$ mTorr.

Results for the investigation of the samples' wetting properties with water revealed similar effects for an increasing water partial pressure during deposition. As for experiments conducted with HD, θ_{adv} increases with increasing $p(H_2O)$ and eventually reaches a plateau of $\theta_{adv} \approx 119.5°$. Here as well, an apparent plateau of $\Delta\theta$ at low $p(H_2O)$ of $\Delta\theta \approx 9°$ is observed followed by a sharp increase in $\Delta\theta$ at $p(H_2O) \approx 200$ mTorr to values > 18°. For depositions accomplished at high $p(H_2O)$ no values for hystereses could be resolved as they were beyond the detection limit of ≈ 20°.

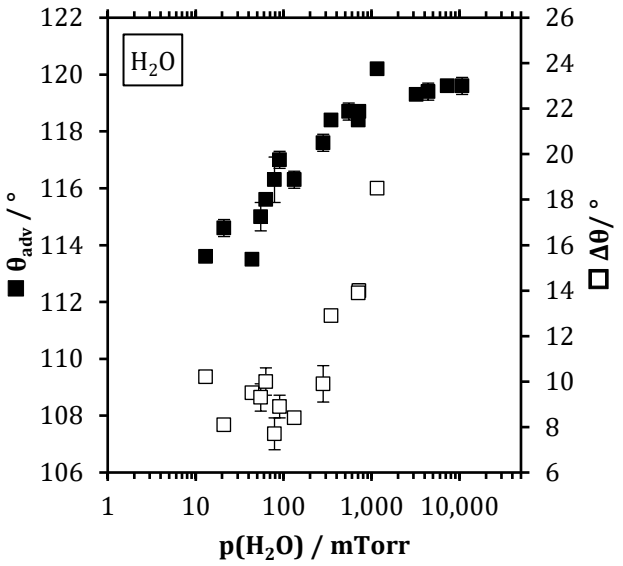

Figure 67: Results of wetting experiments with water for films deposited from F8H2-$SiCl_3$ prepared at varying water partial pressures p(H_2O).

In order to verify the successful deposition of the precursor molecules on the substrate the samples were examined by XPS. As a means of comparison, samples prepared at low and high water partial pressures, respectively, were examined.

XPS analysis of a sample prepared at low water partial pressure of p(H_2O) = 63 mTorr (p(F8H2-$SiCl_3$) = 261 mTorr) yields a survey spectrum of the expected elemental peaks and compositions: 15.0 at% C (C1s: 280-295 eV), 30.6 at% F (F1s: 688 eV), 22.5 at% O (O1s: 533 eV) and 32.0 at% Si (Si2p: 99 eV), see Figure 68. Conducting a detailed C1s analysis (Figure 69) gives three main regions of intensity which can be attributed to distinct carbon species present in the precursor molecule.[124] The broadened peak around 285 eV can be assigned to unresolved peaks representing non-fluorinated methylene units at 284.6 eV ($\underline{C}H_2$) and 285.9 eV ($\underline{C}H_2$-CF_2). Apart from signals originating from the deposited film this region might also contain intensities of possible carbon contaminations adsorbed from atmosphere. Peaks around 291 eV (two unresolved peaks, 290.3 eV CH_2-$\underline{C}F_2$ and 291.3 eV CF_2) and 293.5 eV (CF_3) represent the fluoromethylene units of the precursor molecule as described in literature.[124] The ratio of the fluorocarbon composition CF_3/CF_2(exp.) = 0.20 found experimentally is slightly larger than the value calculated from stoichiometry of CF_3/CF_2(calc.) = 0.17. However, this finding is in agreement

with the expected upright arrangement of the fluoroalkyl chains with the -CF_3 moiety facing the ambient. [212] An increased F/C-ratio is in accordance with the high surface sensitivity of XPS as the outermost surface region of the film consists mainly of fluorine (F/C(exp.) = 2.04; F/C(calc.) = 1.70). The ratio of fluorine to silicon is determined to F/Si = 0.96.

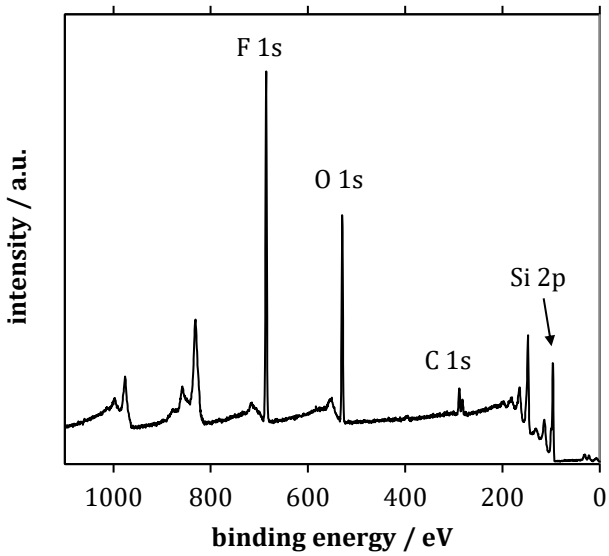

Figure 68: Survey spectrum of an XPS experiment for a sample film deposited from F8H2-$SiCl_3$ at low p(H_2O) = 63 mTorr and p(F8H2-$SiCl_3$) = 261 mTorr.

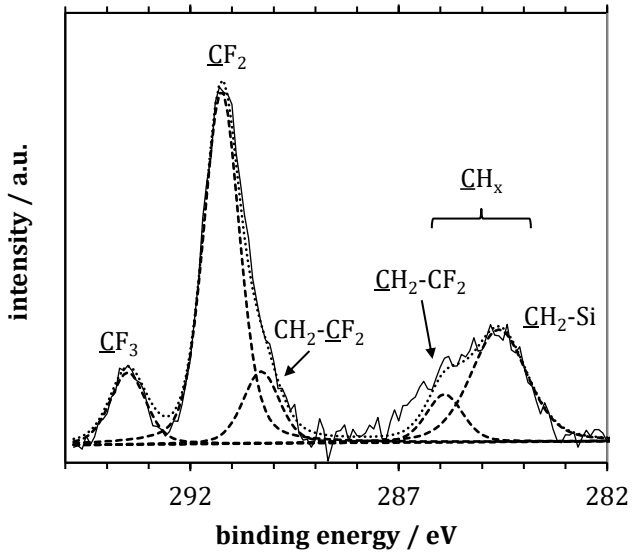

Figure 69: Detailed C1s XP spectrum of a sample deposited at low $p(H_2O)$ = 63 mTorr and $p(F8H2\text{-}SiCl_3)$ = 261 mTorr with Gaussian-Lorentzian fits to $\underline{C}H_2$, $\underline{C}H_2\text{-}CF_2$, $\underline{C}F_2\text{-}CH_2$, $\underline{C}F_2$, $\underline{C}F_3$ (G-L ratio 0.7). Results verify the deposition of a fluoroalkylated layer and suggest the $-CF_3$ moiety facing the ambient. The region of 283-287 eV may contain contaminations from CH_x-species adsorbed from the atmosphere.

XPS analysis of a sample prepared at high water partial pressure of $p(H_2O)$ = 10,691 mTorr ($p(F8H2\text{-}SiCl_3)$ = 259 mTorr) yields the following elemental peaks and compositions: 15.4 at% C, 38.6 at% F, 19.5 at% O and 26.5 at% Si. In comparison to the sample prepared at low $p(H_2O)$ the ratio CF_3/CF_2(exp.) = 0.19 slightly decreases which may be regarded to be a consequence of increased chain disorder. More important is the fact that the ratio F/Si = 1.46 increases which suggests an increased film thickness and will be further discussed later. This effect can be found as a steady increase in F/Si ratio for samples with increasing $p(H_2O)$ (Figure 70).

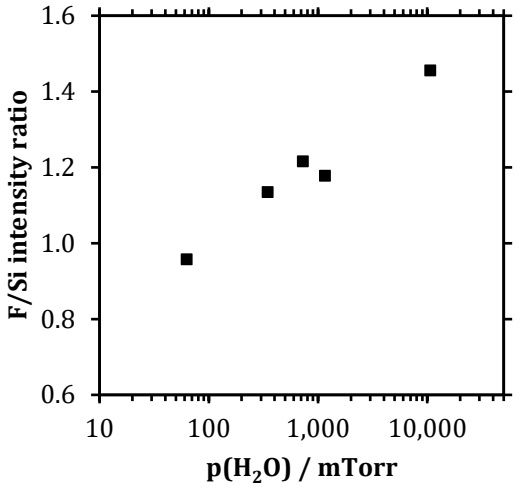

Figure 70: Results of F/Si ratio in films from F8H2-$SiCl_3$ as obtained from XPS experiments. The results indicate thicker layers at increasing p(H_2O) applied during the deposition.

Film thicknesses of samples prepared under varying p(H_2O) were examined by ellipsometry and yielded an increasing thickness with increasing water partial pressure. As given in Figure 71, the ellipsometric film thickness increases from (8.3 ± 0.41) Å at low water partial pressures (p(H_2O) = 63 mTorr) to (12.9 ± 0.4) Å at elevated pressures (p(H_2O) = 10,691 mTorr). It has already been mentioned that ellipsometry cannot be employed in terms of certainty of absolute values. Nonetheless it can help to derive a first understanding concerning the relative development of the film's thickness as a function of p(H_2O).

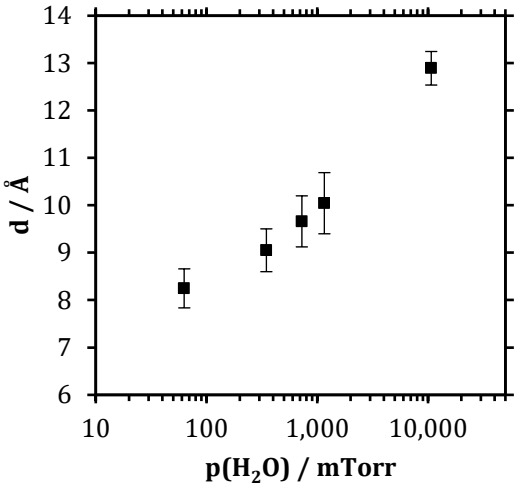

Figure 71: Ellipsometric thickness for films from F8H2-$SiCl_3$.

A film deposited from F8H2-$SiCl_3$ was tested concerning its long-term stability (sample SF-Si-336-A, p(F8H2-$SiCl_3$) = 265 mTorr, p(H_2O) = 58 mTorr). For this, wetting experiments were conducted immediately after deposition of the film and after 80 days of storage under ambient atmosphere conditions. The results reveal that the wetting properties of the film do not change during this period of time, although being exposed to standard ambient humidity (Table 20). The advancing contact angle as well as contact angle hysteresis are constant within the error margins, so that no extensive degradation during this time of storage is assumed.

Day	**θ_{adv} [°]**	**$\Delta\theta$ [°]**
1	74.2 ± 0.4	2.2 ± 0.1
80	74.3 ± 0.3	2.3 ± 0.1

Table 20: Wettability results for long-term stability of sample SF-Si-336-A. Deposition conditions: p(F8H2-$SiCl_3$) = 265 mTorr, p(H_2O) = 58 mTorr.

Initial AFM experiments with samples prepared at low and high p(H_2O) were conducted in order to gain further insight into the samples' surface morphologies and how these results relate to their corresponding wetting properties. It has to be noted that the samples had been under storage for several weeks before AFM-experiments were conducted. These experiments were rather meant as a first impression and starting point for studies following this work, especially in terms of a new deposition system. Hence, it cannot be excluded that the films suffered certain deterioration in the time between deposition and AFM-characterization but the results of the long-term stability experiments suggest that only minor changes may have taken place. As will be shown, the desired "first glimpse" and comparison between high- and low-p(H_2O)-processing as well as chain length differences was successfully accomplished. Sample SF-Si-320 was prepared at p(H_2O) = 132 mTorr (p(F8H2-$SiCl_3$) = 257 mTorr) and exhibited wetting properties with HD of θ_{adv} = 75.9° and $\Delta\theta$ = 2.2°. Sample SF-Si-282 was prepared at p(H_2O) = 1166 mTorr (p(F8H2-$SiCl_3$) = 257 mTorr) with θ_{adv} = 80.2° and $\Delta\theta$ = 8.2°. Other process parameters were applied according to Table 19. AFM-images of both samples are shown in Figure 72 and Figure 74 and are given in identical lateral dimensions.

The images reveal a striking difference between the two deposition conditions. Both samples show signs of circular particles on the surface which similarly vary in size from approximately 20 to 150 nm. However, while the average diameter of the particles is quite constant, the sample prepared at higher p(H_2O) shows a highly increased density of these defects by a factor of 6.5. The maximum diameter of the particles is relatively similar for both samples, although a slight decrease from low to high p(H_2O) is detected. In contrast to this, the average height of the particle increases for the sample prepared at an elevated water partial pressure.

Sample	**p(H_2O) [mTorr]**	**Particle Density [μm^{-1}]**	**Particle Diameter [nm]**			**Particle Height [nm]**		
			mean	**min.**	**max.**	**mean**	**min.**	**max.**
SF-Si-320	132	0.6	60.6	22.0	157.4	6.3	1.4	17.5
SF-Si-282	1166	3.9	60.2	22.0	142.8	8.1	2.6	22.4

Table 21: AFM-results of films deposited from F8H2-$SiCl_3$.

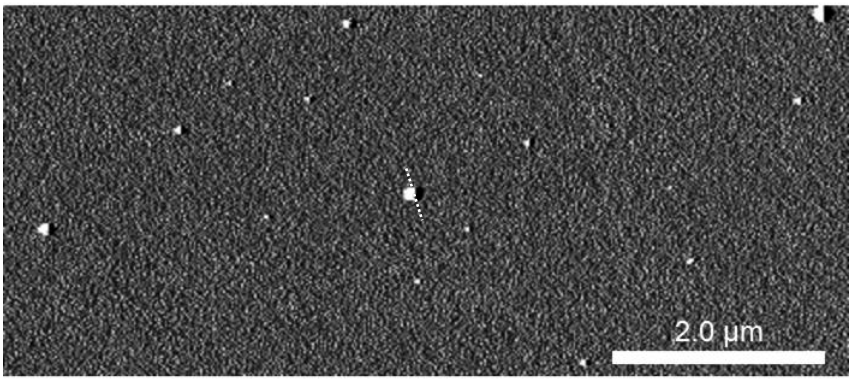

Figure 72: AFM-image of F8H2-$SiCl_3$-sample deposited at low p(H_2O) (SF-Si-320). The dotted line indicates the horizontal section of the line scan.

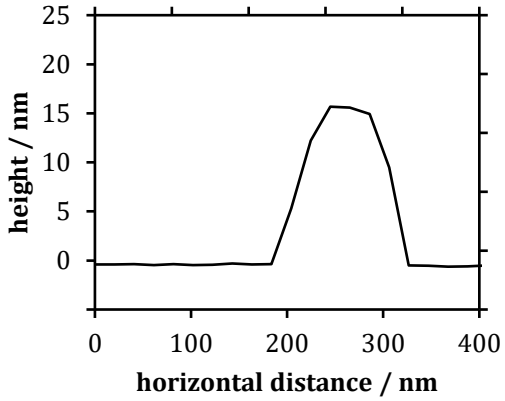

Figure 73: Line scan of F8H2-$SiCl_3$-sample deposited at low p(H_2O) (SF-Si-320).

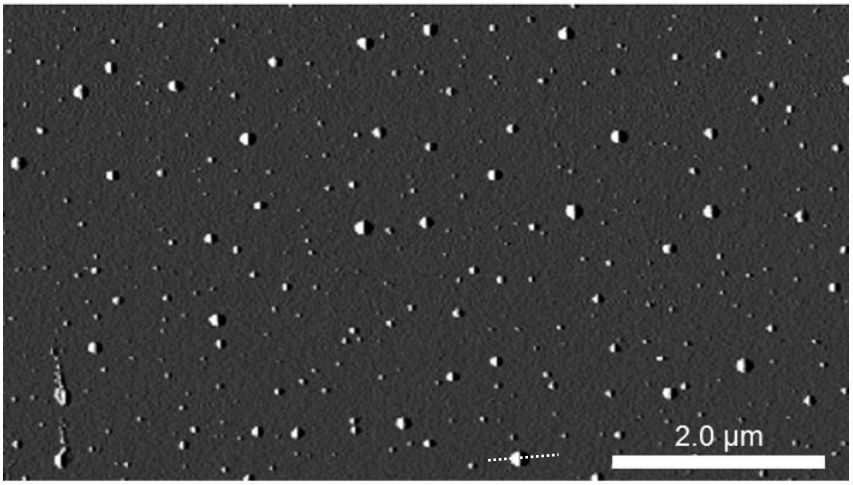

Figure 74: AFM-image of F8H2-$SiCl_3$-sample deposited at high p(H_2O) (SF-Si-282). The dotted line indicates the horizontal section of the line scan.

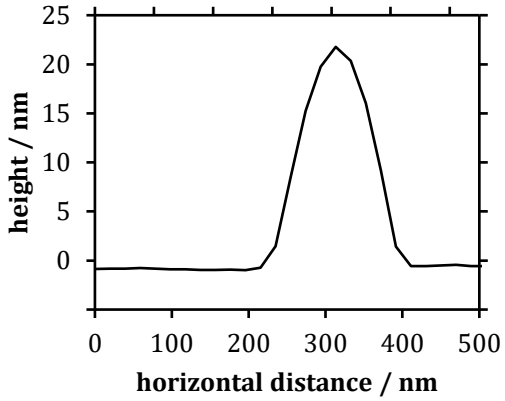

Figure 75: Line scan of F8H2-$SiCl_3$-sample deposited at high p(H_2O) (SF-Si-282).

sSIMS experiments of films from F8H2-$SiCl_3$ revealed an increased concentration of chloride within the surface for high values of p(H_2O) during the deposition of the films (Figure 76). This effect at high water pressures might be due to an increased adsorption of HCl which is liberated during the hydrolysis of the silane precursor. In

order to yield comparable data sets, the results given in Figure 76 are presented as the intensity ratio $\frac{I(Cl^-)}{I(SiO_2^-)}$. The use of the silica substrate's signal for referencing yields a value independent from the current conditions during individual sSIMS experiments.

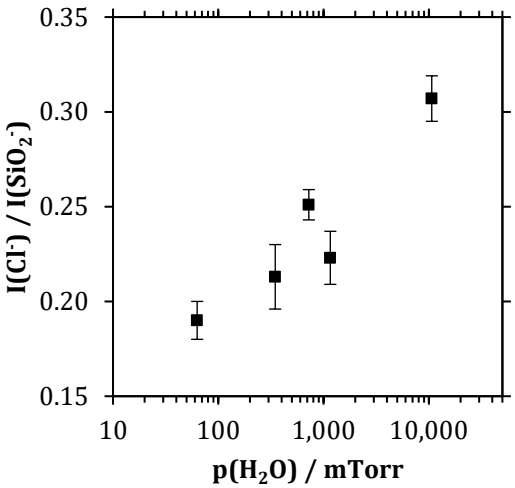

Figure 76: sSIMS experimental results of films from F8H2-$SiCl_3$. Results indicate an increase of chloride within the final film with increasing p(H_2O) during film deposition.

6.1.1.2. Silane partial pressure p(F8H2-$SiCl_3$)

The results of the influence of silane partial pressure during the deposition of films from F8H2-$SiCl_3$ are presented in Figure 77 in terms of dynamic contact angle measurements with HD and Figure 78 for contact angle experiments with water. For HD, experiments show a steady increase of the advancing contact angle from θ_{adv} = 66.5° for depositions accomplished at low p(F8H2-$SiCl_3$) until reaching a plateau value of approximately 75° at elevated partial pressures. Contact angle hysteresis $\Delta\theta$ shows only slight deviations over the whole range of process conditions with $\Delta\theta \approx 2.4°$. Even at low silane concentrations hysteresis was found to be as low as 2.7°. Thus, the results suggest best film quality at optimized conditions (i.e. using the smallest possible amount of silane) when a minimum silane partial pressure is supplied while the plateau value of θ_{adv} is obtained.

Wetting experiments with water yield similar results shifted to larger contact angles as with HD but show stronger differences in Δθ at elevated silane partial pressures.

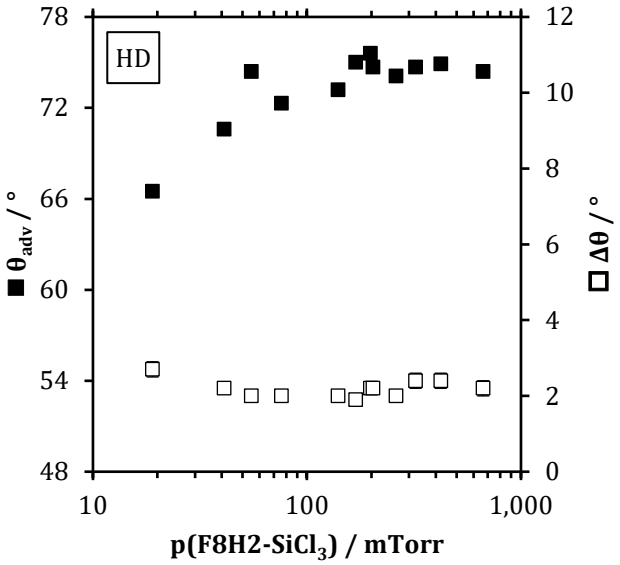

Figure 77: Results of wetting experiments with HD on samples prepared under varying p(F8H2-$SiCl_3$).

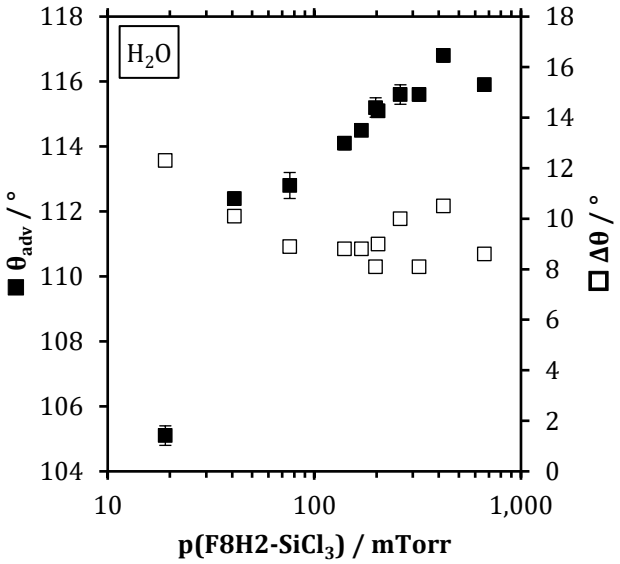

Figure 78: Results of wetting experiments with H_2O on samples prepared under varying p(F8H2-$SiCl_3$).

6.1.1.3. Deposition times

The influence of two important reaction times on the samples' wetting properties has been studied for films deposited from F8H2-$SiCl_3$. During silane adsorption time t(F8H2-$SiCl_3$) the precursor may pre-adsorb onto the substrate's surface prior to the addition of water vapor. During water reaction time t(H_2O) both silane and water vapor are present in the reactor chamber and all components are able to react with the substrate or with each other. Experiments concerning deposition times were conducted after an adaption to the deposition system was made, so that obtained values of θ_{adv} are not directly comparable to prior experiments concerning vapor partial pressures. Experiments of deposition times were all conducted under the same technical set-up, so that these experiments are comparable to each other.

Variation of t(F8H2-$SiCl_3$) was found to have no notable effect on the wetting properties of the final films (Figure 79). Neither advancing contact angles nor contact angle hystereses were affected considerably by varying silane adsorption time over a range of one minute to three hours and samples both at shortest and longest adsorption times gave identical results within the error margins.

The effect of t(H_2O) on the wetting properties is clearly more prominent (Figure 80). For very short water reaction times a low θ_{adv} of only 70.2° is detected. As t(H_2O) increases dewetting increases as well and θ_{adv} apparently reaches a plateau value of about 72.5°, suggesting the necessity of a minimum water reaction time in order to obtain optimum films. In contrast to the change in θ_{adv}, contact angle hysteresis $\Delta\theta$ is rather constant within the error margins for all samples ($\Delta\theta \approx 2.2°$), although a slight increase in $\Delta\theta$ may be observed for very short water reaction times.

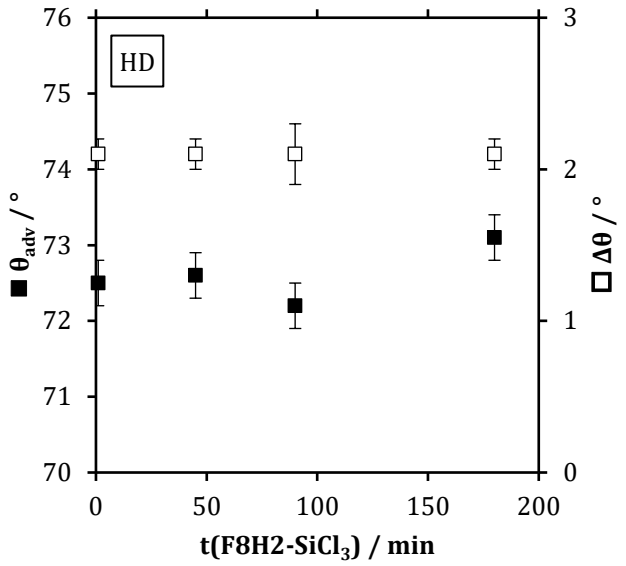

Figure 79: Results of wetting experiments with HD on films deposited from F8H2-$SiCl_3$ prepared at varying silane adsorption times t(F8H2-$SiCl_3$) do not suggest a considerable effect on wetting properties. Experiments are to be interpreted independently from other depositions (see explanation given in the text).

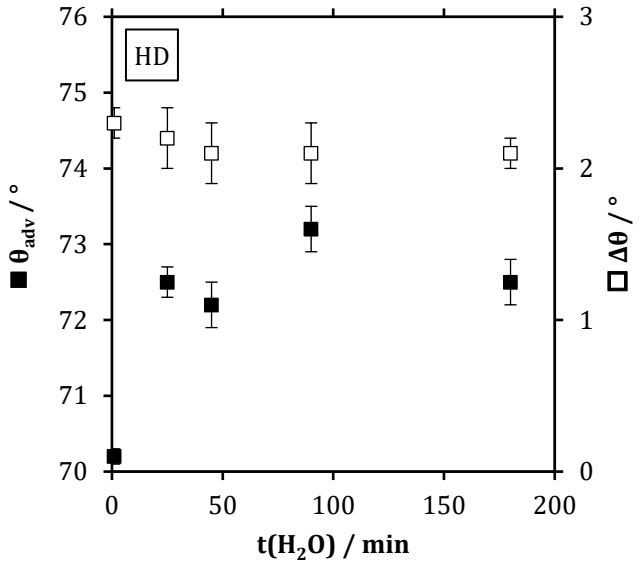

Figure 80: Results of wetting experiments with HD on films deposited from F8H2-$SiCl_3$ prepared at varying water reaction times t(H_2O). Results show improved film quality if t(H_2O) is extended to t(H_2O) ≥ 20 min. Experiments are to be interpreted independently from other depositions (see explanation given in the text).

Variation of the post-deposition desorption process was not studied with major priority, as the majority of physisorbed molecules is expected to be removed from the substrate and deposition system during the nitrogen purging steps prior to the desorption step. Therefore, only a small number of depositions was accomplished under variation of desorption time t(des.) and desorption temperature T(des.) (which can be set individually from the remaining deposition process temperature). The results of these deposition processes are given in Table 22 and did not reveal any significant change in wetting properties within the error margins, neither by desorption temperature nor by desorption duration.

Sample	**t(des.) [min]**	**T(des.) [°C]**	**θ_{adv} [°]**	**$\Delta\theta$ [°]**
SF-Si-0301-A (ref.)	60	*cooling down from 80 °C*	74.1 ± 0.2	2.0 ± 0.1
SF-Si-0252	1	*cooling down from 80 °C*	73.9 ± 0.2	2.2 ± 0.1
SF-Si-0254	60	120	73.7 ± 0.1	2.4 ± 0.1
SF-Si-0251	180	120	73.8 ± 0.2	2.2 ± 0.1

Table 22: Results of wetting experiments with HD on samples deposited from F8H2-$SiCl_3$ under variation of conditions during desorption phase. Sample SF-Si-0301-A serves as reference.

6.1.1.4. Deposition Temperature

Although the range of investigated deposition temperatures was rather small, a detectable influence on the monolayers' wetting properties could be observed and film quality decreases with increasing deposition temperature. Periods of silane adsorption time and water reaction time were not changed during these experiments. The strong decrease of θ_{adv} is particularly prominent while $\Delta\theta$ slightly increases by 1° (Figure 81). This effect may be assumed to be a consequence of reduced sticking probability of precursor molecules to the substrate surface at elevated temperatures.

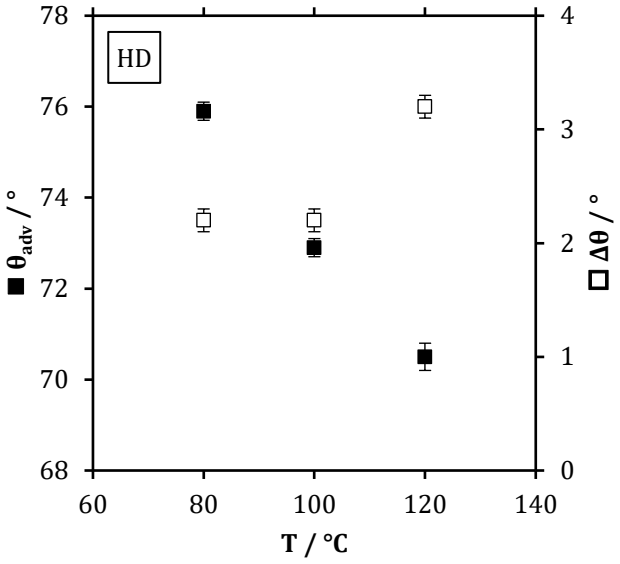

Figure 81: Results of wetting experiments with HD on samples from F8H2-$SiCl_3$ prepared at varying deposition temperature.

6.1.2. Films Deposited from F10H2-$SiCl_3$

6.1.2.1. Water partial pressure p(H_2O)

The investigation of the effect of water partial pressure on the HD wetting properties of films deposited from F10H2-$SiCl_3$ revealed some surprising differences compared to films prepared from short-chain F8H2-$SiCl_3$. As presented in Figure 82, θ_{adv} steadily increases with increasing p(H_2O) from approximately 62.0° at low water pressure to roughly 77.5° at increased amounts of water. Qualitatively, the results are similar to the results obtained from F8H2-$SiCl_3$-films, but differ in such that θ_{adv} at low p(H_2O) is several degrees smaller for films from F10H2-$SiCl_3$. A distinct plateau for θ_{adv} at high p(H_2O) cannot be observed due to the limited range of partial pressures investigated. For F10H2-$SiCl_3$, $\Delta\theta$ was found to exhibit its largest values of $\Delta\theta \approx 4.5°$ at low water partial pressures and decreases with increasing p(H_2O) to approximately $\Delta\theta \approx 2.5°$ at p(H_2O) ≈ 800 mTorr. Further increase of p(H_2O) leads to a slight increase to $\Delta\theta \approx 3.5°$. Although no experiments were conducted for even higher water partial pressures, it is assumed that contact angle hysteresis would further increase at elevated pressures of p(H_2O) > 2,000 mTorr similar to depositions from F8H2-$SiCl_3$. The behavior of $\Delta\theta$ for F10H2-$SiCl_3$-films is strikingly different from the results obtained for films from

F8H2-$SiCl_3$ (see Figure 66 for comparison). Best wetting properties obtainable at optimum conditions ($p(H_2O) \approx$ 1,000 mTorr) are found to be $\theta_{adv} \approx 77.5°$ and $\Delta\theta \approx 2.5°$.

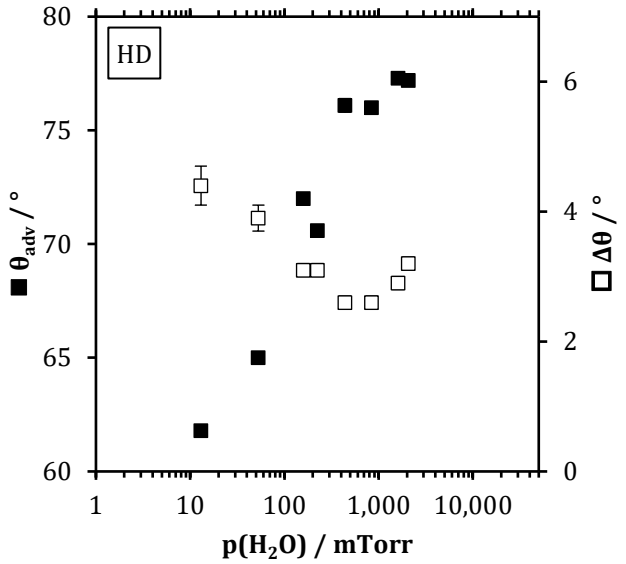

Figure 82: Results of wetting experiments with HD for films deposited from F10H2-$SiCl_3$ prepared at varying water partial pressures $p(H_2O)$.

A film deposited from F10H2-$SiCl_3$ was tested concerning its long-term stability (sample JK096.2, p(F10H2-$SiCl_3$) = 322 mTorr, $p(H_2O)$ = 200 mTorr). For this, wetting experiments were conducted immediately after deposition of the film and after 77 days of storage under ambient atmosphere conditions. The results reveal that the wetting properties of the film do not change significantly during storage (Table 23) but in contrast to the sample from F8H2-$SiCl_3$ do show a slight decrease in θ_{adv}. As contact angle hysteresis remains unaffected, it can be assumed that the samples overall integrity has not changed strongly upon the exposure to ambient humidity.

It has to be mentioned that this sample was one of the very first films that were deposited from F10H2-$SiCl_3$. Process conditions differ in details from those that were used throughout the later part of the study so that this sample and its ratio of water

to silane partial pressures represent unique conditions and are not directly comparable to later samples.

Day	θ_{adv} [°]	$\Delta\theta$ [°]
1	76.5 ± 0.2	3.2 ± 0.1
77	75.3 ± 0.4	3.3 ± 0.1

Table 23: Wettability results for long-term stability of sample JK096.2. Deposition conditions: p(F10H2-$SiCl_3$) = 322 mTorr, p(H_2O) = 200 mTorr.

As for samples prepared from F8H2-$SiCl_3$, AFM experiments have been conducted for depositions from F10H2-$SiCl_3$ at different values of p(H_2O) as well. Here, sample SF-Si-391 was prepared at p(H_2O) = 439 mTorr (p(F10H2-$SiCl_3$) = 240 mTorr) and exhibited wetting properties with HD of θ_{adv} = 76.1° and $\Delta\theta$ = 2.6°. Sample SF-Si-389 was prepared at p(H_2O) = 1609 mTorr (p(F8H2-$SiCl_3$) = 262 mTorr) with θ_{adv} = 77.3° and $\Delta\theta$ = 2.9°. Other process parameters were applied according to Table 19. AFM images of both samples are shown in Figure 83 and Figure 85. The results of AFM experiments are very similar compared to the results obtained for samples from F8H2-$SiCl_3$. Again, apparently circular particles are observed on both samples with a strongly higher particle density on the sample prepared at higher p(H_2O), where density is increased by a factor of 24. The average particle diameter is slightly larger for the low-p(H_2O) sample, which may be a matter of statistics and caused by the very small number of particles to be evaluated in this segment of the sample. As expected, the range of particle diameters broadens with increasing water partial pressure and the maximum particle size increases from 91 nm to 123 nm. The average height of the particles is the same for both samples, although the range of particle height strongly increases. Some particles with vertical dimensions >10 nm are detected, which, however, are present in only very small numbers, so that an average value of 3.5 nm is obtained.

In comparison to the sample prepared from F8H2-$SiCl_3$ the particle density on samples from low p(H_2O) is reduced and hardly any particles are detected on the film from F10H2-$SiCl_3$. The average particle diameter for these samples is slightly

increased for the longer-chain films. The average particle heights are only approximately half the dimensions of the F8H2-$SiCl_3$-films.

Sample	$p(H_2O)$ [mTorr]	Particle Density [μm^{-1}]	Particle Diameter [nm]			Particle Height [nm]		
			mean	min.	max.	mean	min.	max.
SF-Si-391	439	0.1	66.1	49.2	90.8	3.4	2.6	3.9
SF-Si-389	1609	3.5	53.5	22.0	122.7	3.5	1.9	12.7

Table 24: AFM-results of film deposited from F10H2-$SiCl_3$.

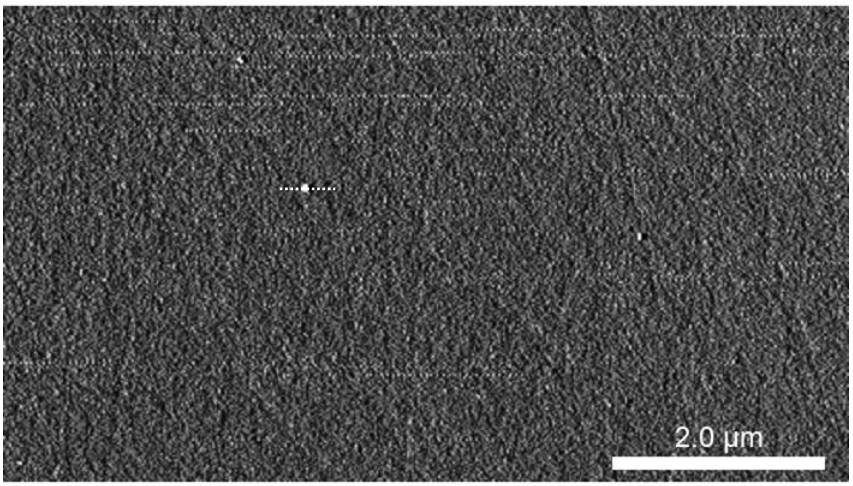

Figure 83: AFM-image of F10H2-$SiCl_3$-sample deposited at low $p(H_2O)$ (SF-Si-391). The dotted line indicates the horizontal section of the line scan.

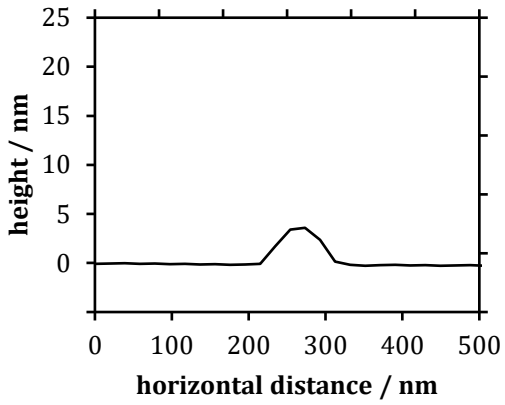

Figure 84: Line scan of F10H2-$SiCl_3$-sample deposited at low p(H_2O) (SF-Si-391).

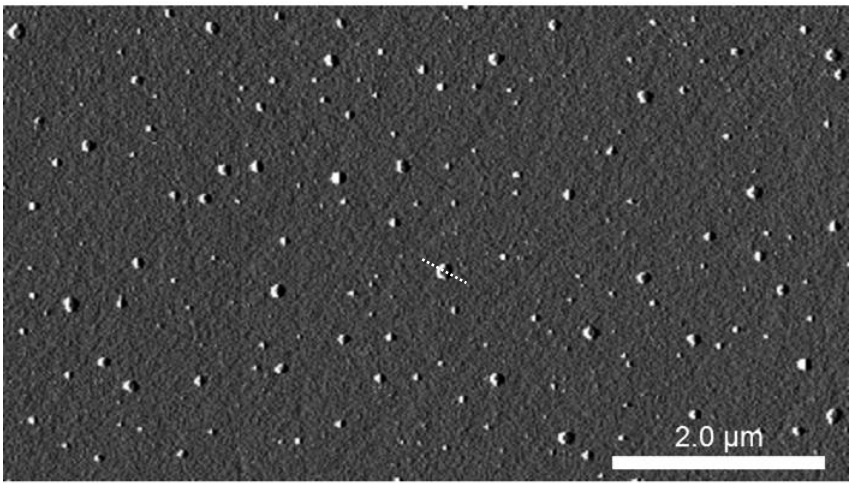

Figure 85: AFM-image of F10H2-$SiCl_3$-sample deposited at high p(H_2O) (SF-Si-389). The dotted line indicates the horizontal section of the line scan.

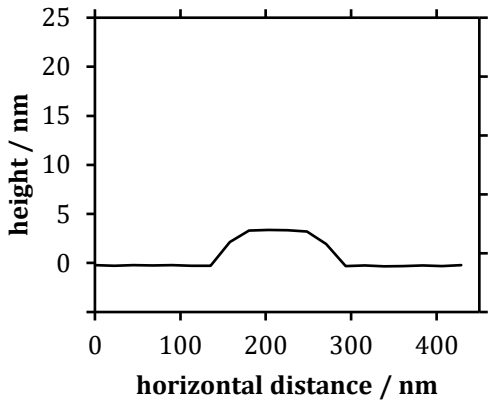

Figure 86: Line scan of F10H2-$SiCl_3$-sample deposited at high p(H_2O) (SF-Si-389).

6.1.2.2. Silane partial pressure p(F10H2-$SiCl_3$)

Results of wetting experiments on films deposited from F10H2-$SiCl_3$ are presented in Figure 87 and reveal a similar yet in details distinctly different behavior compared to F8H2-$SiCl_3$-films. For small values of p(F10H2-$SiCl_3$) ≈ 30 mTorr films with low θ_{adv} and high $\Delta\theta$ are obtained and suggest the formation of low-quality films (θ_{adv} ≈ 54.0°, $\Delta\theta$ ≈ 10.0°). Wetting properties strongly improve with increasing p(F10H2-$SiCl_3$) and approximate plateau values for both θ_{adv} and $\Delta\theta$ are obtained at p(F10H2-$SiCl_3$) > 50 mTorr. These plateaus yield films with θ_{adv} ≈ 72.0° and $\Delta\theta$ ≈ 3.0°. Interestingly, the experiment at the highest silane partial pressure (p(F10H2-$SiCl_3$) = 613 mTorr) resulted in a singular decrease of θ_{adv} while $\Delta\theta$ remained at the low plateau level. This noticeable value is assumed to be caused by irregularities during the measurement but unfortunately, even higher silane partial pressures could not be investigated, so that no tendency for further development of θ_{adv} can be given. Similar to films from F8H2-$SiCl_3$ wetting results appear to improve with increasing silane partial pressure, although the differences between initial and plateau stages are more prominent with F10H2-$SiCl_3$, particularly at low partial pressure. Analogous to films from F8H2-$SiCl_3$ a minimum partial pressure of F10H2-$SiCl_3$ appears to be necessary for the formation of good-quality films.

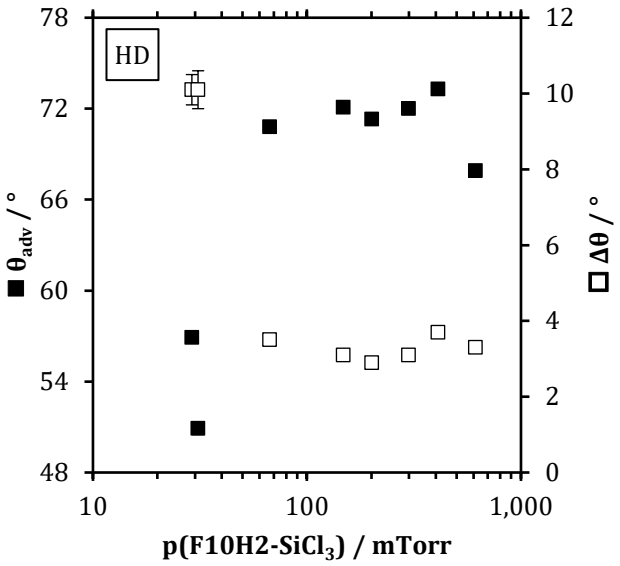

Figure 87: Results of wetting experiments with HD on samples prepared under varying p(F10H2-$SiCl_3$).

6.1.2.3. Deposition Temperature

The effect of deposition temperature for films from solid F10H2-$SiCl_3$ was studied at a reduced silane partial pressure of p(F10H2-$SiCl_3$) = 150 mTorr in order to achieve comparable conditions even at low temperatures. This pressure is above the threshold pressure for F10H2-$SiCl_3$ where good quality films are observed (compare Figure 87).

The observed effects on wetting properties induced by variations in deposition temperature are rather small. Contact angle hysteresis Δθ remains constant at Δθ ≈ 3.2° whereas the advancing contact angle θ_{adv} slightly increases from below 70° at T = 80 °C to approximately 72° at T = 100 °C and decreases again to about 70° at T = 120 °C. In contrast to an evident strong effect of deposition temperature for films from F8H2-$SiCl_3$, no distinct conclusion can be drawn for F10H2-$SiCl_3$. Similar to films deposited from F8H2-SiCl3, the slight decrease in quality at a deposition temperature of 120 °C may be attributed to a decreasing sticking probability of the precursor molecules. On the other hand, the increase of θ_{adv} from 80 °C to 100 °C could be a consequence of improved vaporization of the silane precursor and thus an improved supply of precursor molecules for film formation.

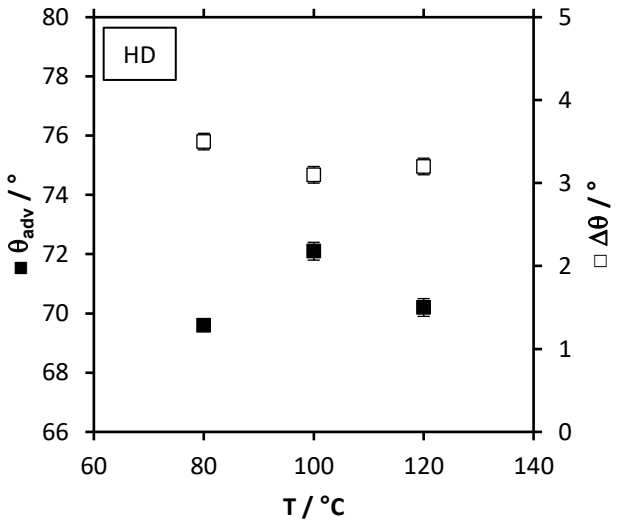

Figure 88: Results of wetting experiments with HD on samples from F10H2-$SiCl_3$ prepared at varying deposition temperature.

6.2. Discussion

The gathered results underline the outstanding influence of water for the deposition of SAMs from fluoroalkylated trichlorosilane precursors and the exact choice of process parameters is crucial for the outcome of the wetting properties of the final films. The main part of this section will therefore be dedicated to the results that are influenced by manipulations of the water addition procedure.

6.2.1. Primary Importance of Water Addition and the Effect of Reactants' Partial Pressures

The obtained wetting properties of films deposited from F8H2-$SiCl_3$ for HD at optimum conditions ($\theta_{adv} \approx 76.5°$, $\Delta\theta \approx 2.0°$) relate well to values published in literature and indicate a comparable or even superior film quality, particularly in terms of film homogeneity expressed by small contact angle hysteresis (see Table 2 in Section 2.3.2). The general applicability of the deposition setup with this specific

system can therefore be confirmed and may even suggest this CVD-system as a means of improved film deposition, particularly concerning the automated and flexible deposition sequence.

F10H2-$SiCl_3$-films exhibit p(H_2O)-dependent wetting properties that are to some degree strikingly contrasting to films from F8H2-$SiCl_3$ and under optimum deposition conditions, wetting properties for films from F10H2-$SiCl_3$ exhibit values of $\theta_{adv} \approx 76.0$ and $\Delta\theta \approx 2.5°$. Published values for films from F10H2-$SiCl_3$ are rarely to be found but the comparison to literature suggests superior properties of the CVD-deposited films described in this work.

The difference to films from F8H2-$SiCl_3$ becomes evident particularly in terms of contact angle hysteresis, which remains at a remarkably low value of 3° for F10H2-$SiCl_3$-films even at water pressures as high as 1,000 mTorr. In this range, F8H2-$SiCl_3$-films already exhibit values of hysteresis of approximately 10°. Regarding contact angle hysteresis as a measure of surface homogeneity this means that films from longer precursor molecules F10H2-$SiCl_3$ appear to form more uniform monolayers than those from F8H2-$SiCl_3$. Looking at the advancing contact angle θ_{adv}, the general effect of increasing p(H_2O) is similar to films from F8H2-$SiCl_3$ but differs in details. Thus, films from F10H2-$SiCl_3$ exhibit lower initial values of θ_{adv} for low water pressures and no plateau behavior appears to be detectable at high partial pressures. This, however, may be due to the fact, that the number of films from F10H2-$SiCl_3$ was limited and no deposition was accomplished applying a water partial pressure exceeding 2,000 mTorr. Therefore, it cannot be excluded that a plateau value for θ_{adv} will be observed at further increased water pressures. This plateau might probably appear at higher p(H_2O) than experimentally detected for films from F8H2-$SiCl_3$, particularly taking into account that contact angle hysteresis with F10H2-$SiCl_3$ showed higher stability against large values of p(H_2O) than for F8H2-$SiCl_3$-films.

Although the resulting wetting properties under optimum deposition conditions are similar for films from F8H2-$SiCl_3$ ($\theta_{adv} \approx 76.5°$, $\Delta\theta \approx 2.0°$) and F10H2-$SiCl_3$ ($\theta_{adv} \approx 76.0°$, $\Delta\theta \approx 2.5°$), the required optimum conditions vary strongly in terms of water partial pressure. While for F8H2-$SiCl_3$ a pressure of $p(H_2O) \approx 200$ mTorr is required, optimum properties with F10H2-$SiCl_3$ are achieved at $p(H_2O) \approx 1{,}000$ mTorr. As described, this is a value at which films from F8H2-$SiCl_3$ already deteriorate in quality. This effect may also be a result of the 20 °C increase in deposition temperature for F10H2-$SiCl_3$, but the overall behavior in p(H_2O)-dependency suggests to be too different as to be a pure consequence of deposition

temperature. Moreover, the results obtained for depositions from different temperatures do not confirm a strong influence of the deposition temperature on the films' wetting properties.

For films from F8H2-$SiCl_3$, XPS experiments revealed a steady increase in the F/Si elemental ratio with increasing $p(H_2O)$ (see Figure 70), which can be attributed to an increased film thickness. This conclusion is supported by ellipsometric measurements of the films' thicknesses. Here, a steady increase in film thickness from d = (8.25 ± 0.41) Å at low water pressure to d = (12.89 ± 0.35) Å at high pressure is observed (Figure 71). The maximum height difference corresponds to approximately half a monolayer. The increase of film thickness is presumably a result of increased cross-linking between silane molecules during the deposition process. This causes an increased disorder within the film accompanied by the development of multilayer growth. It is assumed that the origin of increased cross-linking lies in the over-stoichiometric addition of water which causes the monolayer films to grow in a non-conformal fashion. The impact of cross-linking has its foundations in the hydrolysis of precursor molecules that takes place during the deposition of trichlorosilane-based films. As introduced, SAM formation is thought to proceed via the fast and stoichiometric hydrolysis of trichlorosilane precursors, i.e. the hydrolysis of chloro functionalities to hydroxyl groups. Looking at this hydrolysis in more detail, it becomes obvious that it takes place in a stepwise fashion from trichlorosilane -$SiCl_3$ (S0) to dichlorosilanol -$SiCl_2OH$ (S1), chlorodisilanol -$SiCl(OH)_2$ (S2) and trisilanol -$Si(OH)_3$ (S3) under simultaneous liberation of HCl. The extent of hydrolysis thus depends on the amount of water molecules provided during the deposition process, which is measured directly in terms of water partial pressure $p(H_2O)$. During deposition, all these species may consequently be involved in monolayer formation.

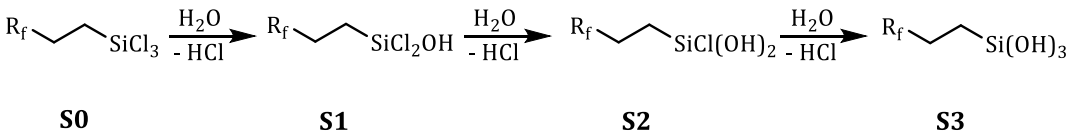

Figure 89: Illustration of step-wise hydrolysis of trichlorosilane precursor under liberation of HCl.

Hydrolyzed species are assumed to self-assemble into a densely-packed monolayer where dense packing is directed by the fluoroalkyl chains. While hydrolyzed silanes can bind covalently to the silica substrate via siloxane bonds, pre- and post-adsorption cross-linking directly between molecules can occur as well. Unlike the siloxane bonding between substrate and precursor, this kind of inter-precursor siloxane cross-linking has been shown to introduce defect-sites and to induce multilayer growth.[157,216] Bringing back to our minds the explanations on the matter of cross-linking in silane SAMs from sections 2.3.4 and 2.5, it is a major requirement for the formation of well-ordered films that cross-linking of silane-headgroups is prevented. According to the reaction scheme in Figure 89, only species S2 and S3 are able to form cross-linked agglomerations of more than two molecules during the deposition process. Molecules S1 may of course form dimeric species, which however would not be able to chemically bind to the substrate (unless further hydrolysis takes place). As the concentration of cross-linkable molecules S2 and S3 directly depends on the amount of supplied water $p(H_2O)$, the risk of cross-linking and its unwanted side-effects are expected to increase with increased $p(H_2O)$.

As a starting point for further interpretation, the relative amount of cross-linkable species can be initially estimated via a simple model and enables the possibility to easily compare different silanes and varying deposition conditions in order to further investigate the cross-linking processes. The model is based on the initial partial pressures of silane and water which are applied for the deposition. For the calculation it is assumed that the formation probabilities of S1, S2 and S3 from water and their non-hydrolyzed forms are identical and that every collision between a water and any silane molecule results in a reaction whereas any silane species does not react with each other. The model yields the relative amounts of individual silane species at a given initial water/silane ratio as depicted in Figure 90. For improved clarity, the relative amounts are given in terms of $p_{rel} = p(H_2O)/[3p(silane)]$ so that full silane conversion ($p_{rel} = 1.0$) is achieved when $p(H_2O)$ is three times the initial silane partial pressure (full hydrolysis of the three chloro functionalities). In cases when $p(H_2O) > 3p(silane)$, the ratio $p(H_2O)/[3p(silane)]$ is defined as $p_{rel} = 1$, neglecting the effect of excess water molecules as required for full hydrolysis. The relative amounts of silane species S0, S1, S2 and S3 are given by:

$$n_{S0} = (1 - p_{rel})^3 \tag{18}$$

$$n_{S1} = 3 \cdot (1 - p_{rel})^2 \cdot p_{rel} \tag{19}$$

$$n_{S2} = 3 \cdot (1 - p_{rel}) \cdot {p_{rel}}^2 \tag{20}$$

$$n_{S3} = {p_{rel}}^3 \tag{21}$$

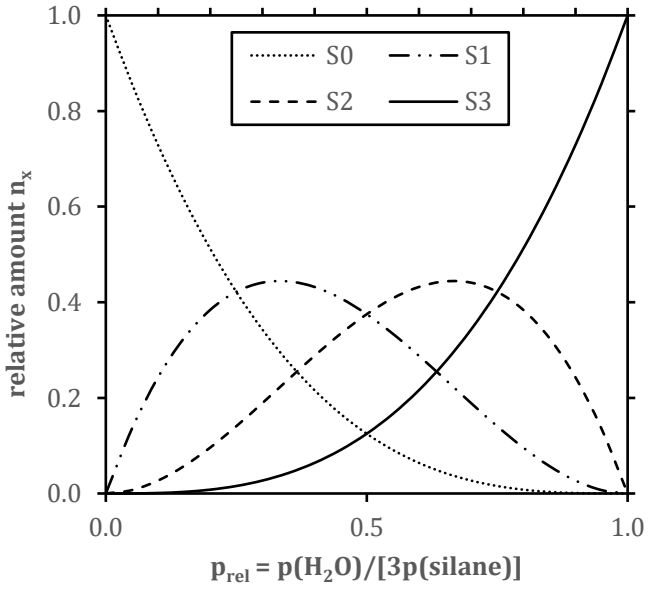

Figure 90: Illustration of the distribution of silane species according to the model introduced in the text. Trichlorosilane precursor S0 is stepwisely hydrolyzed to form dichlorosilanol (S1), chlorodisilanol (S2) and trisilanol (S3) species depending on the initial amount of water and fluoroalkylated trichlorosilane reactants.

Applying this model to the results obtained from the investigation of deposition parameters offers a first method to evaluate the results of varying conditions. Moreover, a direct connection between the quality of a monolayer film and the conditions promoting cross-linking can be drawn. As outlined earlier, only the silanol-species S2 and S3 are able to form cross-linked molecules, so that it is helpful to interpret the results of deposition processes with special regard to the amount of these cross-linkable species. In Figure 91, the results of films from F8H2-$SiCl_3$ deposited under varying process conditions are presented as a function of the total

amount of hydrolyzed species S1, S2 and S3. The amount of species S2 and S3 based relative to this overall silanol partial pressure is depicted in Figure 92.

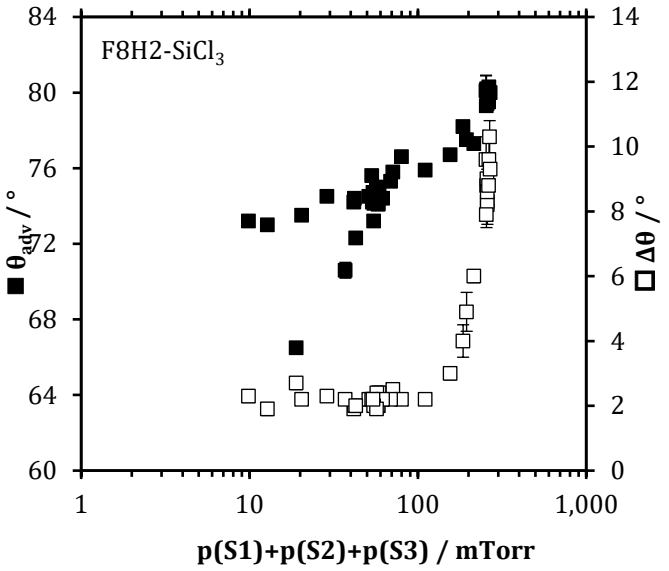

Figure 91: Results of wetting experiments with HD for films deposited from F8H2-$SiCl_3$ prepared at varying p(H_2O) and p(F8H2-$SiCl_3$). Results are given as a function of the sum of hydrolyzed species calculated for complete and stochiometric hydrolysis according to initial partial pressures. Evident discrepancies are associated with depositions at very small values of p(F8H2-$SiCl_3$).

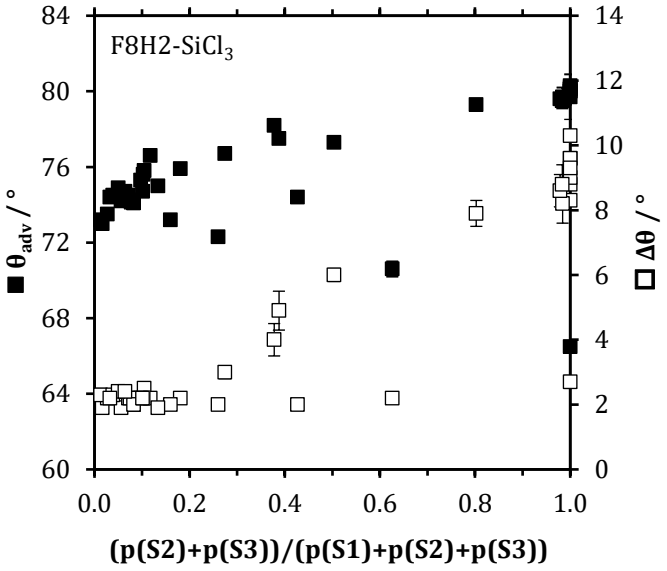

Figure 92: Relative fraction of cross-linkable species for experiments presented in Figure 91, underlining the impracticality of the initially applied model based on complete hydrolysis.

Both graphs make evident, that the assumption of a complete hydrolysis of the precursor molecules according to silane and water partial pressures does not reflect the experimentally obtained results of wetting properties. Inconsistencies arise particularly from depositions accomplished during the study of varying silane partial pressures with very high ratios of $p(H_2O)/3p(F8H2\text{-}SiCl_3)$ caused by very low $p(F8H2\text{-}SiCl_3)$. These depositions lead to low values of θ_{adv} and $\Delta\theta$ at high concentrations of cross-linkable species due to the large excess of water over silane molecules. Assuming a required minimum silane partial pressure (similar to the experimental results of experiments with varying $p(F8H2\text{-}SiCl_3)$) may therefore suit the idea of complete hydrolysis but would not fit in the overall picture. Similar problems are observed when this model is applied to experiments with $F10H2\text{-}SiCl_3$.

Hence, the assumption of complete hydrolysis based on initial partial pressures does not yield satisfying results. In order to evaluate the effect of time-dependent hydrolysis and a system under non-equilibrium conditions, the amounts of the respective silane species are calculated using kinetic modelling software ReactLab KINSIM in a further approach. [268] It allows the estimation of the amounts of S0, S1, S2, S3, H_2O and HCl which are present in the system during monolayer deposition. As no *in-situ* measurements were conducted during deposition experiments, the calculations are based on simple models without assuming too many unknown variables of the system. Thus, calculations are based on the hydrolysis reactions of

species S0, S1 and S2 with water and are assumed to be irreversible (Figure 93). The time scale of the calculations is chosen according to the experimental water reaction time t(H_2O) = 45 min.

$$S0 + H_2O \xrightarrow{k_1} S1 + HCl$$

$$S1 + H_2O \xrightarrow{k_2} S2 + HCl$$

$$S2 + H_2O \xrightarrow{k_3} S3 + HCl$$

Figure 93: Reaction schemes and rate constants applied for KINSIM calculations.

The corresponding velocity constants k_1, k_2, k_3 are assumed to be identical in first approximation. Variation of the reactions' velocity constants and comparison of the resulting gas-phase compositions with the experimentally determined wetting properties show that the development of wetting properties appears to correspond to the overall amount of hydrolyzed species S1, S2 and S3. By slowing down the rate of hydrolysis to $k_{1,2,3} = 1 \cdot 10^{-5}\ (\mathrm{mTorr} \cdot \mathrm{min})^{-1}$, the development of θ_{adv} and $\Delta\theta$ from low to high partial pressures of water and silane can be expressed reasonably (Figure 94). Although kinetic experiments have been reported for liquid-phase hydrolysis of alkyl silanes, reports concerning gas-phase experiments remain scarce. Nonetheless, a kinetic constant of $1 \cdot 10^{-5}\ (\mathrm{mTorr} \cdot \mathrm{min})^{-1}$ (which corresponds to approximately $3.7\ \mathrm{L}/(\mathrm{mol} \cdot \mathrm{s})$ at 80 °C) is within a rough order of magnitude of reported (liquid-phase) constants and is assumed reasonable within these approximations. [174,269,270]

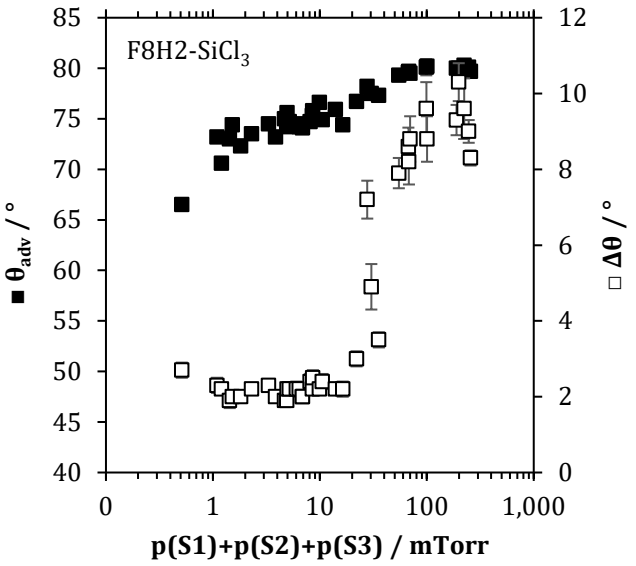

Figure 94: Results of wetting experiments with HD for films deposited from F8H2-$SiCl_3$ prepared at varying p(H_2O) and p(F8H2-$SiCl_3$) as a function of the sum of hydrolyzed species according to KINSIM modelling with $k_{1,2,3} = 1 \cdot 10^{-5}$ (mTorr · min)$^{-1}$. All combinations of initial silane and water partial pressures are reasonably reflected by this model.

This time-dependent and non-instantaneous formation of silanols enables further interpretation of the wetting results. It supports the assumption that a minimum amount of hydrolyzed species has to be present in the deposition system in order to enable the formation of dense films. This can be concluded from the finding, that θ_{adv} increases with an increasing overall amount of silanols and suggests a continuous improvement of the layer. Correspondingly, contact angle hysteresis is slightly increased at low silanol partial pressures and improved results of $\Delta\theta$ are detected if more silanols are supplied for film formation. However, at high partial pressures, $\Delta\theta$ strongly increases and disordered films are formed. Deposition experiments may therefore be divided into approximate regions of low (< 3 mTorr), optimum (≈ 3…10 mTorr) and excessive (> 10 mTorr) amounts of hydrolyzed species. Within the region of low silanol partial pressure, complete and homogeneous monolayer formation appears to be hindered by the reduced amount of silanols which can anchor to the substrate surface. As the total number of silanol molecules already exceeds the number of possible anchoring sites at the substrate surface (roughly 0.01 mTorr of silane molecules are required for complete coverage of a 2" wafer at 80 °C at an assumed coverage of 1 molecule/nm^2), competing effects may be apparent during the stage of water reaction time (e.g. diffusion effects, sticking coefficient of anchoring, temporary adsorption onto chamber walls).

While the overall behavior and wetting at low silanol concentration in particular can be explained by the overall silanol concentration, further information is desirable concerning the increase of film disorder at high amounts of hydrolyzed species. The increase of $\Delta\theta$ within the region of excessive silanol partial pressure is attributed to the presence of cross-linkable silanols S2 and S3. Relative fractions of these silanols increase with increasing overall pressure and are expected to introduce defects into the forming monolayer. For total silanol concentrations exceeding approximately 10 mTorr, the relative amount of cross-linkable species starts to increase noticeably, which is illustrated in Figure 95 and correlates well to the onset of film deterioration in terms of $\Delta\theta$. Thus, as depicted in Figure 96, deterioration of the monolayer in the region of excessive silanol partial pressure starts already if approximately 2 % of the overall silanols belong to the cross-linkable species S2 and S3.

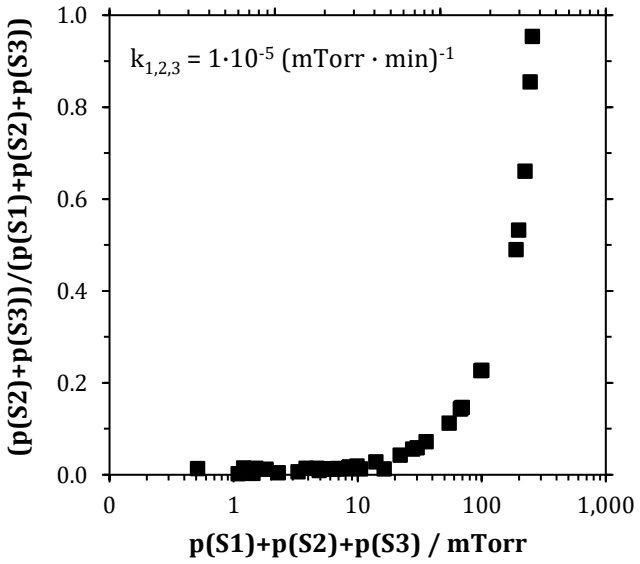

Figure 95: Relative fraction of cross-linkable species as a function of the total amount of hydrolyzed species according to time-dependent KINSIM modelling.

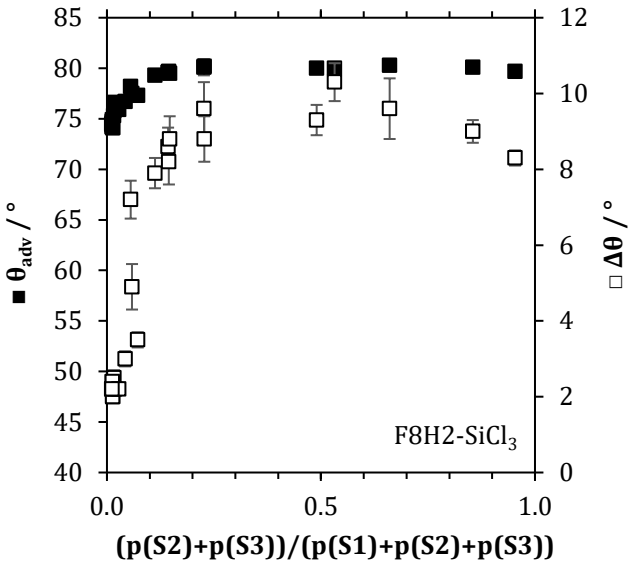

Figure 96: Results of wetting experiments for the region of excessive silanol partial pressure as a function of the relative amount of cross-linkable species.

The assumption of a system, that has not yet reached chemical equilibrium in terms of precursor hydrolysis thus leads to two main aspects of monolayer formation for films from F8H2-$SiCl_3$. First, the overall amount of hydrolyzed species determines the progress of SAM formation, which means that no dense and homogeneous layer is formed until a sufficient amount of silanols is supplied. Second, the relative amount of cross-linkable species S2 and S3 influences the quality of the formed layer in case that sufficient silanol molecules are present. If the partial pressure of S2 and S3 exceed a critical value, film deterioration initiates. Both parameters rely on the initial partial pressures of silane precursor and water vapor and the reaction time given for hydrolysis reaction.

KINSIM calculations were extended to deposition experiments from F10H2-$SiCl_3$ and the model of one global kinetic constant was applied analogously to F8H2-$SiCl_3$. As already experienced during the calculations with F8H2-$SiCl_3$, particularly the wetting results at low overall pressures posed difficulties during modelling. Figure 97 depicts the results of F10H2-$SiCl_3$ experiments as a function of the overall partial pressure of hydrolyzed silane species under the assumption of $k_{1,2,3} = 1 \cdot 10^{-5}$ $(\mathrm{mTorr} \cdot \mathrm{min})^{-1}$, i.e. hydrolysis of short- and long-chain precursors occurs at identical velocity. In general, the model appears to sufficiently represent the observed wetting properties.

However, for very low silanol concentrations, a deviation concerning two samples with large contact angle hysteresis was observed, which would have been expected at smaller partial pressures relative to the low-hysteretic sample at similar partial pressure (or vice versa, respectively). This deviation could not be resolved for kinetic constants in a range from $k_{1,2,3} = 1 \cdot 10^{-12} \ldots 100\ (\mathrm{mTorr} \cdot \mathrm{min})^{-1}$. These samples had been deposited during very low total pressure experiments. Wetting properties of these two samples had already been difficult to determine due to the evident inhomogeneity of the monolayer, which poses the question of the reliability of the samples' results. Nonetheless, this irregularity within the model might as well be caused by the singular measurement, which is found at even lower silanol pressure. Corresponding to the supposed range of low silanol concentration deposition with F8H2-SiCl3, the longer-chain silane F10H2-$SiCl_3$ appears to be more sensitive at this point, which is already reflected by the highly increased value of $\Delta\theta$.

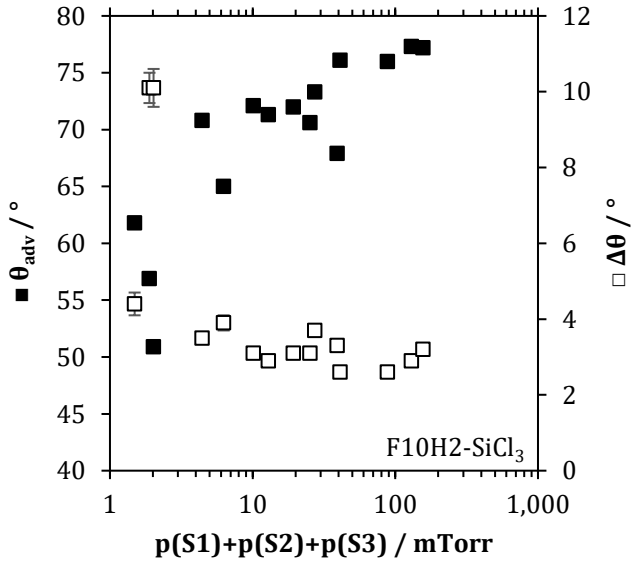

Figure 97: R esults of wetting experiments with HD for films deposited from F10H2-$SiCl_3$ prepared at varying p(H_2O) and p(F10H2-$SiCl_3$) as a function of the sum of hydrolyzed species according to KINSIM modelling with $k_{1,2,3} = 1 \cdot 10^{-5}\ (\mathrm{mTorr} \cdot \mathrm{min})^{-1}$.

Although the segment of low silanol partial pressure deposition (approximately < 5 mTorr) may be reflected by the overall increase of θ_{adv}, no distinct change towards

excessive silanol partial pressure similar to F8H2-$SiCl_3$ can be observed. Taking into account the relative amount of cross-linkable species S2 and S3 for increased silanol partial pressures as depicted in Figure 98, it may perhaps be assumed that the slight increase of Δθ at large relative amounts represents the onset of film deterioration and thus the beginning of the range of excessive silanol partial pressure. Data is, however, too thin to be definitive. Interpreting the slight increase of Δθ as the beginning of film deterioration, this would mean a strong shift to a critical concentration of approximately 30 % S2 and S3 for F10H2-$SiCl_3$ in comparison to 2 % for F8H2-$SiCl_3$. Chain-elongation would thus mean a distinctly more stable environment concerning the effect of cross-linkable silane species.

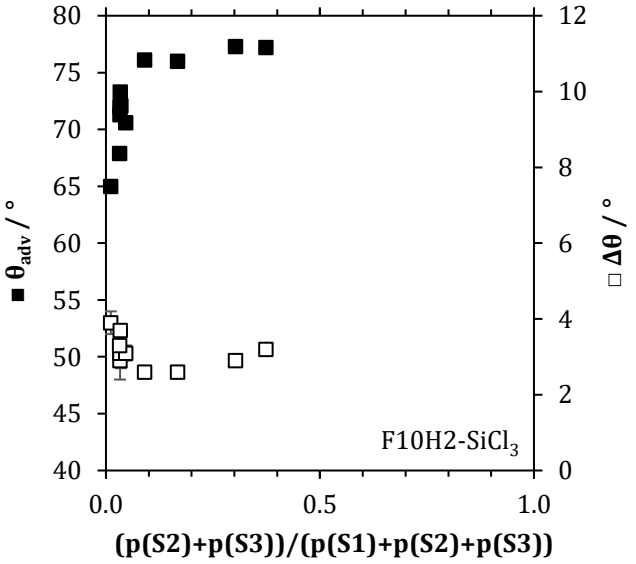

Figure 98: Results of wetting experiments for the region of optimum and excessive silanol partial pressure as a function of the relative amount of cross-linkable species.

In contrast to monolayers from F8H2-$SiCl_3$, film formation from F10H2-$SiCl_3$ is apparently not easily explainable in first approximation by the application of one global kinetic constant. Qualitatively, late onset of film deterioration due to cross-linking for monolayers deposited from F10H2-$SiCl_3$ may, for example, be the result of a preferred anchoring of silanols S1 to the surface before further hydrolysis may take place. Preferential anchoring of any silanol to the surface prior to silanol condensation may also be taken into consideration. Without the knowledge of any *in-situ* data of film formation within the surveyed system, the extension of

concentration modelling including these parameters is, however, very speculative and was not further pursued for the interpretation of the experimental results of F8H2-$SiCl_3$ or F10H2-$SiCl_3$. Extending the system only to dimers of the species S1, S2 and S3 (neglecting further condensation) would already have to include competitive adsorption of all monomers and dimers and may also include desorption phenomena from the substrate surface. As already the assumption of one overall kinetic constant for silane hydrolysis can only be an estimate here, further implementation of unknown variables would not lead to definite clarification.

The conclusions drawn from wetting experiments and modeling of cross-linkable species are supported by the results obtained from AFM experiments. Concerning the decreasing quality in terms of wetting properties that is caused by the application of increased water partial pressures, a distinct correlation is found with the increased number of particulate defects that is observed on the samples' surfaces. This behavior is detected both for films deposited from F8H2-$SiCl_3$ and F10H2-$SiCl_3$ and thus seems to be independent from the choice of precursor. The occurrence of particulates is in agreement with an increasing concentration of cross-linkable species as these species may condense to form cross-linked agglomerates. These agglomerates may then adsorb on the substrate's surface and lead to defects within the film as outlined before. A general increase in the number of occurring particles is therefore not necessarily surprising but a logical consequence if the concentration of cross-linkable species is expected to increase with increasing p(H_2O).

Surprising though are two observations made by AFM about films from F10H2-$SiCl_3$. First, at low p(H_2O) films from the longer chain precursor are found to exhibit a lower concentration of particles on the surface in comparison to films from shorter chain F8H2-$SiCl_3$. Thus, it may be assumed that an increase in chain length can lead to less particles within the final film. It has to be argued, of course, that deposition conditions were not identical for these samples (F8H2: p(H_2O) = 132 mTorr, p(F8H2-$SiCl_3$) = 257 mTorr, T = 80 °C; F10H2-$SiCl_3$: p(H_2O) = 439 mTorr, p(F10H2-$SiCl_3$) = 240 mTorr, T = 100 °C). The relative difference of particle density from low to high p(H_2O) is yet more evident for the samples from F10H2-$SiCl_3$ than from F8H2-$SiCl_3$ (i.e. longer chains do form particles) and the absolute water partial pressure during the deposition of F10H2-$SiCl_3$ was distinctly higher than with F8H2-$SiCl_3$ deposition (i.e. probability for cross-linking increases). On the other hand, a smaller number of particles at low p(H_2O) with F10H2-$SiCl_3$ may be attributed to the increased deposition temperature. Under these conditions, it cannot be ruled out

that defective adsorption of (partly) condensed agglomerates is counteracted by increased thermally induced desorption and displacement of defect sites by properly bound and packed molecules. Increased substrate temperature could as well be thought of leading to a "smoothening" of agglomerate defects. At least in post-deposition experiments, the number of particulate defects was observed to decrease when samples were annealed after they had been immersed in water for several days.[164] The origin of the smaller particle density in F10H2-$SiCl_3$-films is obviously to be determined and as a consequence will require more investigations applying AFM experiments during further studies.

The second surprising observation is the evident difference in wetting properties between the samples from different precursors which were both deposited under high water pressures. AFM experiments yield quite similar results with a high density of particles and similar size distribution of those. While wetting experiments of the sample from F8H2-$SiCl_3$ yielded values of $\theta_{adv} = (80.2 \pm 0.2)°$ and $\Delta\theta = (8.8 \pm 0.6)°$, the films from longer-chain F10H2-$SiCl_3$ gave significantly better results of $\theta_{adv} = (77.3 \pm 0.2)°$ and $\Delta\theta = (2.9 \pm 0.1)°$. Generally, any kind of particulate inhomogeneity would be expected to cause pinning of the triple line of a contacting liquid droplet and would lead to an increased contact angle hysteresis. Although the long-term stability experiments did not show signs of increased degradation by wetting experiments, the increased number of particulates may be the result of partial degradation prior to the conduction of initial AFM-experiments. However, if the samples did not deteriorate in the time between preparation and AFM-experiments, the simple occurrence of particles may apparently be no measure for the wetting properties of a sample, although in both cases an increase in θ_{adv} has been detected. The main difference here comes with the change in contact angle hysteresis, which commonly calls for an increase in surface homogeneity in favor of films from F10H2-$SiCl_3$. Perhaps the particles adsorbed on F10H2-$SiCl_3$ surfaces obtain a higher degree of internal ordering than their short-chain counterparts, so that the wetted surface appears more uniform. Moreover, detected particle height is much smaller for F10H2-$SiCl_3$ than for F8H2-$SiCl_3$ (approximately 3 nm versus 20 nm). If adsorbates are formed from micelle-like structures,[69,176] the longer fluorous chains of F10H2-$SiCl_3$ may as well hinder the penetration by liquids' molecules more effectively simply by increased chain length, although these structures would be less ordered than the neighboring film. One could speculate from these first experiments, that, in these very cases, the advancing contact angle might be mainly influenced by the formation of particles (maybe via a Wenzel mechanism, i.e. the formation of particles increases the total fluorinated surface and thus the contact angle increases due to roughness), whereas a change in contact angle hysteresis is caused by other factors. Possible reasons might be a generally superior packing of the longer precursor

molecules even at high water partial pressures, the size and shape of the formed particles and their own packing of partly cross-linked molecules.

However, in terms of the formation of well-defined SAMs it is the goal to deposit near-perfect, smooth films without major defects and free of particulates, so that the important task remains, how the formation of particles or at least their adsorption on the substrate surface can be prevented. For this, the concerted study of deposition methods of films, the resulting wetting properties and the structural characterization by means of AFM will have to be continued and should be complemented by *in-situ* experimental techniques if possible.

6.2.1.1. Co-adsorption of HCl?

During the characterization of monolayer films from F8H2-$SiCl_3$ it was discovered that an increasing amount of chloride is implemented into the film when the applied water partial pressure during the deposition process is increased (Figure 71). As illustrated in Figure 89, HCl is liberated during the hydrolysis of the silane precursor and was assumed to easily desorb in the course of processing. At least certain amounts of HCl appear to stay within the film or are possibly adsorbed at the substrate surface. Chloride detected by sSIMS may as well result from unhydrolyzed precursor molecules within the film. This origin is however regarded as rather unlikely, as increased conversion of precursor molecules is expected at the water partial pressures leading to chloride implementation and chloride concentration even increases with $p(H_2O)$.

The adsorption of HCl will eventually lead to distortions in the monolayer packing and may cause or promote the observed multilayer growth. The question is if either the adsorption of HCl causes multilayer growth by creating defect sites or if the increased incorporation of HCl is facilitated by prior formation of multilayer structures. Moreover, it can be assumed that an increased excess of water suppresses desorption of HCl or promotes its adsorption, respectively. This concludes from the finding that the amount of chloride detected by sSIMS still increases even at values of $p(H_2O)$ that exceed the amount necessary for full hydrolysis of silane precursor molecules. A possible explanation may be the accumulation of HCl molecules at hydrophilic defect sites of the monolayer at high $p(H_2O)$, maybe in connection with adsorbed excess water molecules at the same site. A direct connection between the appearance of an

increased number of particulates and preferred adsorption of HCl appears plausible as well, as HCl might bind to polar portions of a particle.

For the purpose of creating as-perfect-as-possible monolayers, the issue of incorporated HCl is not of primary importance as increased amounts of chloride have been found at values of $p(H_2O)$ that are beyond the deposition conditions required for high-quality monolayers. Future studies on the influence of HCl during the deposition process can be developed based on the intentional removal of HCl in order to prevent any contact between substrate and HCl vapor. Alternatively, additional amounts of HCl vapor may be added at low $p(H_2O)$ in order to force the incorporation of excess HCl and study its influence on intrinsically HCl-free monolayers. Reducing the amount of HCl within the deposition chamber may be of interest for future modifications of the deposition system and initial methods will be introduced in Section 6.3.

6.2.2. Deposition Times for F8H2-$SiCl_3$

Silane adsorption time t(F8H2-$SiCl_3$) did not show any influence on the film's wetting properties. The results suggest that silane vapor simply has to be added to the deposition system as silane pre-adsorption on the substrate surface does not have a significant effect on the deposition process and precursor molecules are not covalently anchored to the surface. Results mean that at least for adsorption durations up to 180 minutes at 80 °C there is either no direct reaction between silane precursors and silica substrate or the reaction is so fast that it happens instantaneously below the "detection limit" of one minute. The assumption of no direct reaction correlates well to reports by Michalske *et al.*, who observed a substantial desorption of precursor molecules from the substrate surface, when they did not supply water vapor during gas-phase depositions. [179] On the other hand, Tripp *et al.* reported that small vaporized fluoroalkylated silanes in contrast to their non-fluorinated analogs can react directly with silica even at room temperature without the presence of water. [118] They attributed this effect to the increased polarity at the Si atom induced by the electron withdrawing effect of the fluorinated alkyl chain. In their experiments, they found that after one minute of contact time, 20 % of the available hydroxyls at the substrate surface had reacted with precursor molecules. The "detection limit" of one minute at 80 °C in the experiments might therefore lead to the anchoring of a substantial amount of silane on the substrate surface. In-situ analytical techniques will be methods to be used in prospective

studies to confirm the short-time adsorption behavior during the deposition and to clarify the effect of silane adsorption time.

In contrast to silane adsorption time, a variation of water reaction time t(H_2O) was observed to have a significant influence on the properties of the final film. The increasing quality of films with increasing water reaction time suggests that the formation of highly ordered films takes time even though precursor hydrolysis is assumed to happen very fast. Next to the time-dependent formation of reactive silanol species (see Section 6.2.1), this induction period may be caused by adsorption and ordering processes, the covalent anchoring of precursor molecules to the substrate or the simultaneous desorption of molecules like HCl or H_2O, which are not meant to be incorporated into the film. This induction period may be regarded analogously to a minimum deposition time found for the deposition of silane SAMs from deposition solutions. In those experiments, wetting behavior of final films has been described to approach a saturation state, where no further improvement of properties or film development is detected (Chapter 2.5). Further studies employing AFM or simple thickness determinations by e.g. ellipsometry might be helpful if the cause of decreased layer quality was to be determined in detail. Besides the conclusion that a certain minimum water reaction time t(H_2O) is required for the deposition of ordered films (for F8H2-$SiCl_3$ t(H_2O) ≈ 25 min), it can as well be concluded that no further improvement takes place at highly extended t(H_2O).

6.2.3. Deposition Temperature

Overall, the observed changes in wetting behavior caused by a change in deposition temperature only allow a distinct conclusion for depositions from F8H2-$SiCl_3$. For F10H2-$SiCl_3$, no specific rule can be deduced at this point, although for elevated temperatures assumptions in comparison to F8H2-$SiCl_3$ can be made. Thus, increased temperatures appear to promote the formation of films with poor wetting properties. This effect is highly evident for F8H2-$SiCl_3$ and is assumed to reappear during depositions from F10H2-$SiCl_3$. The origin of this effect is assumed to lie in a decreasing sticking probability of the silanol molecules to the substrate surface, so that film formation is not properly completed during the given reaction time. The same assumption was already made by Michalske *et al.* during the gas-phase deposition of monolayers from F6H2-$SiCl_3$. [179] An extension of water reaction time may therefore enable an improvement of the observed wetting properties. In the case of F10H2-

$SiCl_3$, sufficient vaporization of the solid precursor and a reduced supply of silanol molecules to the substrate may have caused the slight decrease in quality at temperatures below 100 °C.

Although no specific inside could be gained concerning the films' properties for the deposition at a wider range of temperatures, it can be concluded that deposition at the final temperatures chosen during the experiments yields films of high quality. It can be assumed that best results are obtained when a minimum temperature is chosen that still guarantees sufficient vaporization and adsorption of the precursor molecules. In principle, this behavior would be comparable to the critical temperature T_c for solution depositions of alkyl trichlorosilanes which has been described in literature. [172,217] The impact of temperature will have to be investigated in a wider range in order to be able to observe general tendencies. Lower limits will be given by the silanes vapor pressures so that sufficient vaporization is possible, whereas upper limits will keep being restricted by technical aspects of the set-up.

6.3. Conclusion & Outlook

In this section, the results of the investigation of deposition conditions for monolayer films from fluorous trichlorosilane precursors were presented. Through variation of individual process parameters, it was possible to determine optimized conditions, under which high-quality films can be reproducibly deposited and wetting properties comparable or better than commonly reported can be obtained.

The strongest effect on film quality results from an improper choice of water partial pressure during the deposition process. Thus, the application of a water partial pressure above the optimum process conditions leads to an increase of defect sites, formation of multilayers and particulates and therefore lowers the film's quality. The main cause for this deterioration is assumed to be the increased probability to form cross-links between precursor molecules, either in the film or in agglomerated particles. In this context, a simple model was applied that describes the influence of precursor hydrolysis on film growth. Improper choice of other process parameters can have deteriorating effects as well, but the effects were found to be smaller as for

$p(H_2O)$ and extreme values have to be chosen in order to influence the final film in the same way even slight changes of $p(H_2O)$ can do.

Moreover, it was shown that the chain lengths of the corresponding systems have an impact not only on the wetting properties and surface structure of the final film but also on their deposition conditions. Improved wetting properties of films deposited from longer chain lengths had been expected and were one reason for the initiation of these studies. The occurrence of characteristic differences in the deposition conditions for longer chains, e.g. stability against high $p(H_2O)$ for F10H2-$SiCl_3$, was, however, surprising and requires further investigations beyond this work. It will be highly interesting to extend the investigations to precursors carrying even longer chains and to discover their properties of wetting and characteristics of deposition.

The study successfully shed light on certain characteristics of SAM processing for this kind of precursors and will help to further improve general knowledge in this area. The series of experiments was, to the best knowledge, the first systematic study of this kind and connected multiple important technically and mechanistically relevant parameters. The results can serve as an initial guideline for practical considerations concerning the deposition of this kind of monolayers and may help to reveal those characteristics, which primarily need to receive further interest in terms of the investigation of mechanistic details.

Nonetheless, the details of SAM formation mechanisms from trichlorosilanes are far from understood and as often, new results lead to new questions, ideas and tasks. Although new insights could be gained and interesting results have been obtained during this work there will be a couple of possibilities to further extend the experimental horizon. The incorporation of an *in-situ* trap in order to remove HCl from the reaction vapor is an important technical aspect that will be regarded in upcoming studies. With the possibility to intentionally bind HCl in a trap it will be possible to study the actual effect of HCl adsorption on the final film. Studies on the influence of HCl gas during the deposition process may not only be limited to the intentional removal of HCl but also include the targeted addition of HCl, for example in cases of low water partial pressures, where under standard conditions only a low partial pressure of HCl would be present. Initial attempts with a selective *in-situ* vapor trap have already been accomplished but are still a matter of further development, so that no results have been presented and only the general idea will be introduced here. For selective removal, a solid substrate of porous alumina (activated alumina 470, C&CS, Germany) was modified by standard methods to obtain tertiary amine endgroups on the surface and was filled in a designated chamber of the deposition

system. [271–273] Thus it is possible to introduce the reactive vapors of water and silane precursor to this additional chamber prior to contact with the deposition substrate, so that HCl gas can be bound to the modified alumina/amine surface. The remaining vapor with an increased concentration of silanol species can then be introduced into the reaction chamber where monolayer deposition on the substrate can occur.

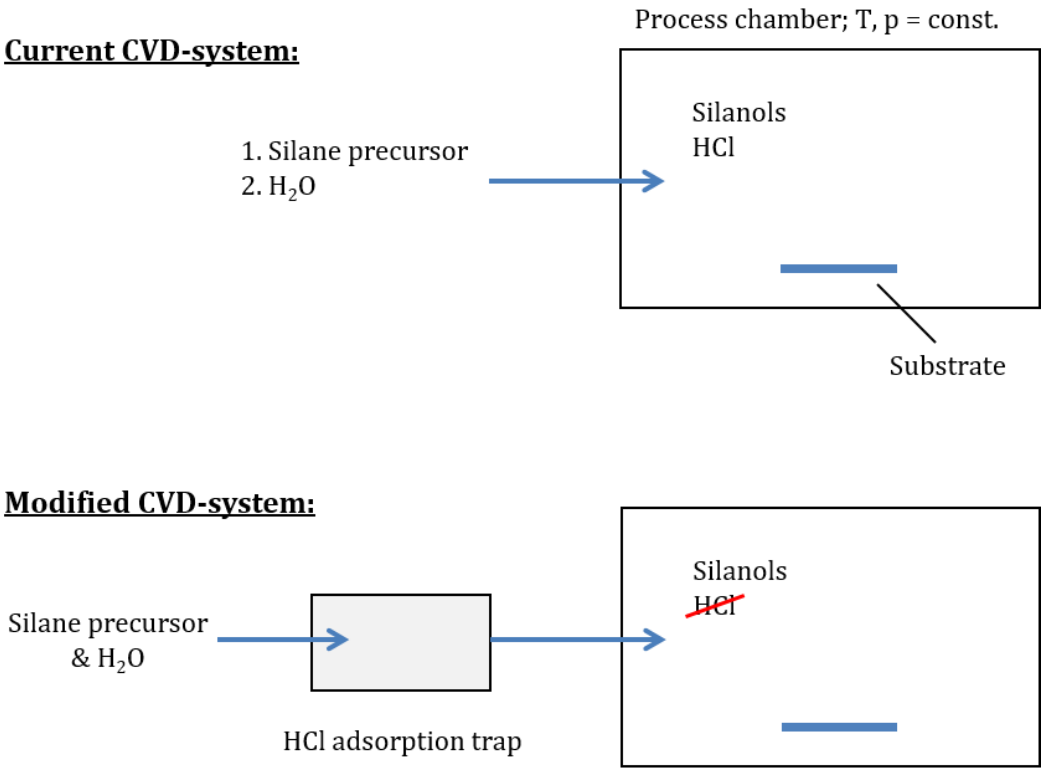

Figure 99: Simplified illustration of the incorporation of the HCl adsorption trap.

Tertiary amines have been selected for modification of the vapor trap as lower amines undergo side-reactions with the silane precursor molecules leading to N-substituted silylamines. [274] HCl-removal is accomplished by a simple acid/base-reaction as illustrated in Figure 100.

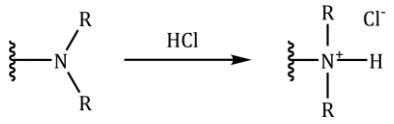

Figure 100: Selective adsorption of HCl by a tertiary-amine-modified solid substrate.

Apart from the HCl-trap, it will be important to improve the thermal capabilities of the deposition system in order to study deposition processes at elevated temperatures above 120 °C. This will be of particular interest regarding the application of longer chain lengths with new solid precursors. With the ability to prepare films within a broader temperature range, the effect of temperature on the film properties can be studied more intensively. Individual heating of the substrate is a further refinement concerning the processing temperature that can be thought of, which is, however, out of scope for the present studies.

The implementation of *in-situ* analytical equipment would mean a tremendous improvement concerning further means of investigation as it would enable a thorough investigation of the mechanisms during film formation. Within the current setup an additional incorporation of further equipment is limited and can be envisaged in upcoming stages of the deposition system. Possible techniques to think of are numerous and for example infrared (IR) spectroscopy, surface plasmon resonance (SPR) spectroscopy, second harmonic generation (SHG), low-energy ion scattering (LEIS) or ellipsometry may be implemented to name only a few. The application of AFM experiments will be extended and will lead to more detailed information on the surface structure under varying deposition conditions and during different stages of deposition, characterization and storage.

The provision of precursor molecules with even larger chain lengths is essential for future investigations. Based on the results of this work it will be possible to provide precursors in the necessary quantity and quality that allow intensive studies not only on mechanistic aspects of the deposition process but will also help to improve technical equipment. For the moment, the separation of telomeric mixtures by means of F-HPLC is the best way to obtain pure substances and further development may minimize the current costs of this method (see Chapter 4). Nonetheless, an easier and less expensive access to substances of this kind is desirable, either by separation of mixtures or new possibilities to synthesize pure compounds directly.

Besides the provision of future precursors, their proper handling will become of further importance in order to enable safe and quick preparation of precursor ampoules while minimizing the risk of pre-deposition deterioration. Moreover, it will be the task of future studies to find out how these new precursors with probably high melting points and low vapor pressures can be processed best. Films from precursor molecules with even longer chain lengths may enable the preparation of films with increased stability during and after the deposition process and may create films with superior properties than already experienced. This could be expressed by denser films that contain less defects and thus would be more stable against the penetration of molecules from contacting liquids. For example, a possible hydrolysis of headgroup/substrate-bonds caused by the intrusion of water molecules might be prevented.

Of particular interest concerning the availability of increased chain lengths will be the transfer of the results that were obtained for binary mixed monolayers of fluorous alkyl thiols on gold. Long-chain fluorous silanes with large differences in the respective chain lengths may be applied similarly for the creation of sub-nm roughness on technically relevant materials like silica. Detailed studies of mixed monolayers from silanes rely on the exact determination of the molar ratios of the corresponding silanes within the film. Exact and reliable dosing of individual silanes during the deposition process will be required, which, however, is expected to be a smaller challenge in relation to the compositional analysis of the final films. The transfer of a mechanism to control wetting by the manipulation of the effective surface tension of a contacting liquid on materials like silica would be a highly exciting topic both for industrial as well as academic purposes.

In general, the deposition of films with increased stability and better performance in terms of wetting can be applied in the general areas of e.g. pure control of wetting properties or in terms of a barrier layer. The possibility to modularly create deposition processes and thus films by control over various aspects of the deposition makes it, moreover, possible to create advanced applications. Besides the creation of molecular structures on flat surfaces it has already been shown that the controlled deposition of such monolayers from fluorous silanes on pre-treated alumina surfaces can lead to systems that exhibit an extraordinarily low friction ("slip flow") in contact with liquid water flow. [32]

7. Appendix

7.1. Precursor Syntheses

Reminder: compounds are designated F*n*H*m*-*X* based on their number of fluoromethylene (*n*) and methylene (*m*) units in combination with the corresponding functional group (*X*). For example, *1H,1H,2H,2H*-perfluorodecyl thiol ($F\text{-}(CF_2)_8\text{-}(CH_2)_2\text{-}SH$) with eight fluoromethylene and two methylene units will be abbreviated F8H2-SH (Figure 5), while for *1H,1H,2H,2H*-perfluorododecyl trichlorosilane ($F\text{-}(CF_2)_{10}\text{-}(CH_2)_2\text{-}SiCl_3$) the form F10H2-$SiCl_3$ and for *n*-hexadecyl thiol ($H\text{-}(CH_2)_{16}\text{-}SH$) the form H16-SH will be used.

Telomeric mixtures of fluoroalkylated iodides FnH2-I (n = 4…30) "Zonyl™ TELB" were obtained from DuPont and were fractionated into narrower mixtures of *n* by vacuum distillation prior to further use (Section 4.1). Fluoroalkylated reagents were used as received: F8H2-I (97 %), F12H2-I (90 %) and F8H2-olefin (99 %) were obtained from ABCR, Germany; F10H2-I (97 %) was obtained from Alfa Aesar, Germany; F10H2-olefin (97 %) and F12H2-olefin (97 %) were obtained from Apollo Scientific, United Kingdom. F8H2-$SiCl_3$ (97 %) for monolayer deposition was obtained from ABCR, Germany. Fluoroalkylated thiol precursors with short chain-lengths were obtained from distributors and were used as received: F4H2-SH (≥ 97 %, Sigma Aldrich, Germany), F6H2-SH (> 99 %, Fluoryx, USA), F8H2-SH (> 99 %, Fluoryx, USA). Thiol precursors carrying chains with n ≥ 12 were synthesized as described below while F10H2-SH was prepared following the same experimental protocol and was kindly supplied by Udo Adels (Qiagen, Germany). Non-fluorinated alkyl thiols Hm-SH with n = 8, 10, 12, 14, 16, 18, 20, 22 were commercially available and were used as received: H8-SH (98 %, Alfa Aesar), H10-SH (96 %, Alfa Aesar), H12-SH (98 %, Alfa Aesar), H14-SH (97 %, TCI), H16-SH (>97 %, TCI), H18-SH (96 %, Alfa Aesar), H20-SH (98 %, Alfa Aesar), H22-SH (>97 %, TCI). Thiols H30-SH and H38-SH were synthesized according to procedures described below.

Further reagents were used as received: *n*-docosyl bromide (>98 %) and phenanthroline monohydrate (>99 %) were obtained from TCI, Germany; *n*-propyl magnesium chloride (1 M solution in Me-THF, Alfa Aesar, Germany); *n*-triacontanol (98 %, Toronto Research Chemicals); imidazole (99 %), Mg (>99 %), LiCl (analytical grade), I_2 (analytical grade), triphenylphosphine (99 %) and $CuCl_2$ (>98 %) were obtained from Merck, Germany; thiourea (99+ %) and PBr_3 (99 %) were obtained from Sigma Aldrich, Germany; HCl (32 wt-% aqueous solution, reagent grade), H_2SO_4

(95 wt-% aqueous solution, analytical grade) and hydrogen peroxide H_2O_2 (35 wt-% aqueous solution, analytical grade) were obtained from Chemsolute Th. Geyer, Germany; Pt(0)-1,3-divinyl-1,1,3,3-tetramethyldisiloxane complex solution in xylene (2.1-2.4 % Pt, "Karstedt catalyst") and 1-chlorooctan-8-ol (98 %) were obtained from ABCR, Germany; $HSiCl_3$ (99 %, Acros, Belgium); NaOH, NaCl, $MgSO_4$ and KOH (all of reagent grade) were obtained from AppliChem, Germany.

Solvents were used as received if not otherwise stated: 1,4-dioxane (analytical grade) was obtained from AppliChem, Germany; (perfluorobutyl)methylether (>99 %) was obtained from Iolitec, Germany; perfluorohexane (99 %) and benzotrifluoride (99 %) were obtained from ABCR, Germany; methanol and *n*-heptane (both of HPLC-grade) were obtained from Carl Roth, Germany; water, toluene, ethanol, dichloromethane (all of analytical grade), ethanol (HPLC grade) and distilled water were obtained from Chemsolute Th. Geyer, Germany.

Test liquids for contact angle measurements were *n*-hexadecane (99%+, SigmaAldrich, Germany), water (p.A., Applichem, Gemany), ethylene glycol (99%, ABCR, Gemany) and squalane (99%, ABCR, Gemany).

7.1.1. General protocol: Thiolation of (fluoro-)alkyl halides with thiourea

The following general procedure is applicable to the synthesis of non-fluorinated and fluorinated alkyl thiols. The preparation of fluoroalkyl thiols was conducted with either pure iodides or with telomeric mixtures of iodides obtained from commercial Zonyl TELB by vacuum distillation. Syntheses were adopted considering literature reports. [227,228] The following general procedure is applicable for the synthesis of pure thiols as well as telomeric mixtures. Exemplarily, the synthesis of F10H2-SH will be described. Chemicals were used as received and the synthesis was conducted under inert atmosphere conditions with dried glassware.

2.28 g *1H,1H,2H,2H*-perfluorododecyl iodide (3.4 mmol, 1.0 equivalent) and 0.30 g thiourea (3.9 mmol, 1.2 eq.) with 8 mL of 1,4-dioxane were placed in a 25 mL round bottom flask equipped with a reflux condenser and oil bath. The mixture was heated to reflux (oil bath: 140 °C) for 4 h during which the solids dissolved completely giving

a slightly yellow solution. After cooling the oil bath to 110 °C, 1.4 mL of a 5 M sodium hydroxide solution (2.1 eq.) were added dropwisely, yielding an intermediate change of color of the solution from yellow over light green to light yellow again. The solution was stirred for 1 h and subsequently, 0.8 ml of 32 wt-% aqueous HCl (10.2 M, 2.4 eq.) were added slowly within the next 30 min, during which the solution temporarily darkened resulting in a clear, slightly green solution after complete addition. The solution was stirred for 14 h at 130 °C oil bath temperature. The hot greenish solution contained some white precipitate and was cooled down to room temperature with subsequently increased precipitation of white solid. The mixture was transferred to a seperating funnel and 100 mL of an aqueous 0.1 M NaCl solution were added. The product was extracted three times with 100 mL (perfluorobutyl)methylether and the combined fluoroorganic fractions were washed three times with 50 mL of 0.1 M aqueous NaCl. The fluorous solution was dried with $MgSO_4$, filtrated and the solvent was removed under reduced pressure. Drying in vacuum yielded the product *1H*,*1H*,*2H*,*2H*-perfluorododecyl thiol as a white solid (1.56 g, 90 %). NMR ($CDCl_3$, 400 MHz): δ = 2.83-2.72 (td(q4), C*H*$_2$SH, 2H), 2.52-2.34 (m, CF_2C*H*$_2$, 2H), δ = 1.61 (t, SH, 1H)

7.1.2. Triacontyl iodide H30-I

1.62 g Triacontanol H30-OH (3.7 mmol, 1.0 eq.), 0.63 g imidazole (9.2 mmol, 2.5 eq.) and 2.42 g triphenylphosphine (9.2 mmol, 2.5 eq.) were prepared with 15 mL toluene in a 50 mL round bottom flask and the mixture was heated at an oil-bath temperature of 70 °C. After complete dissolution of the alcohol, a mixture of 0.69 g iodine (1.12 g, 1.2 eq.) in 15 mL toluene was added slowly under immediate decoloration of the iodine solution and the solution was heated at 70 °C for 12 hours. Residual triphenyl phosphine and imidazole were precipated by the addition of 30 mL *n*-hexane and were subsequently removed by filtration. Triacontyl iodide was obtained by removing the solvents under reduced pressure and the crude product was purified via column chromatography with toluene. H30-I was obtained as a white solid (yield 69 %). NMR ($CDCl_3$, 400 MHz): δ = 3.19 (t, C*H*$_2$I, 2H), 1.82 (q5, C*H2*CH2I, 2H), δ = 1.25 (s, (C*H*$_2$)$_{27}$CH$_3$, 54H), δ = 0.88 (t, (CH$_2$)$_{27}$C*H*$_3$, 3H).

7.1.3. Recursive route to non-fluorinated alkyl thiols

The recursive protocol for the formation of non-fluorinated alkyl thiols is exemplarily described for the synthesis of H30-SH. Further stages of chain-extension can be conducted according to this general protocol.

Formation of the Grignard reagent (stage I): 33.0 g 1-chlorooctan-8-ol (200.6 mmol, 1.0 eq.) and 0.02 g phenanthroline (as indication agent) were prepared in 220 mL THF under inert atmosphere conditions in a three-neck 500 mL round bottom flask and were cooled to -24 °C. 220.7 mL of 1 M solution of *n*-propyl magnesium chloride (220.7 mmol, 1.1 eq.) in 2-methyl tetrahydrofurane were slowly added. 5.1 g Mg (210.6 mmol, 1.05 eq.) and 0.05 mL 1,2-dibromoethane (as initiation agent) were added to the solution, which was subsequently heated to reflux for 6 hours under stirring. The intermediate was not isolated.

Chain-extension (stage II): In a separate flask, 54.7 g H22-Br (140.4 mmol, 1.0 eq.), 0.9 g LiCl (20.1 mmol, 0.14 eq.) and 1.35 g $CuCl_2$ (10.0 mmol, 0.07 eq.) were prepared under inert conditions in 100 mL THF und cooled to 0 °C. Grignard solution was slowly added to the bromide solution over a period of 40 minutes during which the temperature of the reaction mixture raised to approximately 30 °C and a change of color appeared from an initial orange to greenish and dark purple, eventually. The obtained reaction solution was refluxed under stirring for 12 hours. 440 mL aqueous HCl (10 wt-%, 3 M) and 440 mL *n*-hexane were then added to the solution and the mixture was again heated to reflux under stirring for 30 minutes. The hot solution was separated via a separating funnel and the organic fraction was allowed to cool, thus obtaining a solid precipitate, which was isolated by filtration and dried in vacuo. The crude product was recrystallized from MeOH, isolated, again recrystallized from *n*-hexane and subsequently dried in vacuo. H30-OH was obtained as white flakes (yield 54 %). NMR ($CDCl_3$, 300 MHz): δ = 3.64 (t, CH_2OH, 2H), 1.56 (q5, C*H2*CH2OH, 2H), δ = 1.25 (s, (CH_2)$_{27}$CH$_3$, 54H), δ = 0.88 (t, (CH$_2$)$_{27}$CH_3, 3H).

Bromination (stage III): 33 g chain-extended alcohol H30-SH (75.3 mmol, 1.0 eq.) from stage II was prepared under dry argon in 100 mL toluene in a 500 mL three-neck round-bottom flask and was heated under stirring to 110 °C oil-bath temperature. A solution of 22.4 g PBr_3 (82.9 mmol, 1.1 eq.) in 10 mL toluene were added over a period of 10 minutes via a dropping funnel. Upon complete addition, the colorless solution was stirred at 110 °C for 12 hours during which the color changed to orange. The mixture was allowed to cool to room temperature. 100 mL water were carefully and slowly added under stirring and the resulting mixture was heated to reflux for 30 minutes. After the addition of 120 mL *n*-heptane, the hot solution was separated via a

separating funnel and the hot organic fraction was filtered to remove residual solids. Organic solvents were removed under reduced pressure. The resulting solid was recrystallized from MeOH, yielding a white solid product (yield 83 %). NMR ($CDCl_3$, 300 MHz): δ = 3.40 (t, C*H*$_2$Br, 2H), 1.85 (q5, C*H2*CH2Br, 2H), δ = 1.25 (s, (C*H*$_2$)$_{27}$CH$_3$, 54H), δ = 0.88 (t, (CH$_2$)$_{27}$C*H*$_3$, 3H).

Thiolation (stage IV) was conducted according to the general protocol described above. H30-SH as obtained as a white solid (yield 72 %). NMR ($CDCl_3$, 400 MHz): δ = 2.52 (q4, C*H*$_2$SH, 2H), 1.61 (q5, C*H2*CH2SH, 2H), δ = 1.25 (s, (C*H*$_2$)$_{27}$CH$_3$, 54H), δ = 0.88 (t, (CH$_2$)$_{27}$C*H*$_3$, 3H).

7.1.4. *1H,1H,2H,2H*-Perfluoroalkenes F-(CF$_2$)$_n$-CH=CH$_2$

The preparation of fluoroalkyl olefins was conducted with either pure iodides (n = 10, 12) or with telomeric mixtures of iodides obtained from commercial Zonyl TELB by vacuum distillation. Syntheses were adopted considering literature reports. [236,247] The following general procedure is applicable for the synthesis of pure olefins as well as telomeric mixtures. Exemplarily, the conversion of an iodide oligomeric mixture will be described. Chemicals were used as received.

2.33 g KOH (41.5 mmol, 6.3 equivalents) were added to 100 mL of toluene and the mixture was heated to reflux. While residual KOH still remained undissolved, 5.11 g of *1H,1H,2H,2H*-perfluoroalkyl iodide mixture (6.6 mmol, 1.0 eq., calculated based on F12H2-I as the main component) with 50 mL toluene were added. Within the first hour of reflux, a yellowish precipitate formed which soon accumulated as a brown viscous oil on the flask walls. After 18 h of reflux, white and brown solid precipitate had formed and the reaction was cooled to room temperature. Potassium salts were dissolved by the addition of 50 mL of water and the mixture was extracted three times with each 40 mL perfluorohexane. Combined fluorous layers were dried with $MgSO_4$, filtrated and the solvent was removed under reduced pressure. 3.78 g (89 %) olefinic mixture of white solid were obtained after drying in vacuum. NMR (acetone-d$_6$, 400 MHz): δ = 6.34-6.20 (m, C*H*CH$_2$, 1H), 6.14-6.02 (m, CHC*H*$_2$, 2H)

7.1.5. *1H,1H,2H,2H*-Perfluoroalkyl trichlorosilanes F-$(CF_2)_n$-$(CH_2)_2$-$SiCl_3$

Due to the lack of commercial availability, precursor compounds bearing fluoroalkylated chains longer than eight fluoromethylene units had to be synthesized. Syntheses were adapted from literature reports on the common hydrosilylation route.[74,129,236] The following procedure exemplarily describes the synthesis of F10H2-$SiCl_3$ and can be applied for the synthesis of F8H2-$SiCl_3$, F12H2-$SiCl_3$ and telomeric mixtures under slight modifications of the reaction conditions (Chapter 4.3). Chemicals were used as received or as synthesized according to 7.1.4.

1H,1H,2H,2H-Perfluorodecyl trichlorosilane (F10H2-$SiCl_3$): 3.06 g (5.6 mmol, 1.0 eq) *1H,1H,2H*-perfluorododecene were placed in a stainless steel reaction tube containing a PTFE-coated magnetic stirring bar to ensure sufficient mixing of the components. 30 mg of a platinum(0)-1,3-divinyl-1,1,3,3-tetramethyldisiloxane complex solution in xylene (2.1-2.4 % Pt, "Karstedt catalyst") and 0.75 mL $HSiCl_3$ (1.01 g, 7.4 mmol, 1.3 eq.) were added under inert atmosphere conditions and the reaction tube was tightly sealed. The tube was shaken several times and heated at 120 °C for 44 h. The reaction tube was allowed to cool to room temperature before it was carefully opened under inert atmosphere. The reaction product was separated from other residues by suspension in 100 mL toluene and extraction with three times 30 mL perfluorohexane. The fluorous solvent was slowly removed under reduced pressure and the desired product was obtained as a colorless solid (3,74 g, 98 %, m.p. 47-48 °C) and stored under argon. NMR showed no residual olefin or semifluorinated alkane. NMR ($CDCl_3$, 400 MHz): δ = 2.41-2.24 (m, CF_2CH_2, 2H), 1.72-1.62 (m, CH_2Si, 2H)

1H,1H,2H,2H-Perfluorododecyl trichlorosilane (F12H2-$SiCl_3$): F12H2-$SiCl_3$ was prepared analogously to F10H2-$SiCl_3$ at a reaction temperature of 160 °C from *1H,1H,2H*-perfluorotetradecene. The desired product was obtained as a colorless solid (yield 90 %) and stored under argon. NMR showed traces of residual olefin and no semifluorinated alkane. NMR (C_6F_{14} with DMSO-d_6-insert, 400 MHz): δ = 2.02-1.84 (m, CF_2CH_2, 2H), 1.24-1.14 (m, CH_2Si, 2H).

7.2. Wenzel Model for Wetting on Binary Mixed Monolayers

Wetting properties of binary mixed monolayers are calculated using a simple Wenzel model based on both the theoretical approaches by Wenzel and Cassie-Baxter. Modeling parameters applied for the calculations are collected from literature reports and represent repeatedly reported values as stated in Chapter 5.

The substrate surface is constructed from an array of two sets of hexagonally, densely packed cylinders. The two sets differ in cylinder height and represent the varying chain lengths of precursor thiols within a system. The height of each type of cylinders is individually set and cylinders are randomly positioned within the model area according to the relative amount of precursor (molar fraction).

Different wetting properties are assigned to the top and side faces of the cylinders. While top faces are accounted for as trifluoromethyl "CF_3" surfaces (with the corresponding area A(CF_3)), the side walls are represented with fluoromethylene "CF_2" wetting properties (A(CF_2)). For non-fluorinated monolayers, surfaces were assigned accordingly to CH_3/CH_2 and will be omitted here for improved clarity. The modeled surface is schematically depicted in Figure 101.

Thus, the roughness factor r as the ratio of actual over geometric surface area according to Wenzel is given as:

$$r = \frac{actual\ surface}{geometric\ surface} = \frac{A(CF_3) + A(CF_2)}{A(CF_3)} \qquad (22)$$

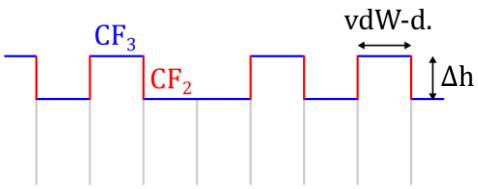

Figure 101: Illustration of the assignment of individual wetting properties and structural parameters. Contact angles, vdW-diameter, and height difference are obtained from literature as well as experiment. Each column/cylinder represents one fluoroalkyl helix.

The relative area fractions of trifluoromethyl and fluoromethylene surfaces are:

$$f(CF_3) = \frac{A(CF_3)}{A(CF_3) + A(CF_2)} \tag{23}$$

$$f(CF_2) = \frac{A(CF_2)}{A(CF_3) + A(CF_2)} \tag{24}$$

The contact angle θ_{CF2} is obtained from literature, while for θ_{CF3} the mean average of experimental contact angles on pure films from both corresponding short- and long-chain thiols is used.

Thus, with the relative surface area fractions, an average surface energy $\cos\theta_{avg}$ can be calculated according to Cassie-Baxter:

$$\cos\theta_{avg} = f(CF_3) \cdot \cos\theta_{CF3} + f(CF_2) \cdot \cos\theta_{CF2} \tag{25}$$

Using Wenzel's law, the expected contact angle θ_{eff} of the model surface can be obtained:

$$\cos\theta_{eff} = r \cdot \cos\theta_{avg} \tag{26}$$

This calculation can be applied for binary mixed systems of varying molar fractions and structural parameters.

Parameter	**FnH2-SH**	**Hm-SH**
vdW-diameter	5.6 Å [184]	4.5 Å [185]
Δh per -$(CX_2)_2$-	2.5 Å [134]	2.2 Å [75]
next-neighbor distance	5.8 Å [87,114,193]	5.0 Å [194–196]
θ_{CF2} / θ_{CH2} (H_2O)	110° [258–261]	105° [275–277]
θ_{CF2}/ θ_{CH2} (Sq)	59° [278]	0° [275,279]

Table 25: Values obtained from literature for Wenzel modelling.

7.3. Analytical Experiments

7.3.1. Dynamic Contact Angle Measurements

Dynamic contact angle measurements were conducted directly after sample preparation. Advancing and receding contact angles (θ_{adv}, θ_{rec}) were obtained from sessile drops at T = (25 ± 0.1) °C using a modified contact angle goniometer (ACA50, Data Physics, Germany). Contact angles of *n*-hexadecane (99%+, SigmaAldrich, Germany), water (p.A., Applichem, Gemany), ethylene glycol (99%, ABCR, Gemany) and squalane (99%, ABCR, Gemany) were determined in an ambient of air from tangent leaning while the triple line of a 20 µl drop moved upon adding 5 µl (advancing contact angle) and subsequently removing 15 µl (receding contact angle) by a 100 µm glass (water) or 200 µm metal (*n*-hexadecane, squalane, ethylene glycol) capillary in contact with the drop at rates of 1.5 µl/s. During the experiment, movies of the motion of the drop contour were recorded and subsequently analyzed after meticulously selecting drop baselines. The advancing contact angle was determined by averaging the contact angle during motion of the liquid droplet, whereas the receding contact angle was determined from the apparent contact angle in the moment of triple line retraction (Figure 102).

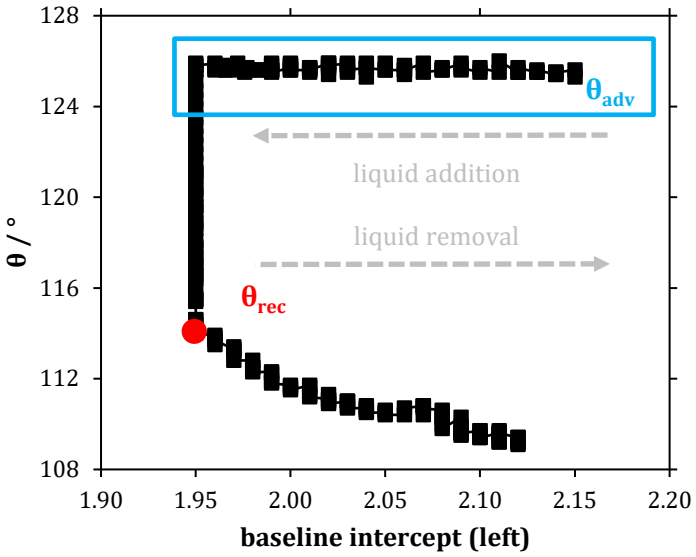

Figure 102: Exemplary explanation of the determination of advancing and receding contact angles from videos of drop motion. The intercept of drop contour and drop baseline moves upon adding and removing liquid from the droplet. θ_{adv} is determined from the average during droplet expansion, while θ_{rec} is determined at the very moment of droplet retraction. Values are obtained from both left and right drop baseline intercepts, with the former depicted here.

The reported values are the average of at least eight independent droplets applied to one sample with approximately 150 individual data points per video. Deviations across the sample were very low with larger error margins for the determination of the receding contact angle (Table 26).

Test liquid	$\Delta\theta_{adv}$ [%]	$\Delta\theta_{rec}$ [%]
water	±0.2	±0.6
n-hexadecane	±0.4	±0.6
squalane	±0.3	±0.7
ethylene glycol	±0.4	±0.6

Table 26: Relative errors of contact angle experiments for individual test liquids.

7.3.2. Ellipsometry

Ellipsometric measurements were conducted using a Dual Mode Waferskan ellipsometer (L115A, Gaertner Scientific, Skokie, IL, USA) with a He-Ne laser (λ = 6328 Å) operated at an incident angle of 70° from the surface normal. The sample stage of the instrument was replaced by a rigid fixture made from aluminum construction profiles equipped with a crossed-roller-bearing stage for sample height adjustment and electrical read-out with micrometer resolution. Data were acquired by repeated measurements at three different sample locations. All measurements were conducted in ambient air with a refractive index of n = 1.

For monolayers deposited from fluoroalkylated trichlorosilane precursors, a simplified model of two parallel and perfectly smooth interfaces was assumed. Since the silicon substrate has a native surface oxide layer a three-interface model might in principle be more accurate. We account for that native oxide layer by measuring its thickness on the uncoated substrate and subtracting it from the measured monolayer thickness that includes both the thicknesses of the monolayer and the native oxide layer. We use a refractive index of n_2 = 3.85 and k_2 = -0.02 for the substrate (bulk silicon). The monolayer was considered to be a transparent medium with a refractive index of n_1=1.46 and k_1 = 0. While other studies have used refractive indices of 1.33 to 1.50 for fluoro-organic monolayers [58,75,87,115,123,134,215,254], a choice of 1.46 is advantageous here as it is also in accordance with the reported value for SiO_2 [280] which is part of our model monolayer.

For thiol monolayers, a refractive index of n_1 = 1.35 was considered, with the imaginary part being zero, thus neglecting adsorption at 6328 Å wavelength. The complex refractive index for gold, n_2 = 0.383 and k_2 = -3.467, have been obtained from reference measurements of uncoated freshly prepared gold substrates of the same kind as those used for monolayer preparation. In contrast to the value applied for silane-based monolayers, a choice of n_1 = 1.35 was applied for thiol-based monolayers. This value seems more suitable for short non-fluorinated chains as most published results were obtained from monolayers with extended non-fluorinated spacer units. The smaller value is assumed to better reflect a situation similar to bulk fluorinated alkane and a similar refractive index of n = 1.33 (measured bulk value) was used by Chidsey and coworkers for F8H2-SH. [115] Tamada and his group determined n = 1.36 ± 0.01 for a layer of F10H2-SH with surface plasmon resonance spectroscopy at a wavelength of 6828 Å. [87]

7.3.3. X-ray Photoelectron Spectroscopy (XPS)

XPS experiments were carried out in an Ultra Axis™ HSA spectrometer (Kratos Analytical, Manchester, UK). Spectra were acquired at a base pressure of 10^{-9} Torr using a 180° hemispherical analyzer and were calibrated using the CH_x line at 284.6 eV as binding energy reference. The samples were irradiated with monoenergetic Al Kα radiation (1486.6 eV) and the spectra were taken at a power of 144 W (12 kV * 12 mA). The spectrometer was operated with a pass energy of 160 eV for survey spectra and 20 eV for high-resolution spectra. Exposure of the monolayer to x-rays may cause significant film degradation caused by a defluorination process. [46,281] In order to avoid misleading data this process was analyzed prior to further measurements. Experimental parameters were adjusted accordingly, so that film degradation did not affect the experimental results. Thus, the number of scans was reduced to five scans for survey spectra (1-1100 eV, step width 0.5 eV) and to two scans for the high-resolution spectra (step width 0.1 eV) of the C1s, F1s, O1s and Si2p regions as a means to reduce film degradation. Charge compensation was used during the measurement that must also be considered as a source of degradation.

7.3.4. Time-of-Flight Secondary-Ion Mass Spectrometry (ToF-SIMS)

ToF-SIMS experiments were conducted with an ToF-SIMS 5 instrument (ION-TOF, Münster, Germany). A Bi^+ primary ion source was used with a primary ion energy of 25 keV at a current of 0.4 pA. Measurements have been conducted at three different locations on the sample, with measured areas of 200 µm × 200 µm for each spot and a primary ion dose density of $6 * 10^{12}$ ions/cm^{-2}. Spectra of positively and negatively charged secondary electrons have been taken which were calibrated using small organic fragment ions and gold cluster ions (e.g. Au^-, Au_2^-, Au_3^-).

7.3.5. Atomic Force Microscopy (AFM)

AFM-images were obtained using a Dimension Icon microscope (Veeco Instruments/Bruker AXS) with an Si AFM probe (TESP, tip radius < 12.5 nm, Bruker). Tapping mode AFM images were conducted at 1 Hz.

7.3.6. Nuclear Magnetic Resonance Spectroscopy (NMR)

1H-NMR spectra were obtained using Bruker Avance 300 and Bruker Avance 400 spectrometers.

7.3.7. Field Desorption Mass Spectroscopy (FDMS)

FD mass spectra were obtained with a double-focus Thermo-Finnigan-MAT MAT95 spectrometer. Analytes were applied onto the sample emitter by repeatedly wetting the emitter with solutions of the analytes in suitable, volatile solvents (commonly, ethanol, acetone or (perfluorobutyl)methylether were used). After loading the emitter into the system, it was heated at a heating current rate of 8.5 mA/min and spectra were obtained at an emission voltage of 4.7 kV and a multiplier voltage of 2.1 kV.

7.3.8. Fluorous Phase High Performance Liquid Chromatography (F-HPLC)

F-HPLC was conducted on an analytical and preparative scale using commercial equipment (Jasco, Japan) with a photodiode array detector for analysis of UV-absorption. The mobile phase consisted of a mixture of methanol and semifluorinated (perfluorobutyl)methylether in a ratio of 4:1 (v/v). Although these

liquids are completely miscible, some vigorous stirring is required to obtain a homogeneous mixture. For this reason, the mobile phase was prepared manually instead of using a commercial mixing unit. Separations were conducted under isocratic conditions and an analytical solvent flow of 1 mL/min or a preparative solvent flow of 8 mL/min was applied. Column temperature was 45 °C.

Pre-packed Chromatographic columns were manufactured by ES industries, USA, and were obtained from MZ-Analysentechnik, Germany (analytical column dimensions: 4.6 x 250 mm, preparative column dimensions: 30 x 250 mm).

8. Bibliography

(1) Barthlott, W.; Neinhuis, C. *Planta* **1997**, *202* (1), 1.

(2) Neinhuis, C.; Barthlott, W. *Ann. Bot.* **1997**, *79* (6), 667.

(3) Franklin, B.; Brownrigg, W.; Farish, R. *Philos. Trans. R. Soc.* **1774**, *64* (1), 445.

(4) Langmuir, I. *J. Am. Chem. Soc.* **1917**, *39* (9), 1848.

(5) Blodgett, K. B. *J. Am. Chem. Soc.* **1934**, *56* (2), 495.

(6) Bigelow, W. C.; Pickett, D. L.; Zisman, W. A. *J. Colloid Sci.* **1946**, *1*, 513.

(7) Nuzzo, R. G.; Allara, D. L. *J. Am. Chem. Soc.* **1983**, *105* (11), 4481.

(8) Maoz, R.; Sagiv, J. *J. Colloid Interface Sci.* **1984**, *100* (2), 465.

(9) Blaszykowski, C.; Sheikh, S.; Benvenuto, P.; Thompson, M. *Langmuir* **2012**, *28* (5), 2318.

(10) Guha Thakurta, S.; Subramanian, A. *Colloids Surfaces A Physicochem. Eng. Asp.* **2012**, *414*, 384.

(11) Ajami, E.; Aguey-Zinsou, K.-F. *J. Colloid Interface Sci.* **2012**, *385* (1), 258.

(12) Avila, J. R.; DeMarco, E. J.; Emery, J. D.; Farha, O. K.; Pellin, M. J.; Hupp, J. T.; Martinson, A. B. F. *ACS Appl. Mater. Interfaces* **2014**, *6* (15), 11891.

(13) Hong, J.; Porter, D. W.; Sreenivasan, R.; McIntyre, P. C.; Bent, S. F. *Langmuir* **2007**, *23* (3), 1160.

(14) Shi, Z.; Walker, A. V. *Langmuir* **2011**, *27* (18), 11292.

(15) Ellsworth, A. A.; Borner, K.; Yang, J.; Walker, A. V. *ECS Trans.* **2014**, *58* (43), 1.

(16) Rymuza, Z. *Microsyst. Technol.* **1999**, *5* (4), 173.

(17) Zhuang, Y. X.; Hansen, O.; Knieling, T.; Wang, C.; Rombach, P.; Lang, W.; Benecke, W.; Kehlenbeck, M.; Koblitz, J. *J. Microelectromech. Syst.* **2007**, *16* (6), 1451.

(18) Ashurst, W. R.; Carraro, C.; Maboudian, R.; Frey, W. *Sensors Actuators A* **2003**, *104* (3), 213.

(19) Halik, M.; Hirsch, A. *Adv. Mater.* **2011**, *23* (22–23), 2689.

(20) Gladysz, J. A.; Curran, D. P.; Horváth, I. T. *Handbook of Fluorous Chemistry*, 1st ed.; Wiley-VCH: Weinheim, 2004.

(21) Young, T. *Miscellaneous Works*; Peacock, G., Ed.; Murray: London, 1855; Vol. 1.

(22) Wenzel, R. N. *Ind. Eng. Chem.* **1936**, *28* (8), 988.

(23) Cassie, A. B. D.; Baxter, S. *Trans. Faraday Soc.* **1944**, *40*, 546.

(24) Extrand, C. W. *Langmuir* **2002**, *18* (21), 7991.

(25) Öner, D.; McCarthy, T. J. *Langmuir* **2000**, *16* (20), 7777.

(26) Shibuichi, S.; Yamamoto, T.; Onda, T.; Tsujii, K. *J. Colloid Interface Sci.* **1998**, *208* (1), 287.

(27) Quéré, D. *Reports Prog. Phys.* **2005**, *68* (11), 2495.

(28) Quéré, D. *Annu. Rev. Mater. Res.* **2008**, *38* (1), 71.

(29) Choi, C. H.; Kim, C. J. *Phys. Rev. Lett.* **2006**, *96* (6), 066001.

(30) Lee, C.; Kim, C.-J. *Langmuir* **2009**, *25* (21), 12812.

(31) Kota, A. K.; Mabry, J. M.; Tuteja, A. *Surf. Innov.* **2013**, *1*, 71.

(32) Reddemann, L.; Knauf, J.; Böker, A.; Reihs, K. contribution in progress.

(33) Kwon, Y.; Patankar, N.; Choi, J.; Lee, J. *Langmuir* **2009**, *25* (11), 6129.

(34) Chen, W.; Fadeev, A. Y.; Hsieh, M. C.; Öner, D.; Youngblood, J.; McCarthy, T. J. *Langmuir* **1999**, *15* (10), 3395.

(35) Allara, D. L. *Biosens. Bioelectron.* **1995**, *10*, 771.

(36) Ulman, A. *Chem. Rev.* **1996**, *96* (4), 1533.

(37) Schwartz, D. K. *Annu. Rev. Phys. Chem.* **2001**, *52*, 107.

(38) Schreiber, F. *J. Phys. Condens. Matter* **2004**, *16* (28), R881.

(39) Blodgett, K. B. *J. Am. Chem. Soc.* **1935**, *57* (6), 1007.

(40) Peterson, I. R. *J. Phys. D Appl. Phys.1* **1990**, *23*, 379.

(41) Bain, C.; Troughton, E.; Tao, Y.-T. *J. Am. Chem. Soc.* **1989**, *111* (1), 321.

(42) Laibinis, P. E.; Whitesides, G. M.; Allara, D. L.; Tao, Y.-T.; Parikh, A. N.; Nuzzo, R. G. *J. Am. Chem. Soc.* **1991**, *113* (19), 7152.

(43) Bain, C.; Biebuyck, H.; Whitesides, G. *Langmuir* **1989**, *5* (3), 723.

(44) Lu, H.; Zeysing, D.; Kind, M.; Terfort, A.; Zharnikov, M. *J. Phys. Chem. C* **2013**, *117* (37), 18967.

(45) Lu, H.; Kind, M.; Terfort, A.; Zharnikov, M. *J. Phys. Chem. C* **2013**, *117* (49), 26166.

(46) Nuzzo, R. G.; Dubois, L. H.; Allara, D. L. *J. Am. Chem. Soc.* **1990**, *112* (2), 558.

(47) Hoffmann, P. W.; Stelzle, M.; Rabolt, J. F. *Langmuir* **1997**, *13* (7), 1877.

(48) Hozumi, A.; Ushiyama, K.; Sugimura, H.; Takai, O. *Langmuir* **1999**, *15* (22), 7600.

(49) Tada, H. *J. Electrochem. Soc.* **1995**, *142* (1), L11.

(50) Tada, H.; Nagayama, H. *Langmuir* **1995**, *11* (1), 136.

(51) Parikh, A. N.; Allara, D. L.; Azouz, I. B.; Rondelez, F. *J. Phys. Chem.* **1994**, *98* (31), 7577.

(52) Hozumi, A.; Kim, B.; McCarthy, T. J. *Langmuir* **2009**, *25* (12), 6834.

(53) Silverman, B. M.; Wieghaus, K. A.; Schwartz, J. *Langmuir* **2005**, *21* (1), 225.

(54) Choi, J.; Sakurai, K.; Kato, T. *Surf. Interface Anal.* **2010**, *42* (6–7), 1373.

(55) Tan, M.; Zhang, H.; Wang, Y.; Ma, H.; Zhu, J.; Han, J. *Appl. Surf. Sci.* **2008**, *254* (20), 6332.

(56) Schlotter, N. E.; Porter, M. D.; Bright, T. B.; Allara, D. L. *Chem. Phys. Lett.* **1986**, *132* (1), 93.

(57) Hare, E. F.; Shafrin, E. G.; Zisman, W. A. *J. Phys. Chem.* **1954**, *58*, 236.

(58) Allara, D. L.; Nuzzo, R. G. *Langmuir* **1985**, *1* (1), 45.

(59) Allara, D. L.; Nuzzo, R. G. *Langmuir* **1985**, *1* (5), 52.

(60) Taylor, C. E.; Schwartz, D. K. *Langmuir* **2003**, *19* (7), 2665.

(61) Benítez, J. J.; Kopta, S.; Ogletree, D. F.; Salmeron, M. *Langmuir* **2002**, *18*, 6096.

(62) Frey, S.; Shaporenko, A.; Zharnikov, M.; Harder, P.; Allara, D. L. *J. Phys. Chem. B2* **2003**, *107*, 7716.

(63) Bergerson, W. F.; Mulder, J. A.; Hsung, R. P. **1999**, No. C, 454.

(64) Hickman, J. J.; Laibinis, P. E.; Auerbach, D. I.; Zou, C. F.; Gardner, T. J.; Whitesides, G. M.; Wrighton, M. S. *Langmuir* **1992**, *8* (1), 357.

(65) Han, S. W.; Lee, S. J.; Kim, K. *Langmuir* **2001**, *17* (22), 6981.

(66) Shaporenko, A.; Ulman, A.; Terfort, A.; Zharnikov, M. *J. Phys. Chem. B* **2005**, *109* (9), 3898.

(67) Shaporenko, A.; Cyganik, P.; Buck, M.; Terfort, A.; Zharnikov, M. *J. Phys. Chem. B* **2005**, *109* (111), 13630.

(68) Hohman, J. N.; Thomas, J. C.; Zhao, Y.; Auluck, H.; Kim, M.; Vijselaar, W.; Kommeren, S.; Terfort, A.; Weiss, P. S. *J. Am. Chem. Soc.* **2014**, *136* (22), 8110.

(69) Kim, H. I.; Boiadjiev, V.; Houston, J. E.; Zhu, X.; Kiely, J. D. *Tribol. Lett.* **2001**, *10* (1), 97.

(70) Niederhauser, T. L.; Jiang, G.; Lua, Y.-Y.; Dorff, M. J.; Woolley, A. T.; Asplund, M. C.; Berges, D. a; Linford, M. R. *Langmuir* **2001**, *17* (4), 5889.

(71) Zaba, T.; Noworolska, A.; Bowers, C. M.; Breiten, B.; Whitesides, G. M.; Cyganik, P. *J. Am. Chem. Soc.* **2014**, No. 111, 2.

(72) McDonagh, A. M.; Zareie, H. M.; Ford, M. J.; Barton, C. S.; Ginic-Markovic, M.; Matisons, J. G. *J. Am. Chem. Soc.* **2007**, *129* (12), 3533.

(73) Wasserman, S. R.; Tao, Y. T.; Whitesides, G. M. *Langmuir* **1989**, *5* (4), 1074.

(74) Yoshino, N.; Yamamoto, Y.; Hamano, K.; Kawase, T. *Bull. Chem. Soc. Jpn.* **1993**, *66* (6), 1754.

(75) Porter, M. D.; Bright, T. B.; Allara, D. L.; Chidsey, C. E. D. *J. Am. Chem. Soc.* **1987**, *109* (12), 3559.

(76) Cheng, H.; Hu, Y. *Adv. Colloid Interface Sci.* **2012**, *171–172*, 53.

(77) Cometto, F. P.; Calderón, C. A.; Berdakin, M.; Paredes-Olivera, P.; Macagno, V. A.; Patrito, E. M. *Electrochim. Acta* **2012**, *61*, 132.

(78) Booth, B. D.; Vilt, S. G.; Lewis, J. Ben; Rivera, J. L.; Buehler, E. A.; McCabe, C.; Jennings, G. K. *Langmuir* **2011**, *27* (10), 5909.

(79) Troughton, E. B.; Bain, C. D.; Whitesides, G. M.; Nuzzo, R. G.; Allara, D. L.; Porter, M. D. *Langmuir* **1988**, *4* (2), 365.

(80) Bain, C.; Whitesides, G. *J. Am. Chem. Soc.* **1988**, *110*, 5897.

(81) Yang, G.; Liu, G. *J. Phys. Chem. B* **2003**, *107*, 8746.

(82) Haensch, C.; Hoeppener, S.; Schubert, U. S. *Chem. Soc. Rev.* **2010**, *39* (6), 2323.

(83) Tranca, I.; Smerieri, M.; Savio, L.; Vattuone, L.; Costa, D.; Tielens, F. *Langmuir* **2013**, *29* (25), 7876.

(84) Nomura, S.; Yamada, T.; Kawai, M. *Chem. Lett.* **2010**, *39* (12), 1297.

(85) Fukushima, H.; Seki, S.; Nishikawa, T.; Takiguchi, H.; Tamada, K.; Abe, K.; Colorado, R.; Graupe, M.; Shmakova, O. E.; Lee, T. R. *J. Phys. Chem. B* **2000**, *104* (31), 7417.

(86) Usui, T.; Koini, T.; R. Lee, T.; Tamada, K.; Nagasawa, J.; Nakanishi, F.; Abe, K.; Hara, M.; Knoll, W.; Ishida, T.; Fukushima, H.; Miyashita, S. *Thin Solid Films* **1998**, *327–329*, 150.

(87) Tamada, K.; Ishida, T.; Knoll, W.; Fukushima, H.; Colorado, R.; Graupe, M.; Shmakova, O. E.; Lee, T. R. *Langmuir* **2001**, *17* (6), 1913.

(88) Love, J. C.; Estroff, L. A.; Kriebel, J. K.; Nuzzo, R. G.; Whitesides, G. M. *Chem. Rev.* **2005**, *105* (4), 1103.

(89) P. Barthel-Rosa, L.; A. Gladysz, J. *Coord. Chem. Rev.* **1999**, *190–192*, 587.

(90) Barriet, D.; Lee, T. R. *Curr. Opin. Colloid Interface Sci.* **2003**, *8* (3), 236.

(91) Zenasni, O.; Jamison, A. C.; Lee, T. R. *Soft Matter* **2013**, *9* (28), 6356.

(92) Owen, M. J.; Williams, D. E. *J. Adhes. Sci. Technol.* **1991**, *5* (4), 307.

(93) Krafft, M. P.; Riess, J. G. *Chem. Rev.* **2009**, *109* (5), 1714.

(94) Krafft, M. P. *J. Fluor. Chem.* **2012**, *134*, 90.

(95) Lehmler, H. J. *Chemosphere* **2005**, *58* (11), 1471.

(96) Fujii, S.; Polprasert, C.; Tanaka, S.; Lien, N. P. H.; Qiu, Y. *J. Water Supply Res. Technol. - AQUA* **2007**, *56* (5), 313.

(97) Domingo, J. L. *Environ. Int.* **2012**, *40*, 187.

(98) Tuteja, A.; Choi, W.; Ma, M.; Mabry, J. M.; Mazzella, S. A.; Rutledge, G. C.; McKinley, G. H.; Cohen, R. E. *Science (80-.).* **2007**, *318* (5856), 1618.

(99) Valipour M., N.; Birjandi, F. C.; Sargolzaei, J. *Colloids Surfaces A Physicochem. Eng. Asp.* **2014**, *448* (43), 93.

(100) Geerken, M. J.; Zanten, T. S. van; Lammertink, R. G. H.; Borneman, Z.; Nijdam,

W.; Rijn, C. J. M. van; Wessling, M. *Adv. Eng. Mater.* **2004**, *6* (9), 749.

(101) Wagner, A. J.; Wolfe, G. M.; Fairbrother, D. H. *J. Chem. Phys.* **2004**, *120* (8), 3799.

(102) Zhuang, Y. X.; Hansen, O.; Knieling, T.; Wang, C.; Rombach, P.; Lang, W.; Benecke, W.; Kehlenbeck, M.; Koblitz, J. *J. Micromech. Microeng.* **2006**, *16* (11), 2259.

(103) Srinivasan, U.; Houston, M. R.; Howe, R. T.; Maboudian, R. *J. Microelectromechanical Syst.* **1998**, *7* (2), 252.

(104) Seo, E. K.; Sung, M. M. *Ultramicroscopy* **2007**, *107* (10–11), 995.

(105) Klein, R. J.; Fischer, D. a; Lenhart, J. L. *Langmuir* **2011**, *27* (20), 12423.

(106) Frey, S.; Heister, K.; Zharnikov, M.; Grunze, M. *Phys. Chem. Chem. Phys.* **2000**, *2*, 1979.

(107) Graupe, M.; Takenaga, M.; Koini, T.; Colorado, R. J.; Lee, T. R. *J. Am. Chem. Soc.* **1999**, *121*, 3222.

(108) Colorado, R. J.; Lee, T. R. *J. Phys. Org. Chem.* **2000**, *13*, 796.

(109) Colorado, R. J.; Lee, T. R. *Langmuir* **2003**, *19* (8), 3288.

(110) Graupe, M.; Koini, T.; Kim, H.; Garg, N. *Colloids Surfaces A …* **1999**, *154*, 239.

(111) Bunn, C. W.; Howells, E. R. *Nature* **1954**, *174* (4429), 549.

(112) Jang, S. S.; Blanco, M.; Goddard, W. A.; Caldwell, G.; Ross, R. B. *Macromolecules* **2003**, *36* (14), 5331.

(113) Clark, E. S. *Polymer (Guildf).* **1999**, *40* (16), 4659.

(114) Alves, C. A.; Porter, M. D. *Langmuir* **1993**, *9* (12), 3507.

(115) Chidsey, C. E. D.; Loiacono, D. N. *Langmuir* **1990**, *6*, 682.

(116) Noll, W. *Chemistry and Technology of Silicones*; Academic Press: New York, 1968.

(117) Anderson, R.; Larson, G. L.; Smith, G. L. *Silicon Compounds: Register and Review*; Hüls America, Inc.: Piscataway, 1991.

(118) Tripp, C. P.; Veregin, R. P. N.; Hair, M. L. *Langmuir* **1993**, *9* (12), 3518.

(119) Banga, R.; Yarwood, J.; Morgan, A. M.; Evans, B.; Kells, J. *Langmuir* **1995**, *11* (11), 4393.

(120) DePalma, V.; Tillman, N. *Langmuir* **1989**, *5*, 868.

(121) Bhushan, B.; Hansford, D.; Lee, K. K. *J. Vac. Sci. Technol. A Vacuum, Surfaces, Film.* **2006**, *24* (4), 1197.

(122) Hozumi, A.; McCarthy, T. J. *Langmuir* **2010**, *26* (33), 2567.

(123) Genzer, J.; Efimenko, K.; Fischer, D. A. *Langmuir* **2002**, *18* (24), 9307.

(124) Fréchette, J.; Maboudian, R.; Carraro, C. *Langmuir* **2006**, *22*, 2726.

(125) Janssen, D.; De Palma, R.; Verlaak, S.; Heremans, P.; Dehaen, W. *Thin Solid Films* **2006**, *515* (4), 1433.

(126) Paso, K.; Helberg, R. M. L.; Raaen, S.; Sjöblom, J. *J. Colloid Interface Sci.* **2008**, *325* (1), 228.

(127) Cichomski, M.; Grobelny, J.; Celichowski, G. *Appl. Surf. Sci.* **2008**, *254* (14), 4273.

(128) Ballav, N.; Terfort, A.; Zharnikov, M. *J. Phys. Chem. C* **2009**, *113* (9), 3697.

(129) Pellerite, M. J.; Wood, E. J.; Jones, V. W. *J. Phys. Chem. B* **2002**, *106*, 4746.

(130) Avnon, E.; Paz, Y.; Tessler, N. *Appl. Phys. Lett.* **2009**, *94*, 013502.

(131) Schreiber, F. *Prog. Surf. Sci.* **2000**, *65*, 151.

(132) Dubois, L. H.; Nuzzo, R. G. *Annu. Rev. Phys. Chem.* **1992**, *43*, 437.

(133) Zharnikov, M.; Grunze, M. *J. Phys. Condens. Matter* **2001**, *13*, 11333.

(134) Colorado, R. J.; Graupe, M.; Shmakova, O. E.; Villazana, R. J.; Lee, T. R. In *Interfacial properties on the submicrometer scale*; Frommer, J., Overney, R. M., Eds.; ACS Symposium Series; American Chemical Society: Washington, 2001; Vol. 781, pp 276–292.

(135) Trapnell, B. M. W. *Proc. Roy. Soc. London, Ser. A* **1953**, *218*, 566.

(136) Ford, K.; Battersby, B. J.; Wood, B. J.; Gentle, I. R. *J. Colloid Interface Sci.* **2012**, *370* (1), 162.

(137) Jung, C.; Dannenberger, O.; Xu, Y.; Buck, M.; Grunze, M. *Langmuir* **1998**, *14* (5), 1103.

(138) Zhang, Y.; Terrill, R. H.; Tanzer, T. a.; Bohn, P. W. *J. Am. Chem. Soc.* **1998**, *120* (11), 2654.

(139) Brewer, N. J.; Janusz, S.; Critchley, K.; Evans, S. D.; Leggett, G. J. *J. Phys. Chem. B* **2005**, *109* (22), 11247.

(140) Huang, J.; Hemminger, J. C. *J. Am. Chem. …* **1993**, *115*, 3342.

(141) DeBono, R. F.; Loucks, G. D.; Manna, D. Della; Krull, U. J. *Can. J. Chem.* **1996**, *74* (5), 677.

(142) Dannenberger, O.; Buck, M.; Grunze, M. *J. Phys. Chem. B* **1999**, *103* (12), 2202.

(143) Tamada, K.; Hara, M.; Sasabe, H.; Knoll, W. *Langmuir* **1997**, *7463* (111), 1558.

(144) Kondoh, H.; Kodama, C.; Sumida, H.; Nozoye, H. *J. Chem. Phys.* **1999**, *111* (3), 1175.

(145) Yamada, R.; Wano, H.; Uosaki, K. *Langmuir* **2000**, *16* (13), 5523.

(146) Kawasaki, M.; Sato, T.; Tanaka, T.; Takao, K. *Langmuir* **2000**, *16* (4), 1719.

(147) Terrill, R. H.; Tanzer, T. a; Bohn, P. W. *Langmuir* **1998**, *14* (4), 845.

(148) Peterlinz, K. a; Georgiadis, R. *Langmuir* **1996**, *12* (20), 4731.

(149) Dannenberger, O.; Wolff, J. J.; Buck, M. *Langmuir* **1998**, *14* (17), 4679.

(150) Schneider, T. W.; Buttry, D. a. *J. Am. Chem. Soc.* **1993**, *115* (12), 12391.

(151) Yamada, R.; Sakai, H.; Uosaki, K. *Chem. Lett.* **1999**, *28* (7), 667.

(152) Heister, K.; Allara, D. L.; Bahnck, K.; Frey, S.; Zharnikov, M.; Grunze, M. *Langmuir* **1999**, *15* (17), 5440.

(153) Azehara, H.; Yoshimoto, S.; Hokari, H.; Akiba, U. *J. Electroanal. Chem.* **1999**, *473*, 68.

(154) Schlenoff, J. B.; Li, M.; Ly, H. *J. Am. Chem. Soc.* **1995**, *117* (50), 12528.

(155) Ulman, A. *Adv. Mater.* **1990**, *2* (12), 573.

(156) Onclin, S.; Ravoo, B. J.; Reinhoudt, D. N. *Angew. Chemie - Int. Ed.* **2005**, *44* (39), 6282.

(157) Fadeev, A.; McCarthy, T. J. *Langmuir* **2000**, *16*, 7268.

(158) Stevens, M. J. *Langmuir* **1999**, *15* (8), 2773.

(159) Cohen, S. R.; Naaman, R.; Sagiv, J. *J. Phys. Chem.* **1986**, *90* (14), 3054.

(160) Wang, M.; Liechti, K. M.; Wang, Q.; White, J. M. *Langmuir* **2005**, *21* (5), 1848.

(161) Kluth, G. J.; Sung, M. M.; Maboudian, R. *Langmuir* **1997**, *13* (14), 3775.

(162) Kluth, G. J.; Sander, M.; Sung, M. M.; Maboudian, R. *J. Vac. Sci. Technol. A* **1998**, *16* (3), 932.

(163) Bhairamadgi, N. S.; Pujari, S. P.; Trovela, F. G.; Debrassi, A.; Khamis, A. A.; Alonso, J. M.; Al Zahrani, A. A.; Wennekes, T.; Al-Turaif, H. A.; Van Rijn, C.; Alhamed, Y. A.; Zuilhof, H. *Langmuir* **2014**, *30* (20), 5829.

(164) Gnanappa, A. K.; O'Murchu, C.; Slattery, O.; Peters, F.; O'Hara, T.; Aszalós-Kiss, B.; Tofail, S. A. M. *J. Phys. Chem. C* **2008**, *112* (38), 14934.

(165) McGovern, M. E.; Kallury, K. M. R.; Thompson, M. *Langmuir* **1994**, *10*, 3607.

(166) Angst, D. L.; Simmons, G. W. *Langmuir* **1991**, *7* (10), 2236.

(167) Flinn, D. H.; Guzonas, D. A.; Yoon, R.-H. *Colloids Surfaces A* **1994**, *87* (3), 163.

(168) Le Grange, J. D.; Markham, J. L.; Kurkjian, C. R. *Langmuir* **1993**, *9* (7), 1749.

(169) Silberzan, P.; Léger, L.; Ausserré, D.; Benattar, J. J. *Langmuir* **1991**, *7* (8), 1647.

(170) Carraro, C.; Yauw, O. W.; Sung, M. M.; Maboudian, R. *J. Phys. Chem. B* **1998**, *102* (23), 4441.

(171) Tripp, C. P.; Hair, M. L. *Langmuir* **1992**, *8* (4), 1120.

(172) Brzoska, J. B.; Azouz, I. B.; Rondelez, F. *Langmuir* **1994**, *10*, 4367.

(173) Ducéré, J.; Estève, A.; Dkhissi, A.; Rouhani, M. D.; Landa, G. *J. Phys. Chem.* **2009**, *113*, 15652.

(174) Baker, M. V.; Watling, J. D. *J. Sol-Gel Sci. Technol.* **2004**, *30* (2), 101.

(175) Kushmerick, J. G.; Hankins, M. G.; De Boer, M. P.; Clews, P. J.; Carpick, R. W.; Bunker, B. C. *Tribol. Lett.* **2001**, *10* (1–2), 103.

(176) Bunker, B. C.; Carpick, R. W.; Assink, R. a.; Thomas, M. L.; Hankins, M. G.; Voigt, J. a.; Sipola, D.; de Boer, M. P.; Gulley, G. L. *Langmuir* **2000**, *16* (20), 7742.

(177) de Boer, M. P.; Knapp, J. A.; Michalske, T. A.; Srinivasan, U.; Maboudian, R. *Acta Mater.* **2000**, *48* (18–19), 4531.

(178) Wanebo, M.; Kobrin, B.; Helmrich, F.; Chinn, J. In *Advanced Packaging Materials, Proceedings*; 2005; pp 136–138.

(179) Mayer, T. M.; de Boer, M. P.; Shinn, N. D.; Clews, P. J.; Michalske, T. A. *J. Vac. Sci. Technol. B Microelectron. Nanom. Struct.* **2000**, *18* (5), 2433.

(180) Untereker, D. F.; Lennox, J. C.; Wier, L. M.; Moses, P. R.; Murray, R. W. *J. Electroanal. Chem* **1977**, *81*, 309.

(181) Kristalyn, C. B.; Watt, S.; Spanninga, S. A.; Barnard, R. A.; Nguyen, K.; Chen, Z. *J. Colloid Interface Sci.* **2011**, *353* (1), 322.

(182) Wang, Y.; Lieberman, M. *Langmuir* **2003**, *19*, 1159.

(183) Kessel, C. R.; Granick, S. *Langmuir* **1991**, *7* (3), 532.

(184) Ulman, A.; Eilers, J. E.; Tillman, N. *Langmuir* **1989**, *5* (14), 1147.

(185) Wunderlich, B. *Macromolecular Physics*, Vol. 1.; Academic Press: New York, 1973.

(186) Sarnthein, J.; Pasquarello, A.; Car, R. *Phys. Rev. Lett.* **1995**, *74* (23), 4682.

(187) Zhao, X.; Kopelman, R. *J. Phys. Chem.* **1996**, *100* (26), 11014.

(188) Britt, D. W.; Hlady, V. *J. Colloid Interface Sci.* **1996**, *178* (2), 775.

(189) Finklea, H. O.; Robinson, L. R.; Blackburn, A.; Richter, B.; Allara, D.; Bright, T. *Langmuir* **1986**, *2* (2), 239.

(190) Allara, D. L.; Parikh, A. N.; Rondelez, F. *Langmuir* **1995**, *11* (7), 2357.

(191) Naik, V. V.; Crobu, M.; Venkataraman, N. V.; Spencer, N. D. *J. Phys. Chem. Lett.* **2013**, *4* (16), 2745.

(192) Tsao, M.-W.; Hoffmann, C. L.; Rabolt, J. F.; Johnson, H. E.; Castner, D. G.; Erdelen, C.; Ringsdorf, H. *Langmuir* **1997**, *13* (16), 4317.

(193) Liu, G.; Fenter, P.; Chidsey, C. E. D.; Ogletree, D. F.; Eisenberger, P.; Salmeron, M. *J. Chem. Phys.* **1994**, *101* (5), 4301.

(194) Liu, G.; Salmeron, M. *Langmuir* **1994**, *10* (2), 367.

(195) Strong, L.; Whitesides, G. M. *Langmuir* **1988**, *4* (3), 546.

(196) Widrig, C. A.; Alves, C. A.; Porter, M. D. *J. Am. Chem. Soc.* **1991**, *113* (8), 2805.

(197) Bain, C. D.; Evall, J.; Whitesides, G. M. *J. Am. Chem. Soc.* **1989**, *111* (18), 7155.

(198) Bain, C. D.; Whitesides, G. M. *J. Am. Chem. Soc.* **1989**, *111* (18), 7164.

(199) Oyerokun, F. T.; Vaia, R. A.; Maguire, J. F.; Farmer, B. L. *Langmuir* **2010**, *26* (14), 11991.

(200) Tielens, F.; Humblot, V.; Pradier, C.-M.; Calatayud, M.; Illas, F. *Langmuir* **2009**,

25 (17), 9980.

(201) Pace, G.; Petitjean, A.; Lalloz-Vogel, M.-N.; Harrowfield, J.; Lehn, J.-M.; Samorì, P. *Angew. Chemie Int. Ed.* **2008**, *47* (13), 2484.

(202) Bayat, H.; Tranchida, D.; Song, B.; Walczyk, W.; Sperotto, E.; Schönherr, H. *Langmuir* **2011**, *27* (4), 1353.

(203) Reddemann, L. Dissertation in progress.

(204) Bain, C. D.; Whitesides, G. M. *J. Am. Chem. Soc.* **1988**, *110*, 6560.

(205) Folkers, J. P.; Laibinis, P. E.; Whitesides, G. M.; Deutch, J. *J. Phys. Chem.* **1994**, *98* (2), 563.

(206) Arezki, B.; Delcorte, A.; Garrison, B. J.; Bertrand, P. *J. Phys. Chem. B* **2006**, *110* (13), 6832.

(207) Tolman, R. C. *J. Chem. Phys.* **1949**, *17* (3), 333.

(208) Fradin, C.; Braslau, A.; Luzet, D.; Alba, M.; Boudet, N.; Mecke, K.; Daillant, J. *Nature* **2000**, *403*, 871.

(209) Mora, S.; Daillant, J.; Mecke, K.; Luzet, D.; Braslau, A.; Alba, M.; Struth, B. *Phys. Rev. Lett.* **2003**, *90* (21), 216101.

(210) Li, D.; Yang, B.; Lin, B.; Meron, M.; Gebhardt, J.; Graber, T.; Rice, S. *Phys. Rev. Lett.* **2004**, *92* (13), 136102.

(211) Mecke, K. R.; Dietrich, S. *Phys. Rev. E* **1999**, *59* (6), 6766.

(212) Tada, H.; Nagayama, H. *Langmuir* **1994**, No. 19, 1472.

(213) Lowe, R. D.; Pellow, M. A.; Stack, T. D. P.; Chidsey, C. E. D. *Langmuir* **2011**, *27* (16), 9928.

(214) Knieling, T.; Lang, W.; Benecke, W. *Sensors Actuators B Chem.* **2007**, *126* (1), 13.

(215) Efimenko, K.; Novick, B.; Carbonell, R. G.; Desimone, J. M.; Genzer, J.; Carolina, N.; Hill, C. *Langmuir* **2002**, *18*, 6170.

(216) Wu, K.; Bailey, T. C.; Willson, C. G.; Ekerdt, J. G. *Langmuir* **2005**, *21*, 11795.

(217) Brzoska, J. B.; Shahidzadeh, N.; Rondelez, F. *Nature* **1992**, *360* (6406), 719.

(218) Rye, R. R. *Langmuir* **1997**, *13* (9), 2588.

(219) Lee, S.; Ishizaki, T.; Saito, N.; Takai, O. *Jpn. J. Appl. Phys.* **2008**, *47* (8), 6442.

(220) Fadeev, A. Y.; McCarthy, T. J. *Langmuir* **1999**, No. 24, 3759.

(221) Beckey, H. D.; Belcher, R.; Frieser, H. *Principles of Field Ionization and Field Desorption Mass Spectrometry*; International series in analytical chemistry; Pergamon Press: Oxford, 1977; Vol. 61.

(222) Beckey, H. D. *J. Mass. Spectrom. Ion Physic* **1969**, *2* (6), 500.

(223) Schulten, H.-R.; Schiebel, H. M. *Naturwissenschaften* **1978**, *65*, 223.

(224) Lattimer, R. P.; Schulten, H.-R. *Anal. Chem.* **1989**, *61* (21), 1201A.

(225) Curran, D. P. *Synlett* **2001**, *9*, 1488.

(226) Kissa, E. *Fluorinated Surfactants and Repellents, Surfactant Science Series Vol. 97*; Marcel Dekker: New York, 2001.

(227) da Costa, R. C.; Jurisch, M.; Gladysz, J. a. *Inorganica Chim. Acta* **2008**, *361* (11), 3205.

(228) Naud, C.; Calas, P.; Blancou, H.; Commeyras, a. *J. Fluor. Chem.* **2000**, *104* (2), 173.

(229) Zakharkin, L. I.; Aksenova, N. P.; Guseva, V. V.; Bavrina, T. V.; Konstantinova, T. N.; Chailakhyan, M. K. *Chem. Nat. Comp.* **1984**, *20*, 344.

(230) Cahiez, G.; Alexakis, A.; Normant, J. F. *Tetrahedron Lett.* **1978**, *33*, 3013.

(231) Umio, S.; Ueda, I.; Nojima, H. *J. Mecinal Chem.* **1972**, *15* (8), 855.

(232) Schaumann, E. In *Methods of Organic Chemistry, Vol. VI/1b*; p 746.

(233) Speier, J. L. *Adv. Organomet. Chem.* **1979**, *17*, 407.

(234) Marciniec, B.; Gulinski, J. *J. Organomet. Chem.* **1993**, *446*, 15.

(235) Lewis, L. N.; Stein, J.; Gao, Y.; Colborn, R. E.; Hutchins, G. *Platin. Met. Rev.* **1997**, *41* (2), 66.

(236) Améduri, B.; Boutevin, B.; Nouiri, M.; Talbi, M. *J. Fluor. Chem.* **1995**, *74* (2), 191.

(237) Haszeldine, R. N. *J. Chem. Soc.* **1952**, 3423.

(238) Pierce, O. R.; McBee, E. T.; Cline, R. E. *J. Am. Chem. Soc.* **1953**, *75* (22), 5618.

(239) Crombie, A.; Kim, S.-Y.; Hadida, S.; Curran, D. P. *Org. Syn.* **2002**, *79*, 1.

(240) Schwinn, D.; Bannwarth, W. *Helv. Chim. Acta* **2002**, *85*, 255.

(241) Benkeser, R. A.; Smith, W. E. *J. Am. Chem. Soc.* **1968**, *90* (19), 5307.

(242) Benkeser, R. A.; Gaul, J. M.; Smith, W. E. *J. Am. Chem. Soc.* **1969**, *91* (13), 3666.

(243) Benkeser, R. A. *Acc. Chem. Res.* **1971**, *4* (3), 94.

(244) Cho, Y. S.; Kang, S.-H.; Han, J. S.; Yoo, B. R.; Jung, I. N. *J. Am. Chem. Soc.* **2001**, *123* (23), 5584.

(245) Kang, S.-H.; Han, J. S.; Yoo, B. R.; Lee, M. E.; Jung, I. N. **2003**, *22* (3), 529.

(246) Jung, D. E.; Kang, S.-H.; Han, J. S.; Lim, W. C.; Park, Y. W.; Yoo, B. R. *J. Organomet. Chem.* **2007**, *692* (18), 3901.

(247) Wróblewska, A.; Meissner, E.; Milchert, E. *J. Fluor. Chem.* **2006**, *127* (3), 345.

(248) Bravo, P.; Bruché, L.; Panzeri, W.; Viani, F.; Vichi, L. *J. Fluor. Chem.* **1998**, *91*, 27.

(249) Bravo, P.; Piovosi, E.; Resnati, G.; de Munari, S. *Gazz. Chim. Ital.* **1988**, *118*, 115.

(250) Dumont, W.; Krief, A. *J. Chem. Soc., Chem. Commun.* **1980**, 673.

(251) Willey, T. M.; Vance, A. L.; Van Buuren, T.; Bostedt, C.; Terminello, L. J.; Fadley, C. S. *Surf. Sci.* **2005**, *576* (1–3), 188.

(252) Tarlov, M. J.; Newman, J. G. *Langmuir* **1992**, *8* (20), 1398.

(253) Knauf, J.; Reddemann, L.; Böker, A.; Reihs, K. contribution in progress.

(254) Wasserman, S. R.; Whitesides, G. M.; Tidswell, I. M.; Ocko, B. M.; Pershan, P. S.; Axe, J. D. *J. Am. Chem. Soc.* **1989**, *111* (15), 5852.

(255) Geer, R. E.; Stenger, D. A.; Chen, M. S.; Calvert, J. M.; Shashidhar, R.; Jeong, Y. H.; Pershan, P. S. *Langmuir* **1994**, *10* (4), 1171.

(256) Naud, C.; Calas, P.; Commeyras, A. *Langmuir* **2001**, *17* (16), 4851.

(257) Frey, S.; Heister, K.; Zharnikov, M.; Grunze, M.; Tamada, K.; Colorado, R. J.; Graupe, M.; Shmakova, O. E.; Lee, T. R. *Isr. J. Chem* **2000**, *40* (2), 81.

(258) Fox, H. .; Zisman, W. . *J. Colloid Sci.* **1950**, *5* (6), 514.

(259) Bernett, M. K.; Zisman, W. A. *J. Phys. Chem.* **1959**, *63* (8), 1241.

(260) Dann, J. . *J. Colloid Interface Sci.* **1970**, *32* (2), 302.

(261) Decker, E. L.; Garoff, S. *Langmuir* **1997**, *13* (15), 6321.

(262) Girifalco, L. A.; Good, R. J. *J. Phys. Chem.* **1957**, *61*, 904.

(263) Gao, L.; McCarthy, T. J. *Langmuir* **2007**, *23* (7), 3762.

(264) Vargaftik, N. B.; Volkov, B. N.; Voljak, L. D. *J. Phys. Chem. Ref. Data* **1983**, *12*, 817.

(265) Korosi, G.; Kovats, E. S. *J. Chem. Eng. Data* **1981**, *26* (3), 323.

(266) Bluestein, B. R.; Hilton, C. L. In *Amphoteric Surfactants, Surfactant Sci. Ser. 12*; Dekker: New York, 1982.

(267) Zhao, X.; Liu, Y.; Inoue, S.; Suzuki, T.; Jones, R. O.; Ando, Y. *Phys. Rev. Lett.* **2004**, *92* (12), 125502.

(268) Norman, S.; King, P.; Maeder, M. 2015, p www.jplusconsulting.com.

(269) Osterholtz, F. D.; Pohl, E. R. *J. Adhes. Sci. Technol.* **1992**, *6* (1), 127.

(270) Brinker, C. J. *J. Non. Cryst. Solids* **1988**, *100*, 31.

(271) Yokoi, T.; Kubota, Y.; Tatsumi, T. *Appl. Catal. A Gen.* **2012**, *421–422*, 14.

(272) Kubota, Y.; Sugi, Y.; Tatsumi, T. *Catal. Surv. from Asia* **2007**, *11* (4), 158.

(273) Hruby, S. L.; Shanks, B. H. *J. Catal.* **2009**, *263* (1), 181.

(274) Fessenden, R.; Fessenden, J. R. *Chem. Rev.* **1961**, *61* (4), 361.

(275) du Toit, F. J.; Sanderson, R. D.; Engelbrecht, W. J.; Wagener, J. B. *J. Fluor. Chem.* **1995**, *74* (1), 43.

(276) Lehocký, M.; Drnovská, H.; Lapčíková, B.; Barros-Timmons, A. M.; Trindade, T.; Zembala, M.; Lapčík, L. *Colloids Surfaces A Physicochem. Eng. Asp.* **2003**, *222* (1–3), 125.

(277) Adam, N. K.; Elliot, G. E. P. *J. Chem. Soc.* **1962**, 2206.

(278) Adamson, A. W.; Gast, A. P. *Physical Chemistry of Surfaces*, 6.; John Wiley & Sons, Inc.: New York, 1997.

(279) Fox, H. W.; Zisman, W. A. *J. Coll. Sci.* **1952**, *7*, 428.

(280) Taft, E. A. *J. Electrochem. Soc.* **1978**, *125*, 968.

(281) Wagner, A. J.; Carlo, S. R.; Vecitis, C.; Fairbrother, D. H. *Langmuir* **2002**, *18* (5), 1542.

9. List of Figures

10. List of Tables

11. Abbreviations & Important Parameters

AFM	atomic force microscopy
$\mathbf{c_{long}}$, $\mathbf{c_{short}}$, $\mathbf{c_{sol}}$	concentration of precursor thiols within a deposition solution (long, short, total concentration)
DFT	density functional theory
FDMS	field-desorption mass spectrometry
FE-SEM	field emission scanning electron microscopy
F-HPLC	fluorous phase high-performance liquid chromatography
GIXD	grazing incidence x-ray diffraction
HD	*n*-hexadecane
IR	infrared
$\mathbf{n_{short}}$, $\mathbf{n_{long}}$	chain-length of short/long precursor thiol in mixed thiol monolayers
$\mathbf{p_{rel}}$	parameter describing the ration of initial water to silane partial pressure in vapor-phase silane CVD-processes
r	roughness factor of surfaces according to Wenzel
$\mathbf{R_0}$	specific concentration ratio of precursor thiols in a deposition solution, which yields a SAM of equimolar composition (mixed thiol monolayers)
RP-HPLC	reversed-phase high-performance liquid chromatography

$\mathbf{R_{sol}}$	concentration ratio of precursor thiols in a deposition solution (mixed thiol monolayers)
S0, S1, S2, S3	relative amounts of hydrolyzed species within modeling of trichlorosilane hydrolysis
SAM	self-assembled monolayer
SHG	second harmonic generation
sSIMS	static secondary-ion mass spectrometry
TBPC	tetrabutylphosphonium chloride
ToF-SIMS	time-of-flight secondary-ion mass spetrometry
vdW	van der Waals
XPS	x-ray photoelectron spectroscopy
$\mathbf{x_{short}}$, $\mathbf{x_{long}}$, $\mathbf{x_{FnH2}}$	molar fraction of specified precursor in mixed thiol monolayers
Δh	chain-length difference in Ångtstroms
Δm	chain-length difference of non-fluorinated SAMs and precursors
Δn	chain-length difference of fluorinated SAMs and precursors
Δθ	contact angle hysteresis
$\mathbf{\Delta\theta_{adv,max}(L)}$	maximum increase/decrease of advancing contact angle for liquid L (used in thiol monolayers)
$\mathbf{\theta_{adv}}$, $\mathbf{\theta_{adv}(L)}$	advancing contact angle (of liquid L)
$\mathbf{\theta_{CB}}$	contact angle according to Cassie-Baxter

θ_{rec}	receding contact angle
θ_W	contact angle according to Wenzel
θ_Y	contact angle according to Young
ω	interaction parameter applied in mixed thiol monolayers

12. Scientific Contributions

Knauf, J.; Reddemann, L.; Böker, A.; Reihs, K. “A Detailed Investigation of the Conditions for Monolayer Deposition from Silane Precursors” (Talk); AVS 59th International Symposium & Exhibition, Tampa 2012

Knauf, J.; Reddemann, L.; Böker, A.; Reihs, K. “Unexpected behaviour of liquid wetting at the limit of small-scale surface topography” (Talk); 19th Interdisciplinary Surface Science Conference (ISSC-19), Nottingham 2013

Knauf, J.; Reddemann, L.; Böker, A.; Reihs, K. "Controlled molecular layer deposition enables extremely low friction of liquid water flow on structured surfaces" (Poster), 13th International Conference on Atomic Layer Deposition (ALD 2013), San Diego 2013

Knauf, J.; Reddemann, L.; Böker, A.; Reihs, K. "Unexpected behaviour of liquid wetting at the limit of small-scale surface topography" (Talk); AVS 60th International Symposium & Exhibition, Long Beach 2013

Knauf, J.; Reddemann, L.; Cheng, K.; Böker, A.; Reihs, K. “Scale Dependent Surface Energies Influence Wetting Behaviour on Ultimately Small Topographies” (Talk), AVS 61st International Symposium and Exhibition, Baltimore 2014

<u>Co-authorship:</u>

Reddemann, L.; Knauf, J.; Böker, A.; Reihs, K. “Extremely Low Friction of Liquid Water Flow on Structured Surfaces” (Talk); 14th International Conference on Organized Molecular Films (ICOMF14 - LB14), Paris 2012

Reddemann, L.; Knauf, J.; Böker, A.; Reihs, K. "Investigation of wetting phenomena at the limit of small-scale surface topography in the sub-nanometer Regime" (Talk); 19th International Vacuum Congress (IVC 19), Paris 2013

Reihs, K.; Reddemann, L.; Knauf, J.; Breitenstein, D.; Hagenhoff, B.; Böker, A. “Limitation of Quantitative Surface Analysis by Static SIMS Using Ar Cluster Ions”

(Talk), 19th International Conference on Secondary ion Mass Spectrometry (SIMS-19), Jeju 2013

Reddemann, L.; Knauf, J.; Cheng, K.; Brock, W.; Hagenhoff, B.; Böker, A.; Reihs, K. "Thermodynamic Properties of Binary Mixed Monolayers Investigated by Static SIMS" (Poster), 9th European Workshop on Secondary Ion Mass Spectrometry (SIMS Europe), Münster 2014

Reihs, K.; Reddemann, L.; Knauf, J.; Cheng, K.; Breitenstein, D.; Fartmann, M.; ter Veen, R.; Hagenhoff, B.; Böker, A. "Unexpected Relations of Ion Intensities in Static SIMS using Ar Cluster Primary Ions" (Talk), 9th European Workshop on Secondary Ion Mass Spectrometry (SIMS Europe), Münster 2014

Reddemann, L.; Knauf, J.; Cheng, K.; Böker, A.; Reihs, K. "A New Principle other than ‚Wenzel' and ‚Cassie' to Modify Wetting Properties by Surface Topography"(Poster), 5th International Colloids Conference, Amsterdam 2015